Vikas Tyagi

compiled thesis file 30-7-25

PHD Thesis

Document Details

Submission ID
trn:oid:::3618:106444020

Submission Date
Jul 30, 2025, 3:40 PM GMT+5:30

Download Date
Jul 30, 2025, 4:18 PM GMT+5:30

File Name
compiled thesis file 30-7-25.pdf

File Size
9.3 MB

157 Pages

46,867 Words

244,915 Characters

11% Overall Similarity

The combined total of all matches, including overlapping sources, for each database.

Filtered from the Report

- Bibliography
- Quoted Text
- Small Matches (less than 8 words)

Exclusions

- 64 Excluded Matches

Match Groups

345 Not Cited or Quoted 11%
Matches with neither in-text citation nor quotation marks

3 Missing Quotations 0%
Matches that are still very similar to source material

0 Missing Citation 0%
Matches that have quotation marks, but no in-text citation

0 Cited and Quoted 0%
Matches with in-text citation present, but no quotation marks

Top Sources

7% Internet sources
8% Publications
9% Submitted works (Student Papers)

Match Groups

- **345** Not Cited or Quoted 11%
  Matches with neither in-text citation nor quotation marks
- **3** Missing Quotations 0%
  Matches that are still very similar to source material
- **0** Missing Citation 0%
  Matches that have quotation marks, but no in-text citation
- **0** Cited and Quoted 0%
  Matches with in-text citation present, but no quotation marks

Top Sources

- 7% Internet sources
- 8% Publications
- 9% Submitted works (Student Papers)

Top Sources

The sources with the highest number of matches within the submission. Overlapping sources will not be displayed.

1	Student papers	
IIT Delhi on 2025-06-19		2%
2	Student papers	
IIT Delhi on 2024-06-21		1%
3	Internet	
www.google.com		1%
4	Student papers	
National Institute of Technology Warangal on 2025-05-28		1%
5	Internet	
dx.doi.org		<1%
6	Publication	
Hossian, Asik, Samir Kumar Bhunia, and Ranjan Jana. "Substrate-Dependent Mec...		<1%
7	Publication	
Greenwood, Nathaniel Scott. "Rhodium(III)-Catalyzed Heterocycle Synthesis and ...		<1%
8	Publication	
Bhatt, Shreeja. "Development of Palladium Catalyzed Olefin Functionalizations: R...		<1%
9	Internet	
hdl.handle.net		<1%
10	Internet	
repository.lsu.edu		<1%

11	Publication	Marek Varga, Florian Ortis, Emily Hank, Kaixin Zhou et al. "Giving an Enzyme Sciss... <1%
12	Publication	Wilson-Konderka, Cody. "Total Synthesis of Syringolin B and Other Urea/Guanidin... <1%
13	Publication	Suraksha Gahalawat, Sneha Ray, Xiaoyu Zhang, Xiaoyi Deng et al. "Optimization o... <1%
14	Publication	Dmitry V. Liskin, Penny Chaloner. "Advanced Organic Synthesis - A Laboratory Ma... <1%
15	Publication	Shiyang Zhai, Irina Honin, Linda Schäker-Hübner, Maria Hanl et al. "Development ... <1%
16	Publication	Mark E. Thompson. "Electrophosphorescent Materials and Devices", Jenny Stanfo... <1%
17	Publication	Parmjeet Kaur, Vikas Tyagi. "Design and preparation of novel bifunctional nanobi... <1%
18	Publication	Jian Xue, Li-Gang Bai, Liang Zhang, Yue Zhou, Xiao-Long Lin, Neng-Jie Mou, Dong-... <1%
19	Publication	Cui, Huarui. "Development of Small Molecule Chemical Probes for BRD4", Univers... <1%
20	Publication	Princess Simeon, Ramu Venkatesan, Xiaoyu Hao, Angelica Carmona, Sohel Daria, ... <1%
21	Publication	Paul Kosma, Tanja Wrodnigg, Arnold Stütz. "Carbohydrate Chemistry - Proven Sy... <1%

CONTENTS

CONTENTS

CONTENTS

CONTENTS

LIST OF ABBREVIATIONS

PPL	Lipase from *Porcine pancreas*
CALB	Lipase from *Candida antarctica*
CRL	Lipase from *Candida rugosa*
RML	Lipase from *Rhizomucor miehei*
PFL	Lipase from *Pseudomonas fluorescens*
PCL	Lipase from *Pseudomonas cepacia*
HNTs	Halloysite nanotubes
E. coli	*Escherichia coli*
CLEA	Cross-linked enzyme aggregates
PdNPs	Pd-nanoparticles
DMSO	Dimethyl sulfoxide
EtOH	Ethanol
MeOH	Methanol
THF	Tetrahydrofuran
EtOAc	Ethyl acetate
K_2CO_3	Potassium carbonate
NaOH	Sodium hydroxide
KO^tBu	Potassium tert-butoxide
^{1}HNMR	Proton Nuclear Magnetic Resonance
^{13}C NMR	Carbon Nuclear Magnetic Resonance
^{19}F NMR	Fluorine Nuclear Magnetic Resonance
TMS	Trimethyl silane
D_2O	Deuterium oxide
$CDCl_3$	Deuterated chloroform
TLC	Thin Layer Chromatography
HPLC	High-Performance Liquid Chromatography
UV	Ultra-violet Spectroscopy
HRMS	High-resolution mass spectrometry
FT-IR	Fourier Transform Infra-Red Spectroscopy

LIST OF ABBREVIATIONS

FT-NMR	Fourier Transform-Nuclear Magnetic Resonance Spectroscopy
XRD	X-Ray Diffraction
EDS	Energy Dispersive X-ray Spectroscopy
FE-SEM	Field Emission Scanning Electron Microscopy
HR-TEM	High-Resolution Transmission Electron Microscopy
KPi	Potassium phosphate
MOFs	Metal Organic Frameworks
$KMnO_4$	Potassium Permanganate
ppm	Parts per million
rpm	Revolutions per minute
mmol/g	Millimole per gram
kcal mol-1	Kilocalories per mole
$^{n}Bu_4N$	Tetrabutyl ammonium
TEMPO	2,2,6,6-tetramethylpiperidin-1-yl)oxyl
BHT	Butylated hydroxytoluene
CV	Cyclic voltammetry
r.t.	Room temperature
n.r.	No reaction

LIST OF SYMBOLS

Symbols	Description
Å	Angstrom
C	Celsius
T	Temperature
g	Gram
mg	Milligram
nm	Nanometre
º	Degree
J	Coupling constant
Min	Minute
h	Hour
s	Second
%	Percentage
Y	Yield
C	Conversion
α	Alpha
β	Beta
μ	Micro
γ	Gamma
v	Frequency
λ	Wavelength
o	Ortho
m	Meta
p	Para
L	Litre
δ	Chemical shift
V	Volts
F	Faraday
Pt	Platinum
MHz	Megahertz
eV	Electron volt
v/v	Volume by volume

LIST OF SYMBOLS

Equiv.	Equivalent
M	Molar
MM	Molar Mass
mA	Milliampere
e.r.	Enantiomeric ratio
e.e.	Enantiomeric excess
E	Enantioselectivity

turnitin Page 12 of 161 - Integrity Submission Submission ID trn:oid:::3618:106444020

LIST OF FIGURES

LIST OF SCHEMES

LIST OF SCHEMES

LIST OF SCHEMES

LIST OF TABLES

ABSTRACT

A major goal in modern synthetic chemistry is to develop sustainable and cost-efficient methodologies for the synthesis of complex, chiral molecules-particularly those with pharmaceutical importance. There are number of approaches being used for the sustainable synthesis of organic molecules, including biocatalysis, electrosynthesis, and photocatalysis. Enzymes, or biocatalysts, are integral to synthetic chemistry, offering exceptional chemo-, regio-, and enantioselectivity while operating under mild and environmentally benign conditions. Despite these advantages, their application is often limited by narrow substrate specificity and restricted reactivity. To overcome these limitations, one promising approach is to integrate biocatalysis with other catalytic techniques. These integrated strategies offer new opportunities for selective and green synthesis. However, a significant challenge lies in the potential deactivation of enzymes when used alongside other catalysts, which can compromise the overall catalytic efficiency. To address this challenge, it is essential to identify reaction conditions that preserve the stability and activity of each catalytic component. Achieving such compatibility is key to enabling efficient multi-catalytic cascade processes for the synthesis of drug-like compounds. The first chapter of thesis emphasizes on recent progress particularly from the last three years in the field of hydrolase catalyzed reactions integrated with chemical, electro-, and photocatalysis, highlighting their emerging role in advanced synthetic methodologies.

In the second chapter, we have developed a chemoenzymatic approach that combines chemical and bio-catalyst and has proven very useful in synthetic chemistry. However, mutual deactivation of chemical and bio-catalyst when employed in the same pot is still a challenge. In this context, the development of nanobiohybrid catalysts has played an important role and overcoming the issue of mutual deactivation between catalysts to a certain extent. Herein, we design and synthesize a novel heterogeneous recyclable nanobiohybrid catalyst comprising palladium nanoparticles and α-amylase from *Aspergillus oryzae* immobilized onto halloysite nanotubes as a solid heterogeneous support. Further, the wider applicability of the developed nanobiohybrid catalyst is revealed in the one-pot chemoenzymatic synthesis of functionalized biphenyls and bis(indolyl)methanes which consists of Pd-catalyzed Suzuki-Miyaura coupling and α-amylase mediated aza-Michael addition or electrophilic substitution reactions respectively. Further, the robustness and generality of the developed one-pot chemoenzymatic synthesis are demonstrated by incorporating different substitutions at the starting materials and obtaining the corresponding products in moderate to good yields.

ABSTRACT

In the third chapter of this thesis, we have developed a sustainable process to synthesize chiral sulfur-based organofluorine compounds by integrating electrosynthesis and biocatalysis within a single vessel while using water as a solvent. In this context, differently substituted 2-fluoro-3-mercaptopropionic acids have been synthesized in good isolated yields using thiophenols and fluorine-containing *α*,*β*-unsaturated alkenes. In addition, molecular docking and control experiments were carried out that suggest the formation of radical species during the electrolysis and participation of the lipase active site during the biocatalysis. The scalability and applicability of the developed protocol have been illustrated through the synthesis of a key intermediate of the MMP-3 inhibitor and by performing a gramscale reaction. Further, the compatibility of the lipase enzyme with electricity highlights the promising potential of enzymatic electrosynthesis in advancing environmentally friendly organic transformations.

In the fourth chapter, we reported a novel metal-free electrochemical strategy for the regioselective *N*-sulfonylation of *in-situ* generated indole-based hydrazones using readily available sodium sulfinates. The feasibility of the protocol was demonstrated by employing differently substituted aldehydes, hydrazines, and sodium sulfinates to access *N*-sulfonylated products up to 81% isolated yield. Further, various control experiments and cyclic voltammetry studies have been performed to get valuable mechanistic insights. These studies suggested the formation of indole-phenyldiazenium as an intermediate while ruling out the possibility of any radical formation during this transformation. In addition, the synthesized compounds were tested for antibacterial activity against Gram-positive and Gram-negative pathogens. Among them, compounds **5d**, **5e**, **5l**, and **5q** were found to have strong and selective antibacterial activity against *Staphylococcus aureus*, with **5d** being the most potent (MIC = 6.87 μM), while showing only moderate activity against Gram-negative pathogens. Furthermore, scanning electron microscopy (SEM) analysis revealed that the most promising hit (**5d**) causes significant morphological alternations and exert its effects by causing considerable cellular damage.

CHAPTER 1

Introduction and Literature Review

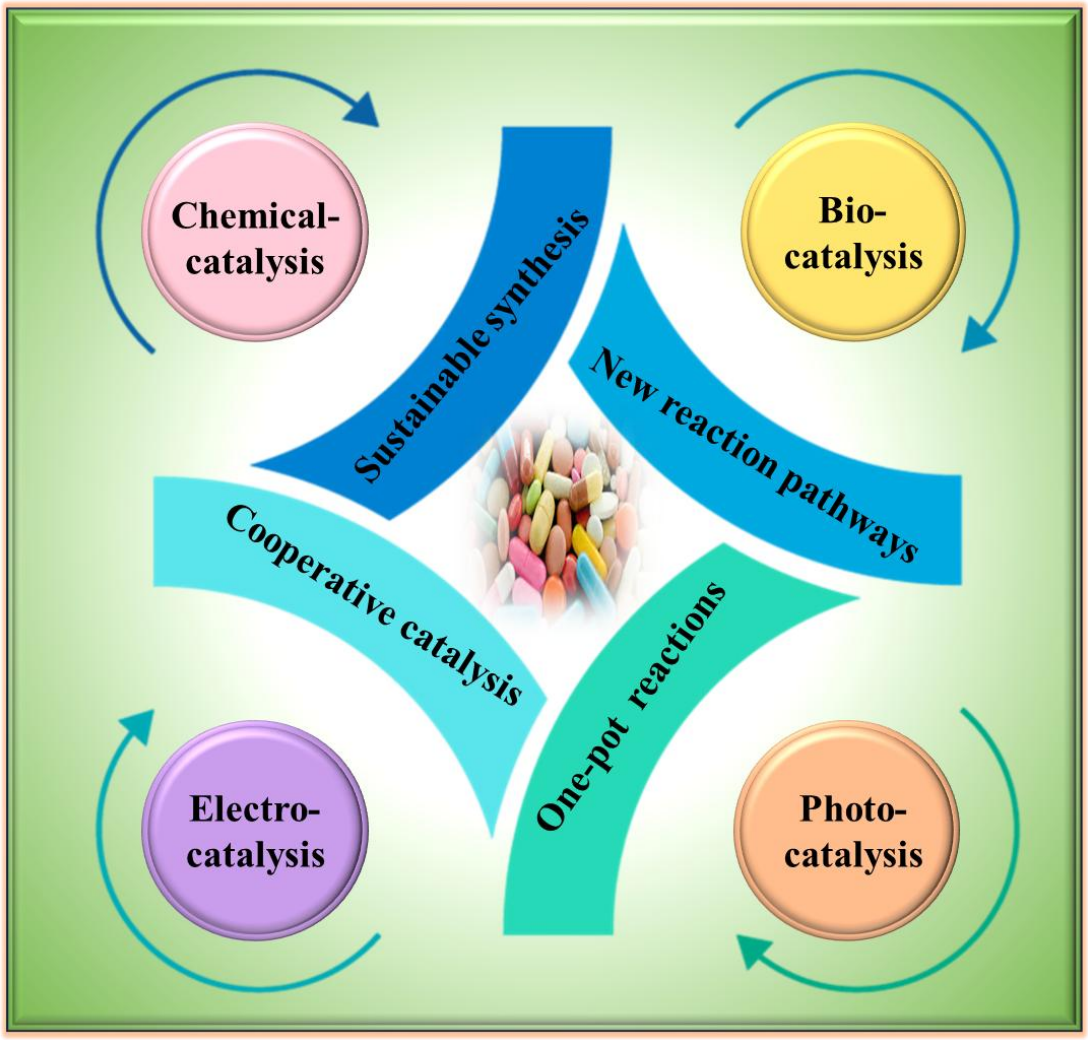

CHAPTER 1

1.1: Introduction

In recent years, the concept of sustainability has gained significant attention across diverse industries, including pharmaceuticals, agrochemicals, polymers, energy, and fuels.[1] In chemistry, sustainability refers to the design and development of chemical methodologies that reduce environmental effects, conserve resources, and ensure long-term ecological stability.[2] It primarily relies on the twelve principles of green chemistry to develop safe, efficient, and environmentally friendly methods for the safer production of pharmaceuticals, chemicals, materials, and beyond.[3] Moreover, sustainability offers several advantages in organic synthesis, such as enhanced selectivity and reactivity, reduced environmental impact, access to novel chemical space, utilization of renewable resources, waste minimization, etc.[4]

In the past decades, synthetic methodologies have focused primarily on achieving high yields and product purity, often overlooking energy consumption, toxicity, and waste generation.[5] Additionally, the traditional synthetic approaches, particularly at industrial scales, rely heavily on harmful chemicals and solvents, leading to massive waste production and a negative impact on both the environment and human health.[6] Therefore, rising environmental and economic concerns have prompted the scientific community to concentrate on inventing new and replacing old synthetic methods that are not only efficient and scalable, but also cost-effective and environmentally beneficial. Furthermore, sustainable synthesis in organic chemistry can be achieved in different ways, such as by using green solvents and catalysts, biomass-derived chemicals, and generating no toxic waste during reactions.[7]

In the last decade, biocatalysis has gained recognition as an environmentally benign and sustainable catalysis in organic synthesis.[8] Moreover, biocatalysis refers to the use of whole cells, isolated enzymes, or other biomolecules to accelerate the rate of chemical reactions.[9] It offers several notable advantages. First, enzymes are exceptionally efficient catalysts, capable of increasing reaction rates by factors of 10^8 to 10^{10} compared to uncatalyzed processes.[10] Second, unlike metal catalysts, enzymes are biodegradable and environmentally safe. Third, they function under mild conditions, typically at temperatures between 20-50 °C and often in aqueous media, without the need to protect functional groups, thereby minimizing undesired side reactions such as isomerization, racemization, decomposition, and rearrangement, which are common in traditional chemical methods. Fourth, enzymes demonstrate high levels of chemo-, regio-, and stereoselectivity when used as a catalyst in the reactions (**Figure 1.1**). [11] As a result, biocatalysis has increasingly become the preferred method for synthesizing chiral molecules and key precursors in the chemical and pharmaceutical industries in recent years.[12]

CHAPTER 1

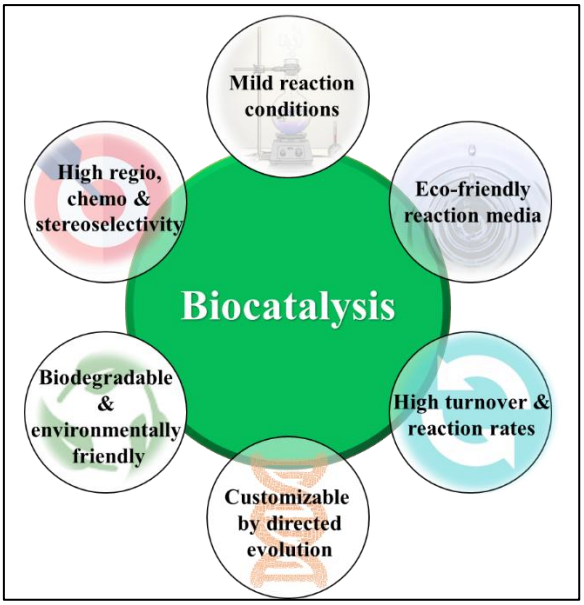

Figure 1.1: Advantages of biocatalysis in sustainable organic synthesis

Further, one of the key breakthroughs in the area of biocatalysis, which has attracted a lot of attention in recent years, has been directed evolution.[13] This technology enables the efficient engineering and customization of enzymes to adapt the diverse reaction conditions. Through this technique, enzymes can be tailored to accept non-natural substrates and operate under a broad range of pH values and extreme temperatures.[14] This has significantly expanded their applicability, allowing for stereoselective, specific, and complex chemical transformations.[15] Enzymes being used in biocatalysis are broadly classified into seven categories based on their catalytic activity, which have been presented in **Table 1.1**.[16]

Table 1.1: Classification of enzymes based on their catalysis

EC class	Enzyme	General catalytic action	Examples
EC1	Oxidoreductases	Redox reactions (electron transfer)	Cytochrome oxidase, NADH dehydrogenase, etc.
EC2	Transferases	Functional group transfer	Kinase, aminotransferase, etc.
EC3	Hydrolases	Water mediated hydrolytic bond cleavage Water mediated hydrolytic bond cleavage	Lipase, amylase, etc.
EC4	Lyases	Addition/removal of groups to form double bonds without hydrolysis	Aldolase, fumarase, etc.
EC5	Isomerases	Isomerization (rearrangement within the molecule)	Racemase, Phosphoglucose isomerase, etc.
EC6	Ligases	Bond formation using ATP	DNA ligase, synthetase etc.
EC7	Translocases	Movement of ions/molecules across membranes	ATP synthase, Sodium/Potassium ATPase, etc.

Among different classes of enzymes, hydrolases are widely utilized biocatalysts in industrial organic synthesis, valued for their impressive features such as high stability in organic solvents, high chemo-, regio-, and stereoselectivity, broad substrate scope, commercial availability, and the ability to operate without cofactors.[17] Their functionality in both aqueous and non-aqueous environments, along with their operational simplicity, makes them highly appealing to chemists. In addition to their well-established roles in hydrolysis, esterification, acylation, and amidation reactions, hydrolases have also demonstrated the ability to catalyse non-natural transformations that extend beyond their classical hydrolytic functions.[18] The discovery and exploration of such unusual reactivities present new opportunities to further expand the scope of hydrolase-mediated transformations in organic synthesis.[19]

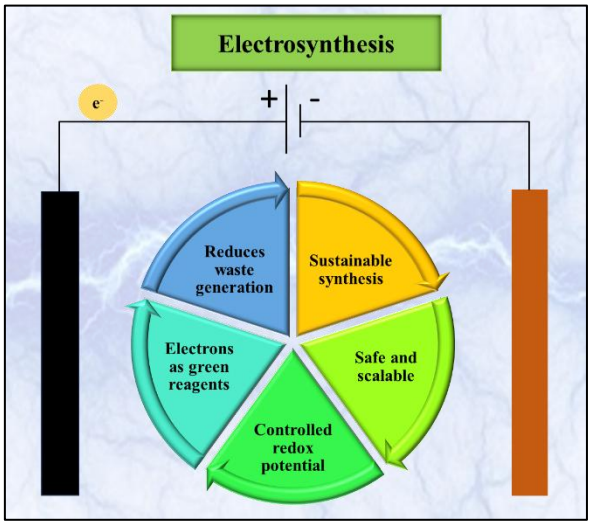

Figure 1.2: Key features of electrosynthesis

On the other hand, organic electrosynthesis is another novel, sustainable, and eco-friendly strategy for synthesizing organic compounds, utilizing inexpensive and potentially renewable electrical energy to drive redox reactions.[20] Since electrochemical processes generally require mild conditions, they eliminate the need for external oxidants. They often produce the desired products in shorter times while conserving energy, as hazardous oxidizing and reducing agents are replaced by electrons (**Figure 1.2**).[21] Moreover, by simply adjusting the applied current, it is possible to precisely control the oxidation and reduction potentials of the system.[22] This tunability offers a significant advantage over conventional methods. This flexibility helps minimize side reactions and byproduct formation, enabling cleaner reactions with high efficiency.[23] However, enantioselective organic synthesis remains a challenge in electrosynthesis due to the high reactivity of free radicals generated during the process.[24] It often requires chiral ligands, catalysts, or transition metals, but the limited compatibility of

these chiral catalysts within electrochemical cells makes it difficult to obtain chiral molecules.[25] Therefore, developing new approaches for asymmetric synthesis is crucial to achieving more sustainable catalytic systems in organic electrosynthesis. In addition, the development of multistep, one-pot cascade reactions has become a central focus in modern green chemistry and synthetic organic methodologies.[5] By combining distinct catalytic modes within a single process, these cascades enhance substrate tolerance, reactivity, and stereoselectivity.[26] Importantly, they improve overall synthetic efficiency by increasing yields, reducing reaction times, and minimizing the need for intermediate purification.[27] In this context, to achieve multistep synthesis in a one-pot fashion, researchers in recent decades have explored the integration of biocatalysis with other catalytic disciplines such as chemocatalysis, electrocatalysis, and photocatalysis.[28] This interdisciplinary approach aims to expand the accessible chemical space and enable the synthesis of a broader range of valuable chiral compounds (**Figure 1.3**).[29] However, merging biocatalysis with other catalytic strategies in a one-pot setup presents significant challenges, primarily due to incompatibilities in optimal reaction conditions.[30] Enzymes typically require mild, aqueous, and neutral pH environments, while chemical catalysts often demand harsh conditions such as elevated temperatures, extreme pH values, or organic solvents, or electricity generally necessitate redox mediators and uncontrollable free radical species.[31] As a result, simultaneous operation of both catalytic systems within a single pot is very limited, as most successful examples rely on sequential

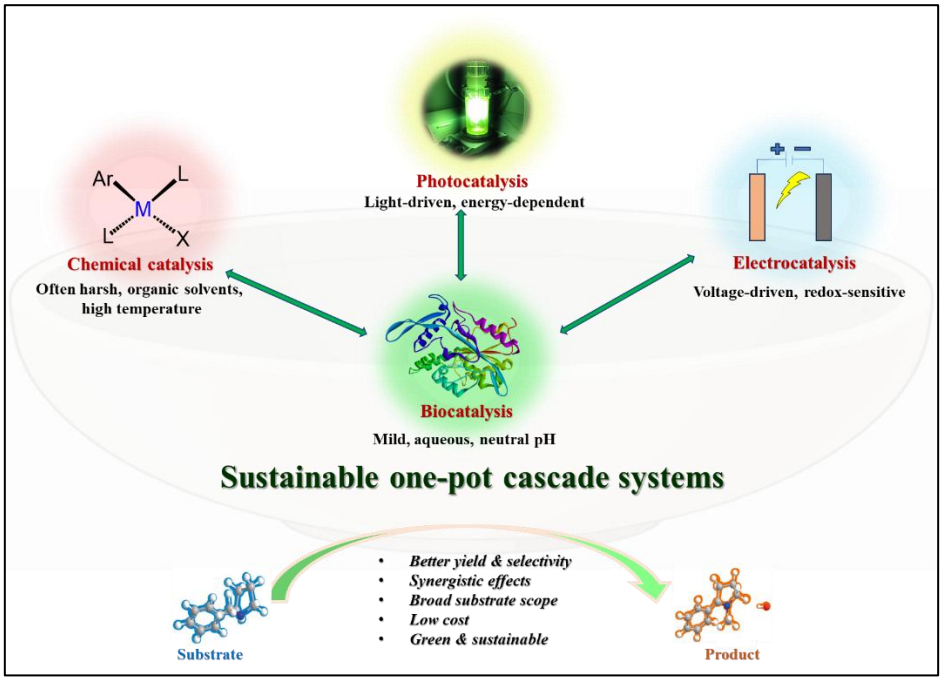

Figure 1.3: A representation of the integration of biocatalysis with chemocatalysis, photocatalysis, or electrocatalysis in a one-pot reaction system and its advantages

strategies that allow each catalyst to operate under its preferred conditions.[32]

This chapter highlights recent advancements mainly reported in the last three years in the designing and execution of hydrolase-based cascade systems in synergy with other catalytic approaches, emphasizing their potential for efficient, sustainable, and environmentally friendly synthesis of complex organic compounds.

1.2: Literature Review

1.2.1: Integration of bio- and chemical-catalysts

The integration of biocatalysis and chemical catalysis offers notable advantages, as it eliminates the need for additional efforts in setting up multicatalytic reactions. In this approach, the product of one step seamlessly serves as the reactant for the next, ultimately saving time, solvents, and costs.[33] However, certain limitations persist, such as low final product conversions and mutual deactivation of enzymes and chemical catalysts in one-pot systems. To address these challenges, chemists have increasingly adopted the metal-enzyme nanohybrid strategy in recent years.[34] In this approach, the hybrid catalysts are designed to spatially separate the chemical catalyst and the enzyme, minimizing direct contact and thereby reducing the risk of deactivating their individual catalytic activities.[35]

In this context, Deska and co-workers reported the design and synthesis of nanobiohybrids comprising gold or silver nanoparticles embedded within a protein matrix (**Scheme 1.1a**).[36] This heterogeneous catalyst, having dual activity, was prepared by incubating the CALB enzyme with the desired metal salts in aqueous solution at room temperature, followed by centrifugation and lyophilization. The dual functionality of the resulting hybrid catalysts was evaluated via a one-pot cascade synthesis of chiral 2,5-dihydrofurans from allenic acetates (**Scheme 1.1b**). In this reaction, the lipase catalyzed the hydrolytic kinetic resolution, while the metal component facilitated allene cycloisomerization. To demonstrate the applicability of the hybrid catalysts, CALB/AuNP-1 was employed for the synthesis of 2,5-dihydrofurans using tetrahydrofuran (THF) as the solvent at 40 ◦C. Intrestingly, more α-substituted allenes underwent cyclization more efficiently than α-monosubstituted allenic alcohols. The CALB/gold nanomaterial provided moderate yields of the desired products i.e. 40-48%, when using allenes containing saturated hydrocarbon chains (**Scheme 1.1c**). In contrast, allenes bearing methyl or aromatic groups in the allylic olefin moiety produced dihydrofurans more efficiently. Additionally, the formation of bisdihydrofurans through dimerization was observed with all hybrid catalysts, but it occurred more prominently with dextran-based polymer-modified CALB/AuNP-2 (**Scheme 1.1d**). The utility and versatility of this catalytic system

were further demonstrated through the synthesis of stereoselective multicyclic structures with excellent enantiopurity (**Scheme 1.1e**).

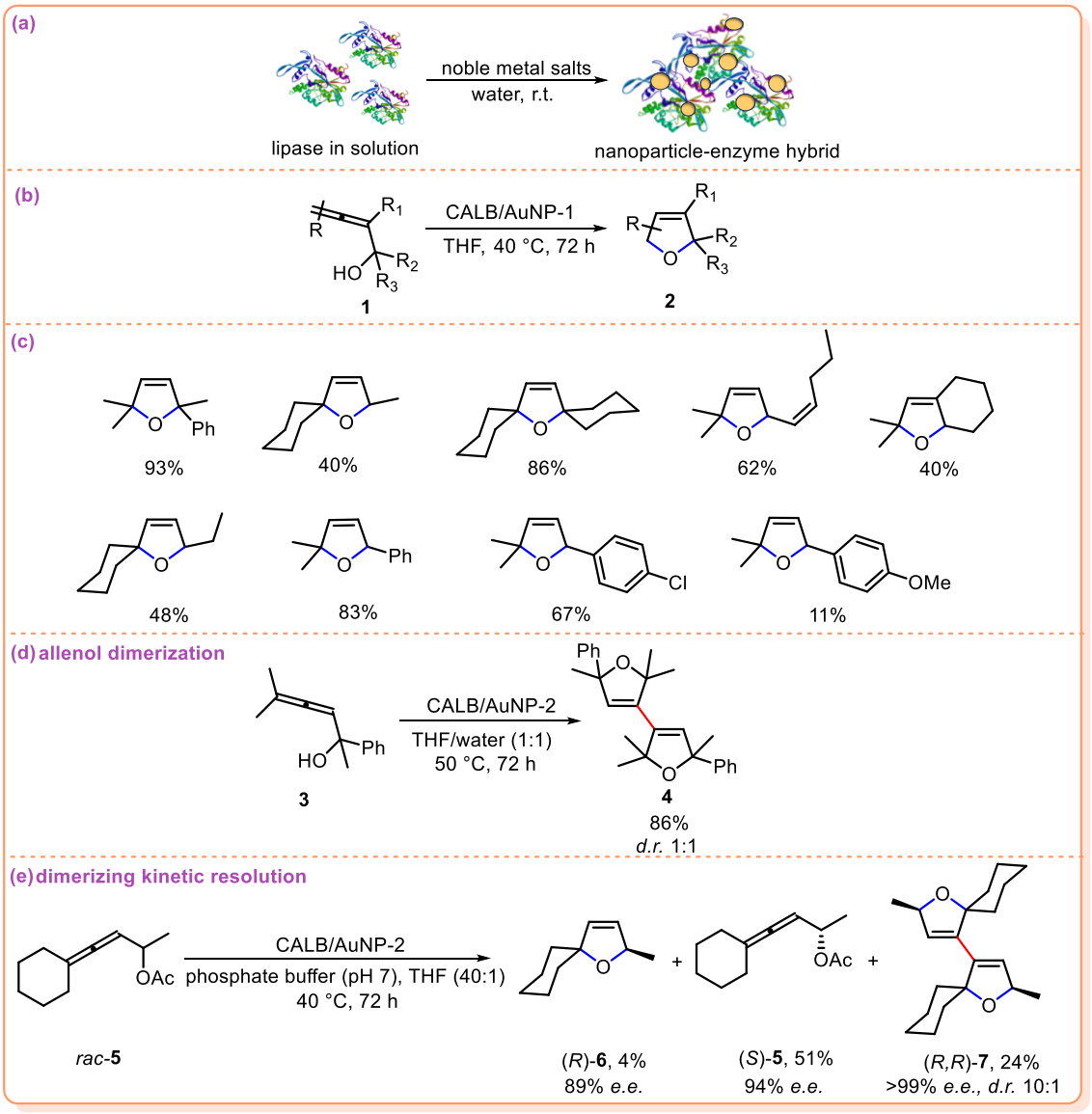

Scheme 1.1: CALB/gold nanobiohybrid catalyzed synthesis of various 2,5-dihydrofurans

Similarly, Palomo and co-workers devised the synthesis of nanohybrids composed of gold (Au) or silver (Ag) nanoparticles integrated with the lipase enzyme (**Table 1.2**).[37] The formation of these metallic nanohybrids is highly influenced by the choice of protein, bioconjugate, and pH. When lipase was modified with a bioconjugate-specifically dextran-aspartic acid polymer (Dext6kDa) and used in the synthesis of Au or Ag nanohybrids, smaller metal nanoparticles were observed. These nanobiohybrids exhibited dual catalytic activity, enabling the synthesis of enantiopure oxygen containing-heterocycles through a cascade reaction involving lipase-catalyzed and metal-catalyzed cycloisomerization of allenic acetates. Among the catalysts, Ag-

based nanobiohybrids generated the (*R*)-2,5-dihydrofuran product with good enantioselectivity, though only moderate conversion. In contrast, the AuNPs-CALB-pH4.5 catalyst produced the desired cyclized product with excellent enantioselectivity in nearly half the time compared to the AgNPs-CALB catalyst, while maintaining a similar conversion rate. The lower conversion observed with AgNPs-CALB-Dext6kDa was attributed to a side reaction, as a significant amount of unreacted allenic acetate was recovered with 99% enantiomeric excess (*e.e.*) (**Table 1.2**).

Table 1.2: Screening of metallic nanohybrids towards cycloisomerization of allenic acetates

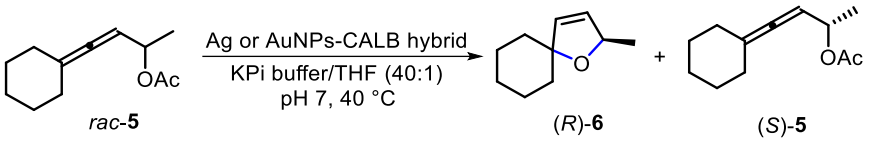

rac-**5** (*R*)-**6** (*S*)-**5**

Entry	Catalyst	Time (d)	Conversion (%)	(*R*) *e.e.* (%)	(*S*) *e.e.* (%)
1	AgNPs-CALB	4	26	88	88
2	AgNPs-CALB-Dext6kDa	3	43	94	94
3	AgNPs-CALB-Dext2000kDa	3	42	95	84
4	AuNPs-CALB-pH4.5	2	21	93	64
5	AuNPs-CALB-Dext6kDa	3	2	93	99

Next, Singhania et al. reported a novel enzymatic protocol employing a commercially available lipase, Palatase 20000L, in combination with the surfactant TPGS-750-M (DL-α-tocopherol methoxypolyethylene glycol succinate) to catalyse esterification reactions in water without the need for any cofactors.[38] This biocatalytic process was integrated into a one-pot which consist a lipase-catalyzed esterification to produce an intermediate (**10**), followed by subsequent palladium-catalyzed cross-coupling reaction to afford the final product (**12**) in 82% yield (**Scheme 1.2a**). Notably, the produced ester (**12**) was proposed to localize within the lipophilic core of micelles rather than the aqueous phase. This hypothesis was supported by observations made when the pH was increased during the coupling step through the addition of a base. The protocol was further extended to mixed-catalysis sequences. In one example, cinnamic acid (**13**) was first catalytically hydrogenated to produce an intermediate acid (**14**), which then underwent esterification with an alcohol (**15**) to generate a gem-dibromocyclopropane (**16**). This intermediate was subsequently reduced using nickel to yield the final product (**17**) in 65%

isolated yield. Overall, this one-pot lipase-catalyzed protocol demonstrates significant potential as an environmentally friendly approach for tandem catalysis in aqueous media (**Scheme 1.2b**).

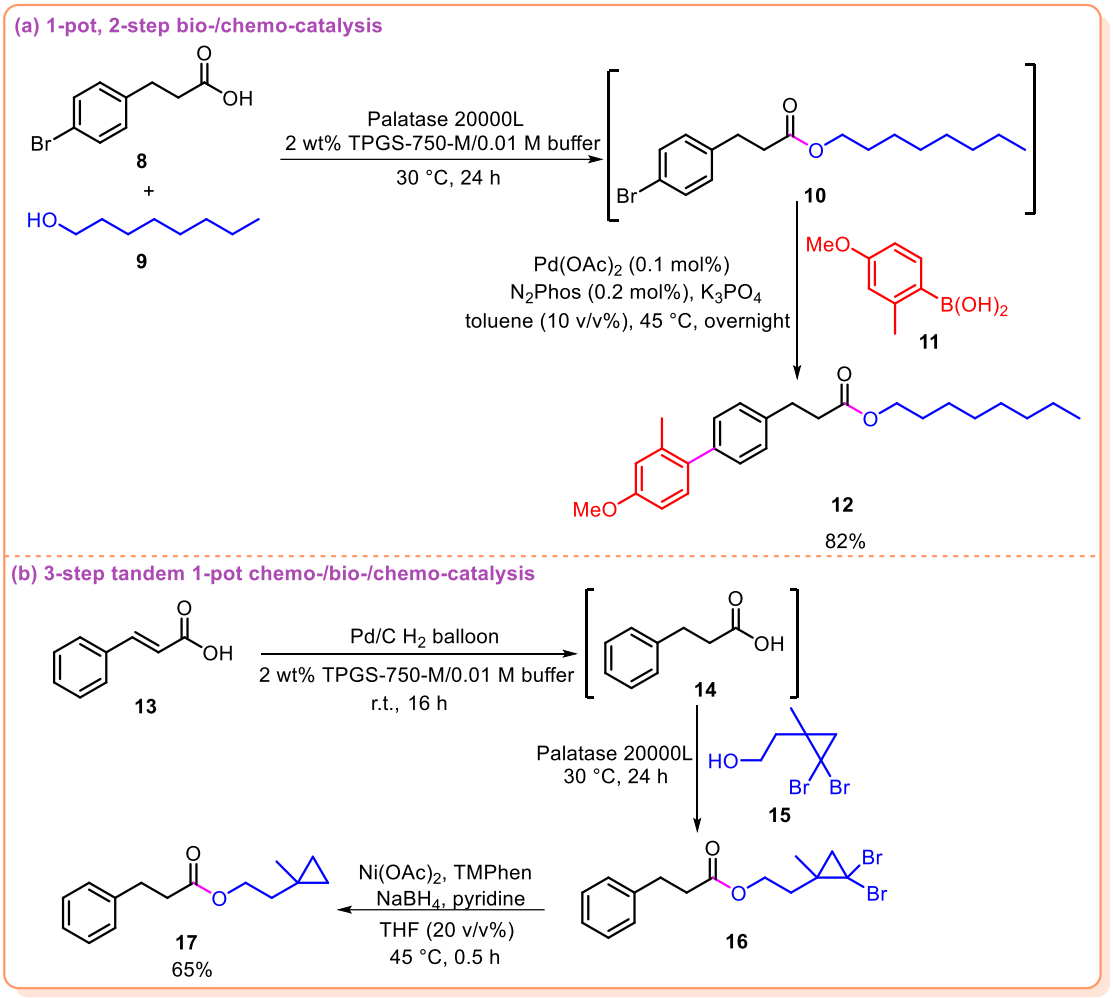

Scheme 1.2: Lipase-catalyzed esterification combined with metal-catalyzed reactions in a one-pot

A one-pot amide bond synthesis involving nitrile hydratase from *E. coli* CGA009, which catalyzed the hydration of nitriles, followed by a copper-catalyzed N-arylation reaction was reported by Micklefield and co-workers (**Scheme 1.3a**).[39] This integrated protocol demonstrated broad substrate scope and excellent functional group tolerance. Various ortho-, meta-, and para-substituted iodoarenes were well tolerated, yielding the desired amides in good yields (**Scheme 1.3b**). Additionally, iodinated heterocycles were smoothly converted to the target products with high efficiency. The versatility of this method was further illustrated using nitriles bearing diverse substituents at the ortho, meta, and para positions, and various heterocyclic nitriles were effectively transformed using the *E. coli* CGA009 enzyme, giving excellent yields of the corresponding amides (**Scheme 1.3b**). The practical utility of this chemoenzymatic strategy was highlighted by the successful synthesis of a sodium channel

inhibitor, suggesting its potential for the preparation of other pharmaceutical intermediates (**Scheme 1.3b**). Notably, nitrile hydratase (AJ270) also enabled asymmetric synthesis of amides within this integrated approach, affording ether-functionalized chiral amides in good

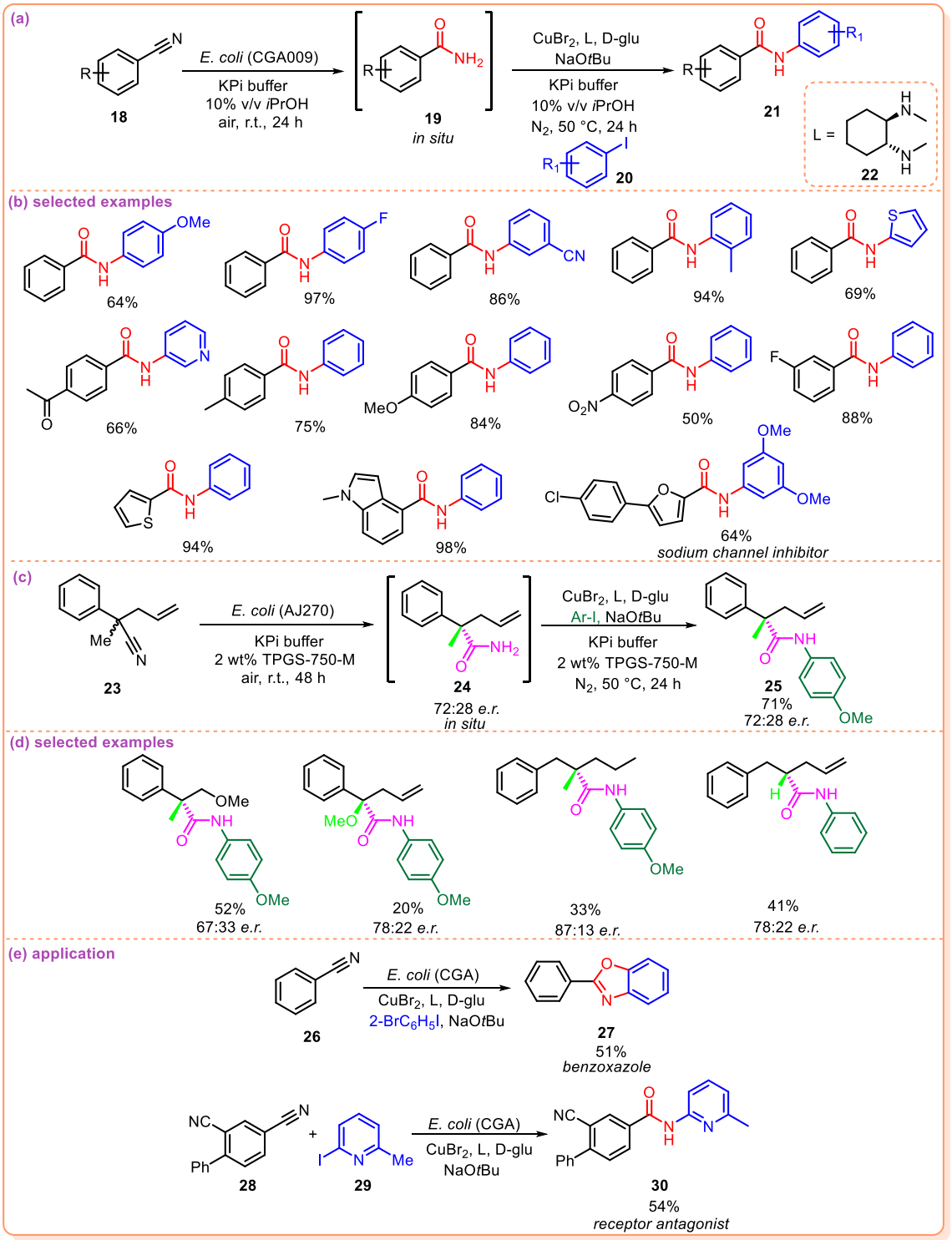

Scheme 1.3: One-pot amide bond synthesis via *E. coli* CGA009-derived nitrile hydratase-catalyzed hydration followed by copper-catalyzed N-arylation.

yields and with favorable diastereomeric ratios (**Scheme 1.3c**). Furthermore, allyl- and propyl-substituted amides were synthesized with good yields and selectivity (**Scheme 1.3d**). The synthetic utility of the method was also demonstrated by the preparation of heterocyclic scaffolds and extended to the synthesis of a drug target (**30**) in 54% overall yield, significantly improving upon a previously reported six-step linear route that gave much lower yield (**Scheme 1.3e**).

In 2022, Jiang and co-workers disclosed the synthesis of a multifunctional nanocatalyst through the co-immobilization of metal nanoparticles and enzymes onto the pores and surface of a stable covalent organic framework (COF) (**Scheme 1.4a**).[40] The COF was prepared via a solvothermal method using triazinyl (Tz) and 2,5-dihydroxyterephthaldehyde (Da) as building blocks. The nitrogen-rich structure of Tz enabled the in-situ reduction and uniform dispersion

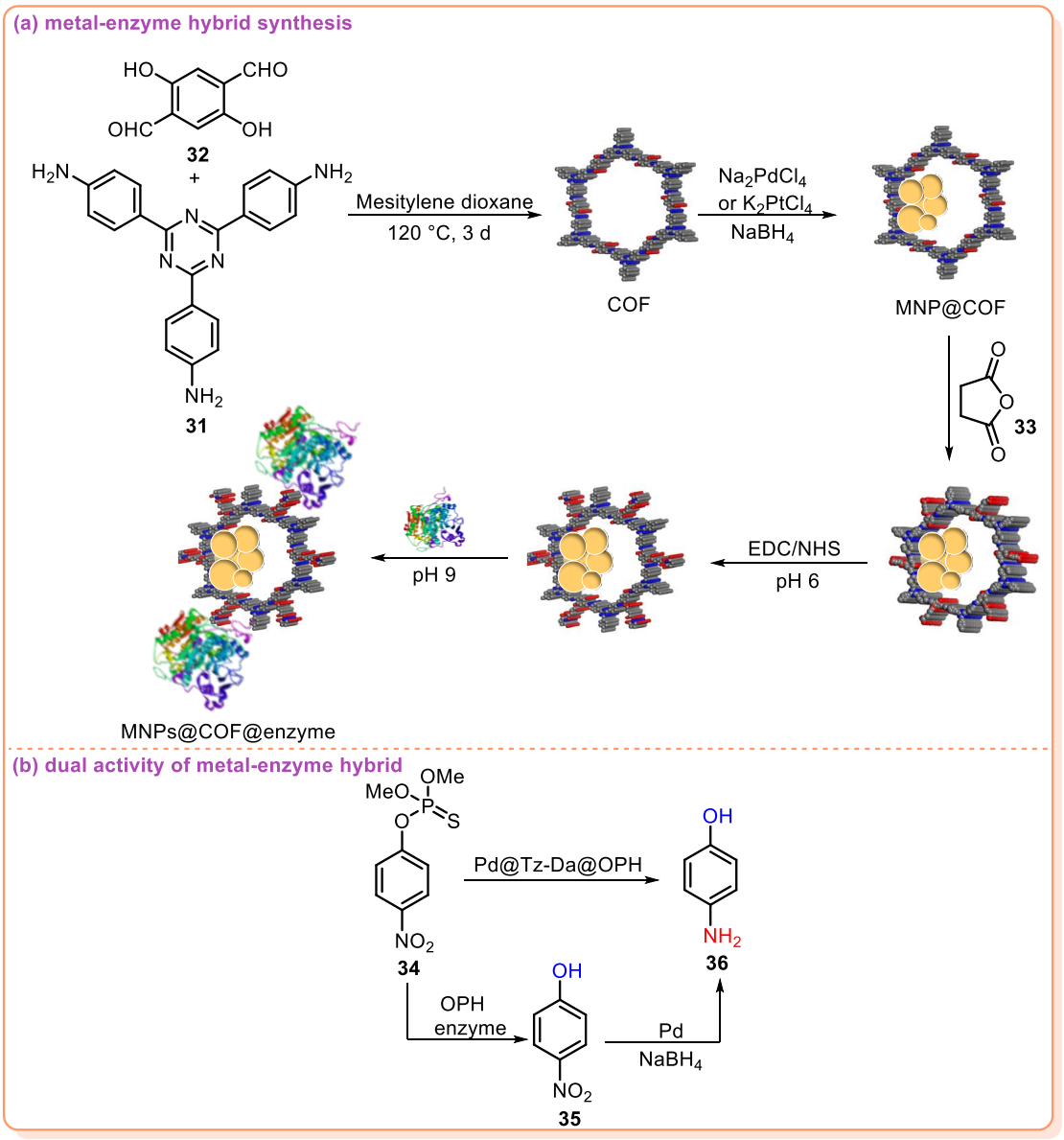

Scheme 1.4: Synthesis of multifunctional Pd@Tz-Da@OPH nanocatalyst and its application

of palladium (Pd) nanoparticles within the COF through the double solvent method, facilitated by strong electronic interactions between nitrogen atoms and Pd. The hydroxyl groups on Da were further functionalized to carboxyl groups using succinic anhydride (SA), allowing for the covalent immobilization of organophosphorus hydrolase (OPH) via EDC/NHS coupling chemistry. The resulting integrated nanocatalyst, Pd@Tz-Da@OPH, exhibited excellent catalytic performance in the degradation of the toxic organophosphate nerve agent methyl parathion. In this cascade reaction, the OPH enzyme first hydrolyzed methyl parathion (**34**) to 4-nitrophenol (**35**), a still-toxic intermediate that is challenging to degrade. Subsequently, the Pd nanoparticles further reduced 4-nitrophenol to the less harmful compound 4-aminophenol (**36**) in the presence of $NaBH_4$. The overall reaction rate was primarily governed by the enzymatic hydrolysis step (**Scheme 1.4b**). This recyclable and stable nanocatalyst demonstrates high versatility and holds significant promise for future applications in environmental remediation.

Further, the synthesis of a nanobiohybrid catalyst composed of glucose oxidase (GOx) and glucoamylase (GA) immobilized onto mesoporous silica nanoparticles (SiO_2) was demonstrated by Sun and colleagues.[41] The presence of both enzymes on the catalyst surface was essential for the efficient production of gluconic acid from starch, as they enable the timely removal of hydrogen peroxide (H_2O_2) and glucose. This synergy was further confirmed through experiments using various catalyst combinations, as detailed in the accompanying **Table 1.3**. In the first three systems, where enzymes were absent on the surface of Au@SiO_2 particles, efficient starch consumption was observed, but gluconic acid formation remained limited. However, when both GA and GOx were co-immobilized onto Au@SiO_2 particles (GA&GOx@Au-SiO_2), there was a significant increase in gluconic acid yield along with improved starch degradation. This system outperformed previously reported enzyme immobilization methods, such as those using graphene as a support. Additionally, varying the GA/GOx ratio influenced the overall reaction yield. Increasing the amount of glucoamylase enhanced starch degradation and glucose generation, thereby improving the efficiency of the entire chemoenzymatic process. Notably, the catalyst exhibited excellent recyclability, maintaining its catalytic activity for up to 10 cycles, making it a promising candidate for the industrial-scale production of gluconic acid.

In 2023, Ge and colleagues reported the synthesis of a hybrid catalyst by immobilizing a Pd-Cu nanoalloy onto cross-linked enzyme aggregates (CLEAs) of *Candida antarctica lipase* B

Table 1.3: Examination of different nanobiohybrids for the production of gluconic acid from starch

Catalytic systems	GA (μg mL^{-1})	GOx (μg mL^{-1})	Au-SiO_2; (mg mL^{-1})	Starch consumption efficiency (%)	Yield of gluconic acid (%)
GA+ GOx	31.1	21.6	0	99.7	60.8
GA+ GOx + Au-SiO_2	31.1	21.6	1.8	99.3	74.9
GA&GOx@SiO_2 + Au-SiO_2	26.6	18.4	1.8	73.6	63.6
GA&GOx@Au-SiO_2 (GA/GOx = 1/1.48)	22.5	33.3	1.8	93.6	93.0
GA&GOx@Au-SiO_2 (GA/GOx = 1.06/1)	29.1	27.5	1.8	96.4	93.8
GA&GOx@Au-SiO_2 (GA/GOx = 1.44/1)	31.1	21.6	1.8	98.7	97.8

(CALB).[42] The incorporation of copper alongside palladium in the nanoalloy was intended to enhance the hybrid catalyst's performance in chemoenzymatic reactions (**Scheme 1.5**). This improvement was attributed to a synergistic effect between the two metals, which significantly boosted the catalytic activity. The resulting hybrid catalyst demonstrated excellent efficiency in Sonogashira coupling reactions, yielding the desired products in high amounts. In this cascade process, the CALB enzyme catalyzed the selective acylation of the ®-enantiomer of an amine, while the Pd-Cu nanoclusters facilitated both the Sonogashira coupling and the racemization of the (*S*)-enantiomer. Overall, the Pd-Cu/CALB CLEAs exhibited remarkable dual functionality, showing high enzymatic as well as metallic catalytic activity in the cascade reaction.

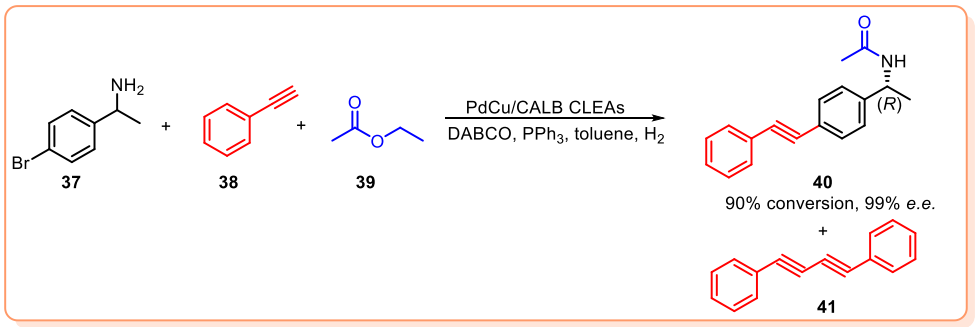

Scheme 1.5: Pd-Cu/CALB CLEAs-catalyzed one-pot selective acylation and Sonogashira coupling reaction

Next, same group designed a hybrid catalyst by anchoring palladium (Pd) single atoms onto the lipase enzyme (CALB), resulting in the formation of Pd/CALB-P (**Scheme 1.6a**).[43] The catalytic activity of this system was first assessed through the Sonogashira coupling of aryl halides with alkynes, where it demonstrated superior efficiency compared to traditional homogeneous Pd-catalysts. Further investigation of its substrate scope revealed broad compatibility, accommodating both electron-donating and electron-withdrawing groups. The hybrid catalyst was employed in a one-pot chemoenzymatic reaction integrating lipase-catalyzed hydrolysis and Pd-catalyzed C–C coupling, efficiently producing a chiral biphenyl alcohol at 30 °C with moderate yield and excellent enantioselectivity (**Scheme 1.6b**).

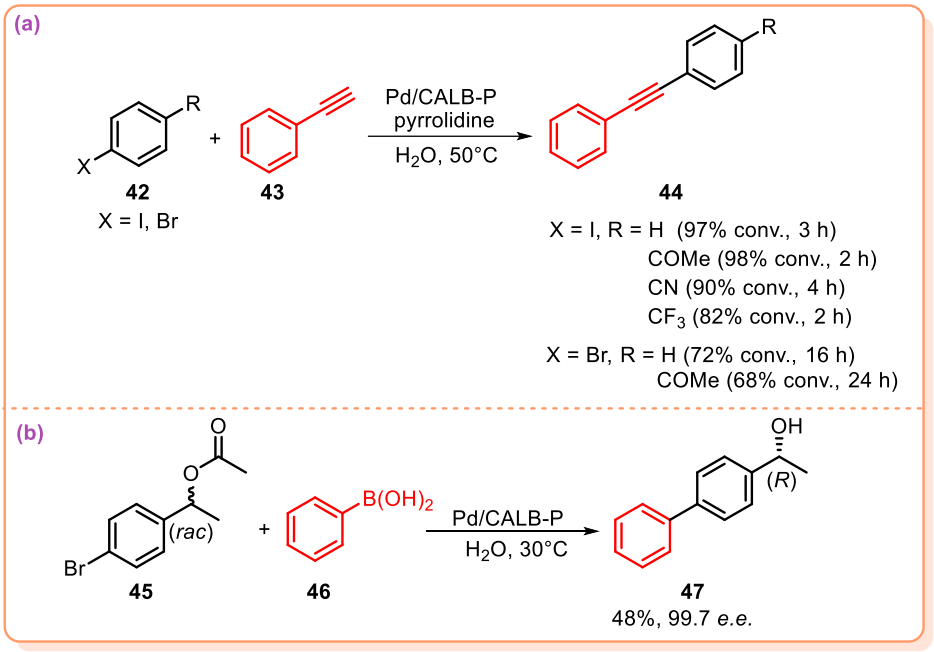

Scheme 1.6: Application of Pd/CALB-P integrated catalyst towards lipase-catalyzed hydrolysis and Pd-catalyzed C–C coupling reaction

Our group has recently developed a nanobiohybrid catalyst by integrating palladium (Pd) metal and the CALB enzyme within a silica matrix, resulting in the formation of Pd(0)-CALB@SiO_2 (**Scheme 1.7a**).[44] This catalyst was employed in a two-step, one-pot chemoenzymatic reaction sequence involving a CALB-catalyzed Groebke-Blackburn-Bienayme (GBB) multicomponent reaction, followed by a Pd-catalyzed Suzuki-Miyaura coupling. The substrate scope was explored by varying substituents on the phenylboronic acids, successfully yielding a series of imidazo[1,2-a]pyridine derivatives in good to excellent yields (**Scheme 1.7b**). The practical applicability of the catalyst was demonstrated through a gram-scale reaction, and the hybrid system proved reusable for up to five cycles. Although a slight decrease in isolated yield was observed after the second cycle, the catalyst retained considerable activity across multiple runs.

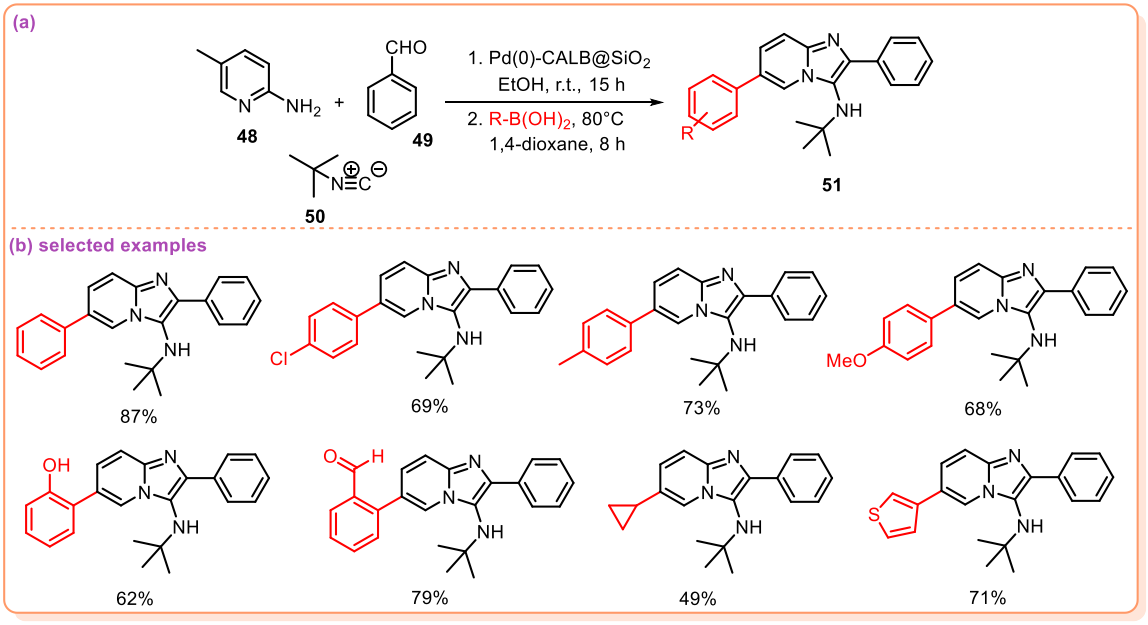

Scheme 1.7: Construction of Pd(0)-CALB@SiO_2 nanocatalyst and its application in the synthesis of imidazo[1,2-a]pyridine derivatives

In 2023, Yang et al. constructed a multicompartmental metal-organic framework (MOF) microreactor using the Pickering double emulsion methodology.[45] This approach leverages multiple liquid-liquid interfaces to guide the controlled growth of dense MOF layers, resulting in microreactors with tailored internal architectures and selective permeability (**Scheme 1.8**). Two distinct catalytic entities-hydrophilic CALB enzyme and hydrophobic Grubb's catalyst-were successfully co-encapsulated within a single microreactor. The catalytic performance was evaluated through a cascade reaction involving Grubb's catalyst-mediated ring-closing metathesis of 1,6-heptadien-4-ol (**52**), followed by CALB-catalyzed transesterification to produce 3-cyclopentenyl acetate (**55**). The resulting MOF microreactor demonstrated a 2-5 fold

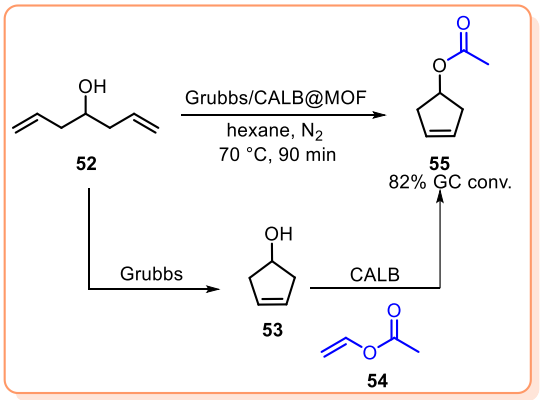

Scheme 1.8: Synthesis of 3-cyclopentenyl acetate from constructed microreactor containing Grubbs catalyst and CALB enzyme

enhancement in catalytic activity compared to individual catalysts, attributed to controlled mutual deactivation and improved substrate channelling.

A simple multistep one-pot platform that integrates chemo- and biocatalysis using nanoparticle-based catalysts was developed by Wu and group members.[46] These catalysts were synthesized in two steps: first, chiral ligand monomers were polymerized onto silica nanoparticles via atom transfer radical polymerization (ATRP); second, the resulting particles were coordinated with $[RuCl_2(p\text{-cymene})]_2$ to form the final catalysts. They efficiently catalyzed the asymmetric transfer hydrogenation of acetophenone (**56**) to 1-phenylethanol (**57**) in water, achieving up to 99% conversion and 93% enantiomeric excess (**Scheme 1.9**). Additionally, the nanoparticles served as emulsifiers to form stable Pickering emulsions. Incorporation of CALB enabled a second-step enantioselective acylation with vinyl butyrate (**58**), reaching up to 38% conversion and 99% *e.e*. This strategy demonstrates a versatile and effective approach for sequential chemoenzymatic cascades in aqueous and emulsion systems.

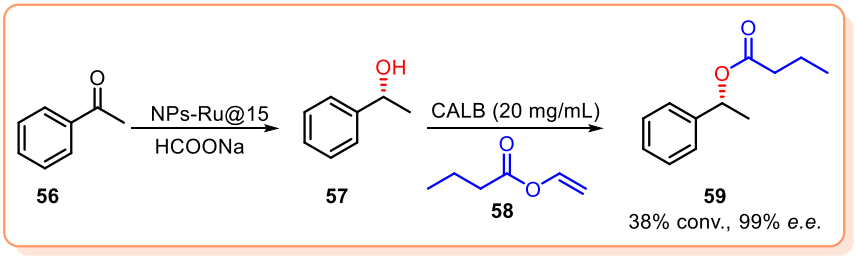

Scheme 1.9: Sequential chemoenzymatic cascade asymmetric synthesis of ®-1-phenylethyl butyrate in water

Also, we have developed a one-pot synthesis for substituted indole derivatives and amino-substituted biaryls in good yields using α-amylase and a Pd-catalyst (**Scheme 1.10a**).[47] Initially, we synthesized indole derivatives via an α-amylase-mediated aza-Michael addition, followed by a transition-metal-catalyzed isocyanide insertion reaction. The substrate scope was then expanded by employing various bromoanilines and isocyanides (**Scheme 1.10b**). It was observed that electronic effects of the substituents had minimal impact on the yields of the desired products. However, when cyclohexyl isocyanide was used, a slight decrease in yield was noted. Encouraged by these results, we extended our methodology to a one-pot sequence combining the enzyme-mediated aza-Michael addition and a metal-catalyzed Suzuki–Miyaura coupling reaction (**Scheme 1.10c**). Under the same optimized conditions, the substrate scope was evaluated using different substituted boronic acids and bromoanilines. In all cases, good yields of the desired amino-substituted biaryl products were obtained (**Scheme 1.10d**).

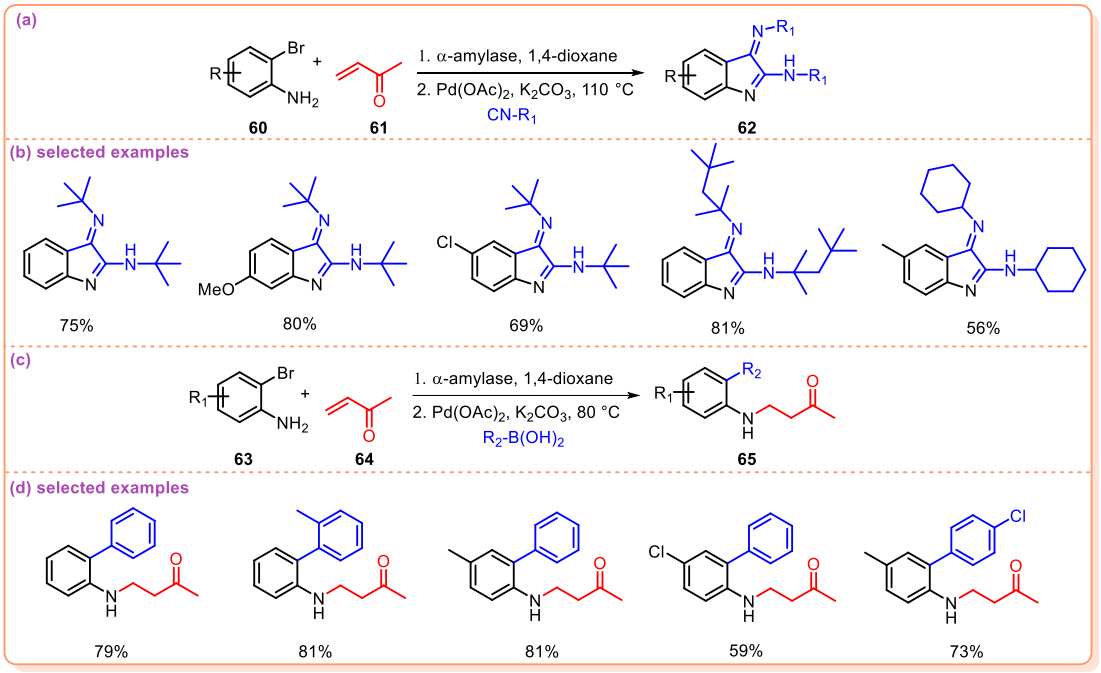

Scheme 1.10: One-pot synthesis and substrate-controlled diversification of β-aminocarbonyl compounds

Recently, Jiang and co-workers reported an innovative strategy for constructing a magnetic wrinkled organosilica (MWOS) core–shell catalyst by co-immobilizing palladium (Pd) nanoparticles and lipase (CALB) within the porous structure of MWOS.[48] This metal-enzyme hybrid catalyst was evaluated for its performance in the dynamic kinetic resolution (DKR) of

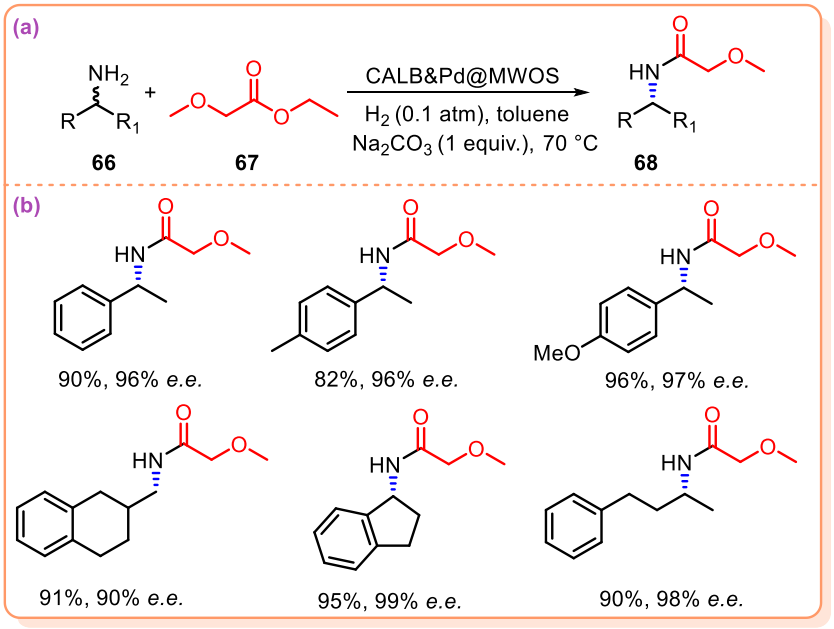

Scheme 1.11: Synthesis of chiral amides from core–shell nanocatalyst CALB&Pd@MWOS

chiral primary amines (**Scheme 1.11a**). Owing to the close proximity of the two catalytic components within the MWOS framework, the integrated catalyst exhibited significantly enhanced reactivity compared to the individual Pd@MWOS and CALB@MWOS systems. The hybrid catalyst demonstrated excellent recyclability, retaining high activity and selectivity over five consecutive cycles. Furthermore, it exhibited a broad substrate scope, producing chiral amides from various primary amines with yields of up to 96% along with enantiomeric excess (*e.e.*) of up to 99% (**Scheme 1.11b**). Notably, the overall catalytic performance, particularly the selectivity and activity, was strongly influenced by the efficiency of the racemization step.

Last year, Rudroff and his team reported a multistep, one-pot cascade synthesis of aldehydes containing flavor and fragrance properties.[49] The process begins with the conversion of phenylpropenes to phenylacetones via Wacker oxidation. This step employs a catalytic system comprising palladium (II) trifluoroacetate [$Pd(TFA)_2$] and sodium trifluoroacetate (NaTFA), with iron(III) chloride ($FeCl_3$) serving as the terminal oxidant. Subsequently, the resulting phenylacetones undergo Baeyer–Villiger oxidation catalyzed by phenylacetone monooxygenase from *Thermobifida fusca*, yielding the corresponding acetate esters. These esters are then hydrolyzed by esterase from *Pseudomonas fluorescens* to form aromatic alcohols. In the final step, enzymatic oxidation using alcohol dehydrogenase converts the alcohols into aldehydes. This four-step cascade reaction successfully produced eight different aldehydes in moderate to good yields (**Table 1.4**). The authors highlighted the green chemistry aspect of their approach, emphasizing the use of Fe(III) as a benign terminal oxidant for the Pd-catalyzed Wacker oxidation. This is in contrast to conventional methods that rely on copper salts, which are considered hazardous.

Table 1.4: Multistep, one-pot cascade synthesis of flavor and fragrance containing aldehydes

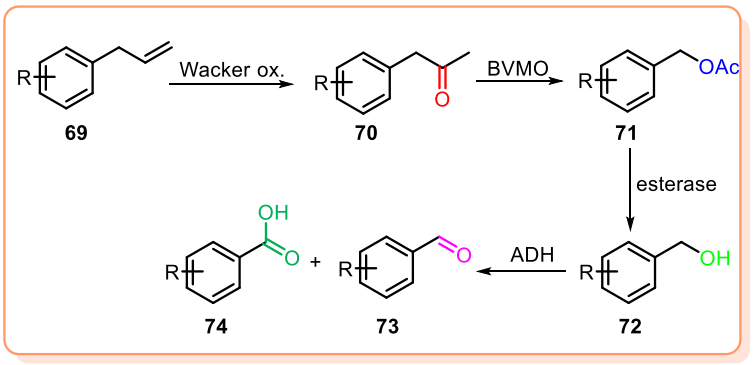

Entry	R	Yield of enzymatic cascade, t = 24 h	Ratio of aldehyde/acid
1	H	53 ± 11%	2.7/1
2	3-CH_3	61 ± 22%	2.9/1
3	4-CH_3	86 ± 11%	6.2/1
4	4-OCH_3	62 ± 19%	11.1/1
5	1,2-OCH_3	58 ± 7%	16.6/1
6	1,2-CH_2-OCH_2	89 ± 7%	14.2/1
7	1-OH, 2-OCH_3	20 ± 10%	500/1
8	1-OAc, 2-OCH_3	16 ± 4%	-

1.2.2: A combind electro-biocatalysis approches

The integration of electrosynthesis with biocatalysis opens new avenues in organic synthesis.[50] However, enzymes often exhibit a limited substrate scope, and achieving stereoselective synthesis under electrochemical conditions can be challenging due to the high reactivity of free radicals.[51,12a] By carefully optimizing the reaction parameters, the synergy between both catalytic systems can be harnessed to produce the desired compounds efficiently.[52]

Guan and colleagues introduced an innovative strategy that integrates organic electrosynthesis with the non-natural catalytic function of wheat germ lipase (WGL) (**Scheme 1.12a**).[53] They demonstrated the effectiveness of this method by successfully synthesizing a range of

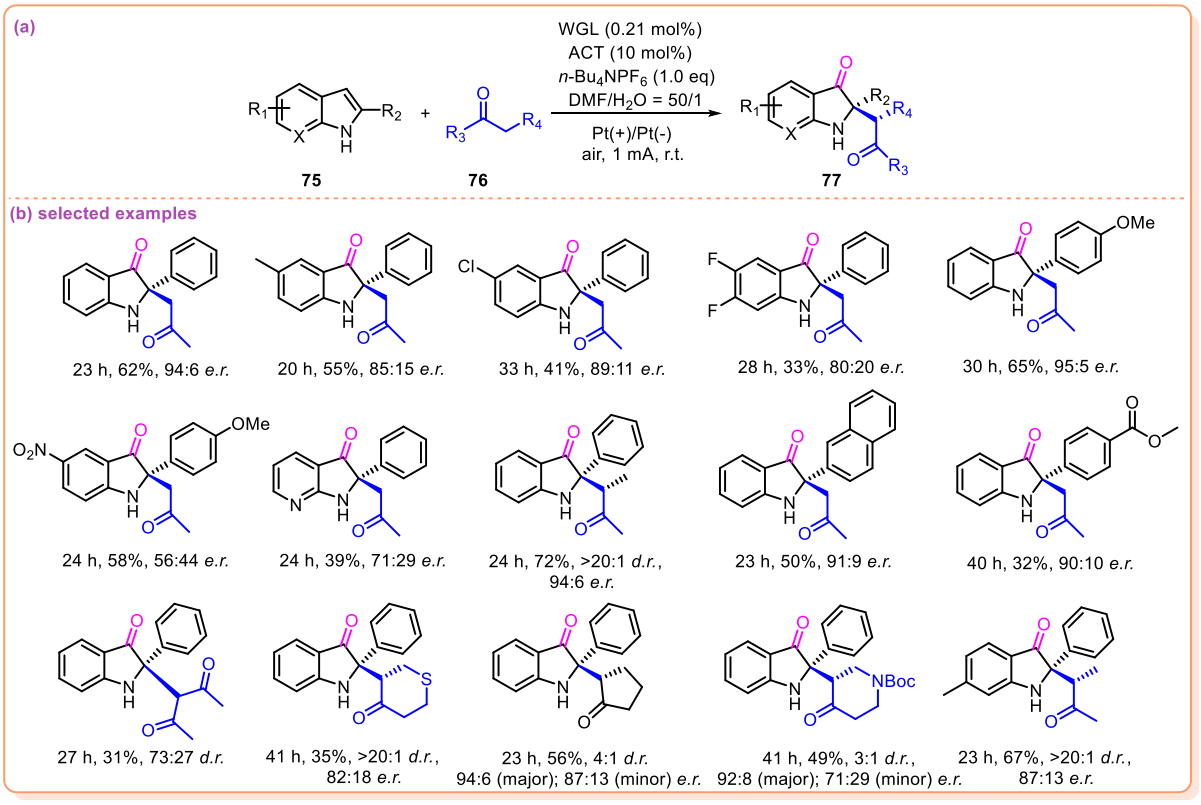

Scheme 1.12: Bioelectrosynthesis of various asymmetric 2,2-disubstituted 3-carbonyl indoles

asymmetric 2,2-disubstituted 3-carbonyl indoles from 2-substituted indoles and various ketones. The introduction of a redox mediator, 4-acetamido-2,2,6,6-tetramethyl-1-piperidinyloxy (ACT), significantly enhanced the oxidation process by operating at lower potentials, thereby minimizing the formation of undesired by-products. This combined catalytic approach proceeds efficiently under mild conditions and delivers products in notable yields. Indole derivatives bearing both electron-donating and electron-withdrawing substituents on the indole core showed good reactivity with acetone (**Scheme 1.12b**). Among the 2-phenylindoles, those with electron-donating groups at the phenyl position produced higher yields compared to their electron-withdrawing counterparts. Furthermore, the reaction was shown to be compatible with a variety of ketones, including cyclic, acyclic, and heterocyclic types. Importantly, this groundbreaking work offers the first demonstration of the compatibility between hydrolase catalysis and organic electrochemical synthesis.

Building on this strategy, our group has recently reported a novel one-pot protocol that merges electrosynthesis with the non-natural catalytic activity of lipase.[54] In this system, CALB facilitates the regioselective C-3 alkylation of indoles, followed by electrochemical C-2 oxidation within the same reaction vessel (**Scheme 1.13a**). This bio-electro-synthetic approach demonstrated its versatility with indole derivatives bearing electron-donating groups, yielding the desired products in moderate to good isolated yields (**Scheme 1.13b**). However, no product formation was observed when indoles containing electron-withdrawing substituents were used. To validate the essential roles of both the enzyme and the electric current, a series of control experiments were performed, confirming that both components are critical for the successful formation of 3-alkylated oxindoles in this integrated one-pot system.

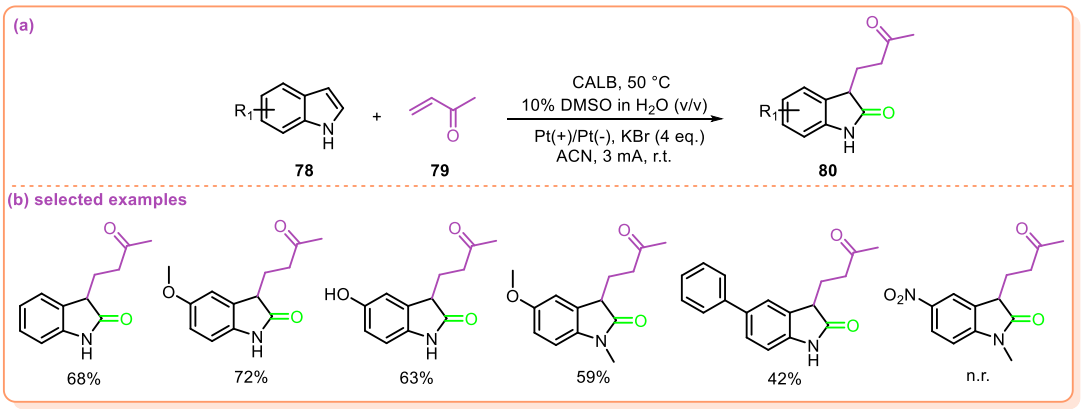

Scheme 1.13: Synthesis of various 3-alkylated oxindoles via an integrated biocatalysis and electrochemical approach

1.2.3: One-pot integration of Bio- and Photo-catalysis

Photocatalysis and biocatalysis have both attracted significant attention in organic synthesis due to their remarkable features, including flexibility, selectivity, atom economy, and strong potential for reaction optimization.[55] Biocatalysis enables the production of highly selective products under mild reaction conditions, while photocatalysis utilizes visible light as an energy source to access a broad range of reactivities.[56] Combining biocatalysis with photocatalysis expands the scope of biocatalytic transformations, offering a sustainable approach for the synthesis of high-value compounds.[57]

In 2022, Zhu and colleagues reported a combinative approach integrating photocatalysis and biocatalysis for the efficient one-pot synthesis of 3-aminoalkyl chromones (**Scheme 1.14a**).[58] This method employed photoredox catalysis in tandem with enzymatic catalysis, using *o*-hydroxyaryl enaminones and *N*-aryl glycine esters as starting materials. Methylene blue (MB^+) was identified as the optimal photocatalyst, while CALB was chosen as the biocatalyst. The reaction was carried out in acetonitrile under 18 W blue LED irradiation at room temperature.

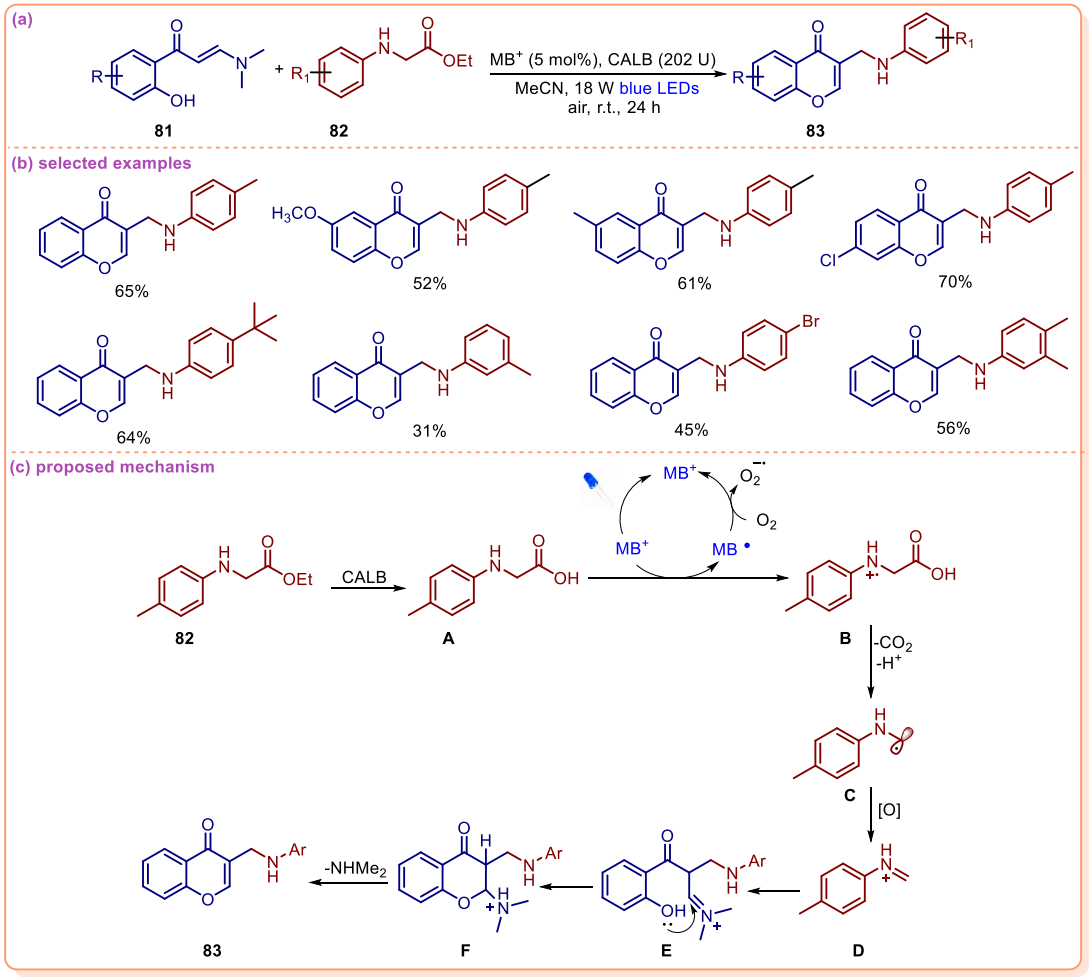

Scheme 1.14: Photobiocatalytic one-pot synthesis of various 3-aminoalkyl chromones

Under these mild conditions, various substituted chromones were synthesized with good yields (**Scheme 1.14b**). Good product yields were obtained when *N*-aryl glycine ethyl ester was reacted with enaminones bearing electron-donating groups or halo substituents. Additionally, the substrate scope was further explored by varying the *N*-aryl glycine esters. It was observed that esters bearing electron-donating groups performed well, while the presence of a methyl group at the *meta*-position led to reduced yields. Based on previous literature and control experiments, the authors proposed a plausible mechanism for this photobiocatalytic transformation. Initially, enzymatic hydrolysis of the *N*-aryl glycine ester by CALB generates the corresponding *N*-aryl glycine (**A**) (**Scheme 1.14c**). Under blue light irradiation, MB^+ mediates a single-electron transfer (SET) process, leading to the formation of a radical cation intermediate (**B**), which undergoes deprotonation and decarboxylation to yield an aminoalkyl radical (**C**). Oxidation of the resulting radical intermediate (**C**) produces an imine intermediate (**D**), which reacts with the enaminone to form an iminium species (**E**). Intramolecular nucleophilic cyclization followed by the elimination of dimethylamine affords the desired 3-aminoalkyl chromone product (**85**).

Jin et al. established a robust photoenzymatic platform by immobilizing wheat germ lipase (WGL) onto mesoporous porphyrin-based covalent organic frameworks (COFs) for asymmetric catalysis (**Scheme 1.15a**).[59] The resulting hybrid photobiocatalysts, referred to as WGL@NKCOF-118(M) (where M = H, Ni, Cu, or Zn), were thoroughly characterized, confirming the successful integration of the enzyme into the photocatalytic COF matrix. These hybrid catalysts were evaluated using asymmetric Mannich reactions as a model to assess their catalytic performance. A notable feature of this system is the close spatial proximity between the photocatalyst and the enzyme's active site, which significantly enhances the selectivity and efficiency of radical-mediated transformations. This proximity effect facilitates precise substrate binding and localized radical generation within the same catalytic microenvironment. Remarkably, this synergistic system enabled the enantioselective formation of $C(sp^3)$–$C(sp^3)$ bonds-reactions that cannot be accomplished by WGL or COFs alone. Mechanistic studies, supported by a range of analytical techniques, revealed that singlet oxygen plays a key role in mediating the observed asymmetric catalysis. Furthermore, the substrate scope was explored using various 2-phenylindole derivatives (**Scheme 1.15b**). It was observed that substrates bearing electron-donating groups on the indole core afforded higher yields, likely due to their ability to better stabilize cationic intermediates. Overall, the WGL@COF composites

demonstrated excellent enzymatic activity, operational stability, and high reusability under visible light irradiation.

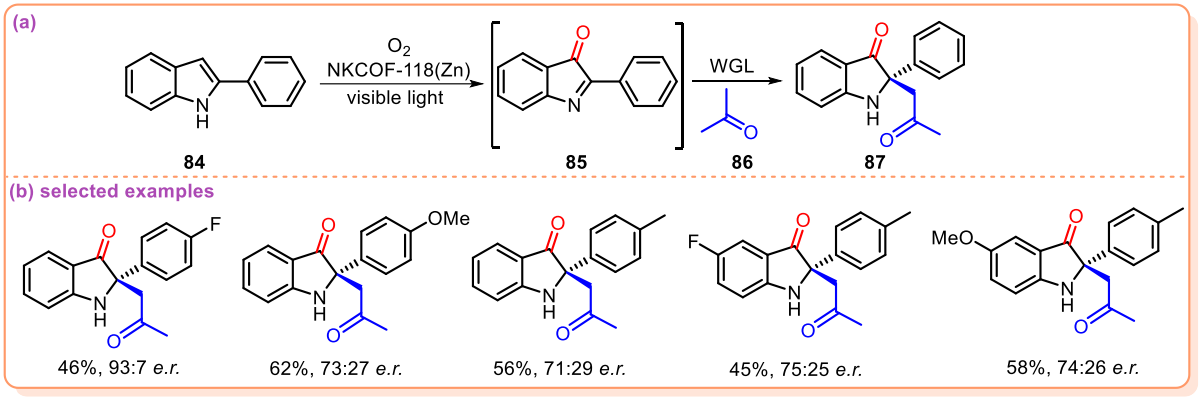

Scheme 1.15: One-pot photobiocatalytic C–C bond formation using wheat germ lipase and a COF matrix

Yu and co-workers devised a hybrid photocatalytic–biocatalytic strategy for the efficient synthesis of diverse C-3 acylated indole derivatives, delivering products in good to excellent yields (**Scheme 1.16a**).[60] The synthetic sequence begins with the introduction of an aminomethyl group onto the indole ring via a multicomponent Mannich reaction involving amines, aldehydes, and indoles. This Mannich product then undergoes photocatalytic

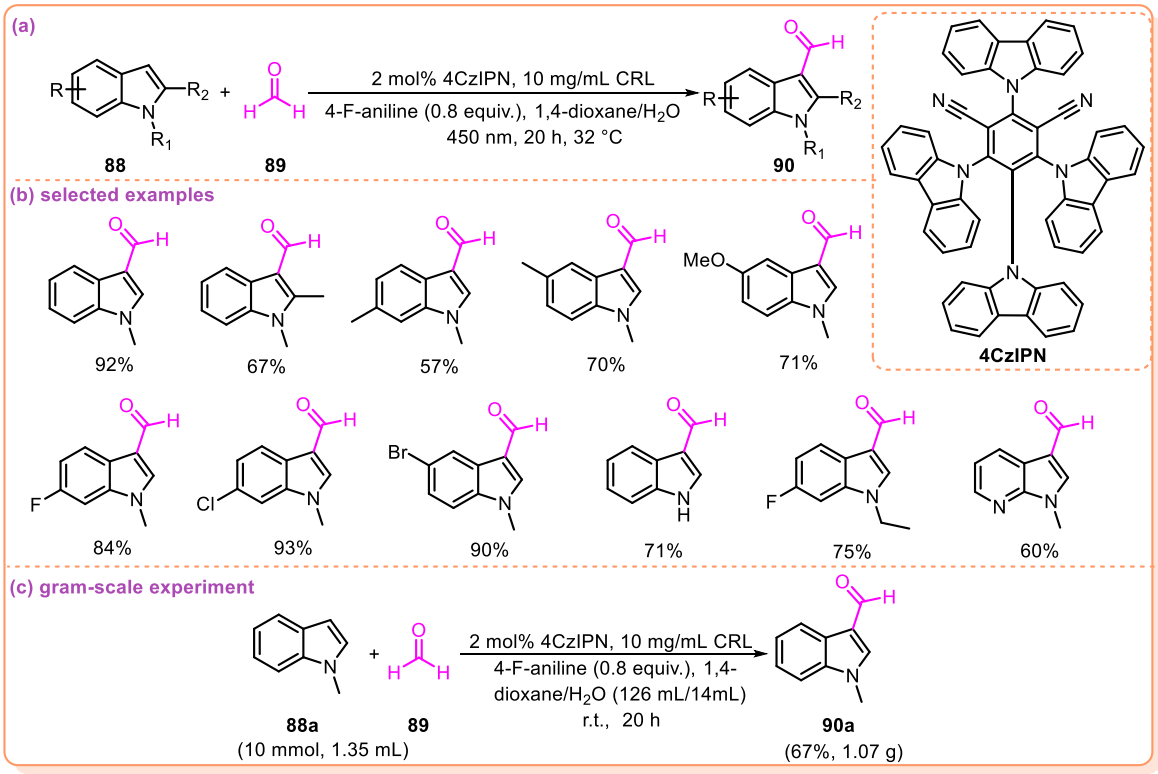

Scheme 1.16: Synthesis of various C-3 acylated indoles via combinative approach using photocatalyst 4CzIPN and CRL enzyme

to afford the desired C-3 acylated indole product. In addition, the substrate scope was thoroughly explored using *N*-methyl indoles bearing both electron-donating and electron-withdrawing substituents, all of which reacted smoothly under the mild photobiocatalytic conditions (**Scheme 1.16b**). Control experiments confirmed that the cascade reaction proceeds via a radical pathway, with the lipase enzyme playing a dual role in both the formation and hydrolysis of key intermediates. To demonstrate the practicality of the method, the reaction was successfully scaled up to gram-scale under optimized conditions, affording the desired cascade acylated product in a 67% yield (**Scheme 1.16c**).

Last year, Li et al. developed a novel strategy to facilitate photobiocatalytic cascade reactions, effectively overcoming the differing behaviours of enzymes and photocatalysts by spatially regulating their distances on Pickering droplet interfaces (**Scheme 1.17a**).[61] Gold nanoparticles immobilized on ultrathin graphitic carbon nitride nanosheets were positioned at the outer layer of oil droplets, where they generated hydrogen peroxide under light irradiation (xenon lamp). Concurrently, CALB was precisely localized at the inner interfacial layer to catalyze enzyme-mediated biooxidations, utilizing the in situ generated H_2O_2 as the oxidant. This methodology was successfully applied to the epoxidation of various alkenes, including aliphatic olefins, challenging α-olefins, and biomass-derived olefins such as α-pinene and limonene (**Scheme 1.17b**). The engineered interfacial system achieved 2-5 times higher reactivity compared to reactions conducted in the bulk aqueous phase. Moreover, this approach not only enhanced the efficiency of the cascade reaction and the transport of H_2O_2 across interfaces but also provided

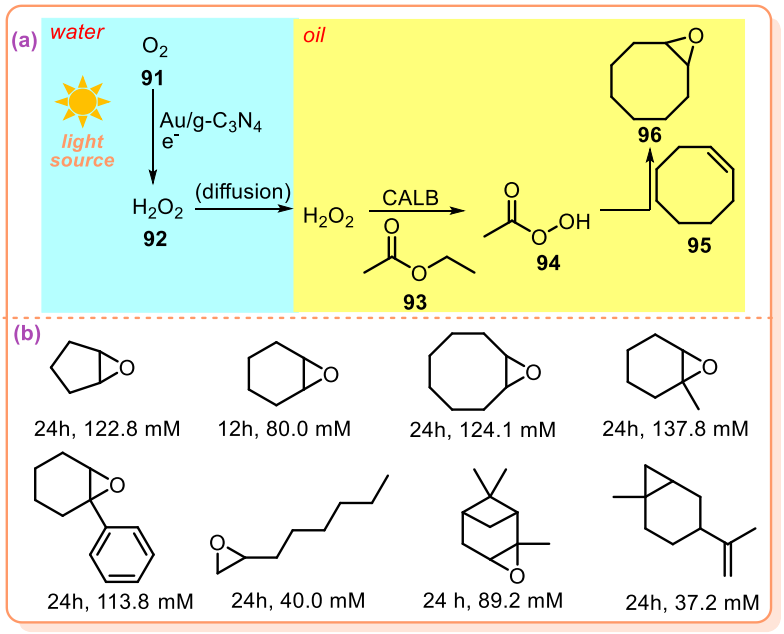

Scheme 1.17: Photobiocatalytic cascade epoxidation of various alkenes at Pickering droplet interfaces

protection to enzymes against oxidative inactivation due to photogenerated reactive species.

Chen and co-workers designed and constructed a heterogeneous Zr-based metal–organic framework (MOF) catalyst, within which both a photocatalyst and wheat germ lipase (WGL) enzyme were simultaneously encapsulated (**Scheme 1.18a**).[62] The rapid synthesis of this photobiocatalyst, achieved without the use of strong acids or organic solvents, demonstrated excellent performance in the asymmetric Mannich reaction, along with good reusability and operational stability. The zirconia-based MOF, UiO-67, was employed to co-immobilize two photosensitizers (Ru- and Cu-based) alongside the WGL enzyme (**Scheme 1.18b**). Depending on the ratio of the two photosensitizers (either 1/2 or 1/3), four different photobiocatalysts were designed. Next, the activity of these catalysts was evaluated for the asymmetric synthesis of various *N*-aryl-substituted tetrahydroisoquinoline (THIQ) derivatives under visible light irradiation (**Scheme 1.18c**). Among them, WGL@UiO-67-Ru1/2 exhibited the best catalytic performance and was subsequently used for the transformation of different 2-phenylindole

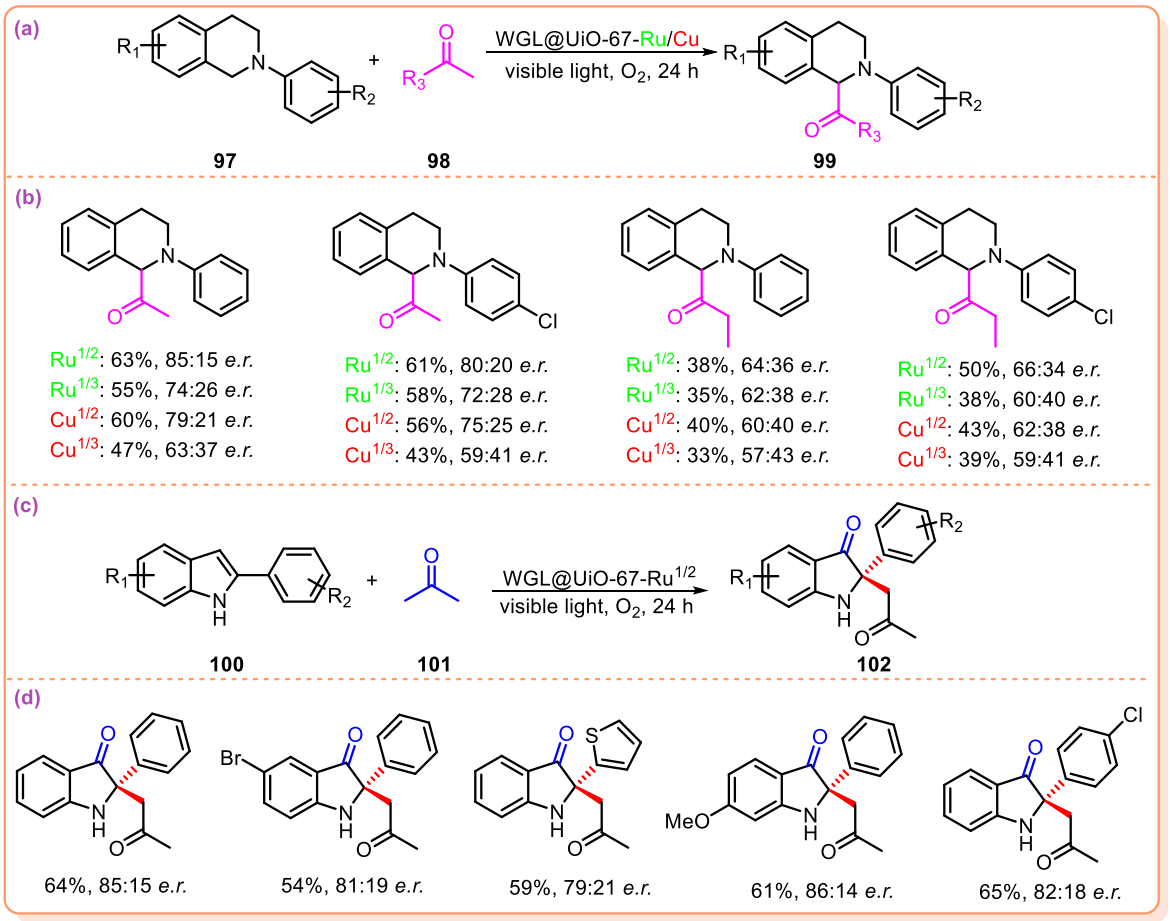

Scheme 1.18: Synthesis of N-aryl-substituted tetrahydroisoquinoline derivatives by newly constructed WGL@UiO-67-Cu/Ru photobiocatalyst

derivatives with acetone. Impressively, the photobiocatalyst maintained high activity regardless of the electronic properties of the substrates (**Scheme 1.18d**). Overall, the UiO-67 framework provided a protective environment for the enzyme, shielding it from the detrimental effects of organic solvents while preserving its catalytic activity.

Very recently, Wu and co-workers developed a photobiocatalyst by encapsulating anthraquinone-2-sulfonate (AQS) as the photocatalyst within the core of cationic liposomes comprised of dioleoyl-3-trimethylammonium propane (DOTAP) and helper cholesterol lipids (**Scheme 1.19a**).[63] Interestingly, Electrostatic stabilization was achieved through interactions between the positively charged liposome surface and the negatively charged membrane of *E. coli* cell. Liposome-coated bacterial cells overexpressing enzymes such as CALB and benzaldehyde lyase (BAL) enabled the efficient synthesis of value-added compounds through multistep cascade reactions. These cascades included two step or three step CALB-catalyzed hydrolysis, BAL-catalyzed condensation, and AQS-mediated photo-oxidation processes (**Scheme 1.19a,b**).

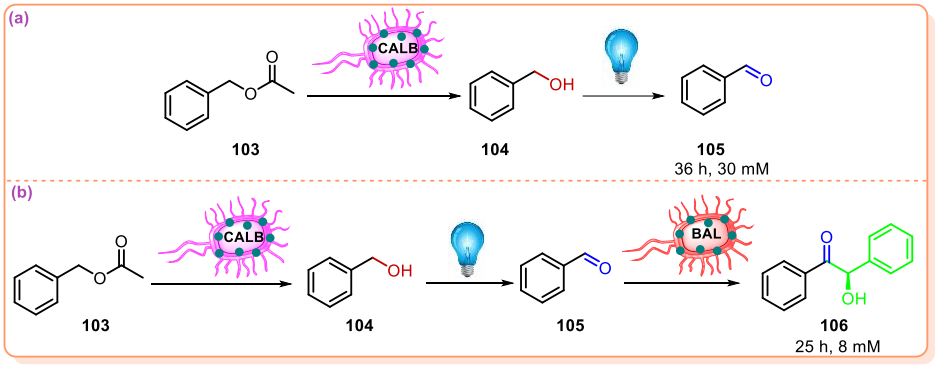

Scheme 1.19: Combining liposomal-coated enzymatic activity with a photocatalyst for multistep cascade reactions

Next, Micklefield and co-workers developed a new strategy combining nitrilase enzyme catalysis with photoredox catalysis to convert inexpensive organonitrile compounds into multifluorinated products (**Scheme 1.20a**).[64] Their approach involved the enzymatic hydrolysis of nitriles using nitrilase in potassium phosphate (KPi) buffer at room temperature for 18 hours, followed by light irradiation for an additional 18 hours after the addition of solvents and chemical reagents. Using this method, they successfully transformed various nitriles into trifluoromethylated compounds with moderate to good isolated yields (**Scheme 1.20b**). Notably, the enzyme exhibited high regioselectivity by selectively hydrolyzing aliphatic nitriles while leaving aromatic nitriles intact. Halogen-substituted substrates further demonstrated the broad applicability of this methodology. Moreover, by employing a hypervalent iodine

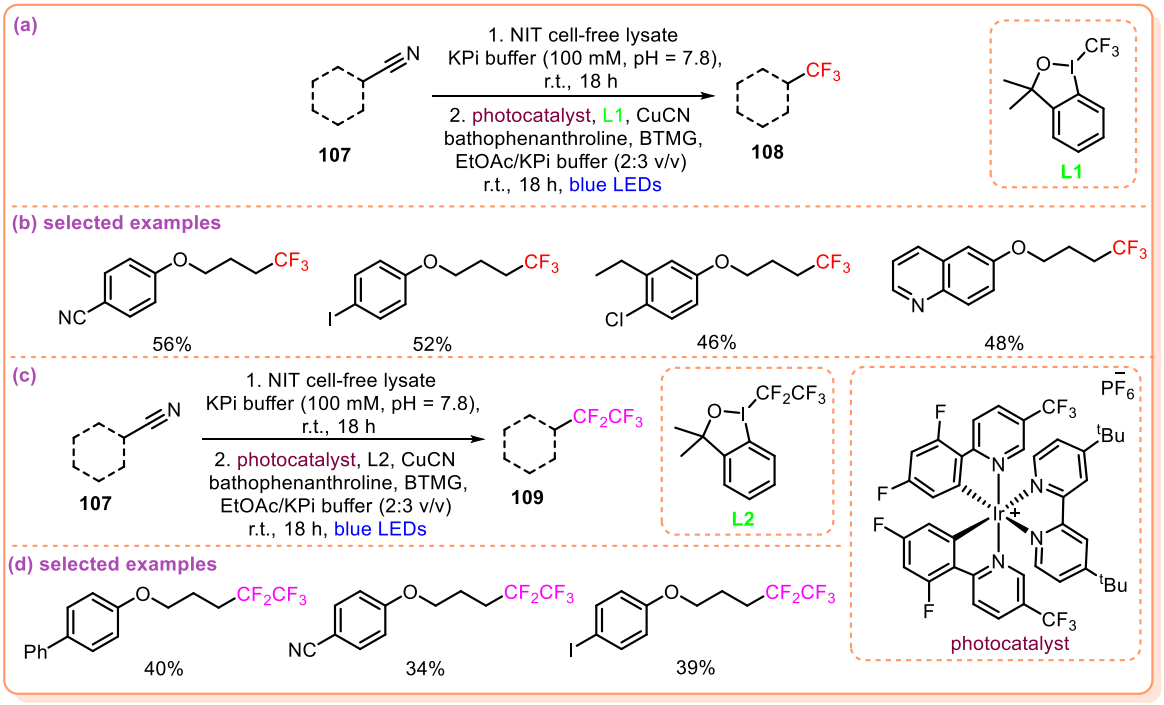

Scheme 1.20: Nitrilase enzyme and photoredox catalysis combined for the efficient synthesis of multifluorinated products

compound (L2) instead of the traditional Togni's reagent (**L1**), they achieved the synthesis of pentafluoroethyl phenol derivatives with yields ranging from 34 to 40% (**Scheme 1.20c,d**).

1.2.4: Electrochemical strategies for the synthesis of bioactive molecule

Electrochemistry has emerged as a key tool in modern synthetic strategies, aligning with green chemistry principles and offering an alternative to traditional methodologies.[21] It enables the direct synthesis of both simple and complex molecules within a highly functionalized chemical space.[22] Thus, electrochemistry effectively bridges the gap between sustainable practices and the synthesis of bioactive molecules.[65]

Yao et al. reported a straightforward electrochemical methodology for the sulfonylation of organoboronic acids using sodium sulfinates (**Scheme 1.21a**).[66] This green approach enables the synthesis of a broad range of organosulfones from aryl, heteroaryl, and alkenyl boronic acids in good to excellent yields at room temperature within 5 hours (**Scheme 1.21b**). The reaction was performed in an undivided electrochemical cell using carbon and platinum as the anode and cathode, respectively. Notably, this sustainable protocol operates without the need for additives or catalysts. Mechanistic studies, including radical trapping and cyclic voltammetry experiments, revealed that the reaction proceeds via the formation of sulfonyl

radicals. Furthermore, the utility of the method was demonstrated through scale-up reactions and the synthesis of the antibacterial drug dapsone (**Scheme 1.21c,d**).

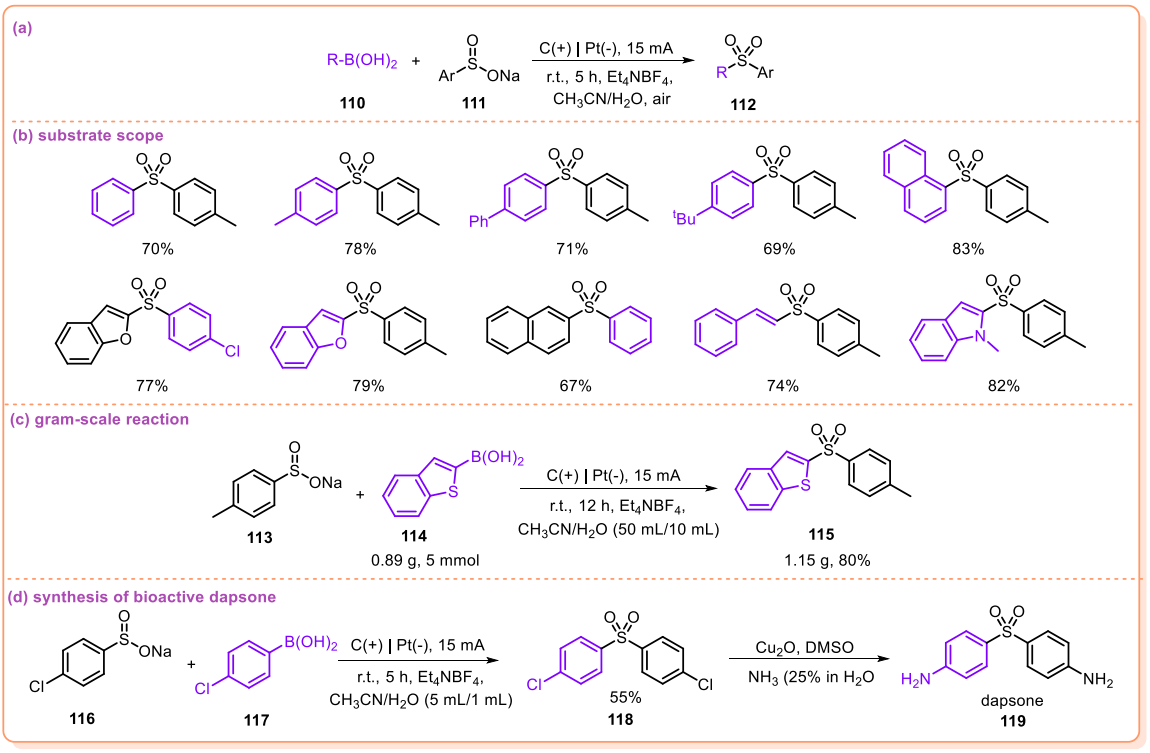

Scheme: 1.21: Electrochemical synthesis of organosulfones

In 2023, Qiu and co-workers developed a metal-free electrocarboxylation strategy that employs electricity and CO_2 as the energy source and carboxylic acid precursor, respectively, for the site-selective C–H carboxylation of unactivated arenes **(Scheme 1.22a)**.[67] This versatile approach demonstrated broad substrate scope, efficiently transforming polycyclic aromatic hydrocarbons, challenging heteroarenes, simple phenyl derivatives, and substituted arenes with excellent chemo- and regioselectivity as well as high atom economy. Notably, the method enabled the reductive activation of challenging substrates such as naphthalenes, pyridines, pyrimidines, and substituted quinolines **(Scheme 1.22b)**. The scalability of the protocol was illustrated through the gram-scale carboxylation of methyl-2-naphthoate (9 mmol) with CO_2, affording the desired product in 82% yield **(Scheme 1.22c)**. Mechanistic investigations, including cyclic voltammetry and control experiments, suggested the formation of CO_2 radical anions at the cathode **(Scheme 1.22d)**. Further DFT studies revealed that these radical anions play a key role in dictating the regioselectivity of the reaction.

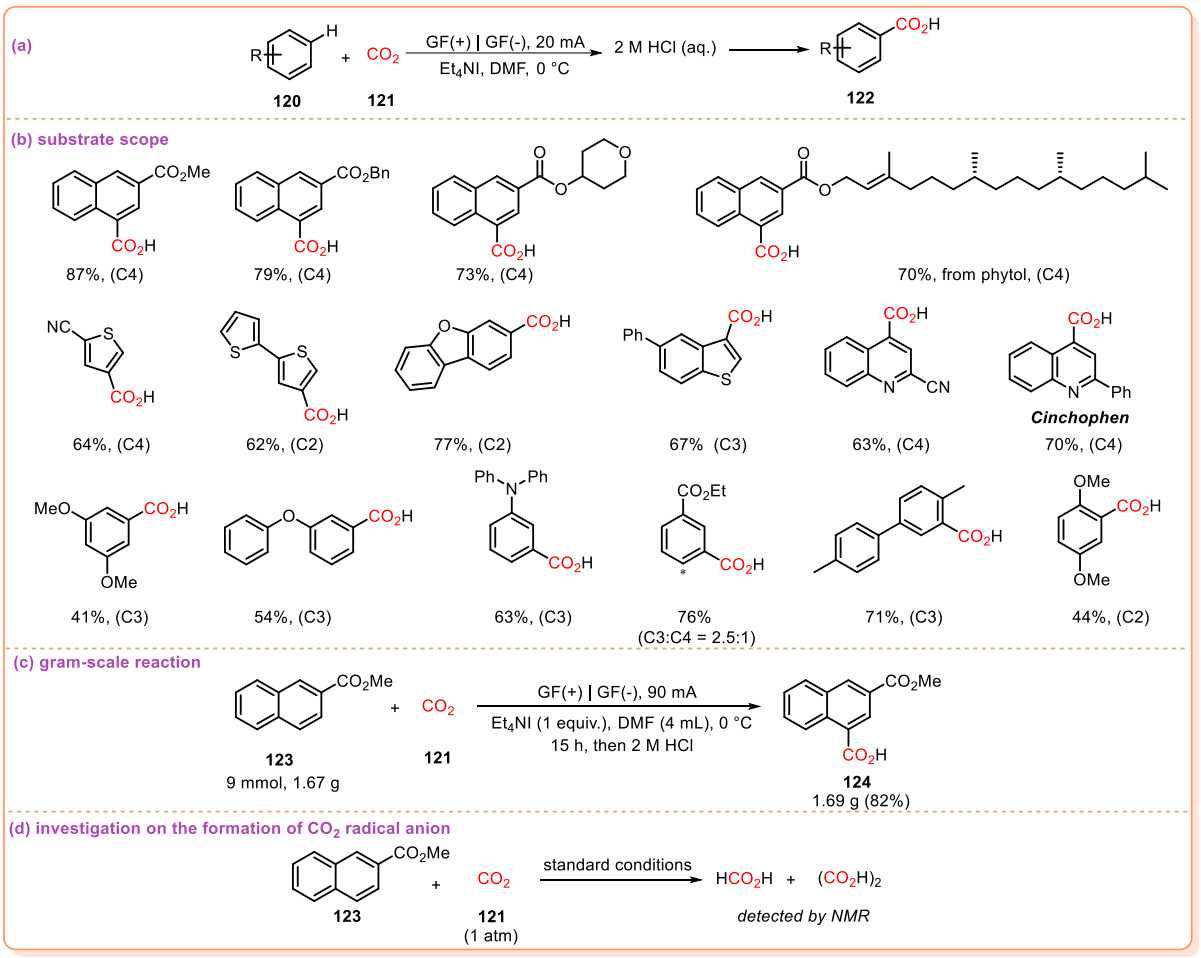

Scheme: 1.22: Electrochemical site-selective C-H carboxylation of arenes

Wang and co-workers reported an electrochemical strategy for the synthesis of 2,5-diaryloxazoles from aryl ketones and benzyl amines or amino acids (**Scheme 1.23a**).[68] This metal-, base-, and chemical oxidant-free protocol enables N–H and C(sp^3)–H functionalization to afford a wide range of functionalized oxazoles using various benzyl amines, α-amino acids, and phenyl glycines in moderate to excellent yields (**Scheme 1.23b**). The versatility of the method was further demonstrated through gram-scale reactions and the synthesis of several bioactive natural products (**Scheme 1.23c,d**). Mechanistic studies, including control experiments, revealed that the transformation proceeds via a radical pathway.

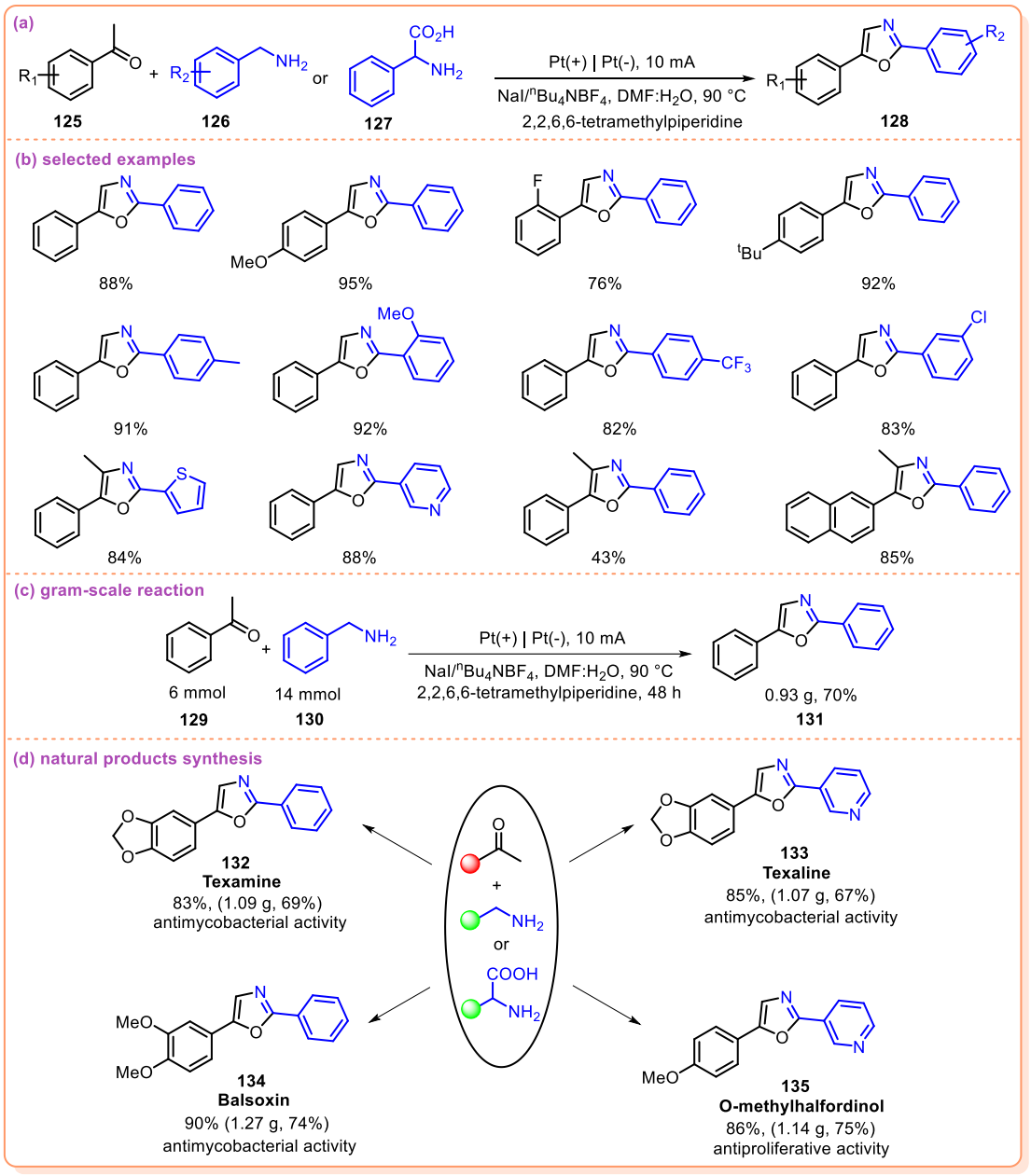

Scheme: 1.23: Synthesis of different 2,5-diaryloxazoles using electricity

1.3 Conclusion

In summary, to achieve sustainability in organic synthesis has become a key focus for chemists in recent years. The primary aim is to design organic reactions that minimize waste, employ green solvents, and utilize catalytic strategies aligned with the principles of green chemistry. Major green catalytic approaches include biocatalysis, electrocatalysis, photocatalysis, and organocatalysis, each offering distinct advantages and limitations. Integrating these diverse catalytic methods expands the accessible chemical space and enables the synthesis of complex molecules that are often unattainable through individual catalytic strategies. Such integrated systems operate in sequential or concurrent multicatalytic cascades, facilitating the efficient

production of pharmaceuticals and their precursors. This review focuses on hydrolase-catalyzed integration strategies that combine biocatalysis with other catalytic disciplines. It also highlights how interdisciplinary, integrative cascade approaches enable the synthesis of clinically important molecules by addressing the challenges inherent in designing multicatalytic systems.

1.4: References

1. (a) Mohanty, A. K.; Wu, F.; Mincheva, R.; Hakkarainen, M.; Raquez, J. M.; Mielewski, D. F.; Narayan, R.; Netravali, A. N.; Misra, M. Sustainable polymers. *Nat. Rev. Methods Primers* **2022**, *2*, 46. (b) Mangla, S. K.; Luthra, S.; Jakhar, S.; Gandhi, S.; Muduli, K.; Kumar, A. A step to clean energy—Sustainability in energy system management in an emerging economy context. *J. Clean. Prod.* **2020**, *242*, 118462. (c) Gade, A.; Ingle, P.; Nimbalkar, U.; Rai, M.; Raut, R.; Vedpathak, M.; Jagtap, P.; Abd-Elsalam, K. A. Nanofertilizers: the next generation of agrochemicals for long-term impact on sustainability in farming systems. *Agrochemicals* **2023**, *2*, 257–278. (d) Richie, C. Environmental sustainability and the carbon emissions of pharmaceuticals. *J. Med. Ethics* **2022**, *48*, 334–337.
2. (a) Glavič, P.; Lukman, R. Review of sustainability terms and their definitions. *J. Clean. Prod.* **2007**, *15*, 1875–1885. (b) Anastas, P. T.; Zimmerman, J. B. The periodic table of the elements of green and sustainable chemistry. *Green Chem.* **2019**, *21*, 6545–6566.
3. Ivanković, A.; Dronjić, A.; Bevanda, A. M.; Talić, S. Review of 12 principles of green chemistry in practice. *Int. J. Sustain. Green Energy* **2017**, *6*, 39–48.
4. Kohansal, M. Advances in Green Chemistry: Sustainable Approaches in Organic Synthesis. *Int. J. New Chem.* **2025**, *12*, 726–737.
5. Ratnani, S.; Mahilkar Sonkar, S.; Kumari, R. Strategies for sustainable organic synthesis. *J. Iran. Chem. Soc.* **2023**, *20*, 495–508.
6. (a) Clarke, C. J.; Tu, W. C.; Levers, O.; Brohl, A.; Hallett, J. P. Green and sustainable solvents in chemical processes. *Chem. Rev.* **2018**, *118*, 747–800. (b) Hessel, V.; Tran, N. N.; Asrami, M. R.; Tran, Q. D.; Long, N. V. D.; Escribà-Gelonch, M.; Tejada, J. O.; Linke, S.; Sundmacher, K. Sustainability of green solvents—review and perspective. *Green Chem.* **2022**, *24*, 410–437.
7. (a) Sheldon, R. A. Green solvents for sustainable organic synthesis: state of the art. *Green Chem.* **2005**, *7*, 267–278. (b) Varma, R. S. Greener and sustainable trends in synthesis of organics and nanomaterials. *Green Chem.* **2016**, *18*, 5287–5303. (c) Cseri,

L.; Razali, M.; Pogany, P.; Szekely, G. Organic solvents in sustainable synthesis and engineering. In *Green Chemistry*; Elsevier: **2018**; pp 513–553.

8. (a) Alcalde, M.; Ferrer, M.; Plou, F. J.; Ballesteros, A. Environmental biocatalysis: from remediation with enzymes to novel green processes. *Trends Biotechnol.* **2006**, *24*, 281–287. (b) Yi, D.; Bayer, T.; Badenhorst, C. P.; Wu, S.; Doerr, M.; Höhne, M.; Bornscheuer, U. T. Recent trends in biocatalysis. *Chem. Soc. Rev.* **2021**, *50*, 8003–8049.
9. Bell, E. L.; Finnigan, W.; France, S. P.; Green, A. P.; Hayes, M. A.; Hepworth, L. J.; Lovelock, S. L.; Niikura, H.; Osuna, S.; Romero, E.; Ryan, K. S. Biocatalysis. *Nat. Rev. Methods Primers* **2021**, *1*, 46.
10. Stroppolo, M. E.; Falconi, M.; Caccuri, A. M.; Desideri, A. Superefficient enzymes. *Cell. Mol. Life Sci.* **2001**, *58*, 1451–1460.
11. (a) Sheldon, R. A.; Woodley, J. M. Role of biocatalysis in sustainable chemistry. *Chem. Rev.* **2018**, *118*, 801–838. (b) Garcia-Urdiales, E.; Alfonso, I.; Gotor, V. Enantioselective enzymatic desymmetrizations in organic synthesis. *Chem. Rev.* **2005**, *105*, 313–354. (c) Bommarius, A. S. Biocatalysis: a status report. *Annu. Rev. Chem. Biomol. Eng.* **2015**, *6*, 319–345. (d) Pyser, J. B.; Chakrabarty, S.; Romero, E. O.; Narayan, A. R. State-of-the-art biocatalysis. *ACS Cent. Sci.* **2021**, *7*, 1105–1116. (e) Wandrey, C.; Liese, A.; Kihumbu, D. Industrial biocatalysis: past, present, and future. *Org. Process Res. Dev.* **2000**, *4*, 286–290.
12. (a) Hughes, G.; Lewis, J. C. Introduction: biocatalysis in industry. *Chem. Rev.* **2018**, *118*, 1–3. (b) Schmid, A.; Dordick, J. S.; Hauer, B.; Kiener, A.; Wubbolts, M.; Witholt, B. Industrial biocatalysis today and tomorrow. *Nature* **2001**, *409*, 258–268.
13. Denard, C. A.; Ren, H.; Zhao, H. Improving and repurposing biocatalysts via directed evolution. *Curr. Opin. Chem. Biol.* **2015**, *25*, 55–64.
14. (a) Turner, N. J. Directed evolution drives the next generation of biocatalysts. *Nat. Chem. Biol.* **2009**, *5*, 567–573. (b) Gargiulo, S.; Soumillion, P. Directed evolution for enzyme development in biocatalysis. *Curr. Opin. Chem. Biol.* **2021**, *61*, 107–113. (c) Jaeger, K. E.; Eggert, T. Enantioselective biocatalysis optimized by directed evolution. *Curr. Opin. Biotechnol.* **2004**, *15*, 305–313.
15. (a) Li, G.; Wang, J. B.; Reetz, M. T. Biocatalysts for the pharmaceutical industry created by structure-guided directed evolution of stereoselective enzymes. *Bioorg. Med. Chem.* **2018**, *26*, 1241–1251. (b) Powell, K. A.; Ramer, S. W.; Del Cardayré, S. B.; Stemmer, W. P.; Tobin, M. B.; Longchamp, P. F.; Huisman, G. W. Directed evolution and biocatalysis. *Angew. Chem., Int. Ed.* **2001**, *40*, 3948–3959.

16. (a) Kuo, C. H.; Huang, C. Y.; Shieh, C. J.; Dong, C. D. Enzymes and biocatalysis. *Catalysts* **2022**, *12*, 993. (b) Tao, Z.; Dong, B.; Teng, Z.; Zhao, Y. The classification of enzymes by deep learning. *IEEE Access* **2020**, *8*, 89802–89811.
17. (a) Méndez-Sánchez, D.; López-Iglesias, M.; Gotor-Fernández, V. Hydrolases in organic chemistry: recent achievements in the synthesis of pharmaceuticals. *Curr. Org. Chem.* **2016**, *20*, 1186–1203. (b) Wandrey, C.; Liese, A.; Kihumbu, D. Industrial biocatalysis: past, present, and future. *Org. Process Res. Dev.* **2000**, *4*, 286–290. (c) Busto, E.; Gotor-Fernández, V.; Gotor, V. Hydrolases: catalytically promiscuous enzymes for non-conventional reactions in organic synthesis. *Chem. Soc. Rev. 39*, 4504-4523.
18. (a) Testa, B.; Krämer, S. D. The biochemistry of drug metabolism—an introduction: part 3. Reactions of hydrolysis and their enzymes. *Chem. Biodivers.* **2007**, *4*, 2031–2122. (b) Dorr, B. M.; Fuerst, D. E. Enzymatic amidation for industrial applications. *Curr. Opin. Chem. Biol.* **2018**, *43*, 127–133.
19. Qiu, M.; Dong, S.; Cui, Q.; Feng, Y.; Xuan, J. Recent progress in the mechanism and engineering of α/β hydrolases for chiral chemical production. *Catalysts* **2023**, *13*, 288.
20. Frontana-Uribe, B. A.; Little, R. D.; Ibanez, J. G.; Palma, A.; Vasquez-Medrano, R. Organic electrosynthesis: a promising green methodology in organic chemistry. *Green Chem.* **2010**, *12*, 2099–2119.
21. (a) Utley, J. Trends in organic electrosynthesis. *Chem. Soc. Rev.* **1997**, *26*, 157–167. (b) Frontana-Uribe, B. A.; Little, R. D.; Ibanez, J. G.; Palma, A.; Vasquez-Medrano, R. Organic electrosynthesis: a promising green methodology in organic chemistry. *Green Chem.* **2010**, *12*, 2099–2119.
22. (a) Meyer, T. H.; Choi, I.; Tian, C.; Ackermann, L. Powering the future: how can electrochemistry make a difference in organic synthesis? *Chem* **2020**, *6*, 2484–2496. (b) Marken, F.; Wadhawan, J. D. Multiphase methods in organic electrosynthesis. *Acc. Chem. Res.* **2019**, *52*, 3325–3338.
23. Cardoso, D. S.; Sljukic, B.; Santos, D. M.; Sequeira, C. A. Organic electrosynthesis: from laboratorial practice to industrial applications. *Org. Process Res. Dev.* **2017**, *21*, 1213–1226.
24. (a) Yamamoto, K.; Kuriyama, M.; Onomura, O. Asymmetric electrosynthesis: recent advances in catalytic transformations. *Curr. Opin. Electrochem.* **2021**, *28*, 100714. (b) Siu, J. C.; Fu, N.; Lin, S. Catalyzing electrosynthesis: a homogeneous electrocatalytic approach to reaction discovery. *Acc. Chem. Res.* **2020**, *53*, 547–560.

25. Yamamoto, K.; Kuriyama, M.; Onomura, O. Asymmetric electrosynthesis: recent advances in catalytic transformations. *Curr. Opin. Electrochem.* **2021**, *28*, 100714.
26. (a) Carceller, J. M.; Arias, K. S.; Climent, M. J.; Iborra, S.; Corma, A. One-pot chemo- and photo-enzymatic linear cascade processes. *Chem. Soc. Rev.* **2024**, *53*, 7875–7938. (b) Bruggink, A.; Schoevaart, R.; Kieboom, T. Concepts of nature in organic synthesis: cascade catalysis and multistep conversions in concert. *Org. Process Res. Dev.* **2003**, *7*, 622–640.
27. Ambrosini, L. M.; Lambert, T. H. Multicatalysis: advancing synthetic efficiency and inspiring discovery. *ChemCatChem* **2010**, *2*, 1373–1380.
28. (a) Huang, X.; Cao, M.; Zhao, H. Integrating biocatalysis with chemocatalysis for selective transformations. *Curr. Opin. Chem. Biol.* **2020**, *55*, 161–170. (b) Rudroff, F.; Mihovilovic, M. D.; Gröger, H.; Snajdrova, R.; Iding, H.; Bornscheuer, U. T. Opportunities and challenges for combining chemo- and biocatalysis. *Nat. Catal.* **2018**, *1*, 12–22. (c) Lee, Y. S.; Lim, K.; Minteer, S. D. Cascaded biocatalysis and bioelectrocatalysis: overview and recent advances. *Annu. Rev. Phys. Chem.* **2021**, *72*, 467–488. (d) Yang, J.; Sou, C. K.; Lu, Y. Cell-free biocatalysis coupled with photo-catalysis and electro-catalysis: efficient CO_2-to-chemical conversion. *Green Energy Environ.* **2024**, *9*, 1366–1383.
29. (a) Denard, C. A.; Hartwig, J. F.; Zhao, H. Multistep one-pot reactions combining biocatalysts and chemical catalysts for asymmetric synthesis. *ACS Catal.* **2013**, *3*, 2856–2864. (b) Lee, J. M.; Na, Y.; Han, H.; Chang, S. Cooperative multi-catalyst systems for one-pot organic transformations. *Chem. Soc. Rev.* **2004**, *33*, 302–312.
30. Schmidt, S.; Castiglione, K.; Kourist, R. Overcoming the incompatibility challenge in chemoenzymatic and multi-catalytic cascade reactions. *Chem. Eur. J.* **2018**, *24*, 1755–1768.
31. Rudroff, F.; Mihovilovic, M. D.; Gröger, H.; Snajdrova, R.; Iding, H.; Bornscheuer, U. T. Opportunities and challenges for combining chemo- and biocatalysis. *Nat. Catal.* **2018**, *1*, 12–22.
32. (a) Zhou, Y.; Wu, S.; Bornscheuer, U. T. Recent advances in (chemo)enzymatic cascades for upgrading bio-based resources. *Chem. Commun.* **2021**, *57*, 10661–10674. (b) Kaspar, F.; Schallmey, A. Chemo-enzymatic synthesis of natural products and their analogs. *Curr. Opin. Biotechnol.* **2022**, *77*, 102759. (c) Seel, C. J.; Gulder, T. Biocatalysis fueled by light: on the versatile combination of photocatalysis and enzymes. *ChemBioChem* **2019**, *20*, 1871–1897.

33. Dumeignil, F.; Guehl, M.; Gimbernat, A.; Capron, M.; Ferreira, N. L.; Froidevaux, R.; Girardon, J. S.; Wojcieszak, R.; Dhulster, P.; Delcroix, D. From sequential chemoenzymatic synthesis to integrated hybrid catalysis: taking the best of both worlds to open up the scope of possibilities for a sustainable future. *Catal. Sci. Technol.* **2018**, *8*, 5708–5734.
34. Chen, T.; Lu, Y.; Xiong, X.; Xu, Z. Co-immobilization of enzymes and chemocatalysts for one-pot chemoenzymatic cascades: scaffold engineering toward more efficient catalysis. *Chem Catal.* **2024**, *4*, 100894.
35. (a) Marciello, M.; Morato, Y. L.; Paredes, K. O.; Chamizo, L. L.; Filice, M. Enzyme-metal nanobiohybrids in chemobiocatalytic cascade processes. In *Nanomaterials for Biocatalysis*; Elsevier: **2022**; pp 189–210 (b) Li, X.; Fu, C.; Luo, L.; Ge, J. Design of enzyme-metal hybrid catalysts for organic synthesis. *Cell Rep. Phys. Sci.* **2022**, *3*, 100982.
36. Naapuri, J. M.; Losada-Garcia, N.; Rothemann, R. A.; Pichardo, M. C.; Prechtl, M. H.; Palomo, J. M.; Deska, J. Cascade catalysis through bifunctional lipase–metal biohybrids for the synthesis of enantioenriched O-heterocycles from allenes. *ChemCatChem* **2022**, *14*, e202200362.
37. Naapuri, J. M.; Losada-Garcia, N.; Deska, J.; Palomo, J. M. Synthesis of silver and gold nanoparticles–enzyme–polymer conjugate hybrids as dual-activity catalysts for chemoenzymatic cascade reactions. *Nanoscale* **2022**, *14*, 5701–5715.
38. Singhania, V.; Cortes-Clerget, M.; Dussart-Gautheret, J.; Akkachairin, B.; Yu, J.; Akporji, N.; Gallou, F.; Lipshutz, B. H. Lipase-catalyzed esterification in water enabled by nanomicelles: applications to one-pot multistep sequences. *Chem. Sci.* **2022**, *13*, 1440–1455.
39. Bering, L.; Craven, E. J.; Sowerby Thomas, S. A.; Shepherd, S. A.; Micklefield, J. Merging enzymes with chemocatalysis for amide bond synthesis. *Nat. Commun.* **2022**, *13*, 380.
40. Zhao, H.; Liu, G.; Liu, Y.; Liu, X.; Wang, H.; Chen, H.; Gao, J.; Jiang, Y. Metal nanoparticles@covalent organic framework@enzymes: a universal platform for fabricating a metal–enzyme integrated nanocatalyst. *ACS Appl. Mater. Interfaces* **2022**, *14*, 2881–2892.
41. Gao, J.; Wang, Z.; Guo, R.; Hu, Y.; Dong, X.; Shi, Q.; Sun, Y. Efficient cascade conversion of starch to gluconic acid by a chemoenzymatic system with co-immobilized Au nanoparticles and enzymes. *Catal. Sci. Technol.* **2023**, *13*, 991–999.

42. Li, X.; Hu, X.; Qiao, Y.; Lu, T.; Bai, Y.; Xiong, J.; Li, X.; Gou, Q.; Ge, J. Enzyme-bimetallic catalyst for one-pot chemoenzymatic reactions. *Chem. Eng. J.* **2023**, *452*, 139356.
43. Li, X.; Cao, Y.; Xiong, J.; Li, J.; Xiao, H.; Li, X.; Gou, Q.; Ge, J. Enzyme-metal-single-atom hybrid catalysts for one-pot chemoenzymatic reactions. *Chin. J. Catal.* **2023**, *44*, 139–145.
44. Budhiraja, M.; Ali, A.; Tyagi, V. Construction of a bifunctional Pd(0)–CALB@SiO_2 hybrid catalyst for the synthesis and arylation of imidazo[1,2-a]pyridine in one pot. *Eur. J. Org. Chem.* **2023**, *26*, e202201426.
45. Tian, D.; Hao, R.; Zhang, X.; Shi, H.; Wang, Y.; Liang, L.; Liu, H.; Yang, H. Multi-compartmental MOF microreactors derived from Pickering double emulsions for chemoenzymatic cascade catalysis. *Nat. Commun.* **2023**, *14*, 3226.
46. Wang, S.; Scandurra, L.; Hübner, R.; Nielsen, U. G.; Wu, C. Tailored particle catalysts for multistep one-pot chemoenzymatic cascade in Pickering emulsions. *ChemCatChem* **2023**, *15*, e202201229.
47. Dutt, S.; Tyagi, V. Synthesis and substrate-controlled modification of β-aminocarbonyl using α-amylase enzyme and Pd-catalyst in one-pot. *Biocatal. Biotransfor.* **2024**, *42*, 262–272.
48. Liu, Y.; Guo, N.; Kong, W.; Gao, S.; Liu, G.; Zhou, L.; Gao, J.; Jiang, Y. Magnetic wrinkled organosilica-based metal–enzyme integrated catalysts for enhanced chemoenzymatic catalysis. *Green Synth. Catal.* **2024**, *5*, 122–125.
49. Giparakis, S.; Winkler, M.; Rudroff, F. Nature stays natural: two novel chemoenzymatic one-pot cascades for the synthesis of fragrance and flavor aldehydes. *Green Chem.* **2024**, *26*, 1338–1344.
50. Lin, Y.; Yu, J.; Ye, K. Y. Integrating electrocatalysis with biocatalysis for asymmetric synthesis. *Org. Chem. Front.* **2024**, *11*, 7243–7248.
51. (a) Phillips, A. M. F.; Pombeiro, A. J. L. Electrochemical Asymmetric Synthesis of Biologically Active Substances. *Org. Biomol. Chem*. **2020**, *18*, 7026–7055. (b) Huang, X.; Zhang, Q.; Lin, J.; Harms, K.; Meggers, E. Electricity-driven asymmetric Lewis acid catalysis. *Nat. Catal.* **2019**, *2,* 34-40.
52. (a) Peñafiel, I.; Dryfe, R. A.; Turner, N. J.; Greaney, M. F. Integrated electrobiocatalysis for amine alkylation with alcohols. *ChemCatChem* **2021**, *13*, 864–867. (b) Srikanth, S.; Kumar, M.; Singh, D.; Singh, M. P.; Puri, S. K.; Ramakumar, S. S. V. Long-term

operation of electrobiocatalytic reactor for carbon dioxide transformation into organic molecules. *Bioresour. Technol.* **2018**, *265*, 66–74.

53. Long, C. J.; Cao, H.; Zhao, B. K.; Tan, Y. F.; He, Y. H.; Huang, C. S.; Guan, Z. Merging the non-natural catalytic activity of lipase and electrosynthesis: asymmetric oxidative cross-coupling of secondary amines with ketones. *Angew. Chem.* **2022**, *134*, e202203666.
54. Singh, K.; Tyagi, V. Combining the nonnatural activity of lipase and electrocatalysis in one pot: sustainable and regioselective synthesis of C-3 alkylated oxindoles. *ChemCatChem* **2025**, *17*, e202401182.
55. Harrison, W.; Huang, X.; Zhao, H. Photobiocatalysis for abiological transformations. *Acc. Chem. Res.* **2022**, *55*, 1087–1096.
56. Emmanuel, M. A.; Bender, S. G.; Bilodeau, C.; Carceller, J. M.; DeHovitz, J. S.; Fu, H.; Liu, Y.; Nicholls, B. T.; Ouyang, Y.; Page, C. G.; Qiao, T. Photobiocatalytic strategies for organic synthesis. *Chem. Rev.* **2023**, *123*, 5459–5520.
57. Singh, P. P.; Sinha, S.; Nainwal, P.; Singh, P. K.; Srivastava, V. Novel applications of photobiocatalysts in chemical transformations. *RSC Adv.* **2024**, *14*, 2590–2601.
58. Hu, J. Y.; Xie, Z. B.; Tang, J.; Le, Z. G.; Zhu, Z. Q. Combining enzyme and photoredox catalysis for the construction of 3-aminoalkyl chromones. *J. Org. Chem.* **2022**, *87*, 14965–14969.
59. Jin, C.; Li, N.; Lin, E.; Chen, X.; Wang, T.; Wang, Y.; Yang, M.; Liu, W.; Yu, J.; Zhang, Z.; Chen, Y. Enzyme immobilization in porphyrinic covalent organic frameworks for photoenzymatic asymmetric catalysis. *ACS Catal.* **2022**, *12*, 8259–8268.
60. Yu, Y.; Lin, R. D.; Yao, Y.; Shi, M. L.; Lu, W. F.; Wang, N.; Yu, X. Q. Development of a metal- and oxidant-free enzyme–photocatalyst hybrid system for highly efficient C-3 acylation reactions of indoles with aldehydes. *ACS Catal.* **2022**, *12*, 12543–12554.
61. Li, K.; Zou, H.; Tong, X.; Yang, H. Enhanced photobiocatalytic cascades at Pickering droplet interfaces. *J. Am. Chem. Soc.* **2024**, *146*, 17054–17065.
62. Wang, S.; Liu, W.; Wang, J.; Yu, J.; Wang, F.; Jin, C.; Wang, K.; Cheng, P.; Zhang, Z.; Chen, Y. Mechanochemical encapsulation of enzymes into MOFs for photoenzymatic enantioselective catalysis. *ACS Mater. Lett.* **2024**, *6*, 2609–2616.
63. Zhang, J.; Batista, V. F.; Hübner, R.; Vogel, S.; Wu, C. Combining liposomal photocatalysts with whole-cell catalysts for one-pot photobiocatalysis. *Small* **2025**, *21*, 2408666.

64. Angiolini, S.; Bruton, I.; Bering, L.; Thomas, S. S.; Thompson, J.; Shepherd, S. A.; Micklefield, J. Integrating enzymes with photoredox catalysis for conversion of nitriles into fluorinated products. *ChemCatChem* **2025**, e202500240.
65. Ghosh, A.; Parida, V. K.; Banerjee, D. Challenges and opportunities on sustainable electrochemical transformations: application towards the synthesis of pharmaceuticals and precursors of drug-like molecules. *Green Chem.* ***2024****, 26,* 5770–5789.
66. Yao, W.; Lv, K.; Xie, Z.; Qiu, H.; Ma, M. Catalyst-free electrochemical sulfonylation of organoboronic acids. *J. Org. Chem.* **2023**, *88*, 2296–2305.
67. Zhao, Z.; Liu, Y.; Wang, S.; Tang, S.; Ma, D.; Zhu, Z.; Guo, C.; Qiu, Y. Site-selective electrochemical C–H carboxylation of arenes with CO_2. *Angew. Chem.* **2023**, *135*, e202214710.
68. Li, T.; Pan, L.; Zhang, Y.; Su, J.; Li, K.; Li, K.; Chen, H.; Sun, Q.; Wang, Z. Electrochemical construction of 2,5-diaryloxazoles via N–H and C(sp^3)–H functionalization. *Chin. Chem. Lett.* **2024**, *35*, 108897.

LITERATURE GAPS AND RESEARCH OBJECTIVES

Literature gaps

By going through the literature, the following gaps have been observed:

1. The area of integration of enzyme catalysis with other catalytic systems, like photo, electro, or chemical catalysts, to synthesize biologically relevant molecules is still underexplored.
2. Metal-based catalysts and enzymes have distinguishable natures; the former generally require harsh reaction conditions, while the latter operate under mild reaction conditions. So, the use of both of the catalysts in a one-pot reaction is a big challenge to synthetic chemists.
3. There is no integrated electro-bio-catalytic approach documented previously to catalyze the combination of Michael addition reaction with other synthetic transformations in one-pot fashion.

Objectives

To overcome the aforementioned gaps, we are proposing the following objectives:

1. Development of one-pot chemo-enzymatic approach for catalyzing the combination of Suzuki-Miyaura and Michael-addition reactions.
2. Exploration of thia-Michael addition reaction using enzyme-based catalyst and further application in the synthesis of pharmaceutical precursors.
3. Investigation of an electrochemical strategy for regioselective *N*-sulfonylation of heterocycles.

CHAPTER 2

Design and Preparation of Novel Bifunctional Nanobiohybrid Catalyst by Combining Palladium and α-Amylase Enzyme: Application in the One-pot Chemoenzymatic Catalysis

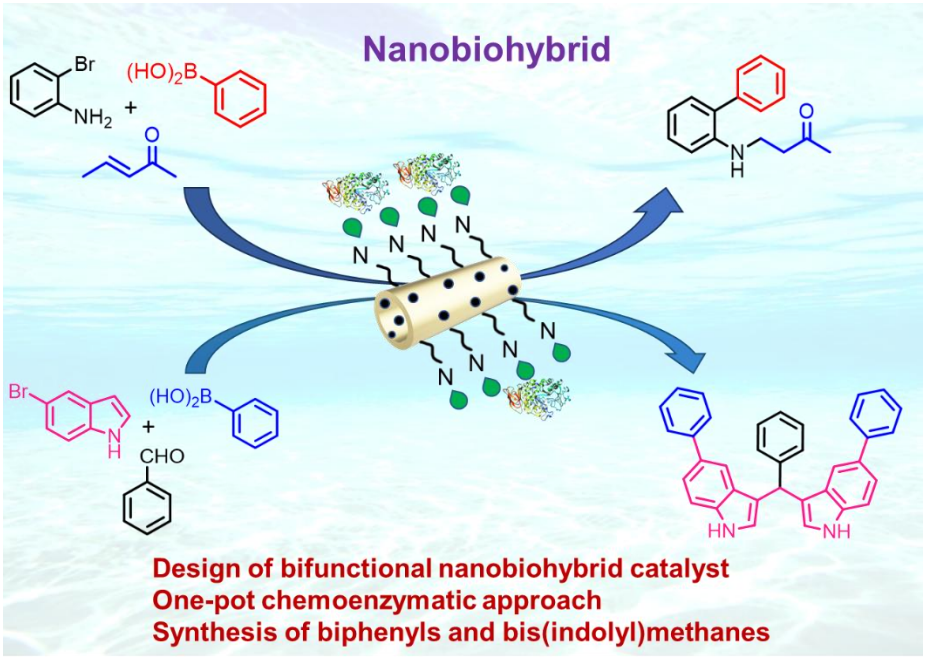

CHAPTER 2

2.1: Introduction

The combining of chemical and bio-catalysis to catalyze dual chemical reactions known as a chemoenzymatic procedure, provides phenomenal opportunities in organic synthesis.[1] Moreover, chemoenzymatic catalysis has the potential to boost overall synthetic productivity by reducing waste production, solvent consumption as well as purification steps.[2] Besides, chemoenzymatic reactions are often classified in two ways either sequential or concurrent. In sequential reactions, usually, a second catalyst and subsequent reagents are added after the completion of the first catalytic transformation. Sometimes, protein removal, dilution/concentration, degassing, and alteration of solvents are also required in this approach. In contrast, in concurrent chemoenzymatic reactions, all reactants and catalysts are added simultaneously in a single pot at the beginning of the reaction.[3] Despite that, it is very challenging to conduct a successful concurrent chemoenzymatic reaction in a single-pot due to the differences in chemical and enzymatic reaction conditions followed by mutual deactivation of both catalysts.[3a, 4] Alternatively, the immobilization of both catalysts on solid surfaces avoids incompatibility between both catalysts and allows their recyclability, physical segregation, and separation.[5] Thus, the construction of heterogeneous nanobiohybrid catalyst fills the gap between chemical and enzymatic catalysis, allowing the chemoenzymatic process to perform in a concurrent manner within a single vessel.[6] The hybrid catalyst allows efficient, green, and sustainable chemoenzymatic reactions due to the slighter distance between dual catalytic active sites which could not be possible for individual metal nanoparticles and immobilized enzymes on various carriers.[7] For instance, the interfacial interactions can impact the catalytic activities of both catalysts which might influence the diffusion of reactants and reaction rates of chemoenzymatic processes. Therefore, while designing the heterogeneous nanobiohybrid catalyst it becomes important to understand the interfacial interactions between both of the catalysts to control the challenges of inherent complexity of chemoenzymatic processes.[8] Recently, certain developments have been made in the field of nanotechnology in the designing of nano-biohybrids.[9] However, among the various approaches used to generate nano-biohybrid catalysts, the immobilization of both entities on the same solid supports has been proven more successful since it offers a strong covalent interaction between the support and enzyme, reducing the likelihood of enzyme leakage.[9h] Additionally, after immobilization, there would be a lower chance of enzyme agglomeration on the support. [9i] On the other hand, in the CLEA (cross-linked enzyme aggregates) methodology, the problem of diffusion might arise due to the uncontrollable immobilization of metal nanoparticles.[6d] In addition, immobilizing the enzyme onto solid support enhances the catalyst's storage stability, and reusability, along with

operational and thermal stability.[9j] One such example of CLEA methodology illustrates the formation of enzyme polymer conjugates in which protein acts as a matrix for the generation of silver or gold nanoparticles retaining the catalytic activities of both entities towards the utilization in the chemoenzymatic process (**Scheme 2.1a**).[10] Likewise, Gallego and group members gave an idea to co-immobilize the gold nanoparticles and CALB onto a magnetic silica shell (**Scheme 2.1b**). They tried to investigate the synergistic kinetic effects of both constituents towards the cascade chemoenzymatic hydrolysis and reduction of para-nitrophenyl esters.[3a]

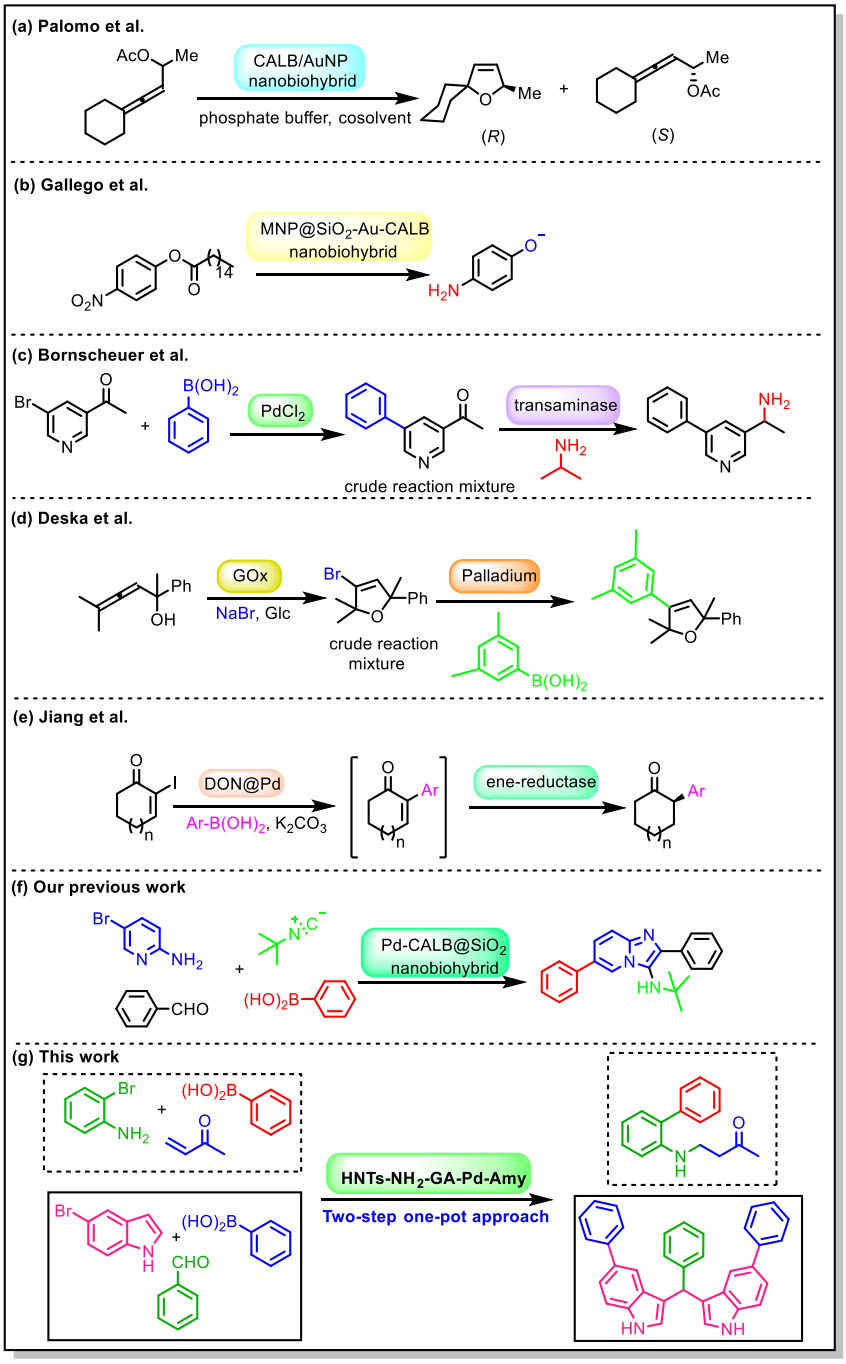

Scheme 2.1: Recently reported chemoenzymatic approaches

On the other hand, certain efforts were made to combine Suzuki-Miyaura coupling with other biocatalytic transformations to meet the chemoenzymatic approach. In this context, Bornscheuer et al. introduced chemoenzymatic two-step one-pot enantioselective synthesis of chiral amines via the Pd-catalyzed Suzuki cross-coupling followed by transaminase catalyzed bioreduction (**Scheme 2.1c**).[11] Furthermore, a combination of glucose oxidase matrix with palladium heterogeneous biohybrid has been disclosed by Deska and coworkers to integrally catalyze the enzyme-mediated biocyclization and metallic Suzuki cross-coupling (**Scheme 2.1d**).[12] In addition, Jiang and group members developed a one-pot synthetic route for the enantioselective synthesis of tertiary α-aryl cyclo ketones by merging the Pd-catalyzed Suzuki-Miyaura coupling and enzymatic stereoselective C-C bond reduction (**Scheme 2.1e**).[13] Moreover, we recently developed a bifunctional Pd-CALB@SiO_2 nanohybrid catalyst by encapsulation of both catalysts within silica (**Scheme 2.1f**). This biohybrid catalyst was utilized for the one-pot synthesis of imidazo[1,2]pyridine derivatives via Groebke-Black-burn-Bienayme (GBB) multicomponent reaction and Suzuki coupling.[14] Besides, HNTs are natural aluminosilicate clay material having a versatile solid surface. They are highly biocompatible, inert to organic solvents & reagents, easier to functionalize towards the immobilization of metal NPs and enzymes.[15] Drawing encouragement from the advantages of biohybrid catalysts and our previous work in this area, herein, we scrutinize the rational design of heterogeneous bifunctional catalyst by immobilization of palladium nanoparticles (PdNPs) and α-amylase from *Aspergillus oryzae* onto halloysite nanotubes (HNTs) in order to maximize the efficiency of chemoenzymatic synthesis of functionalized biphenyls and bisindoles (**Scheme 2.1g**).

2.2: Results and Discussion

2.2.1: Designing and Preparation of Hybrid Catalyst

We started this study by designing and preparing of heterogeneous hybrid catalyst by immobilizing the Pd-nanoparticles (PdNPs) and α-amylase enzyme (Amy) on the surface of halloysite nanotubes (HNTs). First, PdNPs were immobilized at HNTs, followed by the immobilization of α-amylase to deliver the hybrid catalyst i.e., HNTs-Pd-Amy (I) (**Scheme 2.5 & Figure 2.5**). Next, the reactivity of the developed hybrid catalyst (I) was tested to catalyze the one-pot chemoenzymatic reaction consisting of Suzuki-Miyaura and aza-Michael addition reactions respectively. Unfortunately, the prepared hybrid catalyst (I) was not able to perform the model chemoenzymatic reaction (**entry 1, Table 2.1**). Subsequently, we altered the immobilization order, first, α-amylase was immobilized at HNTs followed by the immobilization of PdNPs and as a result, obtained the hybrid catalyst HNTs-Amy-Pd (II) (**Scheme 2.6 & Figure 2.6**). The catalytic activity of the developed hybrid catalyst (II) was

tested, but still, there was no reaction (**entry 2, Table 2.1**). As both of the catalysts were unable to produce the desired product (**5a**), it indicated that both the constituents i.e., enzyme and metal of the hybrid catalyst were in direct contact with each other which might be leading to their mutual deactivation. To actualize our hypothesis, we functionalize the HNTs using OH-bonds situated at the surface. In this context, after the immobilization of PdNPs, the HNTs-Pd were treated with 3-aminopropyl triethoxy silane (APTES) which makes strong Si-O-Si bonds and provides a free NH_2 group away from the surface of HNTs.[16] Further, the amine-functionalized HNTs-Pd-NH_2 were treated with glutaraldehyde (GA) which provided a covalent binder to immobilize the α-amylase enzyme and afforded the hybrid catalyst HNTs-Pd-NH_2-GA-Amy (III) (**Scheme 2.7 & Figure 2.7**). Further, the hybrid catalyst (III) was employed in the chemoenzymatic reaction i.e., Suzuki-Miyaura coupling followed by the aza-Michael addition reaction and there was no reaction occurred (**entry 3, Table 2.1**). However, when we employed the hybrid catalyst (III) to catalyze the chemoenzymatic reaction in reverse order i.e., aza-Michael addition reaction first followed by Suzuki-Miyaura coupling, we obtained only Michael addition product in 58 % yield (**entry 3, Table 2.8**). This indicated that the immobilized enzyme was working well but the catalytic activity of PdNPs was completely lost. Then, we made changes in the immobilization order, first HNTs were functionalized using APTES and GA followed by the immobilization of PdNPs and enzyme respectively which afforded the hybrid catalyst HNTs-NH_2-GA-Pd-Amy (IV) as depicted in **Scheme 2.2**. Fortunately, the developed catalyst (IV) successfully catalyzed the one-pot chemoenzymatic reaction consisting of Suzuki-Miyaura coupling followed by an aza-Michael addition reaction and furnished the product (**5a**) in 47 % yield (**entry 4, Table 2.1**). This indicated that both catalysts were physically segregated over the HNTs, forcing the intermediate to diffuse from one catalyst to another to perform a successful one-pot chemoenzymatic reaction. Further, the hybrid catalyst HNTs-NH_2-GA-Pd-Amy (IV) was characterized by using several techniques like FTIR, XRD, SEM, EDS, HR-TEM, and elemental mapping analysis. When HNTs, HNTs-Pd, and pure α-amylase along with $Pd(OAc)_2$ were employed as a catalyst in the one-pot reaction, product **5(a)** was not observed (**entries 5-7, Table 2.1**). However, the Suzuki-Miyaura product was obtained while using HNTs-Pd as a catalyst (**entry 6, Table 2.8**). Furthermore, we also examined the relative activity of the biohybrid catalyst (IV) for individual reactions i.e. aza-Michael addition and Suzuki-Miyaura coupling reaction (**Table 2.7**). Likewise, the results demonstrated that the biohybrid catalyst (IV) was more effective than the catalysts in their native forms (**entries 1-3, Table 2.7**).

Table 2.1. One-pot chemoenzymatic approach[a]

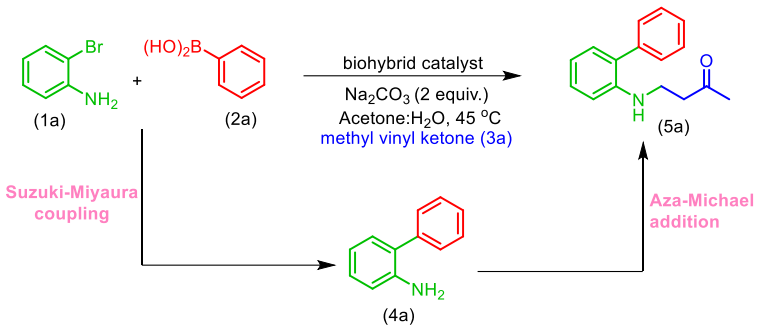

Entry	Catalyst	Product (5a)[c]
1	HNTs-Pd-Amy (I)	-
2	HNTs-Amy-Pd (II)	-
3	HNTs-Pd-NH_2-GA-Amy (III)	-[b]
4	HNTs-NH_2-GA-Pd-Amy (IV)	47% [c]
5	HNTs	-
6	HNTs-Pd	-[d]
7	α-amylase+$Pd(OAc)_2$	-[e]

[a]**Reaction conditions**: 2-Bromoaniline (**1a**) (0.06 mmol, 1.0 equiv.), phenylboronic acid (**2a**) (0.06 mmol, 1.0 equiv.), methyl vinyl ketone (**3a**) (0.06 mmol, 1.0 equiv.), catalyst 5 mg, Na_2CO_3 (0.12 mmol, 2 equiv.), acetone: H_2O (1:1) as a solvent, 45 °C, overnight. [b]Only aza-Michael product was obtained in 58% yield, [c]%conversion using HPLC, [d]Only Suzuki-Miyaura product was obtained in 89% yield, [e]pure enzyme and Pd-catalyst were added in the same pot.

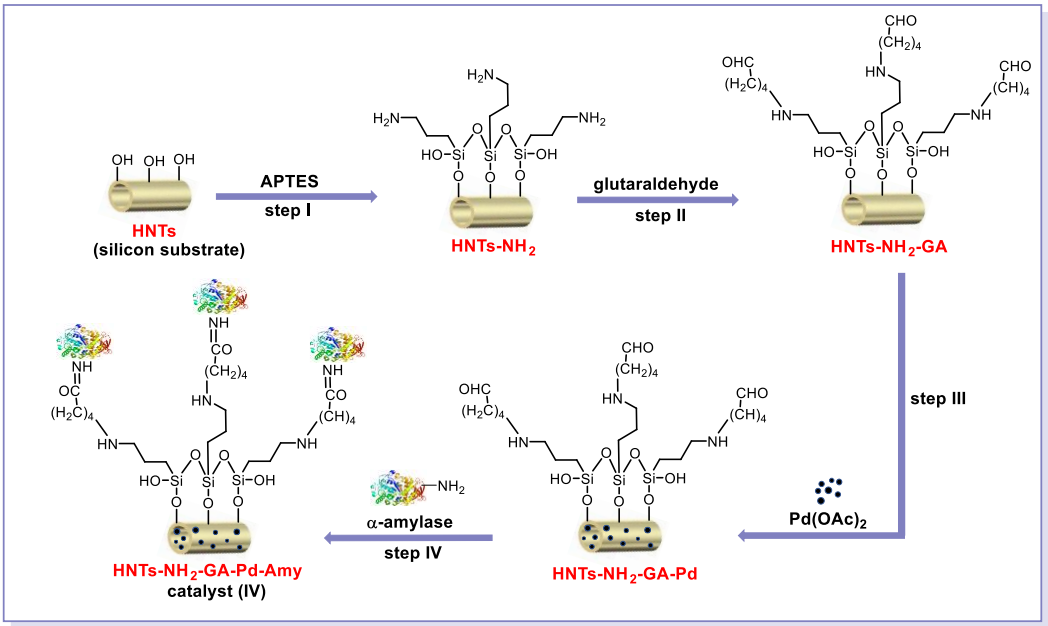

Scheme 2.2: Schematic representation of HNT-NH_2-GA-Pd-Amy (IV) synthesis

2.2.2: Characterization of Catalyst HNTs-NH_2-GA-Pd-Amy (IV)

2.2.2a: FTIR analysis

The immobilization of α-amylase on functionalized HNTs was initially analyzed by FTIR spectroscopy over the range of 4000-400 cm^{-1}. The absorption bands at 3630 and 903 cm^{-1} are attributed to inner Al-OH groups of HNTs.[17] In addition, the stretching bands between 1000-1200 cm^{-1} are due to Si-O-Si bonds of HNTs.[18] The broad peak at 3000 cm^{-1} is assigned to the stretching vibrations of the O-H bond. Further, the absorption peaks at 1580 and 1491 cm^{-1} in catalyst (IV) spectra were allocated to the amide II band as shown in **Figure 2.1**. Additionally, the absorption band positioned at 1286 cm^{-1} is assigned to the amide III bond which is due to the C-O-C stretching vibration. In the literature, similar findings were observed, and the appearance of bands 1400-1600 cm^{-1} and 1100-1300 cm^{-1} were attributed to the amide II and amide III bands respectively.[19] The detected spectral vibrations of catalyst (IV) validate the stable binding of α-amylase over functionalized HNTs. Along with this, it verifies the actual structural integrity of HNTs after profitable anchoring of α-amylase over functionalized HNTs.

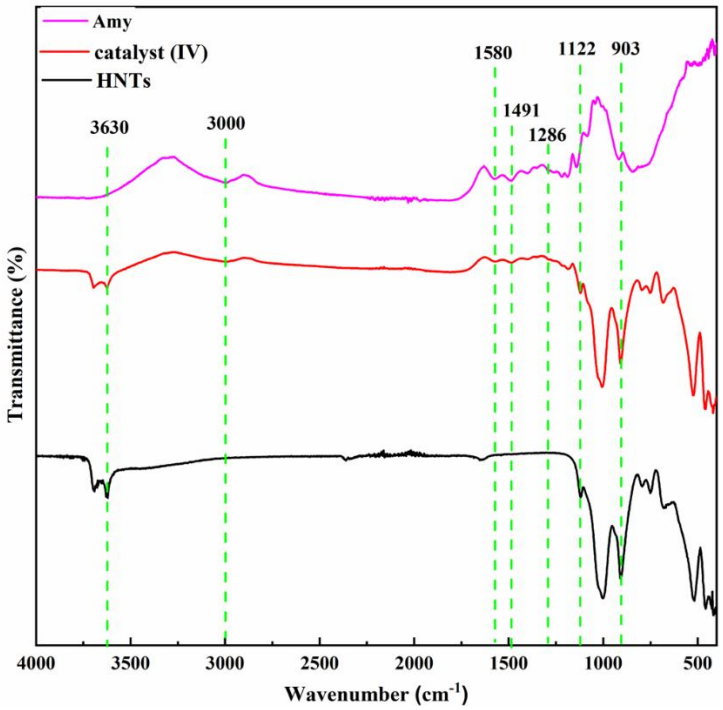

Figure 2.1: FTIR spectra of catalyst (IV)

2.2.2b: XRD analysis

To investigate the core structure or crystalline nature of the prepared nano biohybrid catalyst (IV), XRD analyses were carried out. The incorporation of successful PdNPs on HNTs in catalyst (IV) was confirmed by the appearance of diffraction peaks at 2θ = 40.04°, 45.83°, 68.23°, 82.32°, and 86.64°, corresponding to (111), (200), (220), (311), and (222) planes of PdNPs (JCPDS card no. 05-0681), as is documented in the literature.[20] Additionally, the above characteristic peaks of XRD pattern may be assigned to the face-centered cubic phase of Pd.[20a]

Moreover, proof of the HNTs matrix's sustained crystalline structure in the hybrid catalyst (IV) even after α-amylase immobilization can be seen in **Figure 2.2**, where 2θ diffraction peaks at 11.89°, 19.98° and 24.50° were indexed to the basal planes (001), (020), and (002) of HNTs respectively. However, the immobilization of the enzyme may have caused a slight decrease in peak intensity in the case of hybrid catalyst (IV) compared to pure HNTs powder. A similar modest decrease in peak intensity of the catalyst after enzyme immobilization was also noticed by Ali et al.[21] Overall, the absence of any additional peak indicated that fabricated PdNPs did not alter the structural characteristics of HNTs.

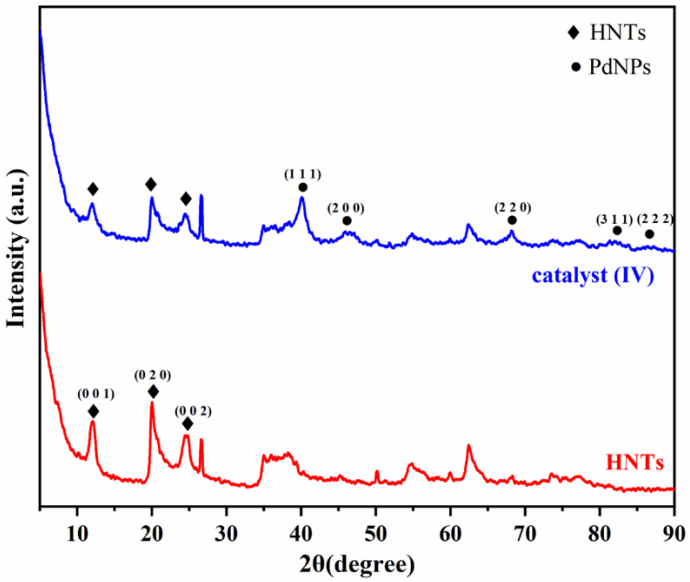

Figure 2.2: XRD analysis of catalyst (IV)

2.2.2c: FE-SEM-EDS, HR-TEM, elemental mapping analysis

The energy-dispersive spectroscopy (EDS) data of hybrid catalyst (IV) are presented in **Figure 2.3f**, which confirmed the successful fabrication of palladium nanoparticles on HNTs. Furthermore, the presence of element nitrogen depicted the loading of α-amylase over HNTs. The appearance of elements carbon, aluminum, silica, and oxygen corroborated towards aluminosilicates of HNTs. The catalyst (IV) was further investigated towards its outer structural morphology through FE-SEM where the uniform existence of PdNPs was found on HNTs (**Figure 2.3a**). Adding to this, no cluster formation of metal PdNPs was observed in the nanobiohybrid catalyst.

Moreover, the elemental mapping shown in **Figure 2.3b** depicted the even distribution of PdNPs and nitrogen on the prepared binary catalyst. Next, to know the inner morphology of the catalyst, HRTEM studies were conducted, which illustrated the presence of cylindrical tubes of HNTs in the range of 400-500 nm. This technique exemplified the existence of spherical nanoparticles of palladium that range in size from ~4-5 nm on the HNTs. The darker

region present over the HNTs might be due to the attachment of the enzyme (**Figure 2.3c-e**). Similar kinds of observations were also reported in the literature.[17] Thus, all these above characterization techniques validate the immobilization of enzyme and metal NPs on HNTs. Furthermore, in order to increase the loading of Pd onto the HNTs, we also tuned the amount of $Pd(OAc)_2$, and discovered that 10 mg of salt provided the highest Pd mass percentage, as shown in **Table 2.6**. Next, we altered the amount of α-amylase to achieve maximum loading onto the HNTs. We discovered that the best immobilization efficiency was 72.11% when enzyme concentration was kept at 3 mg/ml in the reaction (more details are given in section **2.2.8b**, **Figure 2.4)**.

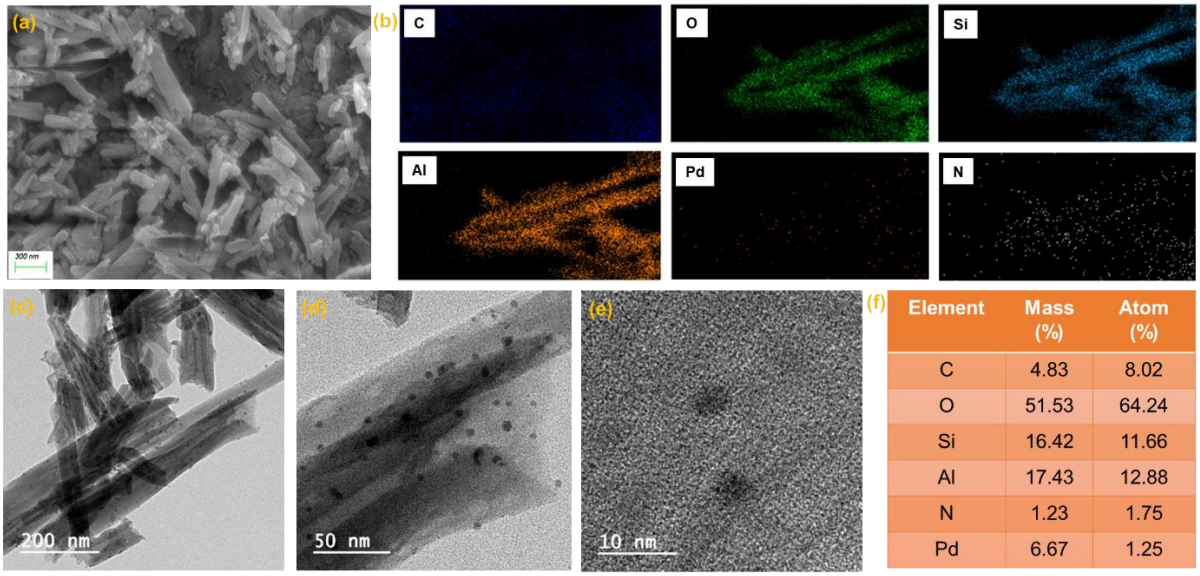

Element	Mass (%)	Atom (%)
C	4.83	8.02
O	51.53	64.24
Si	16.42	11.66
Al	17.43	12.88
N	1.23	1.75
Pd	6.67	1.25

Figure 2.3: (a) FE-SEM image of catalyst (IV) predicting the HNTs matrix remain intact even after immobilization of both metal and enzyme. (b) All elemental mapping images of the corresponding catalyst demonstrate the uniform fabrication of PdNPs on HNTs. (c-e) High-resolution TEM images of the hybrid catalyst (IV) Showing the presence of palladium & enzyme onto the halloysite nanotubes. (f) EDS data of the prepared catalyst HNTs-NH_2-GA-Pd-Amy (IV).

2.2.3: Optimization of the reaction conditions

After successfully developing a nano-biohybrid catalyst (IV), we explored its applications toward the synthesis of functionalized biphenyls using a one-pot chemoenzymatic approach consisting Suzuki-Miyaura and aza-Michael addition reactions. As we have obtained 47% conversion for the one-pot chemoenzymatic reaction (**entry 1, Table 2.2**), next, we decided to optimize the reaction conditions to improve the yield of this transformation. In this context, first, we changed the amount of catalyst (IV) from 5 mg to 2.5 mg, 10 mg, and 15 mg and found that 5 mg was a sufficient amount to obtain the maximum conversion in the model reaction (**entries 2-4, Table 2.2**). Then, we screened the ratio of substrates and found that 1:1.5:1.5

equiv. of 1a:2a:3a respectively was the best combination to achieve the best conversion (**entries 5-10, Table 2.2**). Further, we replaced Na_2CO_3 with Cs_2CO_3 and K_2CO_3, however, Na_2CO_3 remained the best base for this transformation (**entries 11-12, Table 2.2**). In the last, we screened different solvents and their combinations, however, we observed that the reaction gave maximum conversion when 50% acetone in H_2O (v/v) was used as a solvent (**entries 13-16, Table 2.2**). Also, there was no improvement when the temperature was increased, however, the yield dropped if the temperature goes below than 45°C.

Table 2.2: Optimization of reaction conditions[a]

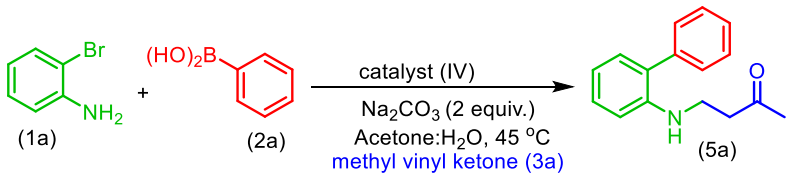

Entry	Deviation from standard reaction conditions	Conversion (5a)[b]
1	No deviation	**47%**
2	2.5 mg catalyst used	33%
3	10 mg catalyst used	48%
4	15 mg catalyst used	43%
5	1.5 equiv. of **2a** used	62%
6	2.0 equiv. of **2a** used	63%
7	3.0 equiv. of **2a** used	62%
8	1.0 equiv. of **3a** used	65%
9	1.2 equiv. of **3a** used	69%
10	1.5 equiv. of **3a** used	71%
11	Cs_2CO_3 instead of Na_2CO_3	37%
12	K_2CO_3 instead of Na_2CO_3	43%
13	H_2O only as a solvent	trace
14	Acetone only as a solvent	trace
15	EtOH in water (1:1, v/v)	19%
16	DMSO in water (1:1, v/v)	27%

[a]**Standard Reaction conditions:** 2-Bromoaniline (**1a**) (0.06 mmol, 1 equiv.), phenylboronic acid (**2a**) (0.06 mmol, 1.0 equiv.), methyl vinyl ketone (**3a**) (0.06 mmol, 1.0 equiv.), catalyst (IV)=5 mg, Na_2CO_3 (0.12 mmol, 2 equiv.), acetone: H_2O (1:1) as a solvent, 45◦C, overnight. [b] %conversion using HPLC.

2.2.4: Substrate scope for Suzuki-Miyaura coupling/aza-Michael addition reaction

Having the best reaction conditions, we explored the substrate scope for the one-pot chemoenzymatic reaction using a catalyst (IV) as shown in **Table 2.3**. In this regard, we checked the effect of substitutions at bromoaniline (**entries 1-6, Table 2.3**). The reaction gave good conversion when electron-donating groups like -CH_3 and halides were installed at the para position of 2-bromoaniline (**entries 2-4, Table 2.3**). However, there was no reaction took place when 4-NO_2 containing 2-bromoaniline was employed (**entry 5, Table 2.3**). Also, the reaction worked well in the case of 4-bromoanline instead of 2-bromoaniline (**entry 6, Table 2.3**). Next, we employed differently substituted phenylboronic acid along with 2-bromoaniline and methyl vinyl ketone. The electron-donating group such as -CH_3 and -OMe were tolerated well but surprisingly, there was no reaction in the case of 4-CN and 4-Br substitutions (**entries 7-10, Table 2.3**). Next, we evaluated the compatibility of substitutions at both 2-bromoanile and phenylboronic acid and obtained the corresponding products in 55% and 58% isolated yield (**entries 11-12, Table 2.3**). In the last, we replaced methyl vinyl ketone with cyclohexenone and cyclopentenone respectively, however, there was no reaction observed and it might be due increment in the steric hindrance during the aza-Michael addition reaction.

Table 2.3: Substrate scope of one-pot chemoenzymatic reaction[a]

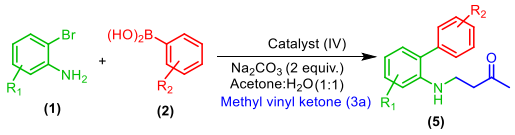

Entry	Bromoaniline (1)	Phenylboronic acid (2)	Product (5), yield[b]
1	 **1a**	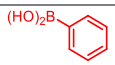 **2a**	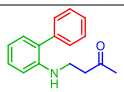 **5a**, 63%
2	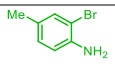 **1b**	**2a**	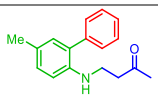 **5b**, 68%
3	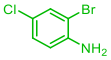 **1c**	**2a**	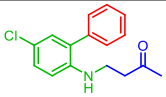 **5c**, 59%
4	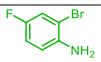 **1d**	**2a**	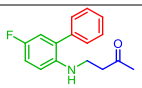 **5d**, 53%
5	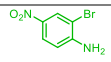		

	1e	**2a**	nr[c]
6	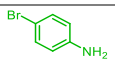 **1f**	**2a**	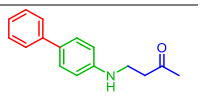 **5e**, 71%
7	**1a**	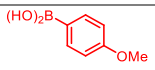 **2b**	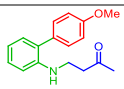 **5f**, 64%
8	**1a**	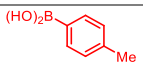 **2c**	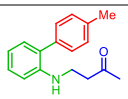 **5g**, 61%
9	**1b**	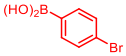 **2d**	nr[c]
10	**1a**	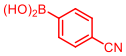 **2e**	nr[c]
11	**1c**	**2b**	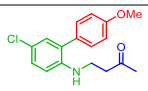 **5h**, 55%
12	**1b**	**2b**	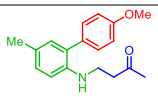 **5i**, 58%

[a]**Reaction conditions**: Bromoaniline (**1**) (1 equiv.), phenylboronic acid (**2**) (1.5 equiv.), methyl vinyl ketone (**3a**) (1.5 equiv.), catalyst (IV)=50 mg, Na_2CO_3 (2 equiv.), acetone: H_2O (1:1) as a solvent, 45 [o]C, overnight. [b]isolated yield, [c]nr=no reaction.

2.2.5: Reaction condition optimization for bis(indolyl)methanes synthesis

In the second phase of our endeavors, we planned to extend the application of constructed nano-biohybrid catalyst in the one-pot synthesis and functionalization of pharmacologically important bis(indolyl)methane derivatives. Initially, one-pot synthesis consisting Pd-catalyzed functionalization of 5-bromoindole using Suzuki-Miyaura coupling reaction followed by enzyme-catalyzed electrophilic synthesis of bis(indolyl)methane was set up using previously optimized reaction conditions (**Table 2.2**). Although, no bis(indolyl)methane product was observed in the one-pot chemoenzymatic reaction (**entry 1, Table 2.4**). Afterward, we changed the solvent system from 50% acetone in water (v/v) to 20% DMSO in H_2O which again did not lead to desired product (**entry 2, Table 2.4**). Subsequently, we put efforts towards the exchange

of solvent from 50% acetone in water (v/v) to 20% DMSO in H_2O after the completion of the first step i.e., Suzuki-Miyaura coupling. As it has been reported previously that 20% DMSO in H_2O is the better solvent system for enzyme-catalyzed synthesis of bis(indolyl)methane.[22] To our delight, we were successful this time to synthesize bis(indolyl)methane derivatives in one pot using chemoenzymatic approach (**entry 3, Table 2.4**). Also, we tried to change the loading of catalyst (IV) and molar ratio of substrates along with the reaction temperature but there was no improvement in the outcome of the reaction (**entries 4-7, Table 2.4**).

Table 2.4: Reaction conditions optimization[a]

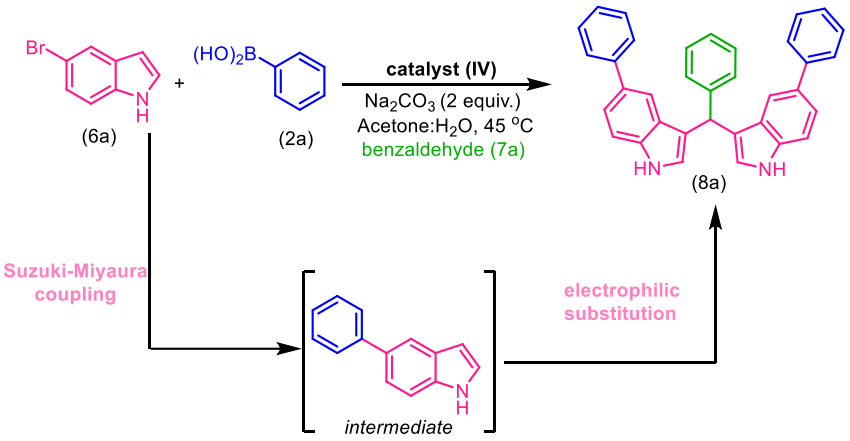

Entry	Deviation from standard reaction conditions	Yield (8a)[b]
1	No deviation	0%
2	20% DMSO in H_2O (v/v)	0%
3	First 50% acetone in H_2O (v/v) then 20%DMSO in H_2O(v/v)	57%
4	Catalyst (IV) 10 mg	53%
5	Molar ratio of **6a**:**2a**:**7a**=1:2:2 equiv.	56%
6	Temperature 60°C	53%
7	Temperature 25°C	-

[a]**Standard Reaction conditions:** 5-bromoindole (**1a**) (0.05 mmol, 1 equiv.), phenylboronic acid (**2a**) (0.08 mmol, 1.5 equiv.), benzaldehyde (**7a**) (0.03 mmol, 1.5 equiv.), catalyst (IV)=5 mg, Na_2CO_3 (0.09 mmol, 2 equiv.), acetone: H_2O (1:1) as a solvent, 45 °C, overnight. [b]%conversion using HPLC.

2.2.6: Substrate scope

Next, to extend the substrate scope of one-pot synthesis of functionalized bis(indolyl)methane, we examined differently substituted boronic acids and benzaldehydes as depicted in **Table 2.5**. Gratifyingly, there was no effect of different substitutions on the outcome of the reaction and we obtained the desired products in good yields (**entries 1-5, Table 2.5**).

Table 2.5: Substrate scope[a]

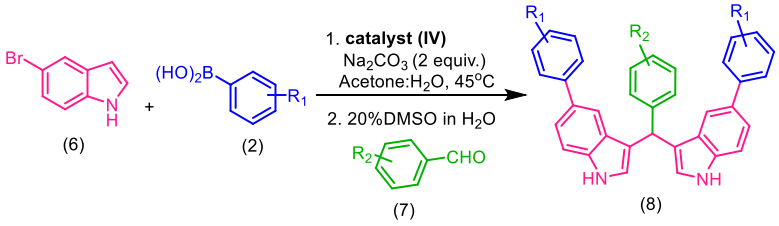

Entry	Phenyl boronic acid	Benzaldehyde	Product
1	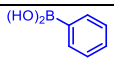 **2a**	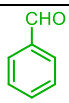 **7a**	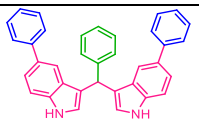 **8a**, 53%
2	**2a**	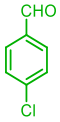 **7b**	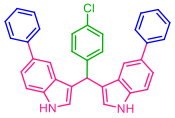 **8b**, 55%
3	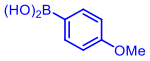 **2b**	 **7a**	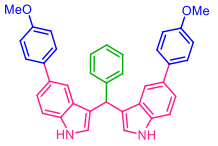 **8c**, 62%
4	**2b**	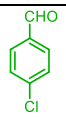 **7b**	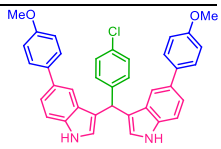 **8d**, 59%
5	**2a**	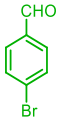 **7c**	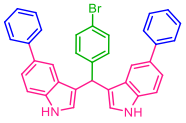 **8e**, 53%

[a]**Reaction conditions**: 5-bromoindole (**6**) (100 mg, 0.5 mmol, 1 equiv.), phenyl boronic acid (**2**) (98 mg, 0.8 mmol, 1.5 equiv.), benzaldehyde (**7**) (30 µL, 0.3 mmol, 1.5 equiv.), catalyst (IV) =50 mg, Na_2CO_3 (105 mg,1.0 mmol, 2 equiv.), acetone: H_2O (1:1) as a solvent which altered to DMSO:H_2O (20%) after completion of Suzuki reaction, 45 °C, overnight. [b]isolated yield.

2.2.7: Catalyst (IV)'s reusability, thermostability and shelf life

Next, we tested the catalyst (IV)'s ability to be reused in the one-pot cascade reaction. In this context, after the completion of the first cycle, the catalyst was separated by centrifugation and the resultant mixture was decanted. The above-separated catalyst was washed with isopropyl alcohol dried in a desiccator and used for a further catalytic cycle to produce the desired

functionalized biphenyls (**5a**). Gratifyingly, there was only a slight decrease in the yield of the desired product in consecutive cycles and catalyst was reusable up to five catalytic cycles (**Scheme 2.3**).

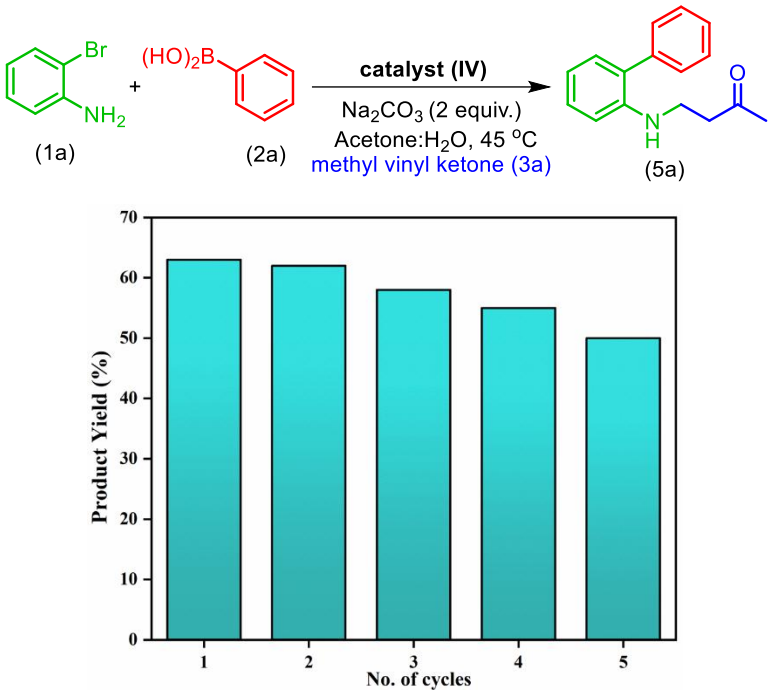

Scheme 2.3: Assessment of catalyst (IV)'s recyclability for the gram scale model reaction. Reaction conditions: 2-Bromoaniline (**1**) (1.00 g, 1 equiv.), phenylboronic acid (**2**) (1.06 g, 1.5 equiv.), methyl vinyl ketone (**3a**) (0.76 mL,1.5 equiv.), catalyst (IV)=500 mg, Na_2CO_3 (1.23 g, 2 equiv.), acetone: H_2O (1:1) as a solvent, 45 °C, overnight. %conversion yield using HPLC.

Moreover, we have tested the thermostability of hybrid catalyst (IV) and pure α-amylase enzyme for the model reaction at different reaction temperatures ranging from 40 to 100 °C (**Scheme 2.4a**). Gratifyingly, there was a slight decrement in the yield in the case of catalyst (IV) whereas the reaction almost diminished in the case of pure enzyme when temperature increased up to 100 °C. These experiments suggested the increment in the thermostability of α-

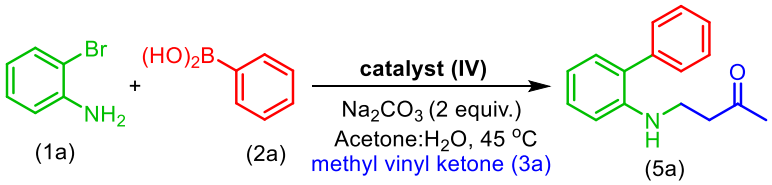

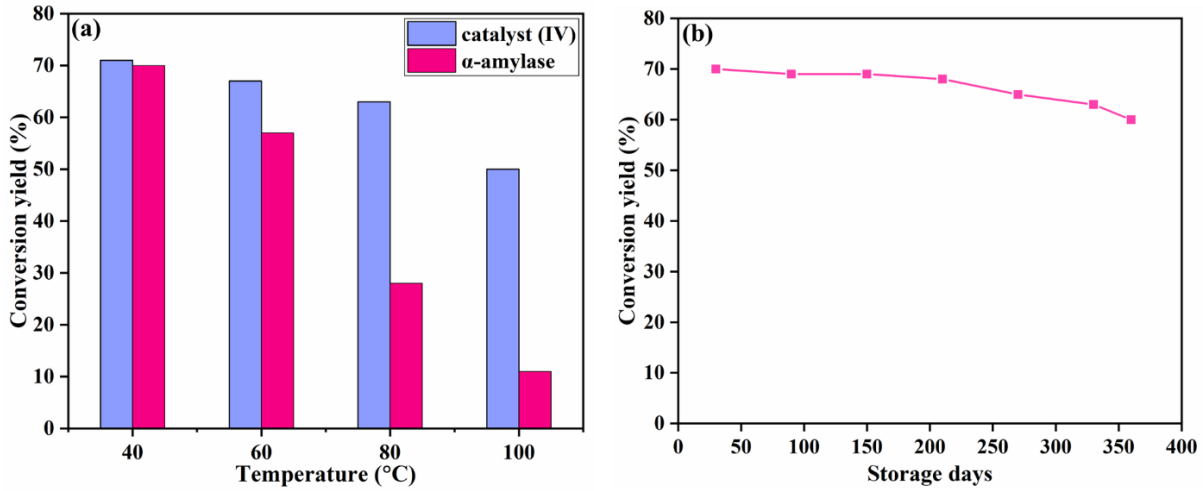

Scheme 2.4. Thermostability and shelf life of hybrid catalyst (IV) (a) Comparison of thermostability of catalyst (IV) with pure α-amylase enzyme. (b) Shelf life of hybrid catalyst (IV).

amylase enzyme after immobilization. Further, after 12 months of storage at room temperature in an airtight container, we examined the catalyst's effectiveness for the model reaction (**Scheme 2.4b**). Gratifyingly, the activity of the biohybrid catalyst (IV) did not much decline, and we successfully produced the cascade product (**5a**) with a 62% yield.

2.2.8: Optimization of Pd and α-amylase loading over HNTs

The immobilization efficiency of both Pd-nanoparticles and α-amylase over HNTs was optimized as given below.

2.2.8a: Effect of palladium concentration on immobilization: The PdNPs immobilization efficiency was checked by adjusting the amount of palladium salt i.e. $Pd(OAc)_2$ from 5 mg to 20 mg. At the very first, in a 50 mL beaker, a solution of $Pd(OAc)_2$ (5 mg to 20 mg, 0.07 equiv. to 0.27 equiv.) in deionized water (D.I.) was made. This solution was then treated with a solution of L-sodium ascorbate (235 mg, 3.5 equiv.) in D.I. water (5 mL), followed by the addition of trisodium citrate.$2H_2O$ (135 mg, 1.35 equiv.) in D.I. water (3.3 mL). The resulting mixture was stirred at room temperature for 15 min which induced black color solution due to the formation of PdNPs. Afterward, the solution was allowed to rest at rt for ~80 min. Then, the PdNPs solution was mixed with HNTs (100 mg, 1 equiv.), and the colloid combination was agitated for 15 min. After the rest of 10 min, the reaction mixture was subjected to centrifugation and the residue was washed with D.I water and isopropyl alcohol.[23] The resultant catalysts were characterized by EDS after drying at room temperature for 24 h in a desiccator. Thus, it was depicted by EDS studies (**Table 2.6**) that whenever we increase the amount of Pd-salt, the immobilization efficiency increases. Also, we tested Pd-HNTs with different loading

of Pd for catalyzing the Suzuki-Miyaura coupling reaction, however, we observed that Pd-HNTs prepared using 10 mg of $Pd(OAc)_2$ per 100 mg of HNTs was sufficient to complete the Suzuki-Miyaura coupling reaction, so we opted 10 mg of $Pd(OAc)_2$ per 100 mg of HNTs for the preparation of catalysts (1-IV)

Table 2.6: mass (%) ratio of Pd detected by EDS

Sr. No.	Pd salt (mg)	Mass (%)
1	5	1.27
2	10	2.51
3	15	3.78
4	20	6.64

2.2.8b: Effect of enzyme concentration: Different enzyme dosages, ranging from 1 mg/mL to 9 mg/mL, have been immobilized with the goal to calculate the amount of α-amylase immobilized onto HNTs. Initially, varied enzyme concentrations were made in a potassium phosphate buffer, and measured the absorbance at 289 nm. Further, 30 mg of imine functionalized HNTs-NH_2-GA support was added to the reaction mixture in order to get enzyme immobilization. Afterward, the solid support was separated by centrifugation and washed with phosphate buffer. Then, used the following formula (equation 1) to determine the enzyme immobilization efficiency of the support, taking into account the absorbance of residual and washings conducted after immobilization.

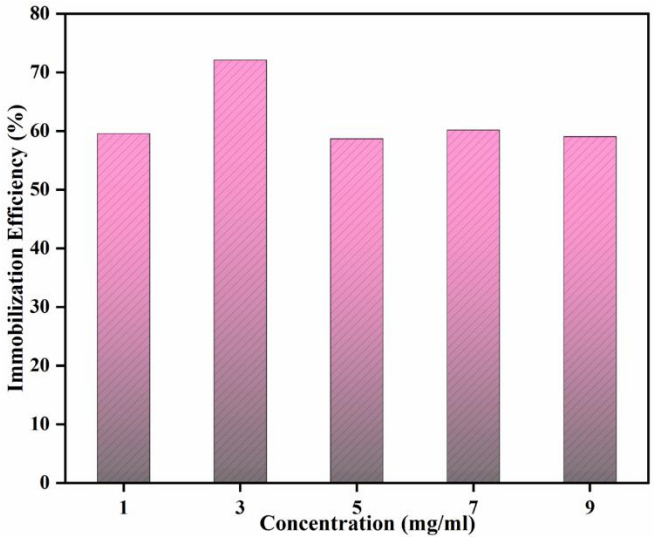

Figure 2.4: impact of α-amylase loading on immobilization efficiency

$$\text{Immobilization Efficiency (\%)} = \frac{A_{(pre)} - A_{(post)}}{A_{(pre)}} \times 100 \qquad (1)$$

Where A is α-amylase's 289 nm absorbance. The absorbance of the solution prior to enzyme immobilization is designated as $A_{(pre)}$, and the absorbance of the solution following enzyme immobilization is designated as $A_{(post)}$.[24]

As shown in the **figure 2.4** higher loading of α-amylase was noted at 3 mg/mL, afterward immobilization saturation occurred.

2.2.9: Comparison of relative activity of the biohybrid catalyst and native catalysts

To compare the catalytic effectiveness of a hybrid catalyst with an individual catalyst, we set up different experiments as displayed in **Table 2.7**. First, the Suzuki-Miyaura coupling reaction was set up using biohybrid catalyst (IV) under the optimized conditions and got the respective product (**4a**) with a conversion of 90% (**entry 1, Table 2.7**). Then, we set up the Michael addition reaction of (**4a**) with methyl vinyl ketone in the presence of biohybrid catalyst (IV) and obtained the resulting product (**5a**) in 71% yield (**entry 1, Table 2.7**). However, when we tested the catalytic effectiveness of the individual catalysts for the corresponding reactions, $Pd(OAc)_2$ yielded the Suzuki-Miyaura coupling product (**4a**) in 92% yield (**entry 2, Table 2.7**) and α-amylase as a biocatalyst for the aza-Michael addition reaction afforded the product (**5a**) in 63% yield (**entry 3, Table 2.7**). These experiments show the effectiveness of biohybrid catalyst (IV) in a sequential manner as compared to the individual catalysts.

Table 2.7: Comparative studies on the relative activity of the biohybrid catalyst (IV) and native catalysts[a]

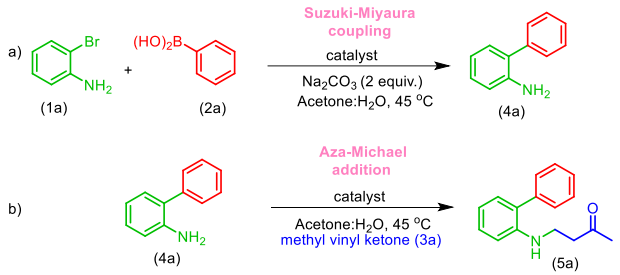

Entry	Catalyst	Conversion (4a)[b]	Conversion (5a)[b]
1	Biohybrid (IV)	90%	71%
2	$Pd(OAc)_2$	92%	-[c]
3	α-amylase	-	63%[d]

[a]**Reaction conditions**: (i) Suzuki-Miyaura coupling reaction: catalyst 5 mg, 2-bromoaniline (**1a**) (1 equiv.), phenylboronic acid (**2a**) (1.5 equiv.), Na_2CO_3 (2 equiv.), 2 ml of acetone:H_2O (1:1) as a solvent, 45 °C, overnight; (ii) aza-Michael addition reaction: **4a** (1 equiv.), methyl vinyl ketone (**3a**) (1.5 equiv.), catalyst 5 mg, 2 ml of acetone:H_2O (1:1) as a solvent, 45 °C. [b]%conversion using HPLC.

2.2.10: Quantification of the chemoenzymatic cascade's intermediates

We have quantified the by-product formed in the one-pot chemoenzymatic approach as shown in **Table 2.8**. We observed only the formation of Suzuki product (**4a**) in 89% when employing HNTs-Pd as a catalyst (**entry 6, Table 2.8**). Also, we observed only the aza-Michael addition product (**4a'**) in 58% yield when using catalyst HNTs-Pd-NH_2-GA-Amy (III) (**entry 3, Table 2.8**).

Table 2.8: Quantification of intermediates for chemoenzymatic cascade synthesis[a]

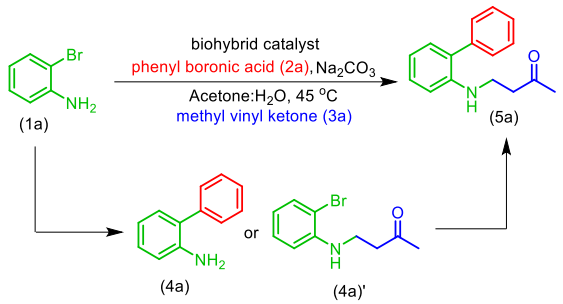

Entry	Catalyst	Product (4a)[b]	Product (4a')[b]	Product (5a)[b]
1	HNTs-Pd-Amy (I)	-	-	-
2	HNTs-Amy-Pd (II)	-	-	-
3	HNTs-Pd-NH_2-GA-Amy (III)	-	58%	-
4	HNTs-NH_2-GA-Pd-Amy (IV)	-	-	47% [b]
5	HNTs	-	-	-
6	HNTs-Pd	89%	-	-
7	α-amylase+$Pd(OAc)_2$	-	-	-[c]

[a]**Reaction conditions**: 2-Bromoaniline (**1a**) (0.06 mmol, 1.0 equiv.), phenylboronic acid (**2a**) (0.06 mmol, 1.0 equiv.), methyl vinyl ketone (**3a**) (0.06 mmol, 1.0 equiv.), catalyst 5 mg, Na_2CO_3 (0.12 mmol, 2 equiv.), acetone: H_2O (1:1) as a solvent, 45 °C, overnight. [b]%conversion using HPLC, [c]pure enzyme and Pd-catalyst were added in the same pot.

2.3: Experimental Section

2.3.1: General information

All solvents and chemicals were purchased commercially and used as such without further purification. HNTs and α-amylase were purchased from Sigma aldrich. The thin layer chromatography technique was used to monitor the progress of the cascade reaction. The desired products were purified by column chromatography using particular ratios of ethyl acetate and hexane as mobile phase over stationary phase silica (60-120 mesh size). The product conversion (%) was analyzed from Thermo scientific Dionex, Ultimate 3000 high

performance liquid chromatography (HPLC). JEOL NMR 400 MHz spectrometer was used to collect NMR spectra of synthesized compounds using $CDCl_3$ having TMS as an internal standard as a deuterated solvent. The coupling constant (*J*) and chemical shift (δ) is expressed in hertz (Hz) and parts per million (ppm) subsequently. The splitting of signals is abbreviated as; singlet (s), doublet (d), triplet (t), doublet of doublet (dd), triplet of doublet (td), doublet of triplet (dt), broad singlet (bs) and multiplet (m). The Fourier transform infrared FTIR spectrum was collected on IRT racer-100 spectrophotometer. The X-ray diffraction (XRD) analysis was performed on Rigaku SmartLab SE instrument with angle range 5 to 90 degree. Field emission scanning electron microscopy (Fe-SEM) and energy dispersive X-ray spectroscopy (EDS) studies were done on Zeiss device. The high-resolution images of the catalyst were captured by JEOL JEM 2100 PLUS instrument.

2.3.2: Procedure for the preparation of catalyst (IV)

2.3.2a: Surface modification of halloysite nanotubes: For the functionalization of HNTs, 200 mg HNTs was combined with 1 mL of 3-aminopropyltriethoxysilane. Then 20 mL of ethanol/acetic acid (3/5; v/v) was added as a co-solvent in a nitrogen environment. The resulting mixture was subjected to a 30 min sonication followed by heating for one hour at 110 ◦C. After the allotted time, the white-colored amine-modified HNTs were cooled and centrifuged at 7000 rpm, washed with ethanol (3 x 10 mL), and dried for an overnight period at 60 ◦C. The following stage involved adding amine functionalized HNTs to a 2.5% (v/v) glutaraldehyde solution and shaking it vigorously for 24 h at room temperature. The resulting mixture was centrifuged (7000 rpm) and the supernatant was separated from the white solid residue. The residue was rinsed multiple times with ethanol to get rid of any remaining glutaraldehyde molecules, then dried at 60 ◦C.

2.3.2b: Procedure for immobilization of palladium onto functionalized HNTs

In a beaker, $Pd(OAc)_2$ salt (15 mg, 0.13 equiv.) was dissolved in deionized water (2.5 mL). The resulted colloidal solution was subsequently treated with a solution of L-sodium ascorbate (350 mg, 3.5 equiv.) in deionized water followed by the addition of trisodium citrate.$2H_2O$ (200 mg, 1.35 equiv.) in deionized water. At room temperature, the mixed solution was allowed to stir for 15 min. The palladium acetate solution mixture's initial orange color changed to black during the first 10 min, signifying the emergence of Pd nanoparticles. The solution was allowed to rest at room temperature and exposed to air for 80 min.[23] Afterward, the resulting solution was mixed with surface functionalized HNTs (150 mg, 1 equiv.), and the colloid combination was stirred for 15 min. After stirring, it was left undisturbed for 10 min. The

reaction mixture was subjected to centrifugation and the residue was washed with D.I water (3 x 10 mL) and isopropyl alcohol (3 x 10 mL). The resultant grey powder was dried at 25 ºC in the desiccator for 24 h.

2.3.2c: Procedure for immobilization of α-amylase onto functionalized HNTs

The α-amylase was immobilized by combining 150 mg of HNT-NH_2-GA-Pd support with an optimized enzyme concentration of 3 mg/mL in 25 mL of potassium phosphate (KPi) buffer (100mM, pH 7.4) at 25 ºC with gentle stirring for overnight. After the mentioned time, it was transferred in a falcon tube and centrifuged at 8000 rpm. The obtained residue was washed with KPi buffer (3 x 10 mL) and then with distilled water (3 x 10 mL). The resultant grey coloured catalyst (IV) was dried at 40 ºC and kept in an air-tight container for further use.

2.3.3: General procedure for the one-pot chemoenzymatic synthesis of functionalized biphenyls

A mixture of 2-bromoaniline (**1a**) (100 mg, 1 equiv.), phenyl boronic acid (**2a**) (106 mg, 1.5 equiv.), catalyst (IV) (50 mg), and sodium carbonate (123 mg, 2 equiv.) in acetone:water (1:1) (10 mL) as a solvent was stirred for 5 hours in a round bottom flask at 45 ºC. The formation of Suzuki-Miyaura product was monitored by TLC, afterwards methyl vinyl ketone (**3a**) (70 µL, 1.5 equiv.) was added to the same reaction vessel and stirred the reaction mixture at 45 ºC for overnight. After completion of aza-Michael addition reaction, as indicated by TLC, the catalyst was separated by centrifugation and the reaction mixture was subjected to work-up using ethyl acetate and water. The final product was purified by column chromatography using silica as a stationary phase and ethyl acetate in hexane as a mobile phase. The resultant yellowish-brown viscous product (5a) was obtained in 63% isolated yield.

2.3.4: General procedure for the one-pot chemoenzymatic synthesis of bis(indolyl)methane derivatives

The 50 mg of biohybrid catalyst (IV) in 10 mL of acetone:H_2O (1:1) was added into a round bottom flask equipped with a stirrer bar. Then, 5-bromo indole (100 mg, 0.5 mmol, 1 equiv.), phenylboronic acid (98 mg, 0.8 mmol, 1.5 equiv.), and sodium carbonate (105 mg, 1.0 mmol, 2.0 equiv.) were added and agitated the reaction mixture at 45ºC. The formation of the Suzuki-Miyaura product was checked by TLC. Thereafter, the catalyst was recovered by centrifugation and the supernatant (reaction mixture) was poured into a separatory funnel for work-up. The crude combination was then re-added to the round bottom flask containing the recovered catalyst along with 20% DMSO in water as a solvent and benzaldehyde (30 µL, 0.3 mmol, 1.5

equiv.). After the overnight stirring at 45 °C, the reaction mixture was subjected to work-up followed by column chromatography using ethyl acetate and hexane as an eluting solvent (20:80) to get the pure product.

2.3.5: Synthesis and characterization of nano-biohybrid catalysts

2.3.5a: HNTs-Pd-Amy (Catalyst I)

HNTs were used as solid support for the preparation of catalyst I and they were treated with freshly made PdNPs according to the procedure followed for the preparation of catalyst (IV). After that, α-amylase was reacted with HNTs-Pd support at room temperature in phosphate buffer to get it immobilize (**Scheme 2.5**).

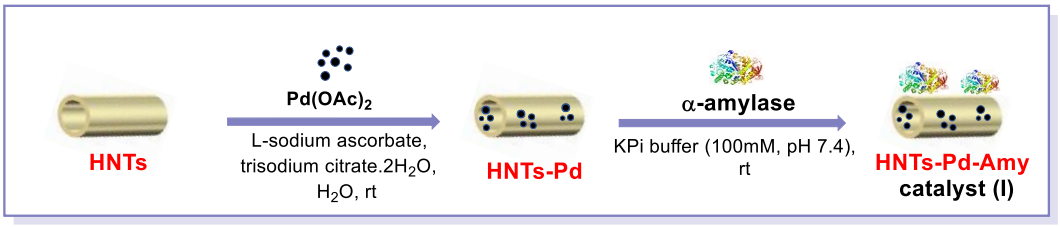

Scheme 2.5: Schematic representation of catalyst (I) preparation

Further, catalyst (I) was characterized by Fe-SEM and EDS to know the outer morphology and elemental composition of the catalyst respectively. The Fe-SEM image as shown in **Figure 2.5(a)** depicted the presence of Pd-nanoparticles in cluster form. Further EDS data provided insight into the presence of Pd and enzyme over HNTs by knowing the weight percentage **(Figure 2.5(b,c)).**

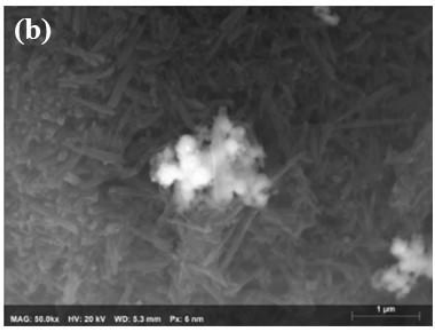

(c)

Element	C	O	Al	Si	Pd	N
Mass (%)	13.78	55.13	15.52	13.02	1.47	1.07

Figure 2.5: (a) Fe-SEM image and (b, c) EDS data of catalyst (I)

2.3.5b: HNTs-Amy-Pd (Catalyst II)

For the preparation of catalyst II, HNTs were treated with a freshly prepared α-amylase solution in phosphate buffer at room temperature. Next, enzyme-supported HNTs were treated with PdNPs in water for Pd-immobilization (**Scheme 2.6**).

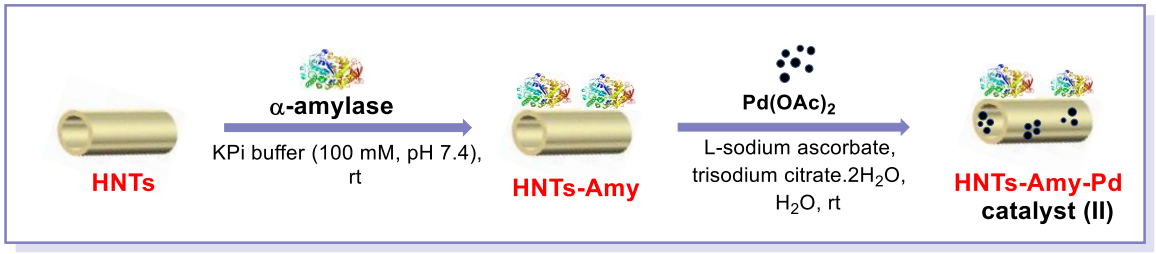

Scheme 2.6: Schematic representation of catalyst (II) preparation

The biohybrid catalyst was characterized by Fe-SEM and EDS for the confirmation of Pd and α-amylase enzyme onto HNTs. Again, PdNPs were in the form of clusters over the HNTs as shown in **Figure 2.6(a)**. Further, the EDS data depicted the presence of Pd (8.06%) and N (1.41%) which gave a clear indication of the successful immobilization of Pd and α-amylase enzyme onto HNTs (**Figure 2.6(b,c)**).

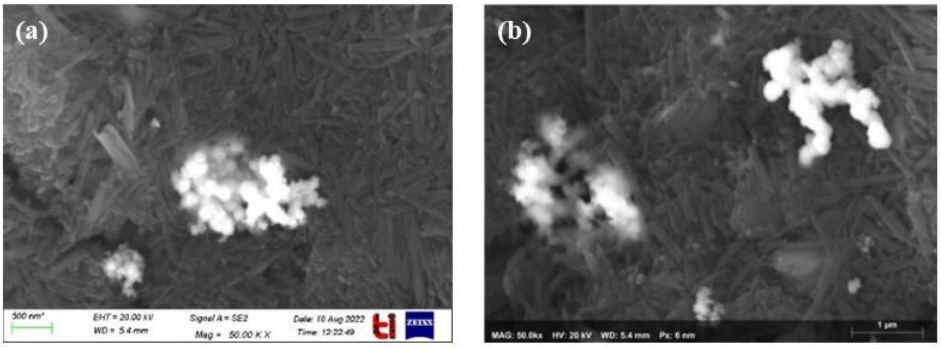

(c)

Element	C	O	Al	Si	Pd	N
Mass (%)	12.82	42.37	19.74	15.60	8.06	1.41

Figure 2.6: (a) FeSEM image and (b, c) EDS data of catalyst (II)

2.3.5c: HNTs-Pd-NH_2-GA-Amy (Catalyst III)

For the construction of catalyst (III), initially, HNTs were mixed with freshly produced PdNPs (according to the procedure used for catalyst (IV)) and then HNTs-Pd were dispersed with APTES solution under a nitrogen atmosphere for the amino-functionalization of HNTs. Afterward, the resulting amino-functionalized HNTs were subjected to glutaraldehyde solution at room temperature to generate HNTs-Pd-NH_2-GA which was further treated with α-amylase for immobilization of enzyme (**Scheme 2.7**).

Next, Fe-SEM and EDS techniques were utilized to know the successful loading of Pd and α-amylase (**Figure 2.7**). In this catalyst (III), uniform distribution of palladium was noticed under the scanning electron microscope. Moreover, EDS data gave an estimation of the presence of Pd and nitrogen in the catalyst.

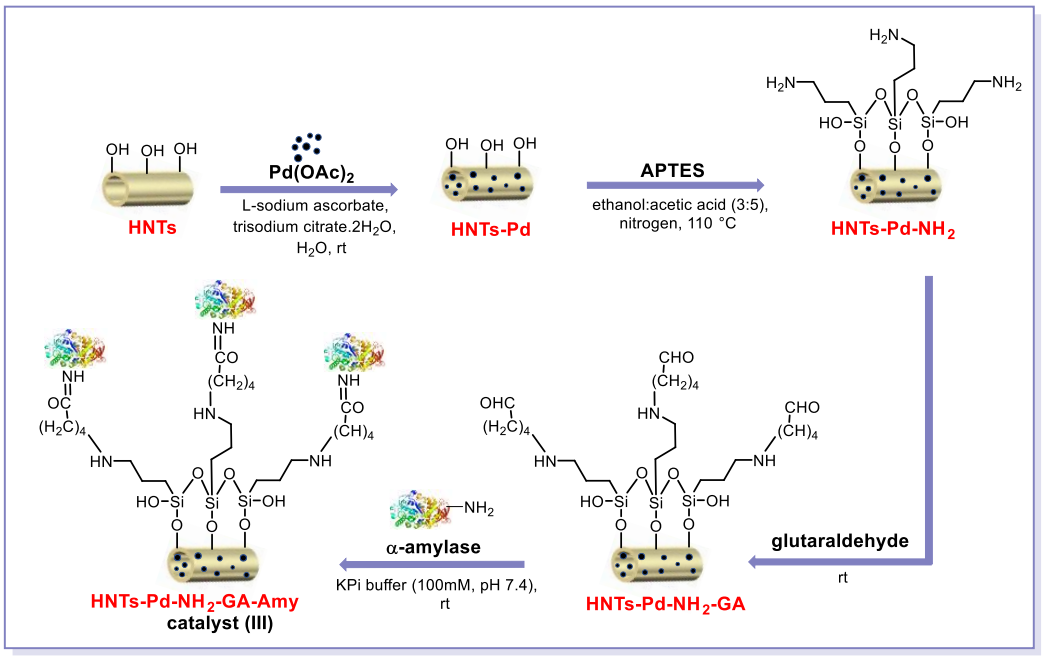

Scheme 2.7: Schematic representation of catalyst (III) preparation

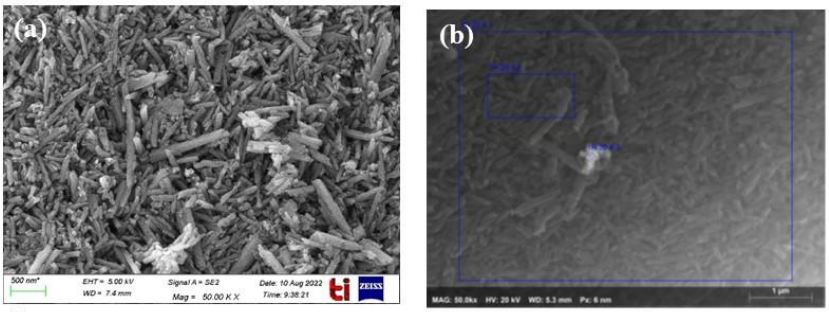

(c)

Element	C	O	Al	Si	Pd	N
Mass (%)	17.69	50.16	13.97	11.42	5.42	1.34

Figure 2.7: (a) FeSEM image and (b, c) EDS data of catalyst (III)

2.3.6: Characterization data of synthesized compounds

4-([1,1'-biphenyl]-2-ylamino)butan-2-one (5a): ^{1}H NMR (400 MHz, $CDCl_3$): δ 7.452-7.414 (m, 2H), 7.372-7.314 (m, 3H), 7.256-7.212 (m, 1H), 7.085 (dd, J = 7.2 Hz, 1.6 Hz, 1H), 6.770 (t, J = 7.6 Hz, 1H), 6.705 (d, J = 8.0 Hz, 1H), 4.167 (bs, 1H), 3.392 (t, J = 7.2 Hz, 2H), 2.689 (t, J = 6.4 Hz, 2H), 2.114 (s, 3H) ppm. ^{13}C NMR: δ 207.767, 144.577, 139.343, 130.532, 129.378, 129.006, 128.787, 128.234, 127.376, 117.288, 110.413, 42.732, 38.527, 30.422 ppm.

4-((5-methyl-[1,1'-biphenyl]-2-yl)amino)butan-2-one (5b): ^{1}H NMR (400 MHz, $CDCl_3$): δ 7.440-7.403 (m, 2H), 7.364-7.304 (m, 3H), 7.049 (dd, J = 8.4 Hz, 2.4 Hz, 1H), 6.917 (d, J = 2 Hz, 1H), 6.634 (d, J = 8 Hz, 1H), 4.014 (bs, 1H), 3.368 (t, J = 6.4 Hz, 2H), 2.674 (t, J = 6.4 Hz, 2H), 2.265 (s, 3H), 2.105 (s, 3H) ppm. ^{13}C NMR: δ 207.920, 142.298, 139.457, 131.276,

129.369, 129.130, 128.940, 128.415, 127.300, 126.527, 110.842, 42.799, 38.909, 30.413, 20.420 ppm.

4-((5-chloro-[1,1'-biphenyl]-2-yl)amino)butan-2-one (5c): ^{1}H NMR (400 MHz, $CDCl_3$): δ 7.453-7.415 (m, 2H), 7.376-7.309 (m, 3H), 7.169 (dd, *J* = 8.4 Hz, 2.8 Hz, 1H), 7.048 (d, *J* = 2.4 Hz, 1H), 6.603 (d, *J* = 8.4 Hz, 1H), 4.156 (bs, 1H), 3.351 (t, *J* = 6.4 Hz, 2H), 2.671 (t, *J* = 6.4 Hz, 2H), 2.112 (s, 3H) ppm. ^{13}C NMR: δ 207.614, 143.271, 138.027, 130.132, 129.569, 129.188, 129.159, 128.329, 127.872, 121.903, 111.500, 42.465, 38.584, 30.441 ppm.

4-((5-fluoro-[1,1'-biphenyl]-2-yl)amino)butan-2-one (5d): ^{1}H NMR (400 MHz, $CDCl_3$): δ 7.460-7.420 (m, 2H), 7.377-7.322 (m, 3H), 6.932 (td, *J* = 8.8 Hz, 3.2 Hz, 1H), 6.837 (dd, *J* = 9.2 Hz, 2.8 Hz, 1H), 6.622 (dd, *J* = 9.2 Hz, 5.2 Hz, 1H), 3.981 (bs, 1H), 3.339 (t, *J* = 6.4 Hz, 2H), 2.663 (t, *J* = 6.4 Hz, 2H), 2.110 (s, 3H) ppm. ^{13}C NMR: δ 207.700, 156.830, 154.484, 141.059, 138.322, 129.188, 129.111, 127.815, 117.288, 117.059, 114.828, 114.618, 111.557, 111.481, 42.637, 39.271, 30.394 ppm.

4-([1,1'-biphenyl]-4-ylamino)butan-2-one (5e): ^{1}H NMR (400 MHz, $CDCl_3$): δ 7.525 (d, *J* = 6.8 Hz, 2H), 7.433 (dt, *J* = 8.8 Hz, 2.8 Hz, 2H), 7.382 (t, *J* = 7.6 Hz, 2H), 7.248 (t, *J* = 8.4 Hz, 1H), 6.668 (dt, *J* =8.8 Hz, 3.2 Hz, 2H), 4.087 (bs, 1H), 3.452 (t, *J* = 6.0 Hz, 2H), 2.769 (t, 6.0 Hz, 2H), 2.170 (s, 3H) ppm. ^{13}C NMR: δ 208.253, 147.171, 141.250, 130.627, 128.759, 128.110, 126.394, 126.222, 113.331, 42.656, 38.413, 30.460 ppm.

4-((4'-methoxy-[1,1'-biphenyl]-2-yl)amino)butan-2-one (5f): ^{1}H NMR (400 MHz, $CDCl_3$): δ 7.284 (dt, *J* = 8.8 Hz, 2.8 Hz, 2H), 7.214 (td, *J* = 8.0 Hz, 1.6 Hz, 1H), 7.065 (dd, *J* = 7.2 Hz, 1.2 Hz, 1H), 6.968 (dt, *J* = 8.4 Hz, 2.8 Hz, 2H), 6.755 (td, *J* = 7.2 Hz, 0.8 Hz, 1H), 6.687 (d, *J* = 8.0 Hz, 1H), 4.265 (bs, 1H), 3.842 (s, 3H), 3.390 (t, *J* = 6.4 Hz, 2H), 2.693 (t, *J* = 6.4 Hz, 2H), 2.119 (s, 3H) ppm. ^{13}C NMR: δ 207.881, 158.890, 144.778, 131.514, 130.599, 130.484, 128.520, 127.910, 117.250, 114.408, 110.298, 55.395, 42.751, 38.518, 30.432 ppm.

4-((4'-methyl-[1,1'-biphenyl]-2-yl)amino)butan-2-one (5g): ^{1}H NMR (400 MHz, $CDCl_3$): δ 7.256-7.207 (m, 5H), 7.083 (dd, *J* = 7.6 Hz, 2.0 Hz, 1H), 6.766 (td, *J* = 7.6 Hz, 1.2 Hz, 1H), 6.7 (d, *J* = 8.0 Hz, 1H), 4.184 (bs, 1H), 3.398 (t, *J* = 6.4 Hz, 2H), 2.696 (t, *J* = 6.4 Hz, 2H), 2.399 (s, 3H), 2.125 (s, 3H) ppm. ^{13}C NMR: δ 207.834, 144.654, 137.054, 136.320, 130.561, 129.731, 129.226, 128.616, 128.205, 117.269, 110.327, 42.761, 38.537, 30.422, 21.326 ppm.

4-((5-chloro-4'-methoxy-[1,1'-biphenyl]-2-yl)amino)butan-2-one (5h): ^{1}H NMR (400 MHz, $CDCl_3$): δ 7.242 (dt, *J* = 8.8 Hz, 2.8 Hz, 2H), 7.145 (dd, *J* = 8.8 Hz, 2.8 Hz, 1H), 7.023 (d, *J* = 2.8 Hz, 1H), 6.959 (dt, *J* = 8.4 Hz, 3.2 Hz, 2H), 6.580 (d, *J* = 8.4 Hz, 1H), 4.137 (bs, 1H), 3.836 (s, 3H), 3.345 (t, *J* = 6.4 Hz, 2H), 2.672 (t, *J* = 6.4 Hz, 2H), 2.115 (s, 3H) ppm. ^{13}C

NMR: δ 207.589, 159.206, 143.448, 130.317, 130.170, 129.314, 128.008, 121.846, 114.526, 111.359, 55.400, 42.483, 38.606, 30.405 ppm.

4-((4'-methoxy-5-methyl-[1,1'-biphenyl]-2-yl)amino)butan-2-one (5i): ^{1}H NMR (400 MHz, $CDCl_3$): δ 7.276 (dt, *J* = 8.8 Hz, 2.8 Hz, 2H), 7.029 (dd, *J* = 8.0 Hz, 2.4 Hz, 1H), 6.957 (dt, *J* = 8.4 Hz, 2.8 Hz, 2H), 6.897 (d, *J* = 2.4 Hz, 1H), 6.615 (d, *J* = 8.4 Hz, 1H), 3.990 (bs, 1H), 3.839 (s, 3H), 3.367 (t, *J* = 6.4 Hz, 2H), 2.675, (t, *J* = 6.4 Hz, 2H), 2.258 (s, 3H), 2.110 (s, 3H) ppm. ^{13}C NMR: δ 207.920, 158.852, 142.489, 131.657, 131.362, 130.456, 128.835, 128.101, 126.480, 114.351, 110.728, 55.395, 42.837, 38.937, 30.394, 20.429 ppm.

3,3'-(phenylmethylene)bis(5-phenyl-1*H*-indole) (8a): ^{1}H NMR (400 MHz, $CDCl_3$): δ 7.951 (bs, 2H), 7.593 (s, 2H), 7.519 (d, *J* = 2.4 Hz, 2H), 7.498 (s, 2H), 7.413 (t, *J* = 1.6 Hz, 4H), 7.381 (d, *J* = 2.8 Hz, 2H), 7.366 (t, *J* = 2.8 Hz, 3H), 7.340 (s, 1H), 7.294 (d, *J* = 6.8 Hz, 2H), 7.265 (s, 1H), 7.228-7.194 (m, 2H), 6.707 (d, *J* = 2.8 Hz, 2H), 5.959 (s, 1H) ppm. ^{13}C NMR: δ 143.977, 142.594, 136.358, 132.935, 128.835, 128.663, 128.406, 127.652, 127.500, 126.318, 124.506, 121.931, 120.110, 118.518, 111.405, 40.320 ppm.

3,3'-((4-chlorophenyl)methylene)bis(5-phenyl-1*H*-indole) (8b): ^{1}H NMR (400 MHz, $CDCl_3$): δ 7.943 (bs, 2H), 7.578 (s, 2H), 7.528 (d, *J* = 8.0 Hz, 4H), 7.444 (d, *J* = 8.8 Hz, 3H), 7.405 (s, 2H), 7.375 (d, *J* = 7.2 Hz, 4H), 7.309 (s, 1H), 7.272-7.239 (m, 4H), 6.656 (s, 2H), 5.940 (s, 1H) ppm. ^{13}C NMR: δ 142.575, 142.499, 136.358, 133.097, 132.000, 130.198, 128.749, 128.568, 127.509, 127.462, 126.441, 124.544, 122.103, 119.567, 118.356, 111.548, 39.719 ppm.

3,3'-(phenylmethylene)bis(5-(4-methoxyphenyl)-1*H*-indole)(8c): ^{1}H NMR (400 MHz, $CDCl_3$): δ 7.940 (bs, 2H), 7.527 (s, 2H), 7.435 (t, *J* = 3.2 Hz, 2H), 7.413 (t, *J* = 2.4 Hz, 2H), 7.373 (s, 4H), 7.358 (s, 1H), 7.275 (t, *J* = 7.2 Hz, 3H), 7.223-7.179 (m, 1H), 6.912 (t, *J* = 3.2 Hz, 2H), 6.891 (t, *J* = 2.0 Hz, 2H), 6.694 (d, *J* = 2.8 Hz, 2H), 5.936 (s, 1H), 3.805 (s, 6H) ppm. ^{13}C NMR: δ 158.461, 144.015, 136.053, 135.252, 132.573, 128.835, 128.415, 128.368, 127.767, 126.298, 124.439, 121.693, 120.034, 118.003, 114.103, 111.328, 55.424 ppm.

3,3'-((4-chlorophenyl)methylene)bis(5-(4-methoxyphenyl)-1*H*-indole) (8d): ^{1}H NMR (400 MHz, $CDCl_3$): δ 7.944 (bs, 2H), 7.500 (s, 2H), 7.433 (d, *J* = 8.8 Hz, 4H), 7.384 (s, 4H), 7.290 (d, *J* = 8.8 Hz, 2H), 7.237 (d, *J* = 8.4 Hz, 2H), 6.916 (d, *J* = 8.8 Hz, 4H), 6.664 (d, *J* = 2.8 Hz, 2H), 5.912 (s, 1H), 3.812 (s, 6H) ppm.^{13}C NMR: δ 158.527, 142.594, 136.034, 135.138, 132.754, 131.943, 130.198, 128.530, 128.444, 127.452, 124.468, 121.865, 119.490, 117.850, 114.151, 111.433, 55.443 ppm.

3,3'-((4-bromophenyl)methylene)bis(5-phenyl-1*H*-indole) (8e): ^{1}H NMR (400 MHz, $CDCl_3$): δ 7.983 (bs, 2H), 7.553 (s, 2H), 7.517 (d, *J* = 1.6 Hz, 2H), 7.495 (s, 2H), 7.427-7.403

(m, 5H), 7.386 (s, 2H), 7.367 (s, 2H), 7.348 (s, 1H), 7.270-7.248 (m, 2H), 7.231 (s, 2H), 6.700 (d, *J* = 2.8 Hz, 2H), 5.918 (s, 1H) ppm. ^{13}C NMR: δ 158.527, 142.594, 136.034, 135.138, 132.754, 131.943, 130.198, 128.530, 128.444, 127.452, 124.468, 121.865, 119.490, 117.850, 114.151, 111.433, 55.443 ppm.

2.4: Conclusion

In summary, we have designed and prepared a bifunctional nano-biohybrid catalyst by immobilization of PdNPs and α-amylase on halloysite nanotubes. Further, the successful incorporation of both the catalysts i.e. PdNPs and α-amylase on halloysite nanotubes was confirmed by using FTIR, XRD, FE-SEM, EDS, HR-TEM techniques. Besides, the synthetic utility of developed nanobiohybrid catalyst was demonstrated by catalyzing one-pot chemoenzymatic reaction consisting Pd-catalyzed Suzuki-Miyaura coupling and α-amylase mediated aza-Michael addition reaction to synthesized functionalized biphenyls. Next, the wider applicability of the constructed nanobiohybrid catalyst was examined on the Pd-catalyzed Suzuki-Miyaura coupling of 5-bromo indoles with aryl boronic acids and subsequent α-amylase catalyzed electrophilic substitution of different benzaldehydes to furnish biologically active substituted bis(indolyl)methanes in good yields. These results indicates that the nanobiohybrid approach has an ample potential to conduct multi-catalytic cycles in a single pot in an efficient manner. Furthermore, the prepared nanobiohybrid catalyst (IV) was found to be recyclable up to five consecutive cycles and highly stable when stored at room temprature for the period of 12 months.

2.5: References

1. (a) Bering, L.; Thompson, J.; Micklefield, J. New Reaction Pathways by Integrating Chemo-and Biocatalysis. *Trends Chem.* **2022**, *4*, 392-408. (b) Heuson, E.; Dumeignil, F. The Various Levels of Integration of Chemo- and Bio-Catalysis towards Hybrid Catalysis. *Catal. Sci. Technol.* **2020**, *10*, 7082–7100. (c) Rudroff, F.; Mihovilovic, M. D.; Gröger, H.; Snajdrova, R.; Iding, H.; Bornscheuer, U. T. Opportunities and Challenges for Combining Chemo- and Biocatalysis. *Nat. Catal.* **2018**, *1*, 12–22. (d) Gröger, H.; Gallou, F.; Lipshutz, B. H. Where Chemocatalysis Meets Biocatalysis: In Water. *Chem. Rev.* **2022**, *123*, 5262–5296.
2. (a) An, C.; Maloney, K. M. Designing for Sustainability with Biocatalytic and Chemoenzymatic Cascade Processes. *Curr. Opin. Green Sustain. Chem.* **2022**, *34*, 100591. (b) Denard, C. A.; Hartwig, J. F.; Zhao, H. Multistep One-Pot Reactions Combining

Biocatalysts and Chemical Catalysts for Asymmetric Synthesis. *ACS Catal.* **2013**, *3*, 2856–2864.c) Simons, C.; Hanefeld, U.; Arends, I. W.; Maschmeyer, T.; Sheldon, R. A. Towards Catalytic Cascade Reactions: Asymmetric Synthesis Using Combined Chemo-Enzymatic Catalysts. *Top. Catal.* **2006**, *40*, 35–44.

3. (a) de Barros, H. R.; Tanaka, L. Y.; da Silva, R. T. P.; Santiago-Arcos, J.; de Torresi, S. I. C.; López-Gallego, F. Assembly of Nano-Biocatalyst for the Tandem Hydrolysis and Reduction of *p*-Nitrophenol Esters. *Part. Part. Syst. Charact.* **2021**, *38*, 2100136. (b) Durchschein, K.; Hall, M.; Faber, K. Unusual Reactions Mediated by FMN-Dependent Ene- and Nitro-Reductases. *Green Chem.* **2013**, *15*, 1764–1772.
4. Yin, H.; Luan, P. Q.; Cao, Y. F.; Ge, J.; Lou, W. Y. Coupling Metal and Whole-Cell Catalysis to Synthesize Chiral Alcohols. *Bioresour. Bioprocess.* **2022**, *9*, 73.
5. (a) Palomo, J. M. Nanobiohybrids: A New Concept for Metal Nanoparticles Synthesis. *Chem. Commun.* **2019**, *55*, 9583–9589. (b) Debecker, D. P.; Smeets, V.; Verren, M. V.; Arango, H. M.; Kinnaer, M.; Devred, F. Hybrid Chemoenzymatic Heterogeneous Catalysts. *Curr. Opin. Green Sustain. Chem.* **2021**, *28*, 100437.
6. (a) de Barros, H. R.; Tanaka, L. Y.; da Silva, R. T. P.; Santiago-Arcos, J.; de Torresi, S. I. C.; López-Gallego, F. Assembly of Nano-Biocatalyst for the Tandem Hydrolysis and Reduction of *p*-Nitrophenol Esters. *Part. Part. Syst. Charact.* **2021**, *38*, 2100136. (b) Durchschein, K.; Hall, M.; Faber, K. Unusual Reactions Mediated by FMN-Dependent Ene- and Nitro-Reductases. *Green Chem.* **2013**, *15*, 1764–1772.
7. Yin, H.; Luan, P. Q.; Cao, Y. F.; Ge, J.; Lou, W. Y. Coupling Metal and Whole-Cell Catalysis to Synthesize Chiral Alcohols. *Bioresour. Bioprocess.* **2022**, *9*, 73.
8. (a) Palomo, J. M. Nanobiohybrids: A New Concept for Metal Nanoparticles Synthesis. *Chem. Commun.* **2019**, *55*, 9583–9589. (b) Debecker, D. P.; Smeets, V.; Verren, M. V.; Arango, H. M.; Kinnaer, M.; Devred, F. Hybrid Chemoenzymatic Heterogeneous Catalysts. *Curr. Opin. Green Sustain. Chem.* **2021**, *28*, 100437.
9. (a) Li, X.; Cao, Y.; Luo, K.; Sun, Y.; Xiong, J.; Wang, L.; Liu, Z.; Li, J.; Ma, J.; Ge, J.; Xiao, H.; Zare, R. N. Highly Active Enzyme–Metal Nanohybrids Synthesized in Protein–Polymer Conjugates. *Nat. Catal.* **2019**, *2*, 718–725. (b) Wang, Y.; Zhang, N.; Zhang, E.; Han, Y.; Qi, Z.; Ansorge-Schumacher, M. B.; Ge, Y.; Wu, C. Heterogeneous Metal–Organic-Framework-Based Biohybrid Catalysts for Cascade Reactions in Organic Solvent. *Chem. Eur. J.* **2019**, *25*, 1716–1721. (c) Qi, L.; Chen, J.; Zhang, B.; Nie, R.; Qi, Z.; Kobayashi, T.; Bao, Z.; Yang, Q.; Ren, Q.; Sun, Q.; Zhang, Z. Deciphering a Reaction Network for the Switchable Production of Tetrahydroquinoline or Quinoline with MOF-Supported Pd Tandem Catalysts. *ACS Catal.* **2020**, *10*, 5707–5714. (d) Zhang, N.; Hübner, R.; Wang, Y.; Zhang, E.; Zhou, Y.; Dong, S.; Wu, C. Surface-Functionalized Mesoporous Nanoparticles as Heterogeneous Supports to Transfer

Bifunctional Catalysts into Organic Solvents for Tandem Catalysis. *ACS Appl. Nano Mater.* **2018**, *1*, 6378–6386. (e) Gao, L.; Wang, Z.; Liu, Y.; Liu, P.; Gao, S.; Gao, J.; Jiang, Y. Co-Immobilization of Metal and Enzyme into Hydrophobic Nanopores for Highly Improved Chemoenzymatic Asymmetric Synthesis. *Chem. Commun.* **2020**, *56*, 13547–13550. (f) Chang, F.; Wang, C.; Chen, Q.; Zhang, Y.; Liu, G. A Chemoenzymatic Cascade Combining a Hydration Catalyst with an Amine Dehydrogenase: Synthesis of Chiral Amines. *Angew. Chem., Int. Ed.* **2022**, *61*, e202114809. (g) Huang, X.; Cao, M.; Zhao, H. Integrating Biocatalysis with Chemocatalysis for Selective Transformations. *Curr. Opin. Chem. Biol.* **2020**, *55*, 161–170. (h) Zdarta, J.; Meyer, A. S.; Jesionowski, T.; Pinelo, M. A General Overview of Support Materials for Enzyme Immobilization: Characteristics, Properties, Practical Utility. *Catalysts* **2018**, *8*, 92. (i) Giri, P.; Pagar, A. D.; Patil, M. D.; Yun, H. Chemical Modification of Enzymes to Improve Biocatalytic Performance. *Biotechnol. Adv.* **2021**, *53*, 107868. (j) Zhai, R.; Zhang, B.; Liu, L.; Xie, Y.; Zhang, H.; Liu, J. Immobilization of Enzyme Biocatalyst on Natural Halloysite Nanotubes. *Catal. Commun.* **2010**, *12*, 259–263.

10. Naapuri, J. M.; Losada-Garcia, N.; Rothemann, R. A.; Pichardo, M. C.; Prechtl, M. H.; Palomo, J. M.; Deska, J. Cascade Catalysis through Bifunctional Lipase Metal Biohybrids for the Synthesis of Enantioenriched O-Heterocycles from Allenes. *ChemCatChem* **2022**, *14*, e202200362.
11. Dawood, A. W.; Bassut, J.; de Souza, R. O.; Bornscheuer, U. T. Combination of the Suzuki–Miyaura Cross-Coupling Reaction with Engineered Transaminases. *Chem. Eur. J.* **2018**, *24*, 16009–16013.
12. Naapuri, J. M.; Åberg, G. A.; Palomo, J. M.; Deska, J. Arylative Allenol Cyclization via Sequential One-Pot Enzyme and Palladium Catalysis. *ChemCatChem* **2021**, *13*, 763–769.
13. Luan, P.; Liu, Y.; Li, Y.; Chen, R.; Huang, C.; Gao, J.; Hollmann, F.; Jiang, Y. Aqueous Chemoenzymatic One-Pot Enantioselective Synthesis of Tertiary α-Aryl Cycloketones via Pd-Catalyzed C–C Formation and Enzymatic C=C Asymmetric Hydrogenation. *Green Chem.* **2021**, *23*, 1960–1964.
14. Budhiraja, M.; Ali, A.; Tyagi, V. Construction of a Bifunctional Pd(0)–CALB@SiO_2 Hybrid Catalyst for the Synthesis and Arylation of Imidazo[1,2-a]pyridine in One Pot. *Eur. J. Org. Chem.* **2023**, *26*, e202201426.
15. (a) Du, M.; Guo, B.; Jia, D. Newly Emerging Applications of Halloysite Nanotubes: A Review. *Polym. Int.* **2010**, *59*, 574–582. (b) Kamble, R.; Ghag, M.; Gaikawad, S.; Panda, B. K. Halloysite Nanotubes and Applications: A Review. *J. Adv. Sci. Res.* **2012**, *3*, 25–29. (c) Danyliuk, N.; Tomaszewska, J.; Tatarchuk, T. Halloysite Nanotubes and Halloysite-Based Composites for Environmental and Biomedical Applications. *J. Mol. Liq.* **2020**, *309*, 113077.
16. (a) Yuan, P.; Southon, P. D.; Liu, Z.; Kepert, C. J. Organosilane Functionalization of Halloysite Nanotubes for Enhanced Loading and Controlled Release. *Nanotechnology* **2012**, *23*, 375705. (b) Terzopoulou, Z.; Papageorgiou, D. G.; Papageorgiou, G. Z.; Bikiaris, D. N. Effect of Surface

Functionalization of Halloysite Nanotubes on Synthesis and Thermal Properties of Poly(ε-Caprolactone). *J. Mater. Sci.* **2018**, *53*, 6519–6541.

17. Pandey, G.; Munguambe, D. M.; Tharmavaram, M.; Rawtani, D.; Agrawal, Y. K. Halloysite Nanotubes—An Efficient 'Nano-Support' for the Immobilization of α-Amylase. *Appl. Clay Sci.* **2017**, *136*, 184–191.
18. Budhiraja, M.; Ali, A.; Tyagi, V. First Biocatalytic Synthesis of Piperidine Derivatives via an Immobilized Lipase-Catalyzed Multicomponent Reaction. *New J. Chem.* **2022**, *46*, 4837–4849.
19. Man, Z.; Feng, Y.; Xiao, J.; Yang, H.; Wu, X. Structural Changes and Molecular Mechanism Study on the Inhibitory Activity of Epigallocatechin against α-Glucosidase and α-Amylase. *Front. Nutr.* **2022**, *9*, 948027.
20. (a) Xu, L.; Wu, X. C.; Zhu, J. J. Green Preparation and Catalytic Application of Pd Nanoparticles. *Nanotechnol.* **2008**, *19*, 305603. (b) Hong, M. C.; Ahn, H.; Choi, M. C.; Lee, Y.; Kim, J.; Rhee, H. Pd Nanoparticles Immobilized on PNIPAM–Halloysite: Highly Active and Reusable Catalyst for Suzuki–Miyaura Coupling Reactions in Water. *Appl. Organomet. Chem.* **2014**, *28*, 156–161.
21. Katiyar, M.; Abida, K.; Ali, A. *Candida rugosa* Lipase Immobilization over SBA-15 to Prepare Solid Biocatalyst for Cotton Seed Oil Transesterification. *Mater. Today: Proc.* **2021**, *36*, 763–768.
22. Kamboj, P.; Tyagi, V. Construction of Bis-Indole Derivatives Using α-Amylase Enzyme: Application in the Gram-Scale Synthesis of Bis-Indole Containing Bioactive Molecules. *Asian J. Org. Chem.* **2023**, *12*, e202200669.
23. Hamdi, J.; Blanco, A. A.; Diehl, B.; Wiley, J. B.; Trudell, M. L. Room-Temperature Aqueous Suzuki–Miyaura Cross-Coupling Reactions Catalyzed via a Recyclable Palladium@Halloysite Nanocomposite. *Org. Lett.* **2019**, *21*, 3471–3475.
24. Gao, X.; Zhai, Q.; Hu, M.; Li, S.; Jiang, Y. Hierarchically Porous Magnetic Fe_3O_4/Fe-MOF Used as an Effective Platform for Enzyme Immobilization: A Kinetic and Thermodynamic Study of Structure–Activity. *Catal. Sci. Technol.* **2021**, *11*, 2446–2455.

CHAPTER 3

Merging Electrosynthesis and Biocatalysis to Access Sulfur-Based Chiral α-Fluorinated Carboxylic Acids

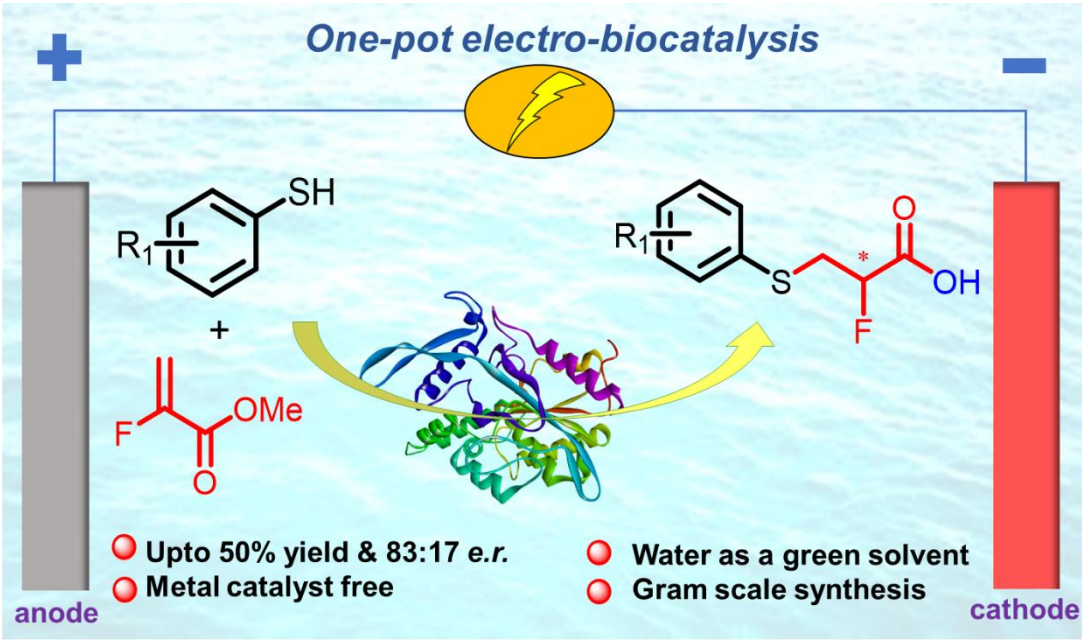

CHAPTER 3

3.1: Introduction

In recent years, the importance of organofluorine compounds has expanded significantly due to their wide range of applications in different areas such as materials science, drug discovery, agrochemicals, and the polymer industry.[1] The incorporation of one or more fluorine atoms into organic compounds often leads to unique physical, chemical, and biological properties, ascribed to the small size, high electronegativity, and low polarizability of the fluorine atom. It is noteworthy that approximately 20 per cent of marketed drugs contain at least one fluorine atom.[2] In particular, chiral sulfur-based organofluorine compounds have gained significant attention as they are used as precursors of numerous drugs or clinically important molecules **(Figure 3.1)**.[3] Previously, these compounds have been predominantly synthesized through sulfa-Michael addition reactions of substituted thiols and fluorine-containing electron-deficient alkenes as starting materials. In this context, Wang and colleagues documented the asymmetric sulfa-Michael addition of thiols and 4,4,4-trifluorocrotonates to obtain organofluorine compounds in high yields and enantioselectivities **(Scheme 3.1a)**.[4] Subsequently, Couve-Bonnaire and group members unveiled the use of the cinchona derivative $(DHQ)_2PYR$ as a catalyst for the sulfa-Michael addition of thiophenols with trisubstituted α-fluoroacrylates to synthesize chiral sulfur-based organofluorinated compounds **(Scheme 3.1b)**.[5] Interestingly, Haufe *et al.* observed the removal of HF as a side product when a base-catalyzed sulfa-Michael addition reaction of 4-methyl thiophenol and methyl-2-fluoro acrylate was performed, as a result, they were unable to synthesize sulfur-based organofluorine compounds.[6] Notwithstanding, most of the methodologies present certain limitations such as the use of organic solvents, complex work-up procedures often required, and the challenges of preserving the fluorine atom in the final product under the established reaction conditions. As a consequence, there is a significant need for the development of an environmentally friendly and efficient methodology to streamline the one-pot synthesis of chiral sulfur-based organofluorine compounds.

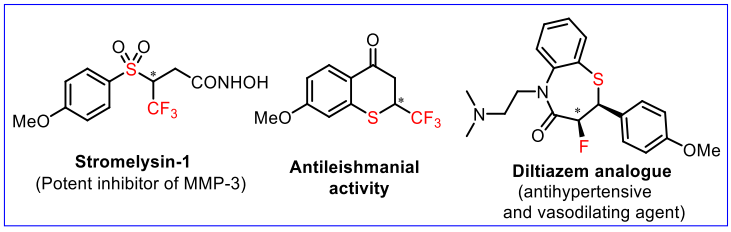

Figure 3.1: Clinically important sulfur-based organofluorine compounds

In recent years, substantial advancements have been made in synthesizing clinically significant molecules using greener methodologies by replacing traditional approaches.[7] Moreover, the

development of greener methodologies involves careful planning of synthetic routes, aiming to avoid the use of hazardous and toxic substances, as well as minimizing the generation of byproducts and chemical waste.[8] In this context, the use of enzymes as catalysts in water has proven highly advantageous in realizing the objectives of green chemistry.[9] Additionally, employing enzymes in organic synthesis has proven highly effective in generating molecules with exceptional chemo-, regio-, and stereoselectivities.[10] On the other hand, organic electrosynthesis is an alternative strategy for replacing the traditional synthetic approaches to achieve green chemistry objectives.[11] Particularly, utilizing electricity in organic synthesis provides numerous benefits such as the use of electron(s) as a reagent by avoiding exogenous oxidants or reductants, fine-tuning of reactions by adjusting the electrode potential, easy scale-up of the reactions without substantial modifications in the reaction conditions, etc.[12] Despite these advantages, achieving enantioselective organic electrosynthesis remains highly challenging due to factors such as the high reactivity of free radicals or intermediates and the

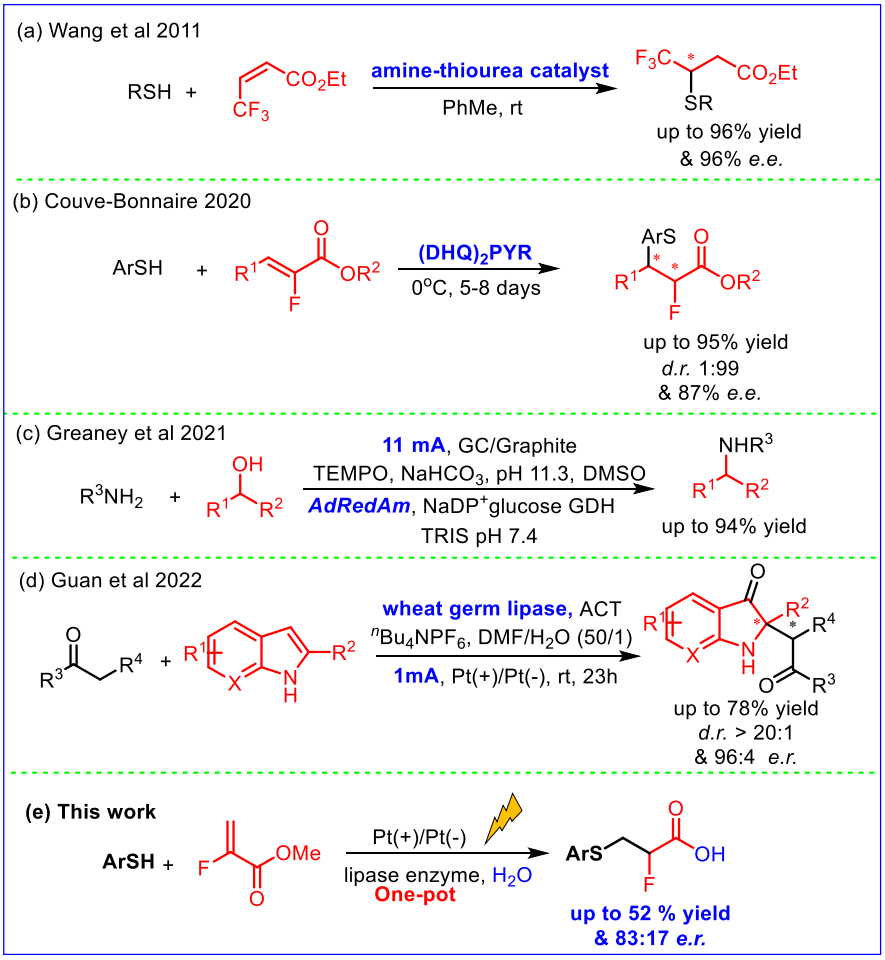

Scheme 3.1: Recent approaches to produce sulfur-based organofluorine compounds (a-b); One-pot integration of electro and biocatalytic approaches (c-e).

limited compatibility of chiral catalysts within an electrochemical cell.[13] To address these challenges, the integration of electrosynthesis and biocatalysis in the same pot offers a promising solution to obtain the compounds in a stereoselective manner.

Previously, the integration of electrosynthesis and biocatalysis was mainly focused either on the production of fuels or chemicals from carbon dioxide or to facilitate electron transfer through electrocatalysis to regenerate the cofactors necessary for enzymatic transformations.[14] However, the integration of electrosynthetic and biocatalytic approaches, which aims to catalyze dual chemical reactions in the same vessel where the product of one reaction serves as the starting material for the next reaction to synthesize biologically important molecules, requires more attention. In this context, Greaney and colleagues reported a one-pot integration of an organic electrosynthesis and biocatalytic approach for amine alkylation with alcohols, comprising TEMPO-mediated electro-catalytic oxidation followed by biocatalytic reductive amination using the *AdRedAm* enzyme **(Scheme 3.1c)**.[15] Very recently, Guan and co-workers discovered enantioselective oxidative cross-coupling of secondary amines with ketones by merging the non-natural catalytic activity of lipase and electrosynthesis **(Scheme 3.1d).**[16] Drawing encouragement from the importance of chiral sulfur-based organofluorine compounds, herein, we hypothesized to combine electrochemical sulfa-Michael addition of thiophenols and 2-fluoroacrylate followed by lipase-catalyzed ester hydrolysis reaction in the same pot to produce chiral sulfur-based organofluorine compounds **(Scheme 3.1e)**. While the sulfa-Michael addition of thiyl radicals to alkenes, alkynes and α, β-unsaturated acid has been previously demonstrated through flash photolysis or using iodine as a chemical oxidant.[3f-g] The electrochemical sulfa-Michael addition involving thiophenol and an α, β-unsaturated ester has not yet been explored. Also, the lipase-catalyzed hydrolysis of 2-fluoro-3-thiopropionate is still undocumented. Taking this into account, initially, we plan to explore both the electrochemical sulfa-Michael addition and the lipase-catalyzed hydrolysis reactions separately and subsequently proceed toward the integration of both approaches in the same vessel.

3.2: Results and Discussion

3.2.1: Optimization of reaction conditions

We started this study by setting up a reaction of thiophenol (**1a**) and methyl 2-fluoro acrylate (**2a**) as model substrates by using tetrabutylammonium iodide ($^{n}Bu_4NI$) as a supporting electrolyte in ethanol under a constant current of 10 mA in an undivided cell with two platinum electrodes at 50 °C and gratifyingly obtain the corresponding product (**3a**) with conversion of65% from this reaction. To enhance the conversion of the model reaction, we screened

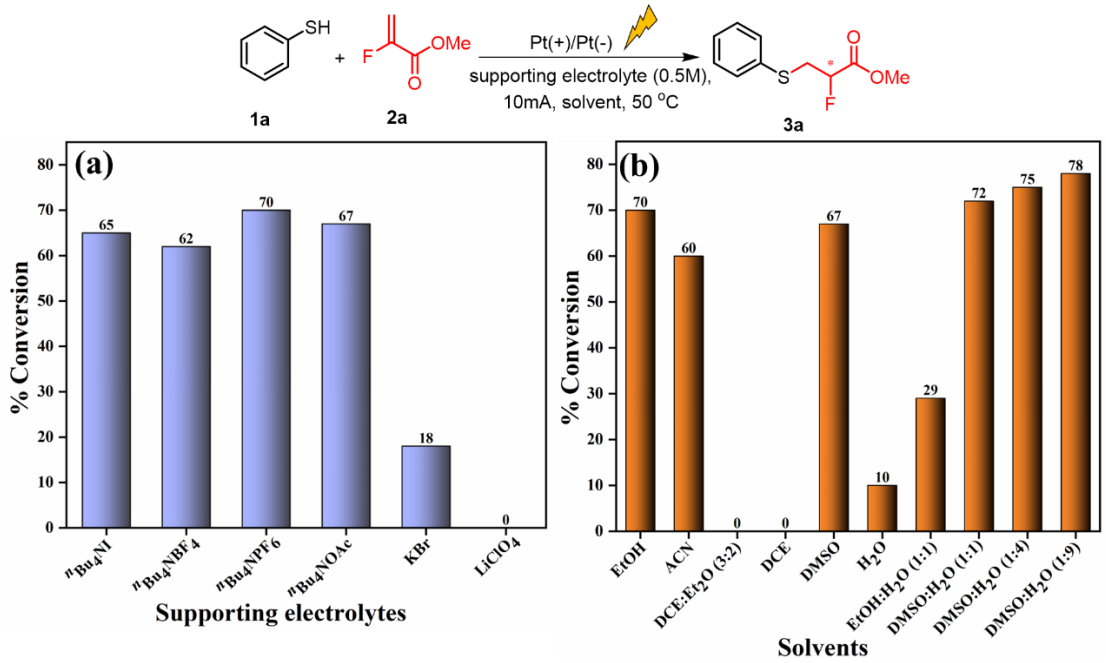

Figure 3.2 (a) Screening of supporting electrolytes for the model reaction (b) Solvent screening for model reaction; **Reaction Conditions**: (a) **1a** (38 µL, 0.4 mmol, 2 equiv.), **2a** (18 µL, 0.2 mmol, 1 equiv.), supporting electrolyte (0.5 M), solvent (2 mL), under a constant current of 10 mA in an undivided cell with two platinum electrodes at 50 ˚C for 1 hour; charge passed with respect to starting material (**2a**) is 2F, % conversion determined by HPLC as given in supporting information, the product **3a** was obtained as a racemic mixture.

tetrafluoroborate ($^{n}Bu_4NBF_4$), tetrabutylammonium hexafluorophosphate ($^{n}Bu_4NPF_6$), and tetrabutylammonium acetate ($^{n}Bu_4NOAc$), however, no notable improvement in the conversion was observed (**Figure 3.2a**). Moreover, when KBr was employed as a supporting electrolyte, the product was obtained with only 18% conversion. Additionally, no reaction was observed when lithium perchlorate ($LiClO_4$) was utilized. Consequently, $^{n}Bu_4NPF_6$ was found as the best supporting electrolyte for the model reaction. Next, we checked the effect of the solvents to improve the efficiency of the model reaction and first switched the solvent from ethanol to acetonitrile, however, there was a slight decrement in the % conversion (**Figure 3.2b**). Afterward, the product was obtained only in trace amounts when DCE (dichloroethane) or the mixture of DCE with diethyl ether (3:2, v/v) was used as a solvent. It is noteworthy that there was an increment in the % conversion when the reaction was conducted in DMSO (**Figure 3.2b**). Subsequently, in an attempt to make the electrochemical sulfa-Michael addition process greener, the model reaction was set up using water as a solvent; however, the formation of the product (**3a**) was only observed in trace amounts, possibly due to the very low solubility of the starting materials in water. Then, we explored the mixture of DMSO or EtOH with water (1:1,

v/v), but the % conversion of the model reaction remained low. Fortunately, an improved % conversion was attained when utilizing a mixture of DMSO in water (1:9 v/v) as the solvent. Consequently, this combination was selected as the best solvent for the electrochemical sulfa-Michael addition reaction. (**Figure 3.2b**).

Afterward, we reduced the supporting electrolyte concentration from 0.5 M to 0.05 M (**entries 1-4, Table 3.1**), as a result, the maximum conversion was obtained when 0.1 M $^{n}Bu_4NPF_6$ was used (**entry 3, Table 3.1**). Further, we varied the current and found that the reaction provides maximum conversion in the case of 5 mA current (**entries 5-6, Table** 3.1). Subsequently, a decrease in the % conversion was noted when the reaction was conducted with an equal amount of both substrates (**entry 7, Table 3.1**). Moreover, there was no enhancement in the % conversion observed when (**1a)** and (**3a)** were employed in a 3:1 molar ratio (**entry 8, Table 3.1**). Next, no improvement in % conversion was observed when the temperature was either decreased or increased from 50°C (**entries 9-10, Table 3.1**). A control reaction was set up to check the role of electricity, and interestingly there was no reaction in the absence of current (**entry 11, Table 3.1**).

Table 3.1: Optimization of reaction conditions for sulfa-Michael addition reaction[a]

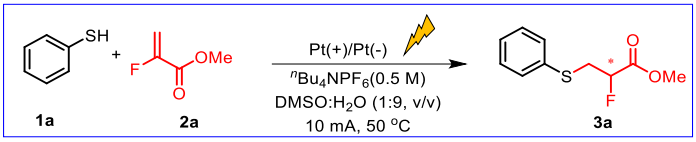

entry	deviation from standard reaction conditions	% conversion (3a)[b]	Charge passed (F)
1	none	78	2
2	0.3 M supporting electrolyte used	82	2
3	0.1 M supporting electrolyte used	88	2
4	0.05 M supporting electrolyte used	57	2
5	15 mA current used	61	3
6	5 mA current used	98	1
7	1 equiv. of 1a used	46	2
8	3 equiv. of 1a used	96	2
9	Temperature 25 ◦C	41	2
10	Temperature 60 ◦C	89	2
11	no electricity	0	0

[a]**Standard reaction conditions: 1a** (38 µL, 0.4 mmol, 2 equiv.), **2a** (18 µL, 0.2 mmol, 1 equiv.), $^{n}Bu_4NPF_6$ (0.5 M), DMSO:H_2O (2 mL), under a constant current of 10 mA flowed in an undivided cell with two platinum electrodes at 50 ◦C for 1 hour. [b]% conversion determined by HPLC.

3.2.2: Substrate scope for electrochemical sulfa-Michael addition reaction

Once the optimized reaction conditions were obtained, the substrate scope for the electrochemical sulfa-Michael addition reaction was investigated to demonstrate the generality of this transformation (**Scheme 3.2**). The reaction provided a very good isolated yield when unsubstituted thiophenol was employed in the reaction (**3a**, **Scheme 3.2**). Then, we tested the scope of the electron-donating group such as methyl-, methoxy-, and hydroxy-containing thiophenols, and obtained the corresponding products in excellent yield (**3b-e, Scheme 3.2**). Next, the reaction provided a slightly lower yield when halide-substituted thiophenols were

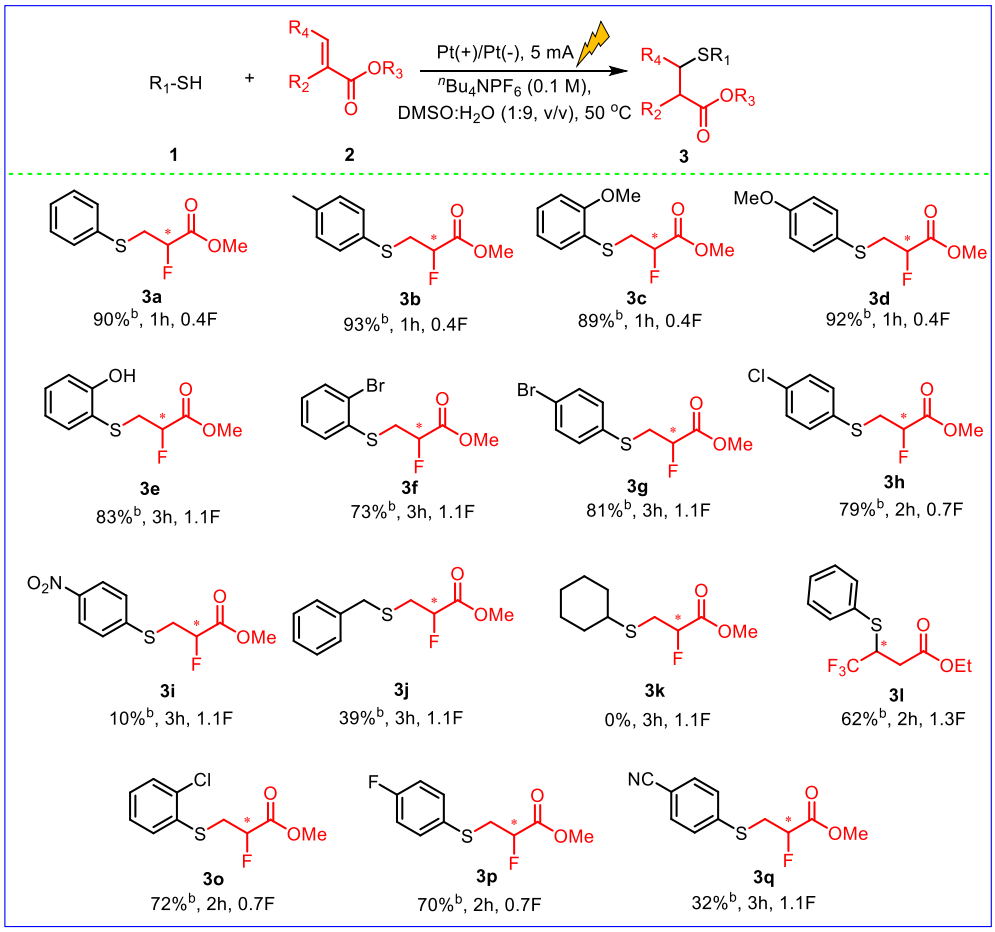

Scheme 3.2: Substrate scope of electrochemical sulfa-Michael addition reaction[a]

[a]**Reaction Conditions**: **1** (1 mmol, 2 equiv.), **2** (0.5 mmol, 1 equiv.), $^{n}Bu_4NPF_6$ (0.1 M), DMSO: H_2O (5 mL), [b]isolated yield.

employed in the reaction (**3f-h, 3o-p, Scheme 3.2**), also reaction took little longer time to get completed. Surprisingly, a very low yield was obtained in the case of 4-NO_2 thiophenol, which might be due to the weakened stabilization of the thiyl radical caused by the strong electron-withdrawing nature of the nitro group, which ultimately impaired the radical's reactivity in the reaction. (**3i**, **Scheme 3.2**).[13c] Also, the reaction yielded the product (**3q**) with an isolated yield

of 32% in the case of 4-CN substituted thiophenol. The reaction provided sulfa-Michael addition product **(3j)** only in 39% isolated yield when thiophenol was replaced with benzyl thiol. Additionally, the current proved insufficient to drive the reaction of cyclohexyl thiol with 2-fluoroacrylate, resulting in no product formation (**3k, Scheme 3.2**). The low yield or no reaction observed in the case of (**3j**) and (**3k**) might be due to the low stability of the aliphatic thiyl radical as compared to the aromatic radical.[13c] Gratifyingly, the reaction afforded the product (**3l**) in a good yield when we replaced methyl-2-fluoro acrylate (**2a**) with a CF_3-containing Michael acceptor i.e. methyl-4,4,4-trifluorobut-2-enoate (**3l**, **Scheme 3.2**).

3.2.3: Reaction condition optimization for enzymatic hydrolysis reaction

In the next phase of our endeavors, we focused on optimizing the reaction conditions for the enzymatic hydrolysis of 2-fluoro-3-mercaptopropanoate derivative **(3d)** to produce chiral 2-fluoro-3-mercaptopropionic acid **(4d)**. First, various lipases from different sources were screened for the asymmetric hydrolysis of **(3d)**, and the results were enclosed in **Table 3.2**. In this context, when lipases from *C. rugosa* and *A. niger* were employed as the catalyst, the desired product **(4d)** was obtained with low enantiomeric ratio and moderate % conversion (**entries 1-2, Table 3.2**). Then, other lipases such as lipase from porcine pancreas and *Candida*

Table 3.2: Screening of lipases for the hydrolysis reaction[a]

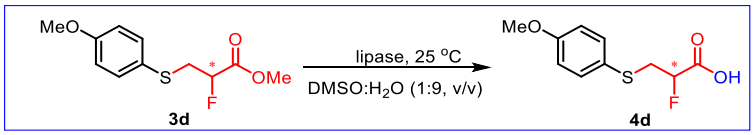

entry	lipase	% conversion[b]	*e.r.*[c]	*% ee*	*E*
1	lipase from *C. rugosa*	39	62:38	24	2
2	lipase from *A. niger*	46	57:43	14	1
3	lipase from Porcine pancreas	62	60:40	20	2
4	*Candida antarctica* lipase B	59	70:30	40	4
5	lipase from *Rhizomucor miehei*	41	64:36	28	2
6	lipase from *Burkhoderia cepacia*	37	72:28	44	3
7	**lipase from *P. Fluorescens***	**52**	**83:17**	**66**	**10**

[a]**Reaction conditions**: **3d** (10 mg, 0.04 mmol, 1 equiv.), lipase (10 mg/mL), DMSO: H_2O (1 mL), incubated at 25°C on 200 rpm for three days; [b]determined by HPLC, [c]determined by chiral HPLC.

antarctica B were used and got product (**4d**) in improved % conversion however the enantiomeric ratios were moderate (**entries 3-4, Table 3.2**). Subsequently, lipase derived from *Rhizomucor miehei* and *Burkhoderia cepacia* produced product (**4d**) with a reduced conversion

and modest enhancement in the enantiomeric ratios (**entries 5-6, Table 3.2**). Gratifyingly, when lipase from *P. fluorescens* (PFL) was used as the catalyst, the reaction provided the desired product (**4d**) in 52% conversion and improved enantiomeric ratio i.e. *e.r.* = 83:17 (**entry 7, Table 3.2**).

Consequently, PFL was selected as the optimal biocatalyst for further optimization of the reaction conditions to improve the enantioselectivity and conversion (**entry 7, Table 3.2**). In this context, a decrement in the % conversion was noticed along with a very slight change in the enantiomeric ratios as enzyme loading was decreased from 10 mg to 5, 3, and 1 mg respectively (**entries 1-4, Table 3.3**). Thus, 10 mg loading of the enzyme was opted as the best for achieving the maximum conversion. Additionally, to further improve the selectivity, water as a solvent was altered by THF, toluene, ethanol, and phosphate buffer (**entries 5-8, Table 3.3**). However, no noticeable rise in the selectivity was observed. Unfortunately, we did not

Table 3.3: Optimization of reaction conditions for enzymatic hydrolysis[a]

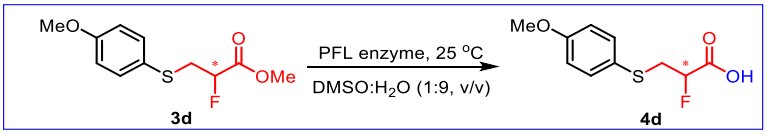

entry	deviation from standard reaction conditions	% conversion[b]	*e.r.*[c]	*% e.e.*	*E*
1	no deviation	52	83:17	66	10
2	5 mg lipase instead 10 mg	31	81:19	62	6
3	3 mg lipase instead 10 mg	23	80:20	60	5
4	1 mg lipase instead 10 mg	19	77:23	54	4
5	THF instead of H_2O	39	75:25	50	4
6	Toluene instead of H_2O	31	69:31	38	3
7	EtOH instead of H_2O	50	67:33	34	3
8	KPi buffer (pH 7, 100 mM), instead of H_2O	32	55:45	10	1
9	Temperature=10 °C instead of 25°C	46	78:22	56	6
10	Temperature=50 °C instead of 25°C	45	77:23	54	5

[a]**Reaction conditions**: **3d** (10 mg, 0.04 mmol, 1 equiv.), enzyme (10 mg/mL), DMSO: H_2O (1 mL), incubated at 200 rpm for three days, [b]determined by HPLC, [c]determined by chiral HPLC.

observe any positive change in enantioselectivity when we decreased or increased the temperature from room temperature to 10 °C or 50 °C respectively **(entries 9-10, Table 3.3)**.

3.2.4: Substrate scope for integrated electrochemical and hydrolysis reaction

In the final phase of our study, we integrate electrochemical sulfa-Michael addition and PFL-catalysed hydrolysis reaction in the same vessel using the optimized reaction conditions. In this context, we performed a one-pot reaction of thiophenol (**1a**) and methyl-2-fluoro acrylate (**2a**) and delightfully obtained the desired product (**4a**) in 47% isolated yield along with the non-hydrolyzed compound (**3a**). Also, we set up sequential electrosynthesis and biocatalysis reactions using the optimized reaction conditions to compare the outcome of a one-pot reaction, however, there was no significant change in the isolated yield of the reaction (**Scheme 3.10**).

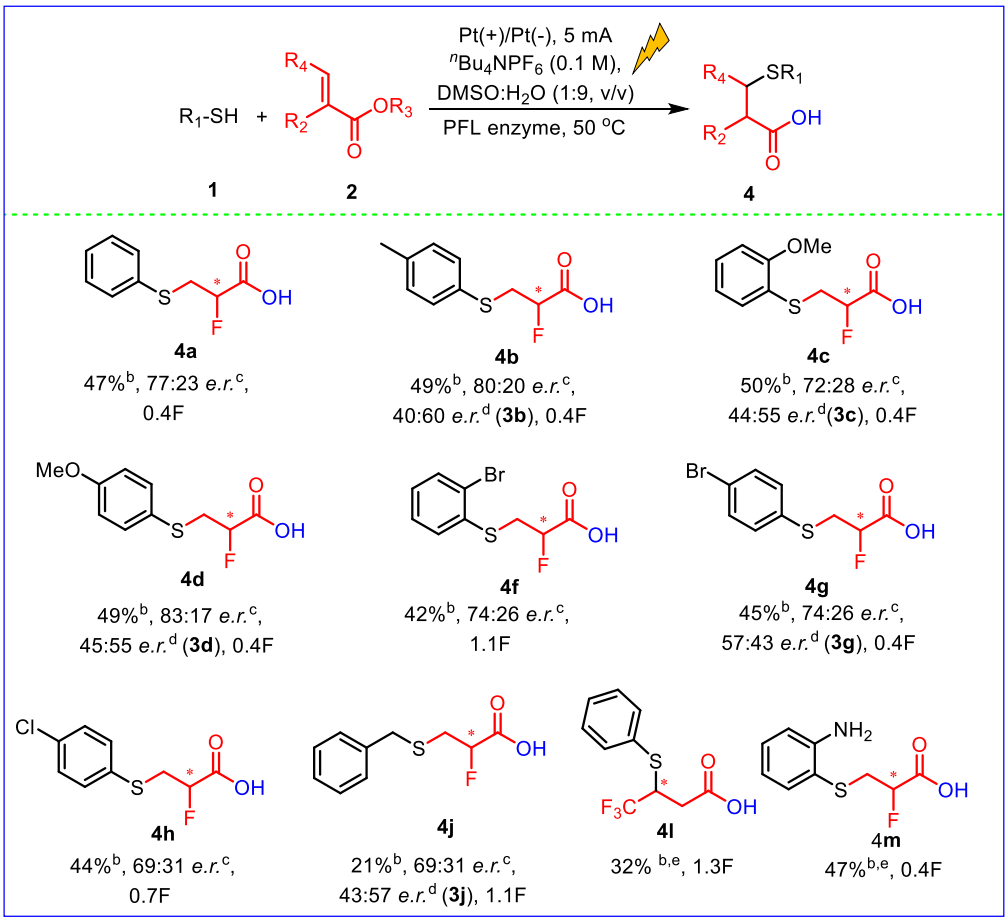

Scheme 3.3: Substrate scope of integrated electrosynthesis and biocatalytic reaction[a]

[a]**Reaction conditions: 1** (1 mmol, 2 equiv.), **2** (0.5 mmol, 1 equiv.), $^{n}Bu_4NPF_6$ (0.1 M), DMSO: H_2O (5 mL), PFL enzyme (10 mg/mL), incubated at 200 rpm for three days after the completion of electrochemical reaction, [b]isolated yield, [c]*e.r.* of product (**4**) as determined by chiral HPLC, [d]*e.r.* of non-hydrolyzed compound (**3**) as determined by chiral HPLC, [e]no enantiomer resolution.

Then, we tested the scope of substituents to show the generality and feasibility of the one-pot integrated electrosynthesis and biocatalytic transformation as depicted in **Scheme 3.3**. There was no significant change observed in the yield and enantiomeric ratio of the product (**4b**) in

comparison to product (**4a**) when thiophenol (**1a**) was replaced by 4-methyl thiophenol in the one-pot reaction (**Scheme 3.3**). Afterward, the effect of 2-methoxy and 4-methoxy substituent on the thiophenol was tested, and a slight increment in the yield, as well as the enantiomeric ratio, was observed (**4c-d, Scheme 3.3).** Next, halide-substituted thiophenols were employed in the one-pot reaction and obtained the corresponding products with good yield and enantiomeric ratios (**4f-h, Scheme 3.3**). Besides, the scope of benzyl thiol was tested, however, the desired product was obtained only in 21% isolate yield (**4j, Scheme 3.3**) accompanied by non-hydrolyzed compound (**3j**). Also, we replaced methyl 2-fluoro acrylate (**2a**) with ethyl 4,4,4-trifluorocrotonate and interestingly reaction provided the corresponding product (**4l**) in 32% isolated yield. The reaction provided the corresponding product (**4m**) in 47% isolated yield when 2-amino thiophenol was employed in the reaction. Noticeably, the lower yield of compounds (**4**) was attributed to the partial recovery of non-hydrolyzed esters intermediates (**3**). The enantiomeric ratios of these recovered esters are presented in **Scheme 3.3**.

3.2.5: Control experiments on electricity and enzyme roles

To understand the role of electricity and PFL enzyme in the one-pot procedure, several experiments were performed as depicted in **Figure 3.3**. First, we monitored the consumption of thiophenol (**1a**) under different reaction conditions and it was found that the concentration

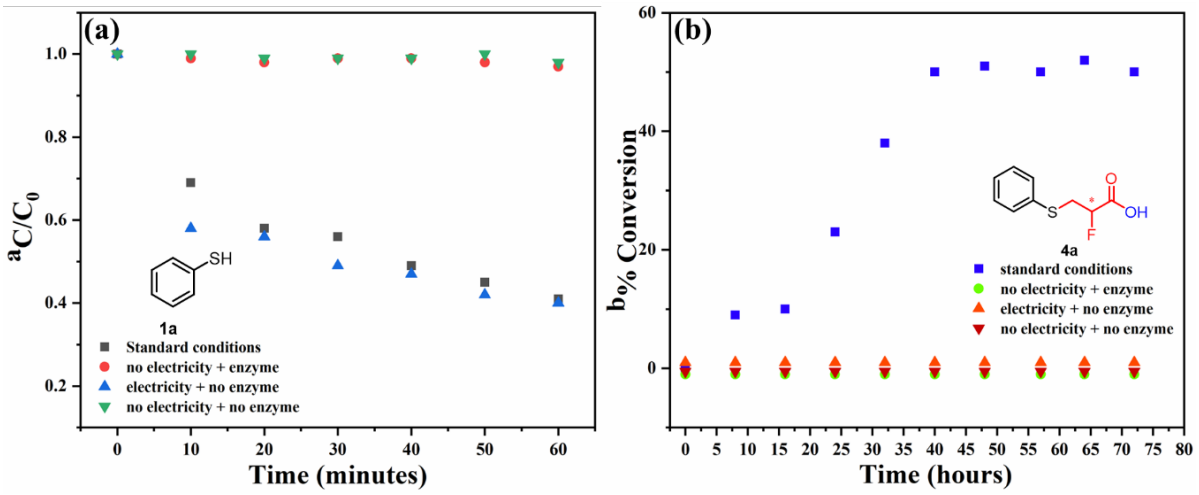

Figure 3.3: (a) Role of electricity and enzyme on the consumption of thiophenol **(1a)** with time (b) Role of electricity and enzyme on the formation of **(4a)** with time; **Standard conditions: 1a** (38 µL, 0.4 mmol, 2.0 equiv.), **2a** (18 µL, 0.2 mmol, 1.0 equiv.), $^{n}Bu_4NPF_6$ (0.1 M), DMSO: H_2O (1:9, v/v, 2 mL), PFL enzyme (10 mg/mL) under a constant current of 5 mA in an undivided cell with two platinum electrodes, maintaining the temperature at 50 °C using an oil bath, total reaction time=72 h, $^{a}C/C_0$ = ratio of thiol concentration at different time intervals with respect to initial concentration (t=0); ^{b}% conversion determined by HPLC.

of thiophenol decreased gradually with time in the presence of electricity, and there was no change in the concentration of thiophenol in the presence of enzyme only (**Figure 3.3a)**. Also, we monitored the formation of acid (**4a**) in different reaction conditions and found that acid was formed only in the presence of the PFL enzyme (**Figure 3.3b)**. These experiments suggested that electricity is required for the sulfa-Michael addition reaction while the PFL enzyme plays a role only in the hydrolysis of ester formed *in-situ* through electrosynthesis.

3.2.6: Mechanistic insights via control experiments

Further, to get insight into the mechanism of electrochemical sulfa-Michael addition, a reaction of **(1a)** and **(2a)** was performed with commonly used radical trapping agent (2,2,6,6-tetramethylpiperidin-1-yl)oxyl (TEMPO) (1 equiv.) and as a result, product (**3a**) was obtained only in 6% yield (**Scheme 3.4a**). By increasing the amount of TEMPO (4 equiv.), product formation was completely inhibited and we were able to detect the adducts formed by the reaction of thia radical (**II**) with TEMPO using HRMS techniques (**Scheme 3.4b**). Besides, we tried another radical scavenger butylated hydroxytoluene (BHT) under the electrochemical conditions, which again terminated the formation of the desired product (**3a) (Scheme 3.4c).** Also, we have detected the formation of diaryldisulfide as a side reaction when the reaction

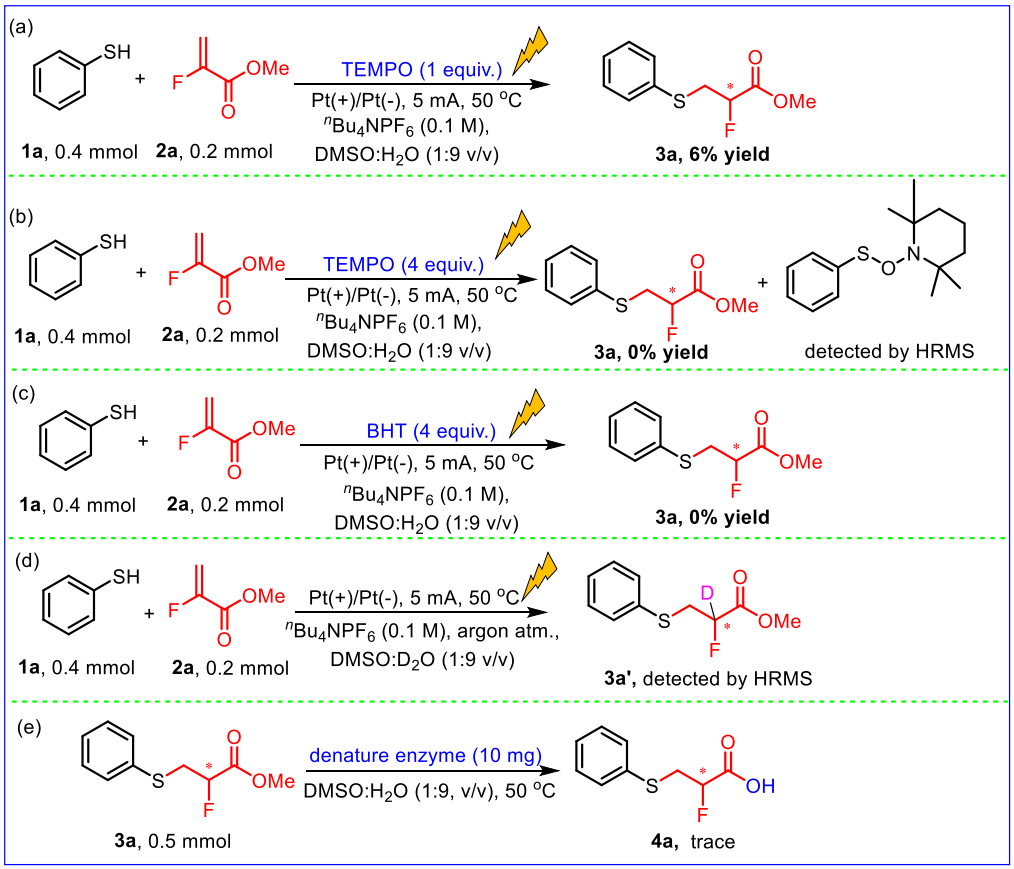

Scheme 3.4: Control experiments

was conducted in the absence of fluoro-acrylate.[18,21] These observations indicated that the reaction may follow a radical process, and thia radical **(II)** may be a possible intermediate in the electrolysis.

3.2.7: Cyclic voltammetry studies

Next, a cyclic voltammetry (CV) study was carried out to examine the redox potential of substrates **(1a)**, **(2a)** and the mixture of substrates and electrolyte (**Figure 3.4I**). There was no oxidation peak in the CV of the blank DMSO:H_2O solution, $^{n}Bu_4NPF_6$ and mixture of $^{n}Bu_4NPF_6$ and (**2a**) (curves a, b & c, **Figure 3.4I**). The oxidation peak for (**1a**) and $^{n}Bu_4NPF_6$ was observed at 0.41 V vs Ag/AgCl (curves c & d, **Figure 3.4I**). Whereas the CV of mixture of (**1a**), (**2a**) and $^{n}Bu_4NPF_6$ exhibited an oxidation peak at 0.48 V. A possible explanation for the modest shift in oxidation potentials observed in the CV of mixtures is due to chemical interaction between (**1a**) and (**2a**) (curve e, **Figure 3.4I**). Xie et al. and Badsara et al. reported similar sorts of observations.[17-18] Next, we conducted experiments using the radical scavenger TEMPO in a DMSO:H_2O (1:9) mixture (curve a **Figure 3.4II**). No appreciable oxidation peak was seen upon the addition of TEMPO to substrate (**2a**), demonstrating a lack of interaction between TEMPO and (**2a**) (curve b **Figure 3.4II**). However, when TEMPO was introduced with thiophenol (**1a**), an oxidation peak was observed at 1.20 V (curve c **Figure 3.4II**). Additionally, when TEMPO was present with both substrates, a new sharp peak appeared at 1.12 V (curve d **Figure 3.4II**), which likely indicates that TEMPO trapped the thiyl radical in the reaction mixture, providing further evidence for the proposed mechanism.

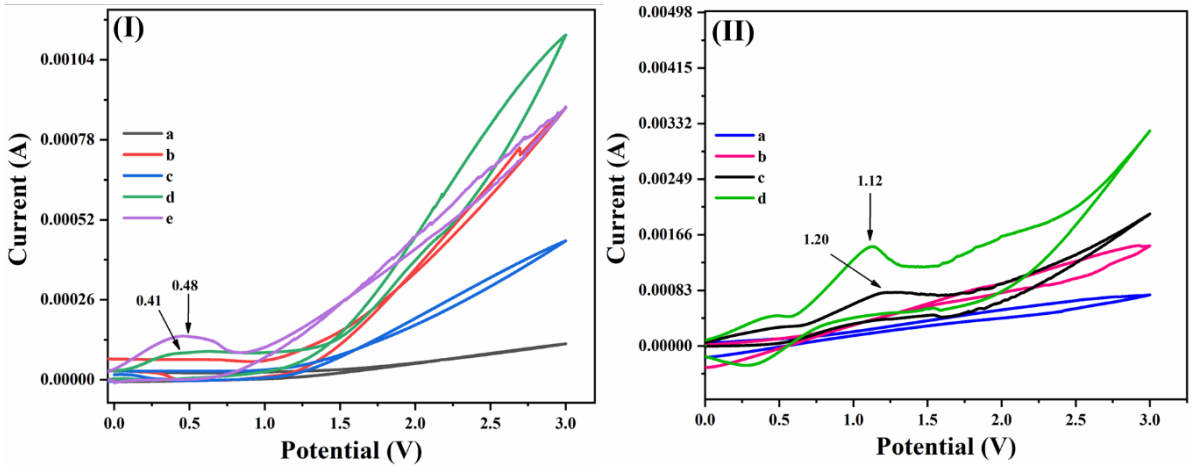

Figure 3.4: Cyclic voltammograms (IUPAC convention) of 0.1 M $^{n}Bu_4NPF_6$ solution in DMSO:H_2O (1:9) at room temperature, using Pt wire as a counter electrode, Pt as working electrode, and Ag/AgCl as a reference electrode, at a scan rate of 0.05 V/s with initial potential = 0 V, the direction of scan = 0 to +3 (oxidative). (I) (a) DMSO:H_2O (1:9) (b) $^{n}Bu_4NPF_6$ (0.1 M), (c) $^{n}Bu_4NPF_6$ (0.1 M) and **2a** (0.001 M) (d) $^{n}Bu_4NPF_6$ (0.1 M) and **1a** (0.002 M) (e) $^{n}Bu_4NPF_6$ (0.1 M), **2a** (0.001 M) and **1a** (0.002 M). (II)

(a) TEMPO (0.004 M) and $^{n}Bu_4NPF_6$ (0.1 M) (b) TEMPO (0.004 M), $^{n}Bu_4NPF_6$ (0.1 M) and **2a** (0.001 M) (c) TEMPO (0.004 M), $^{n}Bu_4NPF_6$ (0.1 M) and **1a** (0.002 M) (d) TEMPO (0.004 M), $^{n}Bu_4NPF_6$ (0.1 M), **2a** (0.001 M) and **1a** (0.002 M).

3.2.8: Molecular docking studies

In addition, the molecular docking study was performed to get insights into the role of the active site of the PFL enzyme during the hydrolysis reaction (**Figure 3.5**). However, due to the non-availability of the crystal structure of the PFL enzyme, we have conducted the docking investigation using *P. cepacia* lipase (PCL) (PDB 3LIP), which is homologous and has sequence similarity with PFL.[19] Previously, it has been reported that the catalytic triad comprising Ser87, Asp264, and His286 amino acids plays an important role in the ester hydrolysis, whereas Leu17 and Tyr29 residues are important for providing selectivity.[19a,20] After performing the docking studies with **(3a)** as a ligand, we have obtained the best-docked pose with the lowest binding energy (-5.7 kcal/mol, **Figure 3.9**) which suggests that Ser87 along with His286 present in the active site may play an important role during the hydrolysis of substrate (**3a)** (**Figure 3.5**). Additionally, Tyr29 and Leu17 residues showed interaction with substrates (**3a**), which may facilitate selectivity during the hydrolysis. [19a,b] To get more insight into the role of the active site of the PFL enzyme in the hydrolysis reaction, we set up the hydrolysis of (**3a**) with denatured PFL *(process for denaturing the enzyme is given in section 3.3.8)* and the desired acid (**4a**) was formed only in trace amounts (**Scheme 3.4**) which suggests that the natural active site (triad of Ser87, Asp264, and His286 residues) is playing a role in the selective hydrolysis reaction.

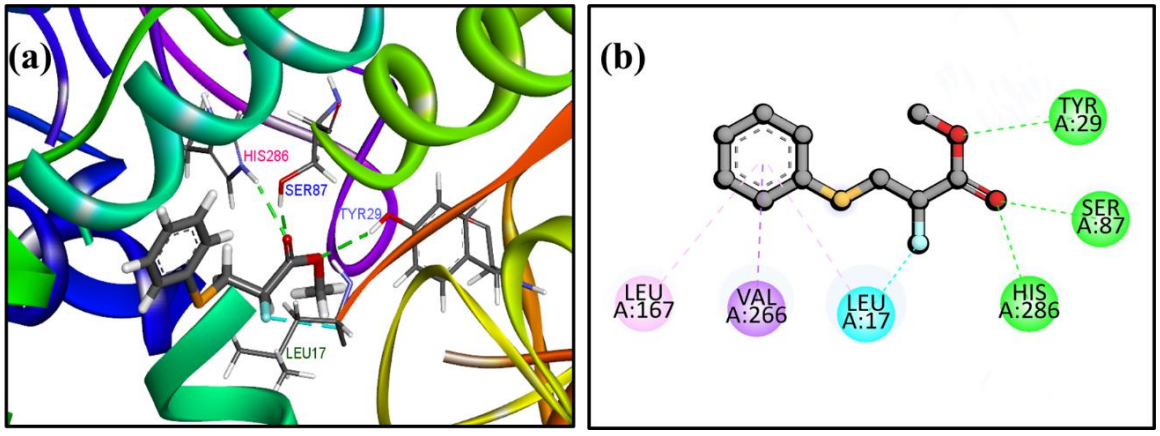

Figure 3.5: Predicted binding interactions of substrate **(3a)** with lipase, dotted lines represent the bonding interactions **(a)** represents the 3D interaction of active site amino acids Ser87 and His286 with the substrate **(3a),** whereas Tyr29 along with Leu17 helps in cooperative binding of substrate to the enzyme active site **(b)** 2D interaction of PCL binding to the substrate (**3a)** along with π-alkyl interactions.

3.2.9: Proposed Mechanism

Based on the above experimental results and literature findings,[21] a plausible mechanism for the formation of (**4a**) was proposed as presented in the **scheme 3.5**. First, thiophenol (**1a**) is anodically oxidized to generate the radical cation species (**I**) which consequently undergo deprotonation to form thia radical (**II**).[21,22] Subsequently, thia radical (**II**) combines with the methyl-2-fluoro acrylate (**2a**) to generate the carbon-centered radical intermediate (**IV**) which undergoes hydrogen abstraction to yield the electrochemical product (**3a**).[21,23] Furthermore, when the reaction was conducted in the presence of deuterated water, the deuterated product (**3a'**) was detected using HRMS, with an $[M + OH]^+$ ion at 232.0563. This result confirmed the formation of (**3a**) from radical intermediate (**IV**) (**Scheme 3.4d**). The stability of the radical intermediate (**IV**) has also been reported by Ito and his group, attributing it to the interaction of the unpaired electron with the ester group.[3f] Then, **3a** enters the active site of the enzyme and binds with the catalytic triad to generate the enzyme-substrate complex (**V**). Afterward, Ser87 attacks at the ester carbonyl atom followed by proton abstraction via His286 to furnish the first tetrahedral intermediate T_d1 (**VI**).[24] After the restoration of the carbon-oxygen double bond, an acyl-enzyme intermediate (**VII**) is formed where His286 allows the release of methanol. Subsequently, water forms a bond with the intermediate acyl-enzyme (**VII**) to deliver (**VIII**). Next, His286 targets the carbonyl carbon of the acyl-enzyme and once again

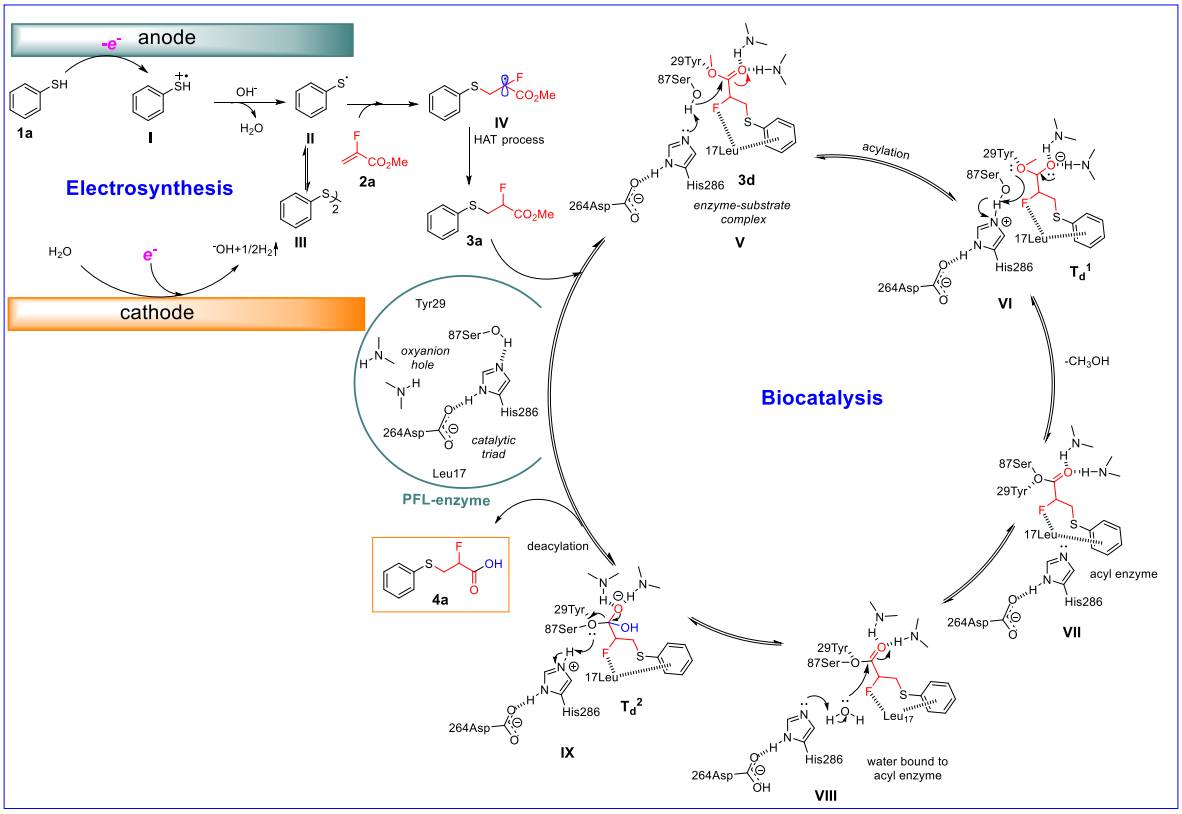

Scheme 3.5: Plausible mechanism for one-pot integrated electrosynthesis and biocatalysis

functions as a base to deprotonate the water as a result the second tetrahedral intermediate T_d2 (**IX**) forms. In the end, 2-fluoro-3-(phenylthio)propanoic acid (**4a**) is released via deacylation, and the free enzyme state is restored after the reformation of the carbon-oxygen double bond.[25]

3.2.10: Gram-scale experiment and application of integrated protocol

To demonstrate the utility of a one-pot integrated electrosynthesis and biocatalysis protocol, a gram-scale reaction involving methyl-2-fluoroacrylate (**2a**) and thiophenol (**1a**) was performed. This resulted in the production of (**4a**) with an isolated yield of 45% (**Scheme 3.6a**). Besides, we showed the application of an integrated electrosynthetic and biocatalytic approach by synthesizing the key intermediate of (R)-γ-trifluoromethyl γ-sulfone hydroxamate which is a potent MMP-3 inhibitor (stromelysin-1) in 39% isolated yield (**Scheme 3.6b**).

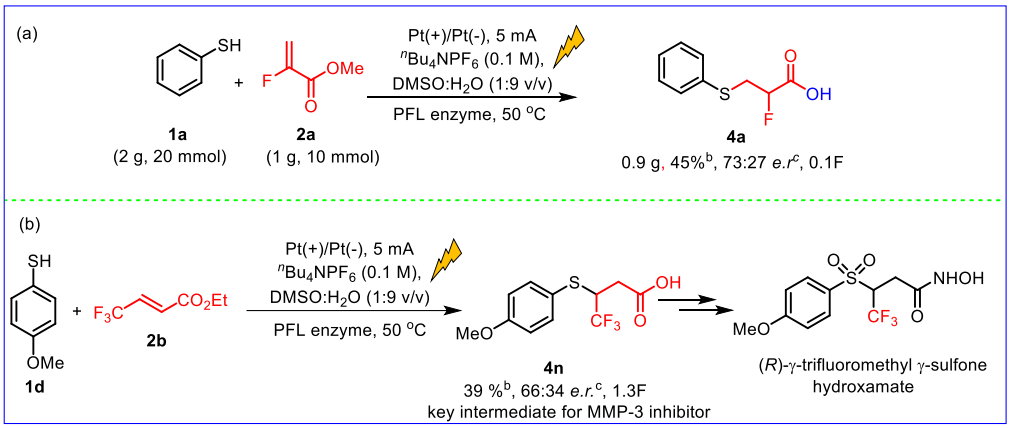

Scheme 3.6: Scale up and application of electrosynthetic and biocatalytic approach

Reaction conditions: (a) **1a** (1900 µL, 20 mmol, 2 equiv.), **2a** (900 µL, 10 mmol, 1 equiv.), ^{n}Bu$_4$NPF$_6$ (0.1 M), DMSO:H$_2$O (100 mL), PFL enzyme (10 mg/mL) under a constant current of 5 mA in an undivided cell with two platinum electrodes, maintaining the temperature at 50 ◦C using an oil bath; (b) **1d** (73 µL, 0.6 mmol, 2 equiv.), **2b** (45 µL, 0.3 mmol, 1 equiv.), ^{n}Bu$_4$NPF$_6$ (0.1 M), DMSO: H$_2$O (5 mL), PFL enzyme (10 mg/mL) under a constant current of 5 mA in an undivided cell with two platinum electrodes, maintaining the temperature at 50 °C using an oil bath; [b]isolated yield, [c]determined by chiral HPLC.

3.3: Experimental section

3.3.1: General information

All chemicals, including starting compounds and solvents, were purchased from commercial suppliers and utilized without any further purification. Lipase from *Candida rugosa* (≥700 U/mg, CAS No. 9001-62-1, Product No. L1754), lipase from *Aspergillus niger* (~200 U/g, CAS No. 9001-62-1, Product No. 62301) lipase from porcine pancreas (≥125U/mg, CAS No. 9001-62-1, Product No. L3126), lipase from *Candida* sp. (recombinant, expressed in *Aspergillus niger*, Lipozyme CALB L) (≥5000 U/g, Product No. L3170), lipase from

Rhizomucor miehei (≥20,000 U/g, CAS No. 9001-62-1, Product No. L4277), and Amano lipase from *Pseudomonas Fluorescens* (≥20,000 U/g, CAS No. 9001-62-1, Product No. 534730) were purchased from Sigma-Aldrich. Amano lipase PS from *Burkholderia cepacia* (CAS No. 9001-62-1, Product No. GLR19.020344) bought from GLR innovations. The electrochemical reactions were conducted on an OWON (P4305) instrument equipped with an undivided cell and magnetic stirrer. The progress of the reaction was monitored by employing thin layer chromatography (TLC, thin layer of silica coated on a glass plates). The ^{1}H NMR, ^{13}C NMR and ^{19}F NMR spectra of the synthesized compounds were recorded on JEOL or Bruker spectrometer on 400 MHz (600/700 MHz), 100 MHz, and 376 MHz respectively. Tetramethylsilane (TMS) was employed as an internal standard in $CDCl_3$ and DMSO-*d*6. The chemical shift is expressed as δ (ppm), whereas the coupling constant is symbolized by *J* (Hz). Chemical shifts were referenced to residual solvent peaks ($CDCl_3$: 7.26 ppm for ^{1}H NMR, 77.16 ppm for ^{13}C NMR; DMSO-*d*6: 2.50 ppm for ^{1}H NMR, 39.51 ppm for ^{13}C NMR. Additional acronyms utilized in NMR follow-up studies include: s, singlet; brs, broad singlet; d, doublet; t, triplet; q, quartet; td, triplet of doublet; dt, doublet of triplet m, multiplet and dd, double doublet. High resolution mass spectra (HRMS) were acquired using a Water QTOF mass spectrometer (XEVO G2 XS) in ESI (-ve) mode. The % conversion (using 1,3-benzodioxole as the internal standard) and enantiomeric ratios (*e.r.*) were determined using a Shimadzu HPLC equipped with an LC-20AD pump, CTO-10AS column oven, and PDA detector. Cyclic voltammograms were acquired using a DY2300 potentiostat instrument.

3.3.2: General procedure for the synthesis of 2-fluoro-3-mercaptopropanoate derivatives (3a-3l):

In a reaction vessel containing stirrer bar were added $^{n}Bu_4NPF_6$ (192 mg, 0.1 M), thiophenol (95 µL, 1.0 mmol, 2.0 equiv.), and methyl 2-fluoroacrylate (45 µL, 0.5 mmol, 1.0 equiv.) in a mixture of DMSO and deionized water (5 mL, 1:9, v/v) and placed on a preheated oil bath at 50 °C. A constant current of 5 mA was applied to the reaction mixture in an undivided cell with two platinum sheet electrodes for certain hours as indicated for each substrate. The progress of the reaction was monitored by TLC. Afterward, the reaction mixture was poured into a separatory funnel and was extracted with an ethyl acetate. The resulting solution was then dried using anhydrous Na_2SO_4. The filtrate was concentrated under vacuum and the residue was purified by column chromatography using silica gel with a mesh size of 60-120 as a stationary phase, while a mixture of ethyl acetate and hexane served as the mobile phase to afford the desired product.

3.3.3: General procedure for the one-pot synthesis of 2-fluoro-3-mercaptopropionic acids:

Thiol (2 equiv.), methyl-2-fluoroacrylate (1 equiv.) and $^{n}Bu_4NPF_6$ (192 mg, 0.1 M) were dissolved in 0.5 mL of DMSO in a reaction tube. Subsequently, a suspension of PFL enzyme (10 mg/mL) in 4.5 mL of water was added to it. A steady current of 5 mA was supplied to the reaction mixture using two platinum electrodes while maintaining the temperature at 50 ◦C in an oil bath. Then, electricity was turned off after the completion of the sulfa-Michael addition reaction, as indicated by TLC. Afterward, the reaction mixture was stirred additionally at 50 °C for 72 h to facilitate the generation of 2-fluoro-3-mercaptopropionic acid derivatives. Next, the reaction mixture was transferred to a Buchner funnel with the sintered disc to remove the electrolyte. The crude residue in the funnel was then washed with ethyl acetate. Following that, the mixture underwent centrifugation at a speed of 9500 rpm to separate the enzyme from the reaction mixture. Next, a solution of saturated $NaHCO_3$ in water (3 x 20 mL) was employed to extract the residual acid present in the EtOAc layer. The pH of all the aqueous layers was adjusted to 2-3 by adding a 2M HCl solution. Following acidification, the desired compound (**4**) was extracted using EtOAc (3 x 20 mL), which was subsequently dried with Na_2SO_4 and evaporated using a rotary evaporator. The residue was once again rinsed with EtOAc into a separate round bottom flask. The pure solid product (**4**) was obtained by washing with a mixture of dichloromethane and hexane in a ratio of 1:9.

3.3.4: General procedure for preparing racemic 2-fluoro-3-mercaptopropionic acids (4) as HPLC standards[26]

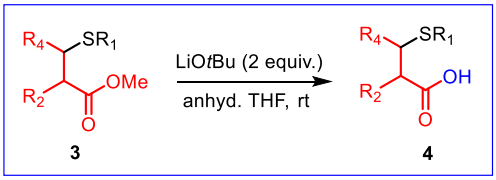

Scheme 3.7: Base-catalyzed racemic synthesis of (**4**)

A round bottom flask, fitted with a magnetic stirrer bar, was charged with lithium *tert*-butoxide (2 equiv.) and ester (**3**) (1 equiv.) dissolved in 2 mL of anhydrous tetrahydrofuran (THF) at room temperature. After the completion of the reaction, as confirmed by thin-layer chromatography (TLC), the tetrahydrofuran (THF) was removed using a rotary evaporator. The pure racemic product was obtained after washing the crude with DCM and hexane respectively.

3.3.5: Procedure to determine % conversion of (3a)

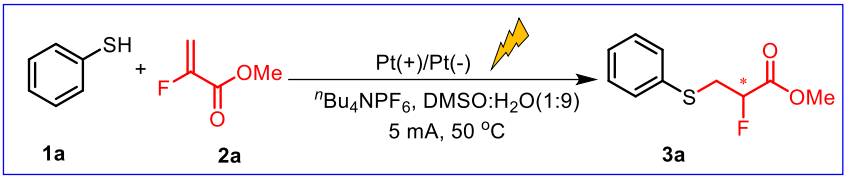

Scheme 3.8: Electrochemical synthesis of (**3a**)

To determine the % conversion, samples (100 µL) were collected after the completion of the reaction and extracted with 300 µL of ethyl acetate. Then, the extracted samples were dried and eluted with isopropyl alcohol (HPLC grade) for HPLC analysis (mobile phase: IPA and hexane) to determine percentage conversion. The following calibration curve was used to calculate the % conversion.

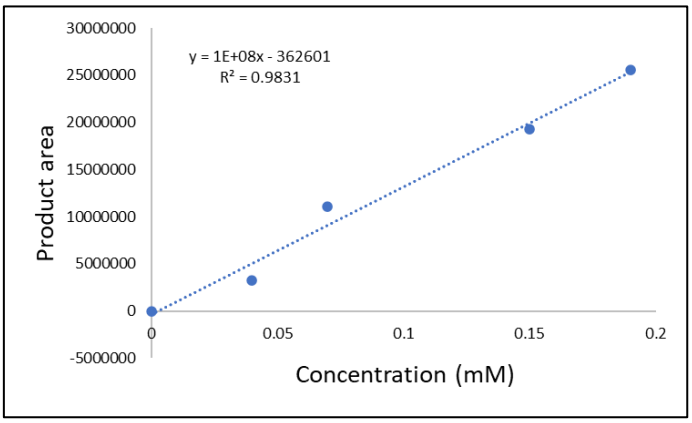

Figure 3.6: Calibration curve of (**3a**)

3.3.6: Procedure to determine the enantiomeric ratio and % conversion of (4d)

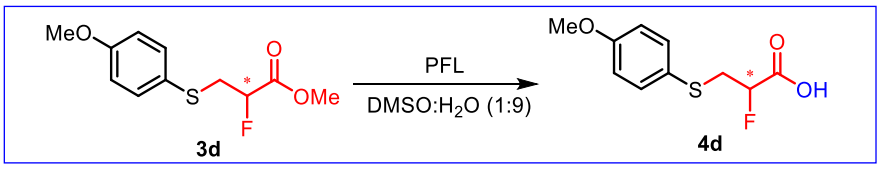

Scheme 3.9: Enzymatic synthesis of (**4d**)

After completion of the reaction, certain aliquots were collected and subjected to extraction using ethyl acetate. The extracted samples were then dried and diluted with isopropyl alcohol to obtain an enantiomeric ratio using Shimadzu HPLC equipped with a chiral column [Lux i-Cellulose-5].

To determine the % conversion, a 10 µL sample was taken and diluted using HPLC grade water followed by injection into Thermo Scientific Dionex Ultimate 3000 HPLC system. The mobile phase consisted of acetonitrile and water, while a C8 column (250 mm x 4.6 mm x 5 µm) served as the stationary phase. The analysis was conducted using the gradient mode. Following calibration curve was used to calculate % conversion.

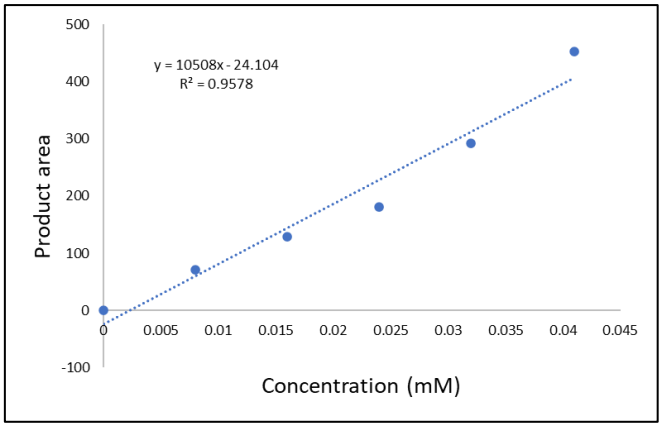

Figure 3.7: Calibration curve of (**4d**)

3.3.7: Representative HPLC chromatograms for one-pot electro-biocatalysis

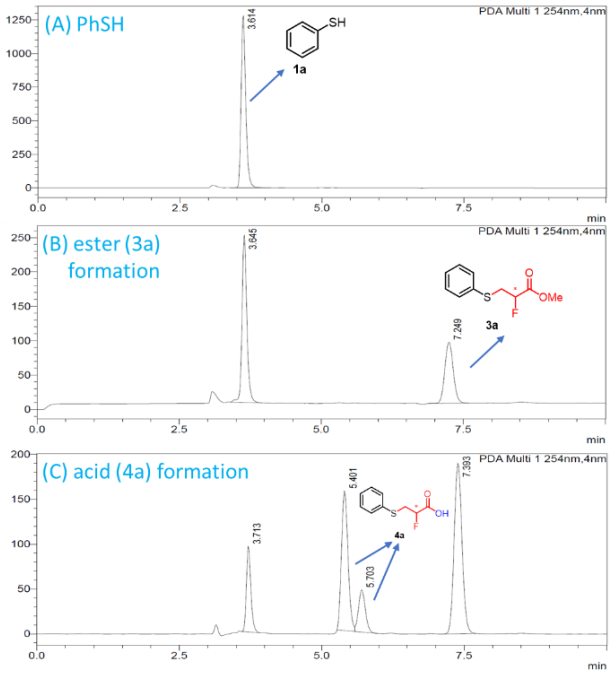

Figure 3.8: HPLC chromatogram for the product (**4a**) formation via electrobiocatalysis

3.3.8: Enzyme denature procedure

By heating: PFL was denatured by heating it to 100 ◦C for 1 h in *N*,*N*-dimethyl formamide.[27]

By urea: PFL was denatured by pre-treatment of urea at 60 ◦C for 3 h.[28]

3.3.9: Procedure for the set-up of sequential electro-biocatalysis

Thiophenol (**1a**) (95 µL, 1.0 mmol, 2 equiv.), methyl-2-fluoroacrylate (**2a**) (45 µL, 0.5 mmol, 1 equiv.) and $^{n}Bu_4NPF_6$ (192 mg, 0.1 M) were dissolved in a mixture of DMSO:H_2O (1:9, v/v, 5 mL). The reaction was initiated by supplying a constant current of 5 mA in an undivided cell with two platinum electrodes at 50 ˚C. After the reaction completion as confirmed by TLC, the reaction mixture was poured into a separatory funnel, and extracted with ethyl acetate. The crude reaction mixture was dried with Na_2SO_4, concentrated under vacuum, and isolated (**3a**) by column chromatography with 90% yield. Afterward, (**3a**) was incubated with PFL enzyme

(10 mg/mL) at ~200 rpm in a DMSO: H_2O (1:9, v/v, 5 mL) for three days. Following that, the mixture underwent centrifugation at a speed of 9500 rpm to separate the enzyme from the reaction mixture. Next, a solution of saturated $NaHCO_3$ in water (3 x 20 mL) was employed to

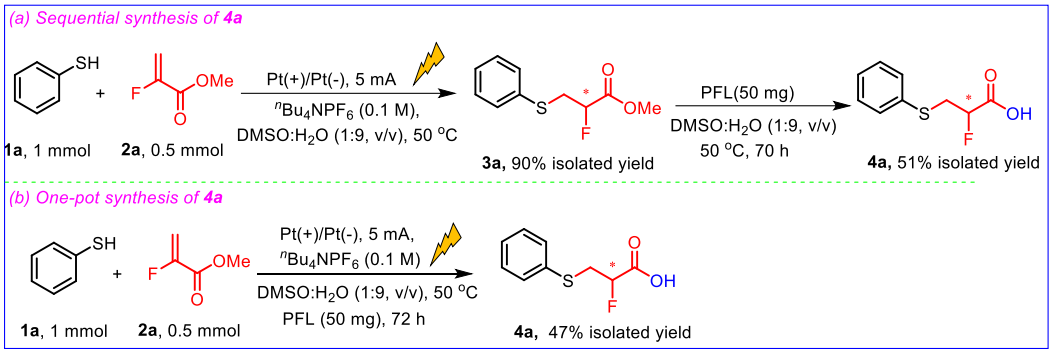

Scheme 3.10: Comparison of sequential and one-pot synthesis of (**4a**) via electro- and biocatalysis

extract the residual acid present in the EtOAc layer. The pH of all the aqueous layers was adjusted to 2-3 by adding a 2M HCl solution. Following acidification, the desired compound (**4a**) was extracted using EtOAc (3 x 20 mL), which was subsequently dried with Na_2SO_4 and evaporated using a rotary evaporator. The residue was once again rinsed with EtOAc into a separate round bottom flask. The pure solid product (**4**) was obtained in 51% yield, after washing the crude with DCM and hexane respectively (**Scheme 3.10**).

3.3.10: Procedure for Gram scale one-pot synthesis of (4a)

Thiophenol (**1a**) (1900 µL, 20 mmol, 2 equiv.), methyl-2-fluoroacrylate (**2a**) (900 µL, 10 mmol, 1 equiv.) and $^nBu_4NPF_6$ (0.1 M) were dissolved in 10 mL of DMSO in a round bottom flask. Subsequently, a suspension of PFL enzyme (10 mg/mL) in 90 mL of water was added to it. A steady current of 5 mA was supplied to the reaction mixture using two platinum electrodes at a temperature of 50 ◦C. Then, electricity was turned off after the completion of the sulfa-Michael addition reaction, as indicated by TLC. Afterward, the reaction mixture was stirred additionally at 50 °C for 72 h to facilitate the generation of (**4a**). Next, the reaction mixture was transferred to a Buchner funnel with the sintered disc to remove the electrolyte. The crude residue in the funnel was then washed with ethyl acetate. Following that, the mixture underwent centrifugation at a speed of 9500 rpm to separate the enzyme from the reaction mixture. Next, a solution of saturated $NaHCO_3$ in water (3 x 250 mL) was employed to extract the residual acid present in the EtOAc layer. The pH of all the aqueous layers was adjusted to 2-3 by adding a 2M HCl solution. Following acidification, the desired compound (**4**) was extracted using EtOAc (3 x 250 mL), which was subsequently dried with Na_2SO_4 and evaporated using a rotary

evaporator. The residue was once again rinsed with EtOAc into a separate round bottom flask. The pure solid product (**4**) was obtained in 45% yield by washing with a mixture of dichloromethane and hexane in a ratio of 1:9.

3.3.11: Docking studies

The binding interactions and approximate binding free energies were predicted using the advanced and extensively used molecular grid-based docking software Autodock (4.2.6).[29] PCL's X-ray crystal coordinates were acquired from the Protein Data Bank (http://www.rcsb.org) with PDB ID 3LIP.[30] Before docking, hydrogen atoms were added and the receptor's structure was changed. The receptor was given Gasteiger charges using AutoDock (MGL) Tools. Using the Discovery studio 2021 client, ligand structures were constructed.[31] The substrate (**3a**) was docked at PCL's active site using an in-silico technique. The grid dimension with center_x ,y,z are 10.966 ,0.552 ,17.911 respectively having each grid size spacing of 40 Å.

Table 3.4: Predicted binding affinity and root mean square deviations (R.S.M.D.) (both lower and upper binding) of substrate (**3a**) upto 9 best poses

Mode	Binding Affinity (kcal/mol)	Distance from the best mode	
		R.S.M.D L.B	R.S.M.D U.B
1	-5.7	0.000	0.000
2	-5.7	6.287	8.071
3	-5.6	0.401	1.323
4	-5.4	2.803	6.462
5	-5.2	6.381	7.752
6	-5.0	2.690	6.260
7	-4.9	10.783	11.500
8	-4.9	3.051	6.485
9	-4.9	6.345	7.755

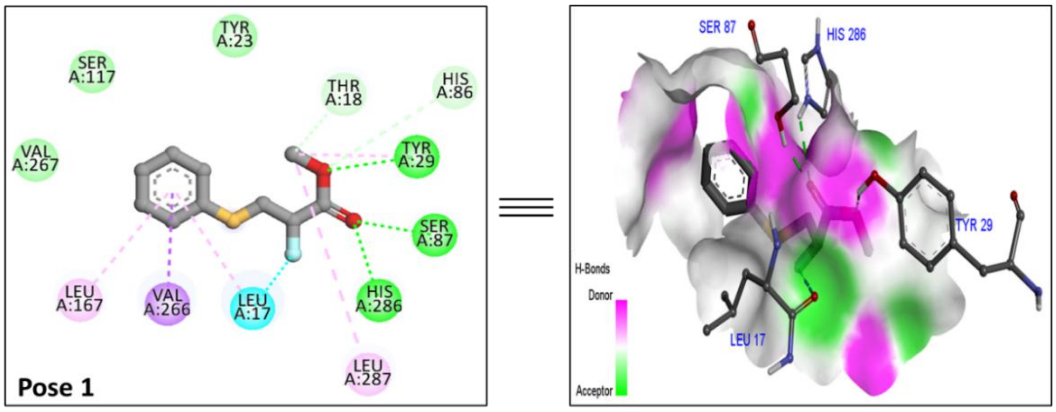
TYR A:23
SER A:117
THR A:18
HIS A:86
VAL A:267
TYR A:29
SER A:87
LEU A:167
VAL A:266
LEU A:17
HIS A:286
LEU A:287
Pose 1
SER 87
HIS 286
TYR 29
LEU 17
H-Bonds
Donor
Acceptor

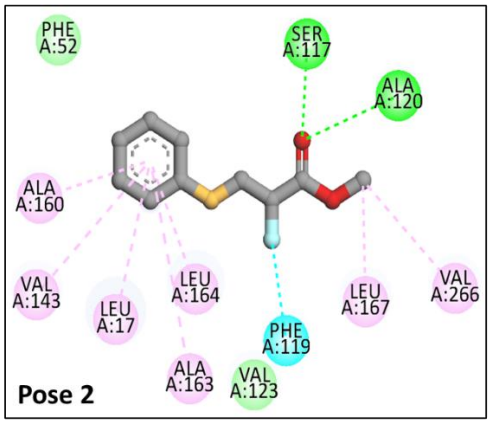
PHE A:52
SER A:117
ALA A:120
ALA A:160
VAL A:143
LEU A:17
LEU A:164
PHE A:119
LEU A:167
VAL A:266
ALA A:163
VAL A:123
Pose 2

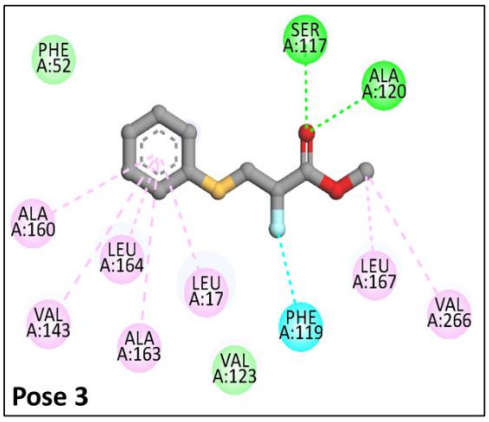
PHE A:52
SER A:117
ALA A:120
ALA A:160
LEU A:164
LEU A:17
LEU A:167
VAL A:143
ALA A:163
PHE A:119
VAL A:266
VAL A:123
Pose 3

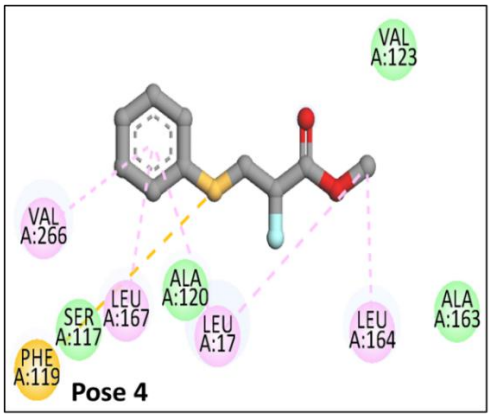
VAL A:123
VAL A:266
ALA A:120
LEU A:167
SER A:117
LEU A:17
ALA A:163
LEU A:164
PHE A:119
Pose 4

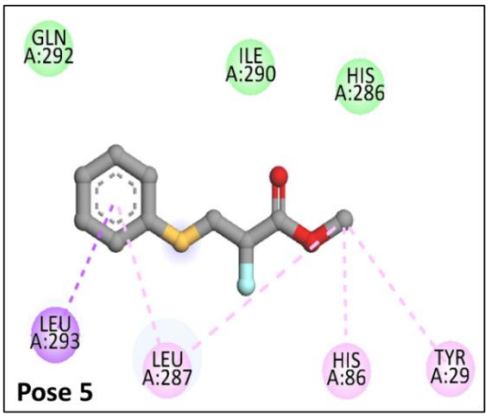
GLN A:292
ILE A:290
HIS A:286
LEU A:293
LEU A:287
HIS A:86
TYR A:29
Pose 5

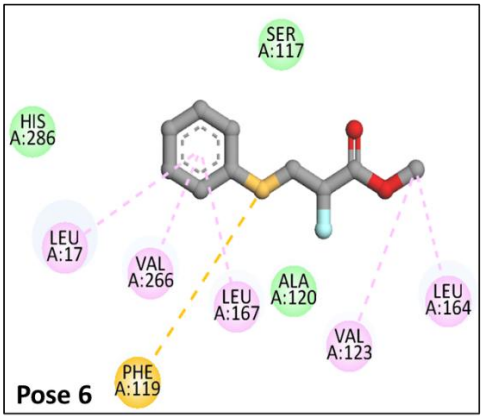
SER A:117
HIS A:286
LEU A:17
VAL A:266
LEU A:167
ALA A:120
LEU A:164
VAL A:123
PHE A:119
Pose 6

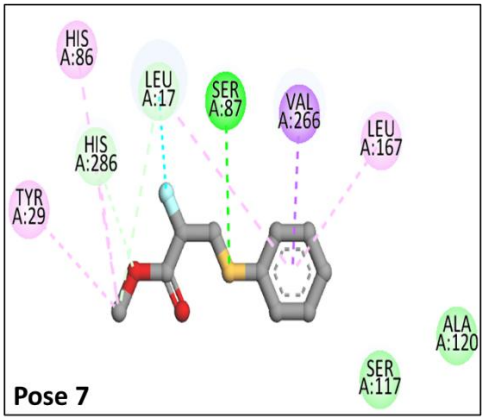
HIS A:86
LEU A:17
SER A:87
VAL A:266
HIS A:286
LEU A:167
TYR A:29
ALA A:120
SER A:117
Pose 7

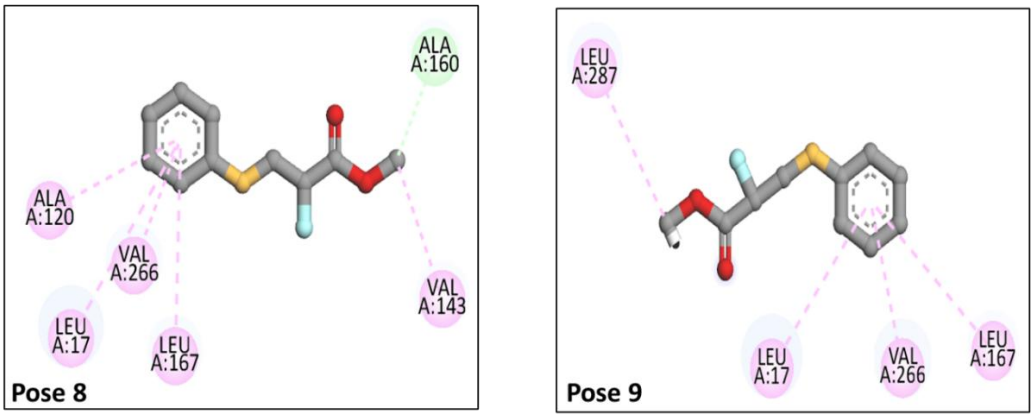

Figure 3.9: 2D interaction of substrate (**3a**) with various amino acids of PCL enzyme up to 9 poses

3.3.12: Procedure for electrolysis and cyclic voltammetry

The electrochemical reactions were carried out using an OWON (P4305) instrument equipped with an undivided cell and a magnetic stirrer. A platinum rectangular plate (25 mm × 6 mm × 1 mm) was used as both the counter and working electrodes, purchased from SmartChemSynths Machine PVT LTD, Hyderabad, India. The distance between the working and counter electrodes was maintained at 1 cm. The electrochemical sulfa-Michael addition reaction was not sensitive to stirring; however, during the hydrolysis reaction, the stirring speed (stir bar: 5 mm × 10 mm) was maintained between 200–300 rpm. Additionally, no homemade electrode was used.

The electrochemical workstation for cyclic voltammetry (CV) was manufactured by SmartChemSynths Machine PVT LTD, Hyderabad, India. . A 30 mm cylindrical platinum wire with a 6 mm shaft, mounted on a Teflon rod and connected via a gold-coated copper rod (2 mm), was used as the working electrode. Before recording each CV, the electrodes were thoroughly cleaned and rinsed with acetone, and the solutions were purged with argon for at least 3 minutes. The initial potential was set to 0 V, and the scan direction ranged from 0 to +3 V (oxidative) at room temperature. The peak potential was measured against an Ag/AgCl reference electrode.

3.3.13: Experimental set-up

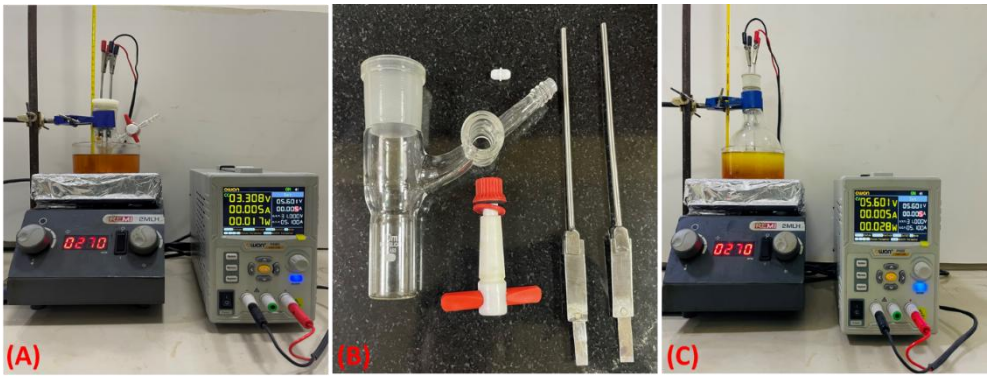

Figure 3.10: (A) Experimental-setup assembly (B) Electrochemical vial, magnetic stirrer bar, and platinum sheet electrodes (C) Gram-scale reaction set-up

3.3.14: Characterization data of synthesized compounds

methyl 2-fluoro-3-(phenylthio)propanoate (3a). The product was prepared according to general procedure (3.3.2) from **1a** (95 µL, 1.0 mmol) and **2a** (45 µL, 0.5 mmol). The crude was purified by column chromatography (mobile phase: EtOAc/Hexane, 1:99 v/v, stationary phase: silica 60-120 mesh), affording **3a** as a colorless liquid in 90% yield (96 mg, 0.45 mmol). ^{1}H NMR (400 MHz, $CDCl_3$): δ_H 7.42-7.39 (m, 2H), 7.28 (td, J = 7.2 Hz, 2.0 Hz, 2H), 7.23-7.19 (m, 1H), 5.06-4.92 (m, 1H), 3.69 (s, 3H), 3.46-3.24 (m, 2H) ppm. $^{13}C\{^{1}H\}$ NMR (100 MHz, $CDCl_3$): δ_C 168.6 (d, $^{2}J_{C-F}$ = 30.0 Hz), 134.3, 131.0, 129.2, 127.3, 87.5 (d, $^{1}J_{C-F}$ = 190.0 Hz), 52.6, 36.6 (d, $^{2}J_{C-F}$ = 20.0 Hz) ppm. HRMS (ESI-TOF) m/z: $[M + OH]^+$ Calcd for $C_{10}H_{12}FO_3S$ 231.0491; Found 231.0486.

methyl 2-fluoro-3-(*p*-tolylthio)propanoate (3b). The product was prepared according to general procedure (3.3.2) from **1b** (119 mg, 1 mmol) and **2a** (45 µL, 0.5 mmol). The crude was purified by column chromatography (mobile phase: EtOAc/Hexane, 1.5:98.5 v/v, stationary phase: silica 60-120 mesh), affording **3b** as a colorless liquid in 93% yield (106 mg, 0.46 mmol). ^{1}H NMR (400 MHz, $CDCl_3$): δ_H 7.34 (dt, J = 8.4 Hz, 2.4 Hz, 2H), 7.11 (d, J = 8.4 Hz, 2H), 5.06-4.91 (m, 1H), 3.72 (s, 3H), 3.43-3.21 (m, 2H), 2.32 (s, 3H) ppm. $^{13}C\{^{1}H\}$ NMR (100 MHz, $CDCl_3$): δ_C 168.7 (d, $^{2}J_{C-F}$ = 20.0 Hz), 137.7, 131.9, 130.5, 129.9, 87.5 (d, $^{1}J_{C-F}$ = 190.0 Hz), 52.5, 37.2 (d, $^{2}J_{C-F}$ = 30.0 Hz), 21.1 ppm. HRMS (ESI^+) m/z: $[M + OH]^+$ calcd for $C_{11}H_{14}FO_3S$: 245.0648, found: 245.0642.

methyl 2-fluoro-3-((2-methoxyphenyl)thio)-2λ^3-propanoate (3c). The product was prepared according to general procedure (3.3.2) from **1c** (116 µL, 1 mmol) and **2a** (45 µL, 0.5 mmol). The crude was purified by column chromatography (mobile phase: EtOAc/Hexane, 3:97 v/v, stationary phase: silica 60-120 mesh), affording **3c** as a colorless liquid in 89% yield (108 mg, 0.44 mmol). ^{1}H NMR (400 MHz, $CDCl_3$): δ_H 7.41 (dd, J = 7.6 Hz, 2.0 Hz, 1H), 7.26, (td, J = 7.6 Hz, 2.0 Hz, 1H), 6.92-6.87 (m, 2H), 5.06-4.91 (m, 1H), 3.89 (s, 3H), 3.69 (s, 3H), 3.45-3.24 (m, 2H) ppm. $^{13}C\{^{1}H\}$ NMR (100 MHz, $CDCl_3$): δ_C 168.8 (d, $^{2}J_{C-F}$ = 20.0 Hz), 158.6, 133.1, 129.3, 121.5, 121.0, 111.0, 87.8 (d, $^{1}J_{C-F}$ = 180.0 Hz), 55.9, 52.6, 34.8 (d, $^{2}J_{C-F}$ = 20.0 Hz) ppm. HRMS (ESI-TOF) m/z: $[M + OH]^+$ Calcd for $C_{11}H_{14}FO_4S$ 261.0597; Found 261.0590.

methyl 2-fluoro-3-((4-methoxyphenyl)thio)-2λ^3-propanoate (3d). The product was prepared according to general procedure(3.3.2) from **1d** (117 µL, 1 mmol) and **2a** (45 µL, 0.5 mmol).

The crude was purified by column chromatography (mobile phase: EtOAc/Hexane, 4:96 v/v, stationary phase: silica 60-120 mesh), affording **3d** as a colorless liquid in 92% yield (112 mg, 0.46 mmol). ^{1}H NMR (400 MHz, $CDCl_3$): δ_H 7.41 (d, J = 8.4 Hz, 2H), 6.83 (d, J = 8.8 Hz, 2H), 5.02-4.87 (m, 1H), 3.77 (s, 3H), 3.71 (s, 3H), 3.34-3.14 (m, 2H) ppm. ^{13}C{^{1}H} NMR (100 MHz, $CDCl_3$): δ_C 168.6 (d, $^{2}J_{C\text{-}F}$ = 30.0 Hz), 159.7, 134.8, 124.3, 114.7, 87.5 (d, $^{1}J_{C\text{-}F}$ = 190.0 Hz), 55.3, 52.5, 38.3 (d, $^{2}J_{C\text{-}F}$ = 20.0 Hz) ppm. HRMS (ESI-TOF) m/z: $[M + OH]^+$ Calcd for $C_{11}H_{14}FO_4S$ 261.0597; Found 261.0596.

methyl 2-fluoro-3-((2-hydroxyphenyl)thio)-2λ^3-propanoate (3e). The product was prepared according to general procedure (3.3.2) from **1e** (97 µL, 1 mmol) and **2a** (45 µL, 0.5 mmol). The crude was purified by column chromatography (mobile phase: EtOAc/Hexane, 5:95 v/v, stationary phase: silica 60-120 mesh), affording **3e** as a colorless liquid in 83% yield (95 mg, 0.41 mmol). ^{1}H NMR (400 MHz, $CDCl_3$): δ_H 7.46 (d, J = 8.0 Hz, 1H), 7.23 (t, J = 8.4 Hz, 1H), 6.95 (d, J = 8.4 Hz, 1H), 6.84 (t, J = 6.0 Hz, 1H), 6.69 (s, 1H), 4.97-4.82 (m, 1H), 3.70 (s, 3H), 3.22-3.05 (m, 2H) ppm. ^{13}C{^{1}H} NMR (100 MHz, $CDCl_3$): δ_C 168.5 (d, $^{2}J_{C\text{-}F}$ = 30.0 Hz), 157.4, 136.5, 131.9, 121.2, 117.2, 115.5, 87.0 (d, $^{1}J_{C\text{-}F}$ = 180.0 Hz), 52.8, 38.2 (d, $^{2}J_{C\text{-}F}$ = 20.0 Hz) ppm. ^{19}F NMR (376 MHz, $CDCl_3$): δ_F -189.66 – -190.03 (m) ppm. HRMS (ESI-TOF) m/z: $[M + OH]^+$ Calcd for $C_{10}H_{12}FO_4S$ 247.0440; Found 247.0453.

methyl 3-((2-bromophenyl)thio)-2-fluoro-2λ^3-propanoate (3f). The product was prepared according to general procedure (3.3.2) from **1f** (116 µL, 1 mmol) and **2a** (45 µL, 0.5 mmol). The crude was purified by column chromatography (mobile phase: EtOAc/Hexane, 2.5:97.5 v/v, stationary phase: silica 60-120 mesh), affording **3f** as a colorless liquid in 73% yield (107 mg, 0.36 mmol). ^{1}H NMR (400 MHz, $CDCl_3$): δ_H 7.57 (dd, J = 8.0 Hz, 1.6 Hz, 1H), 7.43 (dd, J = 7.6 Hz, 1.2 Hz, 1H), 7.27 (td, 7.2 Hz, 1.2 Hz, 1H), 7.09 (td, J = 7.2 Hz, 1.2 Hz, 1H), 5.14-4.99 (m, 1H), 3.76 (s, 3H), 3.52-3.31 (m, 2H) ppm. ^{13}C{^{1}H} NMR (100 MHz, $CDCl_3$): δ_C 168.4 (d, $^{2}J_{C\text{-}F}$ = 30.0 Hz), 135.5, 133.4, 131.1, 128.3, 128.0, 125.7, 87.5 (d, $^{1}J_{C\text{-}F}$ = 190.0 Hz), 52.7, 35.5 (d, $^{2}J_{C\text{-}F}$ = 20.0 Hz) ppm. HRMS (ESI-TOF) m/z: $[M - HBr]^+$ Calcd for $C_{10}H_{10}FO_2S$ 213.0386; Found 213.0377.

methyl 3-((4-bromophenyl)thio)-2-fluoro-2λ^3-propanoate (3g). The product was prepared according to general procedure (3.3.2) from **1g** (182 mg, 1 mmol) and **2a** (45 µL, 0.5 mmol). The crude was purified by column chromatography (mobile phase: EtOAc/Hexane, 1.5:98.5 v/v, stationary phase: silica 60-120 mesh), affording **3g** as a colorless liquid in 81% yield (118 mg, 0.40 mmol).^{1}H NMR (400 MHz, $CDCl_3$): δ_H 7.34 (dt, J = 8.8 Hz, 2.8 Hz, 2H), 7.24 (dt, J = 8.8 Hz, 2.4 Hz, 2H), 5.05-4.89 (m, 1H), 3.69 (s, 3H), 3.41-3.20 (m, 2H) ppm. ^{13}C{^{1}H} NMR (100 MHz, $CDCl_3$): δ_C 168.4 (d, $^{2}J_{C\text{-}F}$ = 20.0 Hz), 133.6, 132.6, 132.2, 121.4, 87.6 (d, $^{1}J_{C\text{-}F}$ =

190.0 Hz), 52.7, 36.6 (d, $^{2}J_{C\text{-}F}$ = 30.0 Hz) ppm. HRMS (ESI-TOF) m/z: $[M - H]^+$ Calcd for $C_{10}H_9BrFO_2S$ 290.9491; Found 290.9505.

methyl 3-((4-chlorophenyl)thio)-2-fluoro-2λ^3-propanoate (3h). The product was prepared according to general procedure (3.3.2) from **1h** (138 mg, 1 mmol) and **2a** (45 µL, 0.5 mmol). The crude was purified by column chromatography (mobile phase: EtOAc/Hexane, 2.5:97.5 v/v, stationary phase: silica 60-120 mesh), affording **3h** as a colorless liquid in 79% yield (98 mg, 0.39 mmol). ^{1}H NMR (700 MHz, $CDCl_3$): δ_H 7.35 (dt, J = 9.1 Hz, 2.8 Hz, 2H), 7.26 (dt, J = 8.4 Hz, 2.8 Hz, 2H), 5.05-4.96 (m, 1H), 3.73 (s, 3H), 3.42-3.36 (m, 1H), 3.32-3.26 (m, 1H) ppm. ^{13}C{^{1}H} NMR (175 MHz, $CDCl_3$): δ_C 168.4 (d, $^{2}J_{C\text{-}F}$ = 17.5 Hz), 133.5, 132.9, 132.5, 129.3, 87.7 (d, $^{1}J_{C\text{-}F}$ = 192.5 Hz), 52.7, 36.8 (d, $^{2}J_{C\text{-}F}$ = 17.5 Hz) ppm. HRMS (ESI-TOF) m/z: $[M + OH]^+$ Calcd for $C_{10}H_{11}ClFO_3S$ 265.0101; Found 265.0107.

methyl 2-fluoro-3-((4-nitrophenyl)thio)-2λ^3-propanoate (3i). The product was prepared according to general procedure (3.3.2) from **1i** (149 mg, 1 mmol) and **2a** (45 µL, 0.5 mmol). The crude was purified by column chromatography (mobile phase: EtOAc/Hexane, 6:94 v/v, stationary phase: silica 60-120 mesh), affording **3i** as a yellow liquid in 10% yield (13 mg, 0.05 mmol). ^{1}H NMR (400 MHz, $CDCl_3$): δ_H 8.09 (dt, J = 9.2 Hz, 2.8 Hz, 2H), 7.42 (dt, J = 9.2 Hz, 2.8 Hz, 2H), 5.21-5.06 (m, 1H), 3.78 (s, 3H), 3.63-3.40 (m, 2H) ppm. ^{13}C{^{1}H} NMR (100 MHz, $CDCl_3$): δ_C 168.0 (d, $^{2}J_{C\text{-}F}$ = 20.0 Hz), 145.8, 144.9, 127.7, 124.0, 87.5 (d, $^{1}J_{C\text{-}F}$ = 190.0 Hz), 52.9, 34.4 (d, $^{2}J_{C\text{-}F}$ = 30.0 Hz) ppm. ^{19}F NMR (376 MHz, $CDCl_3$): δ_F -188.84 (dt, $^{2}J_{F\text{-}H}$ = 50.9 Hz, $^{3}J_{F\text{-}H}$ = 25.4 Hz) ppm, HRMS (ESI-TOF) m/z: $[M + OH]^+$ Calcd for $C_{10}H_{11}FNO_5S$ 276.0342; Found 276.0346.

methyl 3-(benzylthio)-2-fluoro-2λ^3-propanoate (3j). The product was prepared according to general procedure (3.3.2) from **1j** (119 µL, 1 mmol) and **2a** (45 µL, 0.5 mmol). The crude was purified by column chromatography (mobile phase: EtOAc/Hexane, 2:98 v/v, stationary phase: silica 60-120 mesh), affording **3j** as a colorless liquid in 44% yield (13 mg, 0.19 mmol). ^{1}H NMR (700 MHz, $CDCl_3$): δ_H 7.27-7.24 (m, 4H), 7.21-7.17 (m, 1H), 5.04-4.96 (m, 1H), 3.75 (d, J = 3.5 Hz, 2H), 3.74 (s, 3H), 2.87-2.74 (m, 2H) ppm. ^{13}C{^{1}H} NMR (175 MHz, $CDCl_3$): δ_C 168.7 (d, $^{2}J_{C\text{-}F}$ = 17.5 Hz), 137.6, 129.2, 128.7, 127.4, 89.7 (d, $^{1}J_{C\text{-}F}$ = 192.5 Hz), 52.6, 36.9, 32.4 (d, $^{2}J_{C\text{-}F}$ = 17.5 Hz) ppm. HRMS (ESI-TOF) m/z: $[M + OH]^+$ Calcd for $C_{11}H_{14}FO_3S$ 245.0648; Found 245.0643.

ethyl 4,4,4-trifluoro-3-(phenylthio)-3λ^3-butanoate (3l).[4] The product was prepared according to general procedure (3.3.2) from **1a** (65 µL, 0.4 mmol) and **2b** (42 µL, 0.2 mmol). The crude was purified by column chromatography (mobile phase: EtOAc/Hexane, 1:99 v/v, stationary phase: silica 60-120 mesh), affording **3l** as a colorless liquid in 62% yield (51 mg,

0.18 mmol). ^{1}H NMR (400 MHz, $CDCl_3$): δ_H 7.59-7.57 (m, 2H), 7.35-7.32 (m, 3H), 4.27-4.19 (m, 2H), 3.99-3.89 (m, 1H), 2.87 (dd, J = 16.8 Hz, 4.0 Hz, 1H), 2.65 (dd, J = 16.8 Hz, 10.8 Hz, 1H), 1.29 (t, J = 7.6 Hz, 3H) ppm. ^{13}C{^{1}H} NMR (100 MHz, $CDCl_3$): δ_C 169.5, 134.2, 132.3, 129.3, 129.0, 128.9, 127.7, 124.9, 61.6, 48.7 (q, $^1J_{C\text{-}F}$ = 30.0 Hz), 34.6, 14.2 ppm.

methyl 3-((2-chlorophenyl)thio)-2-fluoro-3λ^3-propanoate (3o). The product was prepared according to general procedure (3.3.2) from **1o** (112 µL, 1 mmol) and **2a** (45 µL, 0.5 mmol). The crude was purified by column chromatography (mobile phase: EtOAc/Hexane, 2:98 v/v, stationary phase: silica 60-120 mesh), affording **3o** as a colorless liquid in 72% yield (89 mg, 0.36 mmol). ^{1}H NMR (300 MHz, $CDCl_3$): δ_H 7.49-7.41 (m, 2H), 7.28-7.18 (m, 2H), 5.17-4.99 (m, 1H), 3.77 (s, 3H), 3.56-3.32 (m, 2H) ppm. ^{13}C{^{1}H} NMR (75 MHz, $CDCl_3$): δ_C 168.4 (d, $^2J_{C\text{-}F}$ = 22.5 Hz), 135.5, 133.3, 131.6, 130.1, 128.4, 127.4, 87.6 (d, $^1J_{C\text{-}F}$ = 187.5 Hz), 52.7, 35.1 (d, $^2J_{C\text{-}F}$ = 22.5 Hz) ppm. HRMS (ESI-TOF) m/z: [M - HCl]$^+$ Calcd for $C_{10}H_{10}FO_2S$ 213.0386; Found 213.0381.

methyl 2-fluoro-3-((4-fluorophenyl)thio)-2λ^3-propanoate (3p). The product was prepared according to general procedure (3.3.2) from **1p** (102 µL, 1 mmol) and **2a** (45 µL, 0.5 mmol). The crude was purified by column chromatography (mobile phase: EtOAc/Hexane, 2:98 v/v, stationary phase: silica 60-120 mesh), affording **3p** as a colorless liquid in 70% yield (81 mg, 0.35 mmol). ^{1}H NMR (300 MHz, $CDCl_3$): δ_H 7.44 (t, J = 5.4 Hz, 2H), 6.99 (t, J = 8.7 Hz, 2H), 5.08-4.89 (m, 1H), 3.72 (s, 3H), 3.41-3.18 (m, 2H) ppm. ^{13}C{^{1}H} NMR (75 MHz, $CDCl_3$): δ_C 168.5 (d, $^2J_{C\text{-}F}$ = 22.5 Hz), 162.5 (d, $^1J_{C\text{-}F}$ = 240.0 Hz), 134.3 (d, $^4J_{C\text{-}F}$ = 7.5 Hz), 129.2 (d, $^3J_{C\text{-}F}$ = 7.5 Hz), 116.3 (d, $^2J_{C\text{-}F}$ = 15.0 Hz), 87.6 (d, $^1J_{C\text{-}F}$ = 187.5 Hz), 52.6, 37.7 (d, $^2J_{C\text{-}F}$ = 22.5 Hz) ppm. HRMS (ESI-TOF) m/z: [M + OH]$^+$ Calcd for $C_{10}H_{11}F_2O_3S$ 249.0397; Found 249.0391.

methyl 3-((4-cyanophenyl)thio)-2-fluoropropanoate (3q). The product was prepared according to general procedure (3.3.2) from **1q** (130 mg, 1 mmol) and **2a** (45 µL, 0.5 mmol). The crude was purified by column chromatography (mobile phase: EtOAc/Hexane, 15:85 v/v, stationary phase: silica 60-120 mesh), affording **3q** as a yellow liquid in 32% yield (38 mg, 0.16 mmol). ^{1}H NMR (300 MHz, $CDCl_3$): δ_H 7.55 (d, J = 8.7 Hz, 2H), 7.41 (d, J = 8.1 Hz, 2H), 5.21-5.03 (m, 1H), 3.79 (s, 3H), 3.61-3.34 (m, 2H) ppm. ^{13}C{^{1}H} NMR (75 MHz, $CDCl_3$): δ_C 168.2 (d, $^2J_{C\text{-}F}$ = 30.0 Hz), 142.3, 132.5, 128.5, 118.6, 109.7, 87.6 (d, $^1J_{C\text{-}F}$ = 187.5 Hz), 52.9, 34.7 (d, $^2J_{C\text{-}F}$ = 22.5 Hz) ppm. HRMS (ESI-TOF) m/z: [M + OH]$^+$ Calcd for $C_{11}H_{11}FNO_3S$ 256.0444; Found 256.0449.

2-fluoro-3-(phenylthio)-2λ^3-propanoic acid (4a). The product **4a** was prepared following General Procedure (3.3.3) using **1a** (95 µL, 1 mmol) and **2a** (45 µL, 0.5 mmol). The crude product was obtained as a white powder with a 47% yield (47 mg, 0.23 mmol).^{1}H NMR (600

MHz, DMSO-d^6): δ_H 8.32-8.30 (m, 1H), 7.35-7.27 (m, 4H), 7.17-7.16 (m, 1H), 4.64-4.53 (m, 1H), 3.52-3.46 (m, 1H), 3.22-3.14 (m, 1H) ppm. $^{13}C\{^1H\}$ NMR (100 MHz, $CDCl_3$): δ_C 170.4 (d, $^2J_{C-F}$ = 20.0 Hz), 136.6, 129.1, 128.1, 125.7, 89.8 (d, $^1J_{C-F}$ = 180.0 Hz), 36.6 (d, $^2J_{C-F}$ = 20.0 Hz) ppm. HRMS (ESI-TOF) m/z: $[M - H]^+$ Calcd for $C_9H_8FO_2S$ 199.0229; Found 199.0233. 77:23 *e.r.*, determined by chiral HPLC [Lux i-Cellulose-5 column, isopropanol/hexane (0.1% trifluoroacetic acid) = 7/97, flow rate 1.0 mL/min, λ = 254 nm], retention time: 6.28 min (major), 6.81 min (minor).

2-fluoro-3-(*p*-tolylthio)-2λ^3-propanoic acid (4b). The product **4b** was prepared following General Procedure (3.3.3) using **1b** (119 mg, 1 mmol) and **2a** (45 µL, 0.5 mmol). The crude product was obtained as a white powder with a 49% yield (52 mg, 0.24 mmol).^{1}H NMR (400 MHz, DMSO-d^6): δ_H 7.25 (dt, J = 8.4 Hz, 2.0 Hz, 2H), 7.12 (dt, J = 8.4 Hz, 2.8 Hz, 2H), 4.57-4.41 (m, 1H), 3.48 (dd, J = 14.4 Hz, 2.4 Hz, 1H), 3.40 (dd, J = 14.4 Hz, 2.4 Hz, 1H), 3.16-3.06 (m, 1H), 2.26 (s, 3H) ppm. $^{13}C\{^1H\}$ NMR (100 MHz, DMSO-d^6): δ_C 170.0 (d, $^2J_{C-F}$ = 20.0 Hz), 135.3, 132.7, 129.7, 128.9, 89.8 (d, $^1J_{C-F}$ = 180 Hz), 37.3 (d, $^2J_{C-F}$ = 30.0 Hz), 20.6 ppm. HRMS (ESI-TOF) m/z: $[M - H]^+$ Calcd for $C_{10}H_{10}FO_2S$ 213.0386; Found: 213.0389. 80:20 *e.r.*, determined by chiral HPLC [Lux i-Cellulose-5 column, isopropanol/hexane (0.1% trifluoroacetic acid) = 5/95, flow rate 1.0 mL/min, λ = 254 nm], retention time: 7.90 min (major), 8.66 min (minor).

2-fluoro-3-((2-methoxyphenyl)thio)-2λ^3-propanoic acid (4c). The product **4c** was prepared following General Procedure (3.3.3) using **1c** (116 µL, 1 mmol) and **2a** (45 µL, 0.5 mmol). The crude product was obtained as an off-white powder with a 50% yield (57 mg, 0.25 mmol). ^{1}H NMR (300 MHz, $CDCl_3$): δ_H 7.72 (d, J = 15.0 Hz, 1H), 7.44- 7.35 (m, 1H), 6.99-6.93 (m, 1H), 6.85-6.79 (m, 1H), 5.56- 5.50 (m, 1H), 3.84 (s, 3H), 3.13-3.05 (m, 2H) ppm. $^{13}C\{^1H\}$ NMR (100 MHz, DMSO-d^6): δ_C 170.5 (d, $^2J_{C-F}$ = 20.0 Hz), 156.3, 127.6, 126.6, 124.8, 121.2, 110.9, 89.8 (d, $^1J_{C-F}$ = 180.0 Hz), 55.9, 34.9 (d, $^2J_{C-F}$ = 20.0 Hz) ppm. HRMS (ESI-TOF) m/z: $[M - H]^+$ Calcd for $C_{10}H_{10}FO_3S$ 229.0335; Found 229.0339. 72:28 *e.r.*, determined by chiral HPLC [Lux i-Cellulose-5 column, isopropanol/hexane (0.1% trifluoroacetic acid) = 10/90, flow rate 1.0 mL/min, λ = 254 nm], retention time: 8.39 min (major), 9.26 min (minor).

2-fluoro-3-((4-methoxyphenyl)thio)-2λ^3-propanoic acid (4d). The product **4d** was prepared following General Procedure (3.3.3) using **1d** (117 µL, 1 mmol) and **2a** (45 µL, 0.5 mmol). The crude product was obtained as an off-white powder with a 49% yield (56 mg, 0.24 mmol). ^{1}H NMR (400 MHz, DMSO-d^6): δ_H 7.35 (dt, J = 8.8 Hz, 3.6 Hz, 2H), 6.90 (dt, J = 8.4 Hz, 3.2 Hz, 2H), 4.52-4.36 (m, 1H), 3.73 (s, 3H), 3.39-3.28 (m, 1H), 3.09-2.99 (m, 1H) ppm. $^{13}C\{^1H\}$ NMR (100 MHz, DMSO-d^6): δ_C 169.8 (d, $^2J_{C-F}$ = 10.0 Hz), 158.4, 132.3, 126.3, 114.9, 89.8 (d,

$^{1}J_{C\text{-}F}$ =190.0 Hz), 55.2, 38.8 (d, $^{2}J_{C\text{-}F}$ = 10.0 Hz) ppm. HRMS (ESI-TOF) m/z: $[M - H]^+$ Calcd for $C_{10}H_{10}FO_3S$ 229.0335; Found 229.0339. 83:17 *e.r.*, determined by chiral HPLC [Lux i-Cellulose-5 column, isopropanol/hexane (0.1% trifluoroacetic acid) = 10/90, flow rate 1.0 mL/min, λ = 254 nm], retention time: 6.87 min (major), 7.42 min (minor).

3-((2-bromophenyl)thio)-2-fluoro-2λ^3-propanoic acid (4f). The product **4f** was prepared following General Procedure (3.3.3) using **1f** (116 µL, 1 mmol) and **2a** (45 µL, 0.5 mmol). The crude product was obtained as a white powder with a 42% yield (58 mg, 0.21 mmol). ^{1}H NMR (400 MHz, DMSO-d^6): δ_H 7.63-7.53 (m, 1H), 7.36 (dd, J = 19.2 Hz, 7.6 Hz, 2H), 7.04 (t, 7.6 Hz, 1H), 4.59 (dd, $^{2}J_{H\text{-}F}$ = 52.2 Hz, $^{2}J_{H\text{-}H}$ = 52.4 Hz, 9.2 Hz, 1H), 3.25-3.12 (m, 2H) ppm. ^{13}C{^{1}H} NMR (100 MHz, DMSO-d^6): δ_C 169.8 (d, $^{2}J_{C\text{-}F}$ = 10.0 Hz), 138.1, 135.4, 133.2, 132.7, 130.3, 128.8, 128.4, 127.1, 126.5, 123.1, 121.4, 89.4 (d, $^{1}J_{C\text{-}F}$ = 180.0 Hz), 35.8 (d, $^{2}J_{C\text{-}F}$ = 20.0 Hz) ppm. HRMS (ESI-TOF) m/z: $[M - H]^+$ Calcd for $C_9H_7BrFO_2S$ 276.9334;, Found 276.9338. 74:26 *e.r.*, determined by chiral HPLC [Lux i-Cellulose-5 column, isopropanol/hexane (0.1% trifluoroacetic acid) = 1/99, flow rate 1.0 mL/min, λ = 254 nm], retention time: 12.56 min (major), 13.43 min (minor).

3-((4-bromophenyl)thio)-2-fluoro-2λ^3-propanoic acid (4g). The product **4g** was prepared following General Procedure (3.3.3) using **1g** (182 mg, 1 mmol) and **2a** (45 µL, 0.5 mmol). The crude product was obtained as a white powder with a 45% yield (62 mg, 0.22 mmol). ^{1}H NMR (400 MHz, DMSO-d^6): δ_H 7.44 (d, J = 8.8 Hz, 2H), 7.26 (d, J =8.8 Hz, 2H), 4.57-4.41 (m, 1H), 3.52-3.40 (m, 1H), 3.20-3.10 (m, 1H) ppm. ^{13}C{^{1}H} NMR (100 MHz, DMSO-d^6): δ_C 169.5 (d, $^{2}J_{C\text{-}F}$ = 20.0 Hz), 136.5, 131.8, 129.9, 118.4, 89.8 (d, $^{1}J_{C\text{-}F}$ = 190.0 Hz), 36.5 (d, $^{2}J_{C\text{-}F}$ = 30.0 Hz) ppm. HRMS (ESI-TOF$^-$) m/z: $[M - H]^+$ Calcd for $C_9H_7BrFO_2S$ 276.9334; Found 276.9343. 74:26 *e.r.*, determined by chiral HPLC [Lux i-Cellulose-5 column, isopropanol/hexane (0.1% trifluoroacetic acid) = 1/99, flow rate 1.0 mL/min, λ = 254 nm], retention time: 29.09 min (major), 31.40 min (minor).

3-((4-chlorophenyl)thio)-2-fluoro-2λ^3-propanoic acid (4h). The product **4h** was prepared following General Procedure (3.3.3) using **1h** (138 mg, 1 mmol) and **2a** (45 µL, 0.5 mmol). The crude product was obtained as a white powder with a 44% yield (51 mg, 0.22 mmol). ^{1}H NMR (400 MHz, DMSO-d^6): δ_H 7.39-7.34 (m, 4H), 4.57-4.41 (m, 1H), 3.54-3.43 (m, 1H), 3.23-3.12 (m, 1H) ppm. ^{13}C{^{1}H} NMR (100 MHz, DMSO-d^6): δ_C 169.2 (d, $^{2}J_{C\text{-}F}$ = 20.0 Hz), 135.9, 130.1, 129.6, 128.9, 89.8, (d, $^{1}J_{C\text{-}F}$ = 190.0 Hz), 36.8 (d, $^{2}J_{C\text{-}F}$ = 20.0 Hz) ppm. HRMS (ESI-TOF) m/z: $[M - H]^+$ Calcd for $C_9H_7ClFO_2S$ 232.9839; Found 232.9844. 69:31 *e.r.*, determined by chiral HPLC [Lux i-Cellulose-5 column, isopropanol/hexane (0.1%

trifluoroacetic acid) = 1/99, flow rate 1.0 mL/min, λ = 254 nm], retention time: 29.86 min (major), 32.35 min (minor).

3-(benzylthio)-2-fluoro-2λ^3-propanoic acid (4j). The product **4j** was prepared following General Procedure (3.3.3) using **1j** (119 µL, 1 mmol) and **2a** (45 µL, 0.5 mmol). The crude product was obtained as an off-white powder with a 21% yield (52 mg, 0.10 mmol). ^{1}H NMR (400 MHz, DMSO-d^6): δ_H 7.31-7.28 (m, 4H), 7.24-7.20 (m, 1H), 4.64-4.48 (m, 1H), 3.77 (s, 2H), 2.95-2.82 (m, 1H), 2.73-2.63 (m, 1H) ppm. ^{13}C{^{1}H} NMR (100 MHz, DMSO-d^6): δ_C 170.4 (d, $^2J_{C\text{-}F}$ = 20.0 Hz), 138.8, 128.9, 128.3, 126.7, 91.2 (d, $^1J_{C\text{-}F}$ = 180.0 Hz), 36.1, 34.4 (d, $^2J_{C\text{-}F}$ = 30.0 Hz) ppm. HRMS (ESI-TOF) m/z: [M - H]$^+$ Calcd for $C_{10}H_{10}FO_2S$ 213.0386; Found 213.0351. 69:31 *e.r.*, determined by chiral HPLC [Lux i-Cellulose-5 column, isopropanol/hexane (0.1% trifluoroacetic acid) = 10/90, flow rate 1.0 mL/min, λ = 254 nm], retention time: 5.43 min (major), 5.95 min (minor).

4,4,4-trifluoro-3-(phenylthio)-3λ^3-butanoic acid (4l). The product **4l** was prepared following General Procedure (3.3.3) using **1a** (65 µL, 0.4 mmol) and **2b** (42 µL, 0.2 mmol). The crude product was obtained as an off-white powder with a 32% yield (24 mg, 0.09 mmol). ^{1}H NMR (400 MHz, DMSO-d^6): δ_H 7.59-7.49 (m, 2H), 7.35-7.23 (m, 3H), 6.47-6.31 (m, 1H), 4.29 (brs, 1H), 2.43 (brs, 1H), 2.21-2.15 (m, 1H) ppm. ^{13}C{^{1}H} NMR (100 MHz, DMSO-d^6): δ_C 170.9, 133.8, 131.9, 129.2, 127.8 124.4, 48.9, 37.3 ppm. HRMS (ESI-TOF$^-$) m/z: [M - H]$^+$ Calcd for $C_{10}H_8F_3O_2S$ 249.0197; Found 249.0203.

3-((2-aminophenyl)thio)-2-fluoro-2λ^3-propanoic acid (4m). The product **4m** was prepared following General Procedure (3.3.3) using **1m** (102 µL, 1 mmol) and **2a** (45 µL, 0.5 mmol). The crude product was obtained as yellow powder with a 47% yield (50 mg, 0.23 mmol).^{1}H NMR (400 MHz, DMSO-d^6): δ_H 7.25 (d, J = 7.2 Hz, 1H), 7.02 (t, J = 6.4 Hz, 1H), 6.70 (d, J = 8.4 Hz, 1H), 6.49 (t, J = 7.6 Hz, 1H), 5.38 (s, 2H), 4.51-4.35 (m, 1H), 3.22-3.10 (m, 1H), 2.97-2.87 (m, 1H) ppm. ^{13}C{^{1}H} NMR (100 MHz, DMSO-d^6): δ_C 170.2 (d, $^2J_{C\text{-}F}$ = 20.0 Hz) 149.8, 135.4, 129.5, 116.3, 115.7, 114.4, 89.8 (d, $^1J_{C\text{-}F}$ = 180.0 Hz), 79.3, 38.0 (d, $^2J_{C\text{-}F}$ = 20.0 Hz) ppm. HRMS (ESI-TOF) m/z: [M - H]$^+$ Calcd for $C_9H_9FNO_2S$ 214.0338; Found 214.0331..

4,4,4-trifluoro-3-((4-methoxyphenyl)thio)butanoic acid (4n).[4] The product **4n** was prepared following General Procedure (3.3.3) using **1d** (73 µL, 0.6 mmol), **2b** (45 µL, 0.3 mmol). The crude product was obtained as an off-white powder with a 39% yield (32 mg, 0.11 mmol). ^{1}H NMR (700 MHz, DMSO-d^6): δ_H 7.55-7.43 (m, 2H), 6.91-6.86 (m, 2H), 4.05 (s, 1H), 3.74 (s, 3H), 2.42-2.39 (m, 1H), 2.19-2.15 (m, 1H) ppm. HRMS (ESI-TOF) m/z: [M - H]$^+$ Calcd for $C_{11}H_{10}F_3O_3S$ 279.0303; Found 279.0310.

3.4: Conclusion

In summary, an asymmetric synthesis of sulfur-based organofluorine compounds has been developed via the integration of organic electrosynthesis with lipase-mediated biocatalysis. Further, a variety of 2-fluoro-3-mercaptopropionic acids have been synthesized in moderate yields and good enantioselectivities by using thiophenols and fluorine-containing α, β-unsaturated alkenes in water as a solvent. To get an insight about the mechanism of the one-pot protocol, molecular docking, and other control experiments were carried out that suggested the role of electricity and enzyme active site in the catalysis. The scalability of the developed protocol was shown by setting up a gram-scale reaction. Besides, the practical efficacy has been illustrated via synthesizing a key intermediate of MMP-3 inhibitor. Notably, this metal, ligand, and additional oxidant-free electro-biocatalyst protocol enable further applications of enzymatic electrosynthesis in asymmetric organic transformations.

3.5: References

1. (a) Politanskaya, L. V.; Selivanova, G. A.; Panteleeva, E. V.; Tretyakov, E. V.; Platonov, V. E.; Nikul'shin, P. V.; Vinogradov, A. S.; Zonov, Y. V.; Karpov, V. M.; Mezhenkova, T. V.; Vasilyev, A. V.; Koldobskii, A. B.; Shilova, O. S.; Morozova, S. M.; Burgart, Y. V.; Shchegolkov, E. V.; Saloutin, V. I.; Sokolov, V. B.; Aksinenko, A. Yu.; Nenajdenko, V. G.; Moskalik, M. Yu.; Astakhova, V. V.; Shainyan, B. A.; Tabolin, A. A.; Ioffe, S. L.; Muzalevskiy, V. M.; Balenkova, E. S.; Shastin, A. V.; Tyutyunov, A. A.; Boiko, V. E.; Igumnov, S. M.; Dilman, A. D.; Adonin, N. Yu.; Bardin, V. V.; Masoud, S. M.; Vorobyeva, D. V.; Osipov, S. N.; Nosova, E. V.; Lipunova, G. N.; Charushin, V. N.; Prima, D. O.; Makarov, A. G.; Zibarev, A. V.; Trofimov, B. A.; Sobenina, L. N.; Belyaeva, K. V.; Sosnovskikh, V. Ya.; Obydennov, D. L.; Usachev, S. A. Organofluorine Chemistry: Promising Growth Areas and Challenges. *Russ. Chem. Rev.* **2019**, *88*, 425–569. (b) O'hagan, D. Understanding Organofluorine Chemistry. An Introduction to the C–F Bond. *Chem. Soc. Rev.* **2008**, *37*, 308–319. (c) Ogawa, Y.; Tokunaga, E.; Kobayashi, O.; Hirai, K.; Shibata, N. Current Contributions of Organofluorine Compounds to the Agrochemical Industry. *iScience* **2020**, *23*, 101467. (d) Bégué, J.- P.; Bonnet-Delpon, D. Bioorganic and Medicinal Chemistry of Fluorine; John Wiley & Sons, Inc.: Hoboken, NJ, **2008**. (e) Meanwell, N. A. Fluorine and Fluorinated Motifs in the Design and Application of Bioisosteres for Drug Design. *J. Med. Chem.* **2018**, *61*, 5822−5880.
2. (a) Wang, Y.; Tong, J.; Wu, W.; Xu, Z.; Lu, Y. Organic Fluorines as Halogen Bond Donors: Theoretical Study and Crystallographic Evidence. *Int. J. Quantum Chem.* **2015**, *115*, 884–890. (b) Babudri, F.; Farinola, G. M.; Naso, F.; Ragni, R. Fluorinated Organic Materials for Electronic and Optoelectronic Applications: The Role of the Fluorine Atom. *Chem.*

Comm. **2007**, *10*, 1003–1022. (c) Varadwaj, A.; Varadwaj, P. R.; Marques, H. M.; Yamashita, K. Revealing Factors Influencing the Fluorine-Centered Non-Covalent Interactions in Some Fluorine-Substituted Molecular Complexes: Insights from First-Principles Studies. *ChemPhysChem* **2018**, *19*, 1486–1499. (d) Ilardi, E. A.; Vitaku, E.; Njardarson, J. T. Data-Mining for Sulfur and Fluorine: An Evaluation of Pharmaceuticals to Reveal Opportunities for Drug Design and Discovery. *J. Med. Chem.* **2014**, *57*, 2832–2842. (e) Mei, H.; Han, J.; Fustero, S.; Medio-Simon, M.; Sedgwick, D. M.; Santi, C.; Ruzziconi, R.; Soloshonok, V. A. Fluorine-Containing Drugs Approved by the FDA in 2018. *Chem. Eur. J.* **2019**, *25*, 11797–11819. (f) Purser, S.; Moore, P. R.; Swallow, S.; Gouverneur, V. Fluorine in Medicinal Chemistry. *Chem. Soc. Rev.* **2008**, *37*, 320–330. (g) Wang, J.; Sánchez-Roselló, M.; Aceña, J. L.; del Pozo, C.; Sorochinsky, A. E.; Fustero, S.; Soloshonok, V. A.; Liu, H. Fluorine in Pharmaceutical Industry: Fluorine-Containing Drugs Introduced to the Market in the Last Decade (2001−2011). *Chem. Rev.* **2014**, *114*, 2432−2506.

3. (a) Inoue, M.; Sumii, Y.; Shibata, N. Contribution of Organofluorine Compounds to Pharmaceuticals. *ACS Omega* **2020**, *5*, 10633–10640. (b) Ismail, F. M. D. Important Fluorinated Drugs in Experimental and Clinical Use. *J. Fluor. Chem.* **2002**, *118*, 27–33 (c) O'Hagan, D. Fluorine in Health Care: Organofluorine Containing Blockbuster Drugs. *J. Fluor. Chem.* **2010**, *131*, 1071–1081. (d) Zhou, Y.; Wang, J.; Gu, Z.; Wang, S.; Zhu, W.; Acenã, J. L.; Soloshonok, V. A.; Izawa, K.; Liu, H. Next Generation of Fluorine-Containing Pharmaceuticals, Compounds Currently in Phase II-III Clinical Trials of Major Pharmaceutical Companies: New Structural Trends and Therapeutic Areas. *Chem. Rev.* **2016**, *116*, 422–518. (e) Hagmann, W. K. The Many Roles for Fluorine in Medicinal Chemistry. *J. Med. Chem*. **2008**, *51*, 4359–4369. (f) Ito, O.; Omori, R.; Matsuda, M. Determination of Addition Rates of Benzenethiyl Radicals to Alkynes by Flash Photolysis. Structures of Produced Vinyl-type Radicals. *J. Am. Chem. Soc.* **1982**, *104*, 3934–3937. (g) Vargas, E.; Echeverri, F.; Vélez, I.D.; Robledo, S.M.; Quiñones, W. Synthesis and Evaluation of Thiochroman-4-one Derivatives as Potential Leishmanicidal Agents. *Mol.* **2017**, *22*, 2041.

4. Dong, X. Q.; Fang, X.; Wang, C. J. Organocatalytic Asymmetric Sulfa-Michael Addition of Thiols to 4,4,4-Trifluorocrotonates. *Org. Lett.* **2011**, *13*, 4426–4429.

5. Huang, X.; David, E.; Jubault, P.; Besset, T.; Couve-Bonnaire, S. Organocatalyzed Sulfa-Michael Addition of Thiophenols on Trisubstituted α-Fluoroacrylates, a Straightforward Access to Chiral Fluorinated Compounds. *J. Org. Chem.* **2020**, *85*, 14055–14067.

6. Ramb, D. C.; Lerchen, A.; Kischkewitz, M.; Beutel, B.; Fustero, S.; Haufe, G. Addition of Nucleophiles to Fluorinated Michael Acceptors. *Eur. J. Org. Chem.* **2016**, *2016*, 1751–1759.

7. (a) Tao, J.; Xu, J. H. Biocatalysis in Development of Green Pharmaceutical Processes. *Curr. Opin. Chem. Biol.* **2009**, *13*, 43–50. (b) Kharissova, O. V.; Kharisov, B. I.; González, C. M. O.; Méndez, Y. P.; López, I. Greener Synthesis of Chemical Compounds and Materials. *R. Soc. Open Sci*. **2019**, *6*, 191378. (c) Castiello, C.; Junghanns, P.; Mergel, A.; Jacob, C.; Ducho, C.; Valente, S.; Rotili, D.; Fioravanti, R.; Zwergel, C.; Mai, A. GreenMedChem: The Challenge in the next Decade toward Eco-Friendly Compounds and Processes in Drug Design. *Green Chem*. **2023**, *25*, 2109–2169. (d) Kar, S.; Sanderson, H.; Roy, K.; Benfenati, E.; Leszczynski, J. Green Chemistry in the Synthesis of Pharmaceuticals *Chem. Rev.* **2022**, *122*, 3637–3710.

8. (a) Varma, R. S. Greener and Sustainable Trends in Synthesis of Organics and Nanomaterials. *ACS Sustain. Chem. Eng.* **2016**, *4*, 5866–5878. (b) Hafez, E. A. A.; Al-Mousawi, S. M.; Moustafa, M. S.; Sadek, K. U.; Elnagdi, M. H. Green Methodologies in Organic Synthesis: Recent Developments in Our Laboratories. *Green. Chem. Lett. Rev.* **2013**, *6*, 189–210. (c) Sheldon, R. A. Green Solvents for Sustainable Organic Synthesis: State of the Art. *Green Chem.* **2005**, *7*, 267–278. (d) Gawande, M. B.; Bonifácio, V. D. B.; Luque, R.; Branco, P. S.; Varma, R. S. Benign by Design: Catalyst-Free in-Water, on-Water Green Chemical Methodologies in Organic Synthesis. *Chem. Soc. Rev.* **2013**, *42*, 5522–5551. (e) Vaccaro, L. Green Shades in Organic Synthesis. *Eur. J. Org. Chem*. **2020**, *28*, 4273–4283.

9. (a) Winkler, C. K.; Schrittwieser, J. H.; Kroutil, W. Power of Biocatalysis for Organic Synthesis. *ACS Cent. Sci.* **2021**, *7*, 55–71. (b) Nestl, B. M.; Hammer, S. C.; Nebel, B. A.; Hauer, B. New Generation of Biocatalysts for Organic Synthesis. *Angew. Chem., Int. Ed.* **2014**, *53*, 3070–3095. (c) Hudlicky, T.; Reed, J. W. Applications of Biotransformations and Biocatalysis to Complexity Generation in Organic Synthesis. *Chem. Soc. Rev*. **2009**, *38*, 3117–3132. (d) Reetz, M. T. Biocatalysis in Organic Chemistry and Biotechnology: Past, Present, and Future. *J. Am. Chem. Soc*. **2013**, *135*, 12480–12496. (e) Sheldon, R. A.; Brady, D. Broadening the Scope of Biocatalysis in Sustainable Organic Synthesis. *ChemSusChem*. **2019**, *12*, 2859–2881.

10. (a) Kaur, P.; Tyagi, V. Recent Advances in Iron–Catalyzed Chemical and Enzymatic Carbene–Transfer Reactions. *Adv. Synth. Catal.* **2021**, *363*, 877–905. (b) Hönig, M.; Sondermann, P.; Turner, N. J.; Carreira, E. M. Enantioselective Chemo- and

Biocatalysis: Partners in Retrosynthesis. *Angew. Chem., Int. Ed.* **2017**, *56*, 8942–8973. (c) Corrado, M. L.; Knaus, T.; Mutti, F. G. High Regio- and Stereoselective Multi-Enzymatic Synthesis of All Phenylpropanolamine Stereoisomers from β-Methylstyrene. *ChemBioChem* **2021**, *22*, 2345–2350. (d) Pintor, A.; Lavandera, I.; Volkov, A.; Gotor-Fernández, V. Chemoselective Lipase-Catalyzed Synthesis of Amido Derivatives from 5-Hydroxymethylfurfurylamine. *ACS Sustain. Chem. Eng.* **2023**, *11*, 10284–10292. (e) Le-Huu, P.; Heidt, T.; Claasen, B.; Laschat, S.; Urlacher, V. B. Chemo-, Regio-, and Stereoselective Oxidation of the Monocyclic Diterpenoid -Cembrenediol by P450 BM3. *ACS Catal.* **2015**, *5*, 1772–1780. (f) Tyagi, V.; Fasan, R. Myoglobin-Catalyzed Olefination of Aldehydes. *Angew. Chem., Int. Ed.* **2016**, *55*, 2512–2516. (g) Yang, Y.; Arnold, F. H. Navigating the Unnatural Reaction Space: Directed Evolution of Heme Proteins for Selective Carbene and Nitrene Transfer. *Acc. Chem. Res.* **2021**, *54*, 1209–1225.

11. (a) Sbei, N.; Hardwick, T.; Ahmed, N. Green Chemistry: Electrochemical Organic Transformations via Paired Electrolysis. *ACS Sustainable Chem. Eng*. **2021**, *9*, 6148–6169. (b) Martins, G. M.; Shirinfar, B.; Hardwick, T.; Murtaza, A.; Ahmed, N. Organic Electrosynthesis: Electrochemical Alkyne Functionalization. *Catal. Sci. Technol*. **2019**, *9*, 5868–5881. (c) Cembellín, S.; Batanero, B. Organic Electrosynthesis Towards Sustainability: Fundamentals and Greener Methodologies. *Chem. Rec*. **2021**, *21*, 2453–2471.
12. Martins, G. M.; Zimmer, G. C.; Mendes, S. R.; Ahmed, N. Electrifying Green Synthesis: Recent Advances in Electrochemical Annulation Reactions. *Green Chem*. **2020**, *22*, 4849–4870.
13. (a) Phillips, A. M. F.; Pombeiro, A. J. L. Electrochemical Asymmetric Synthesis of Biologically Active Substances. *Org. Biomol. Chem*. **2020**, *18*, 7026–7055. (b) Huang, X.; Zhang, Q.; Lin, J.; Harms, K.; Meggers, E. Electricity-driven asymmetric Lewis acid catalysis. *Nat. Catal.* **2019**, *2,* 34-40. (c) Kooyman, E. C. Thiyl radicals. *Pure Appl. Chem.* **1967**, *15*, 81-88.
14. (a) Tan, X.; Nielsen, J. The Integration of Bio-Catalysis and Electrocatalysis to Produce Fuels and Chemicals from Carbon Dioxide. *Chem. Soc. Rev*. **2022**, *51*, 4763–4785. (b) Qiao, Y.; Wu, X. S.; Ma, C. X.; He, H.; Li, C. M. A Hierarchical Porous Graphene/Nickel Anode That Simultaneously Boosts the Bio- and Electro-Catalysis for High-Performance Microbial Fuel Cells. *RSC Adv.* **2014**, *4*, 21788–21793.
15. Peñafiel, I.; Dryfe, R. A. W.; Turner, N. J.; Greaney, M. F. Integrated Electro-Biocatalysis for Amine Alkylation with Alcohols. *ChemCatChem* **2021**, *13*, 864–867.

16. Long, C. J.; Cao, H.; Zhao, B. K.; Tan, Y. F.; He, Y. H.; Huang, C. S.; Guan, Z. Merging the Non-Natural Catalytic Activity of Lipase and Electrosynthesis: Asymmetric Oxidative Cross-Coupling of Secondary Amines with Ketones. *Angew. Chem., Int. Ed.* **2022**, *134*, e202203666.
17. Yadav, L.; Maneesha, M.; Dabaria, K. K.; Jat, P. K.; Gurjar, A.; Badsara, S. S. Electrochemical Cascade Thia-Michael and Thioacetalization of Cyclic Enones. *Synthesis* **2022**, *54*, 5479–5490.
18. Li, D.; Jia, J.; Zhao, X.; Zhang, Z.; Wang, H.; Li, S.; Xu, Z.; Xie, Z. Electrochemical Oxidation Cross Dehydrogenative Coupling of Enamines and Thiophenols for the Synthesis of Vinyl Sulfides. *ChemistrySelect* **2021**, *6*, 6460–6463.
19. (a) Panja, A.; Banerjee, D. R.; Basak, A. Reversal of Regioselectivity in Acetylation and Deacetylation of Aryl-Naphthalene Diols and Diacetates by Amano Lipase. *RSC Adv.* **2014**, *4*, 54235–54243. (b) Tafi, A.; Van Almsick, A.; Corelli, F.; Crusco, M.; Laumen, K. E.; Schneider, M. P.; Botta, M. Computer Simulations of Enantioselective Ester Hydrolyses Catalyzed by Pseudomonas Cepacia Lipase. *J. Org. Chem.* **2000**, *65*, 3659–3665. (c) Soni, S.; Dwivedee, B. P.; Sharma, V. K.; Patel, G.; Banerjee, U. C. Exploration of the Expeditious Potential of Pseudomonas Fluorescens Lipase in the Kinetic Resolution of Racemic Intermediates and Its Validation through Molecular Docking. *Chirality* **2018**, *30*, 85–94. (d) Ehlert, J.; Kronemann, J.; Zumbrägel, N.; Preller, M. Lipase-Catalyzed Chemoselective Ester Hydrolysis of Biomimetically Coupled Aryls for the Synthesis of Unsymmetric Biphenyl Esters. *Molecules* **2019**, *24*, 4272.
20. Carvalho, A. C. L. de M.; de Oliveira, B. R.; Lima, G. V.; Negreiro, J. M.; Oliveira, M. C. F.; de Lemos, T. L. G.; da Silva, M. R.; Fonseca, T. de S.; Bezerra, R. M.; dos Santos, J. C. S.; Gonçalves, L. R. B.; Rios, N. S.; Zanatta, G.; de Mattos, M. C. Resolution of Racemic Aryloxy-Propan-2-Yl Acetates via Lipase-Catalyzed Hydrolysis: Preparation of Enantiomerically Pure/Enantioenriched Mexiletine Intermediates and Analogs. *Catalysts* **2022**, *12*, 1566.
21. Guan, Z.; Zhu, S.; Wang, S.; Wang, H.; Wang, S.; Zhong, X.; Bu, F.; Cong, H.; Lei, A. Electrochemical Oxidative Carbon-Atom Difunctionalization: Towards Multisubstituted Imino Sulfide Ethers. *Angew. Chem., Int. Ed.* **2021**, *133*, 1597–1601.
22. (a) He, T. J.; Ye, Z.; Ke, Z.; Huang, J. M. Stereoselective Synthesis of Sulfur-Containing β-Enaminonitrile Derivatives through Electrochemical Csp^3 –H Bond Oxidative Functionalization of Acetonitrile. *Nat. Commun.* **2019**, *10*, 833. (b) Wang, D.; Wang, P.;

Wang, S.; Chen, Y. H.; Zhang, H.; Lei, A. Direct Electrochemical Oxidation of Alcohols with Hydrogen Evolution in Continuous-Flow Reactor. *Nat. Commun.* **2019**, *10*, 2796.

23. Sun, C. C.; Xu, K.; Zeng, C. C. Transition Metal- and Base-Free Electrochemical Aza-Michael Addition of Aromatic Aza-Heterocycles or Ts-Protected Amines to α,β-Unsaturated Alkenes Mediated by NaI. *ACS Sustain. Chem. Eng.* **2019**, *7*, 2255–2261.
24. Rauwerdink, A.; Kazlauskas, R. J. How the Same Core Catalytic Machinery Catalyzes 17 Different Reactions: The Serine-Histidine-Aspartate Catalytic Triad of α/β-Hydrolase Fold Enzymes. *ACS Catalysis*. **2015**, *5*, 6153–6176.
25. (a) Kamal, M. Z.; Mohammad, T. A. S.; Krishnamoorthy, G.; Rao, N. M. Role of Active Site Rigidity in Activity: Md Simulation and Fluorescence Study on a Lipase Mutant. *PLoS One* **2012**, *7,* 35188. (b) Ribeiro, B. D.; De Castro, A. M.; Coelho, M. A. Z.; Freire, D. M. G. Production and Use of Lipases in Bioenergy: A Review from the Feedstocks to Biodiesel Production. *Enzyme Res*. **2011**, *2011*, 615083.
26. Yang, H. S.; Macha, L.; Ha, H. J.; Yang, J. W. Functionalisation of esters *via* 1,3-chelation using NaO*t*Bu: mechanistic investigations and synthetic Applications. *Org. Chem. Front.* **2021**, *8*, 53-60.
27. Yang, F.; Wang, Z.; Wang, H.; Zhang, H.; Yue, H.; Wang, L. Enzyme catalytic promiscuity: lipase catalyzed synthesis of substituted 2*H*-chromenes by a three-component reaction. *RSC Adv.* **2014**, *4*, 25633-25636.
28. Li, K.; He, T.; Li, C.; Feng, X.-W.; Wang, N.; Yu, X.-Q. Lipase-catalysed direct Mannich reaction in water: utilization of biocatalytic promiscuity for C–C bond formation in a “one-pot” synthesis. *Green Chem.* **2009**, *11*, 777-779.
29. Trott, O.; Olson, A. J. AutoDock Vina: Improving the speed and accuracy of docking with a new scoring function, efficient optimization, and multithreading. *J. Comput. Chem.* **2010**, *31*, 455-461.
30. (a) Panja, A.; Banerjee, D. R.; Basak, A. Reversal of regioselectivity in acetylation and deacetylation of aryl-naphthalene diols and diacetates by Amano lipase. *RSC Adv.* **2014**, *4*, 54235-54243. (b) Ehlert, J.; Kronemann, J.; Zumbragel. N.; Preller, M. Lipase-Catalyzed Chemoselective Ester Hydrolysis of Biomimetically Coupled Aryls for the Synthesis of Unsymmetric Biphenyl Esters. *Molecules* **2019**, *24*, 4272**.**
31. https://www.3ds.com/products-services/biovia/products/molecular-modeling simulation/bioviadiscovery-studio/visualization

CHAPTER 4

Electrochemical N-sulfonylation of in-situ Generated Indole-based Hydrazones and Antimicrobial Evaluation

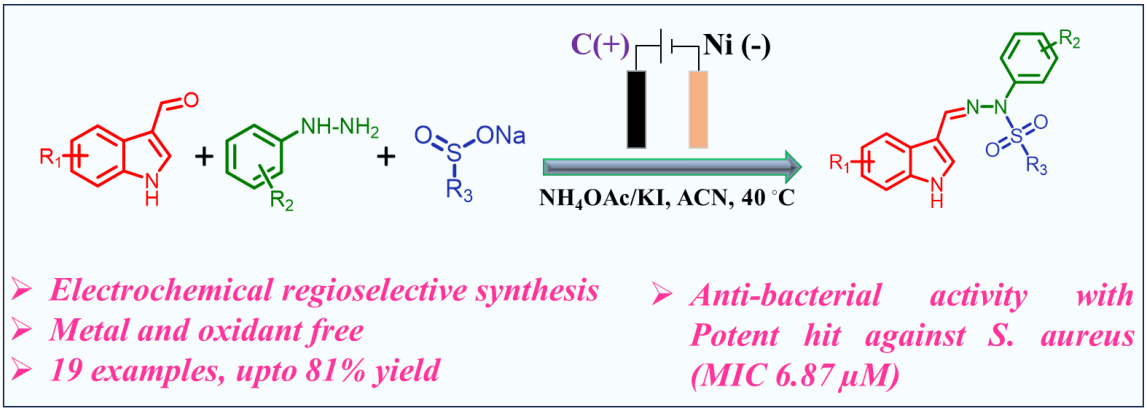

- *Electrochemical regioselective synthesis*
- *Metal and oxidant free*
- *19 examples, upto 81% yield*
- *Anti-bacterial activity with Potent hit against S. aureus (MIC 6.87 µM)*

CHAPTER 4

4.1: Introduction

Hydrazone formation is a powerful strategy for functionalizing carbonyl compounds, enabling the introduction of diverse functional groups into organic molecules, biomolecules, and polymers.[1] Further, hydrazones also represent a key class of biologically active compounds with a wide range of medicinal properties, drawing considerable interest from pharmaceutical chemists.[2] In particular, numerous indole-based hydrazone derivatives have been developed and systematically studied for their therapeutic potential, including antibacterial, antimalarial, antitumor, antitubercular, anti-inflammatory, anti-breast cancer and MIF-inhibitory activities (**Figure 4.1**).[3] Their broad pharmacological profiles make them promising drug candidates with the potential for enhanced efficacy and reduced toxicity.[4] Hence, synthetic strategies for the synthesis and functionalization of hydrazones have garnered significant attention over the past years.[5]

On the other hand, organosulfones constitute an important class of compounds with broad utility in pharmaceuticals, advanced materials, and synthetic chemistry.[6] They display a wide range of biological activities, including antibacterial and anticancer properties, and are frequently incorporated as key structural units in therapeutic agents (**Figure 4.1**).[7] Furthermore, organosulfones can be synthesized through various methods using sulfonylating agents such as sulfonyl chlorides,[8] sulfonyl hydrazides[9] and sodium sulfinates.[10] Traditional approaches, including the oxidation of sulfides[11] and electrophilic aromatic substitution[12] often involve strong oxidants,[13] odorous thiols[14] or harsh acidic conditions, limiting functional group compatibility.[15] Modern strategies such as transition-metal-catalyzed couplings,[16] C-H activation,[17] and multi-component reactions with SO_2 surrogates[18] have broadened synthetic scope but still face challenges like high temperatures, toxic by-products, and limited substrate tolerance. In this context, sodium sulfinates have emerged as highly effective sulfonyl donors owing to their bench stability, ease of synthesis, and compatibility with mild reaction conditions, making them a preferred choice for constructing sulfones.[19] Interestingly, the integration of sulfone scaffolds with hydrazones within a single structural unit holds significant promise for the search for new bioactive compounds. The combination of sulfone and hydrazone functionalities in the same structural unit not only offers potential for innovative drug development but also opens new avenues in the design of advanced organic optoelectronic materials.[20] As a result, the sulfonylation of hydrazones has received considerable attention in recent years. In this context, Liu and co-workers reported an oxidative sulfonylation approach to synthesize β-ketosulfones using a dual-metal co-catalytic system involving copper and silver

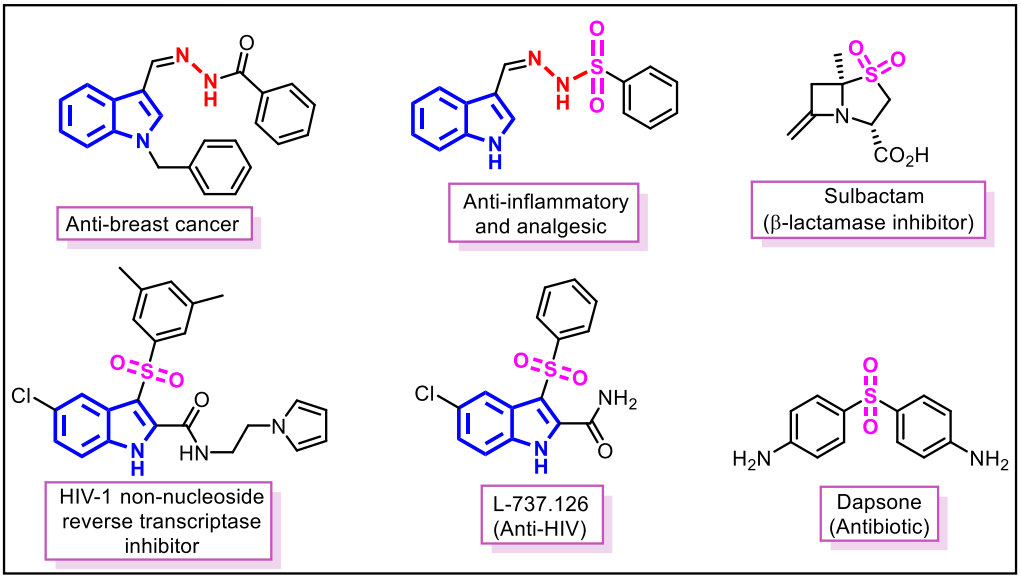

Figure 4.1: Pharmacologically relevant indole-based hydrazones and organosulfones

salts (**Scheme 4.1a**).[21] Further, Zhang and colleagues introduced a heterogeneous chitosan@Cu catalyst for C-H sulfonylation of hydrazones by employing sodium sulfinates as sulfonyl donors to access β-ketosulfones (**Scheme 4.1b**).[22]

Next, electrochemical synthesis has emerged as a green and sustainable alternative in organic chemistry.[23] It utilizes electricity as a clean reagent, minimizes waste generation, reduces reliance on hazardous chemicals, and typically proceeds under mild conditions, making it an eco-friendly and energy-efficient approach.[24] In this context, Hazra et al. developed an electrochemical method for the direct C-H sulfonylation of aldehyde hydrazones using sodium sulfinates as sulfonylating agents, leading to the synthesis of various (*E*)-sulfonylated hydrazones (**Scheme 4.1c**).[7c] Subsequently, Guo and co-workers reported a related C-H sulfonylation approach employing a range of sodium sulfinates to obtain both alkylated and arylated sulfonylated hydrazones (**Scheme 4.1d**).[25]

Herein, we aim to develop a novel electrochemical strategy for the regioselective *N*-sulfonylation of *in-situ* generated indole-based hydrazones using sodium sulfinates (**Scheme4.1e**). This method offers a sustainable and operationally simple route to access a broad range of clinically important *N*-sulfonylated hydrazones under environmentally benign conditions.

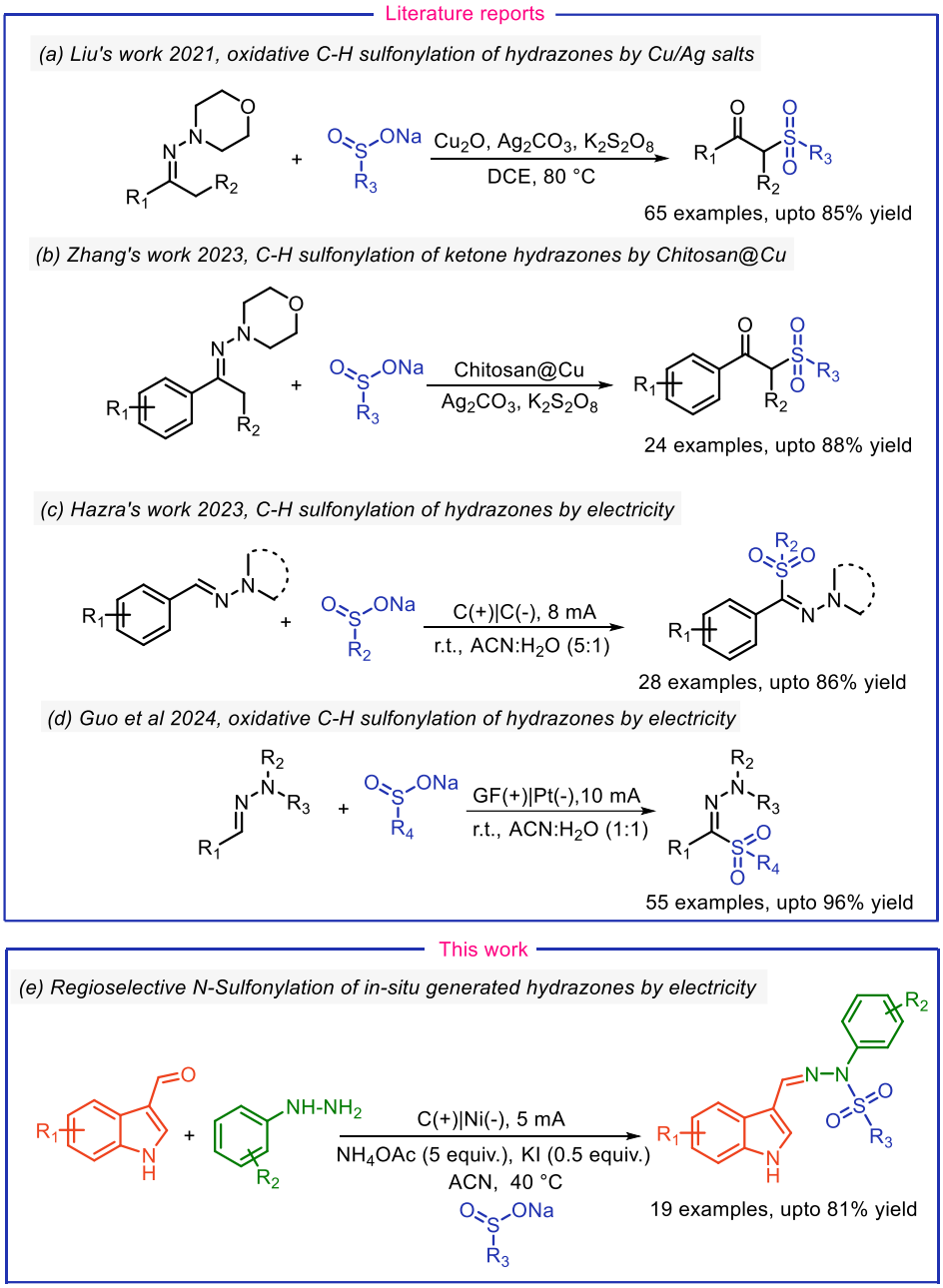

Scheme 4.1: Recent methods for sulfonylation of hydrazones using sodium sulfinates

4.2: Results and Discussion

4.2.1: Optimization of electrochemical reaction conditions

To establish the optimal reaction conditions for the one-pot synthesis of compound (**5a**), we initiated our study using indole-3-carboxaldehyde (**1a**), phenylhydrazine (**2a**), and sodium *p*-toluenesulfinate (**3a**) as model substrates. The reaction was initially performed in an undivided electrochemical cell using a carbon anode and a nickel cathode under a constant current of 5 mA (**entry 1, Table 4.1**). A mixture of ammonium acetate (NH_4OAc) and potassium iodide (KI) served as the supporting electrolyte, with acetonitrile (ACN) as the solvent. Under this

condition, compound (**5a**) was achieved in 82% conversion (**entry 1, Table 4.1**). Subsequent screening of various electrode combinations (**entries 2-6, Table 4.1**), while keeping all other reaction parameters unchanged, did not lead to improved yields. When iron and copper were used as cathodes, the product was formed but starting material (**1a**) was also recovered (**entries 5-6, Table 4.1**). Further, the reaction provided almost similar yield, when platinum or nickel electrodes were employed as a cathode along with carbon as anode (**entries 1 & 3, Table 4.1**), however, nickel was preferred over the platinum owing to its cost-effectiveness, and selected for further optimization. Additionally, when the reaction was carried out in the absence of electricity, only trace amounts of product (**5a**) were detected after 1 hour (**entry 7, Table 4.1**). Next, we examined the impact of the electrolyte on the reaction. In this context, replacing the NH_4OAc/KI combination with single salts such as tetrabutylammonium iodide (TBAI), tetrabutylammonium acetate (TBAOAc), or lithium perchlorate ($LiClO_4$) resulted in no product formation (**entries 8-10, Table 4.1**), suggesting that a synergistic effect of both ammonium acetate and iodide salts is essential. Further investigations showed that when NH_4OAc or KI were used individually, no product (**5a**) was formed (**entries 11-12, Table 4.1**). However, combining TBAOAc with various halide salts revealed that the reaction proceeded efficiently only with KI (**entry 13, Table 4.1**), while the use of KBr or $MgBr_2$ led to significantly lower conversions (**entries 14-15, Table 4.1**). These observations highlights the important role of iodide and acetate ions in this reaction. Additionally, reactions using TBAI in combination with NH_4OAc also led to successful product formation, further confirming the necessity of both iodide and acetate ions (**entries 16, Table 4.1**).

Table 4.1: Optimization of Reaction conditions[a]

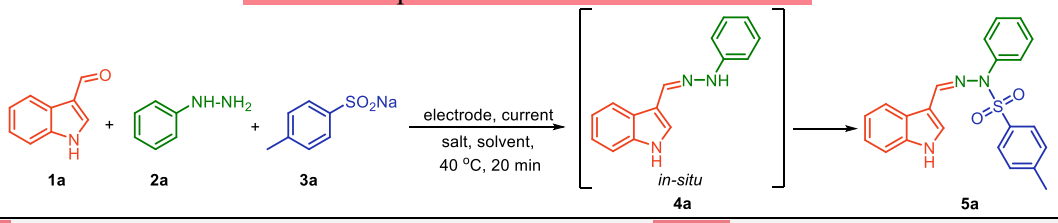

entry	electrode	current	salts	equiv. of salts	solvent	conversion (%)[b]
1	C(+)|Ni(-)	5 mA	NH_4OAc/KI	5:0.5	ACN	82
2	Pt(+)|Pt(-)	5 mA	NH_4OAc/KI	5:0.5	ACN	77
3	C(+)|Pt(-)	5 mA	NH_4OAc/KI	5:0.5	ACN	79
4	C(+)|C(-)	5 mA	NH_4OAc/KI	5:0.5	ACN	70
5	C(+)|Fe(-)	5 mA	NH_4OAc/KI	5:0.5	ACN	68
6	C(+)|Cu(-)	5 mA	NH_4OAc/KI	5:0.5	ACN	66
7	-	-	NH_4OAc/KI	5:0.5	ACN	4
8	C(+)|Ni(-)	5 mA	TBAI	5.0	ACN	0
9	C(+)|Ni(-)	5 mA	TBAOAc	5.0	ACN	0

10	C(+)|Ni(-)	5 mA	$LiClO_4$	5.0	ACN	0
11	C(+)|Ni(-)	5 mA	NH_4OAc	5.0	ACN	0
12	C(+)|Ni(-)	5 mA	KI	5.0	ACN	0
13	C(+)|Ni(-)	5 mA	TBAOAc/KI	5:0.5	ACN	72
14	C(+)|Ni(-)	5 mA	TBAOAc/KBr	5:0.5	ACN	40
15	C(+)|Ni(-)	5 mA	$TBAOAc/MgBr_2$	5:0.5	ACN	36
16	C(+)|Ni(-)	5 mA	$TBAI/NH_4OAc$	5:0.5	ACN	73
17	C(+)|Ni(-)	5 mA	$LiClO_4$/KI	5:0.5	ACN	0
18	C(+)|Ni(-)	5 mA	I_2	5.0	ACN	0
19	C(+)|Ni(-)	5 mA	NH_4OAc/ KI	5:0.5	ACN:H_2O (1:1, v/v)	22
20	C(+)|Ni(-)	5 mA	NH_4OAc/KI	5:0.5	DCE	5
21	C(+)|Ni(-)	5 mA	NH_4OAc/KI	5:0.5	DMSO	0
22	C(+)|Ni(-)	1 mA	NH_4OAc/KI	5:0.5	ACN	70
23	C(+)|Ni(-)	10 mA	NH_4OAc/KI	5:0.5	ACN	77
24	C(+)|Ni(-)	5 mA	NH_4OAc/KI	5:0.5	ACN	54[c]
25	C(+)|Ni(-)	5 mA	NH_4OAc/KI	5:0.5	ACN	65[d]
26	C(+)|Ni(-)	5 mA	NH_4OAc/KI	5:1	ACN	79
27	C(+)|Ni(-)	5 mA	NH_4OAc/KI	3:0.5	ACN	63

[a]**Reaction conditions: 1a** (10 mg, 0.07 mmol), **2a** (8 µL, 0.08 mmol), **3a** (24 mg, 0.13 mmol), solvent (2 mL) under a constant current flowed in an undivided cell with electrodes at 40 °C [b]determined by HPLC, [c]temperature 30 °C, [d]temperature 50 °C.

The use of $LiClO_4$ with KI again failed to yield the product, reinforcing the specificity of the required electrolyte system (**entry 17, Table 4.1**). Importantly, the use of elemental iodine (I_2) instead of iodide salts resulted in no product formation, further emphasizing the crucial role of the iodide ion (**entry 18, Table 4.1**).

Next, solvent screening showed that replacing acetonitrile (ACN) with ACN:H_2O (1:1, v/v), 1,2-dichloroethane (DCE), or DMSO resulted in significantly reduced conversions (**entries 19-21, Table 4.1**). In the case of ACN:H_2O (1:1, v/v), 22% conversion of **(5a)** was observed, with the recovery of starting material (**1a**). Similarly, the reaction in DCE led to 5% conversion only. In contrast, no conversion was observed in DMSO, and (**1a)** was recovered unchanged. These findings confirmed that acetonitrile is the optimal solvent for achieving higher product yields. Variation of the applied current also affected the reaction outcome. Reducing the current to 1 mA resulted in a substantial drop in yield, likely due to insufficient conductivity, which prevented the reaction from proceeding efficiently (**entry 22, Table 4.1**). Conversely, increasing the current to 10 mA led to partial decomposition of the reactants; however, a moderate 77% conversion to product (**5a)** was still attained (**entry 23, Table 4.1**). Finally, changing the reaction temperature (**entries 24-25, Table 4.1**) did not lead to any notable

improvement in yield. Next, the ratios of NH4OAc and KI were varied; however, the reaction gave an inferior yield (**entries 26-27, Table 4.1**). Moreover, a change in the substrate's molar ratio does not improve the reaction outcome.

4.2.2: Substrate scope

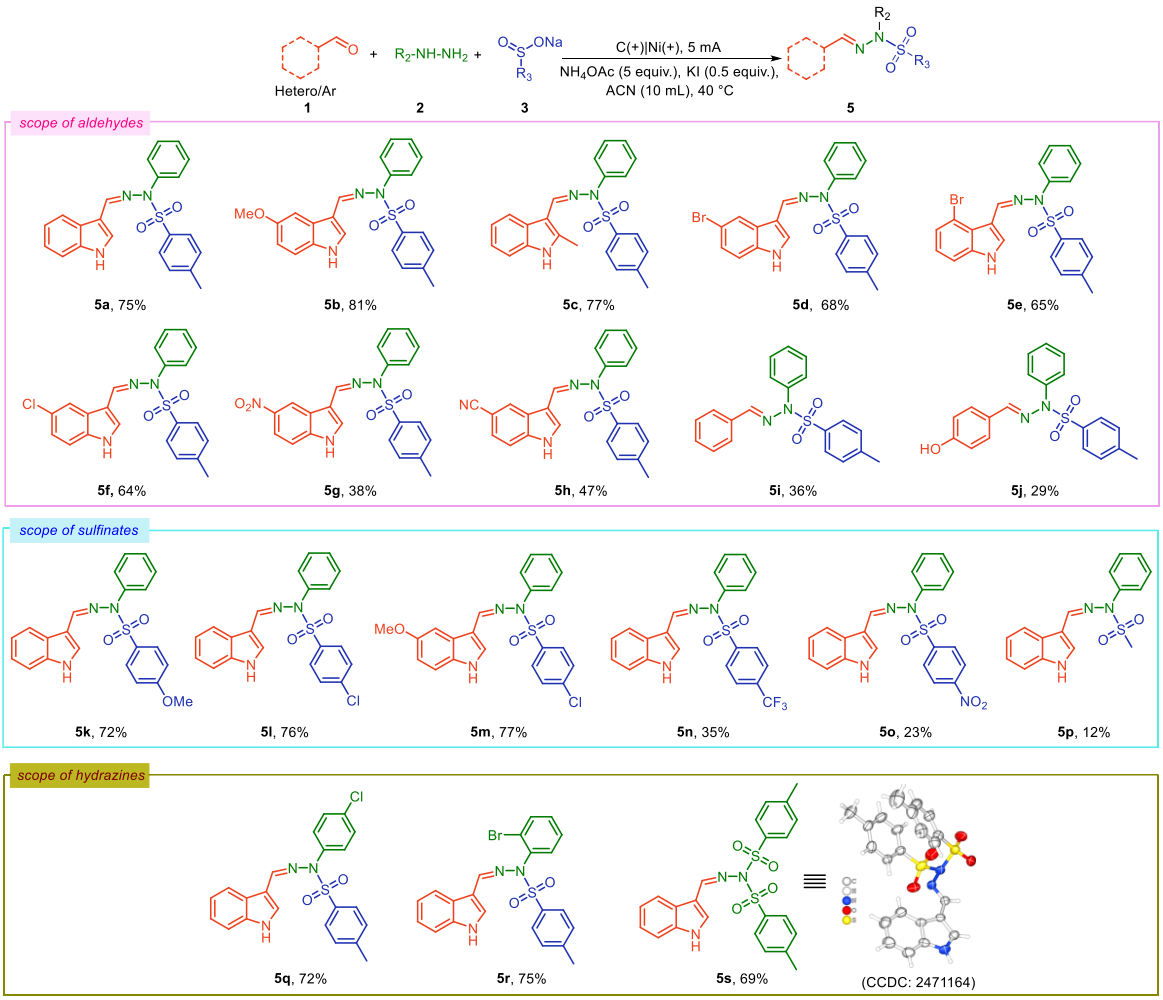

Scheme 4.2: Substrate scope of electrochemical *N*-sulfonylation of *in-situ* generated hydrazones[a]

[a]**Reaction conditions**: C anode, Ni cathode, aldehydes **1** (100 mg, 0.68 mmol, 1 equiv.), hydrazines **2** (81 µL, 0.82 mmol, 1.2 equiv), sodium sulfinates **3** (245 mg, 1.37 mmol, 2 equiv.), NH_4OAc (265 mg, 3.4 mmol, 5 equiv.), KI (57 mg, 0.34 mmol, 0.5 equiv.), ACN (10 mL) under a constant current of 5 mA flowed in an undivided cell with electrodes at 40 °C, isolated yields.

Having the best reaction conditions, we explored the substrate scope by employing a range of electronically and structurally diverse aldehydes, sulfinate salts, and hydrazines. Further, indole-3-carboxaldehydes bearing electron-donating groups afforded higher yields compared to the unsubstituted indole-3-carboxaldehydes (**5a-5c, Scheme 4.2**). Moreover, indole-3-carboxaldehydes containing halide substituents on the C-4 and C-5 position gave moderate yields of the desired products (**5d-5f**, **Scheme 4.2**). However, a significant drop in yield was

observed when aldehydes containing strong electron-withdrawing groups such as NO_2 and CN were used under the same electrochemical conditions with phenyl hydrazine and sodium tosyl sulfinate (**5g** and **5h**, **Scheme 4.2**). Further extending the methodology to benzaldehydes, we observed that these compounds showed a marked decline in product yields than the indole-3-carboxaldehydes (**5i-5j**, **Scheme 4.2**). Further, phenyl sulfinate salts bearing electron-donating group or halide substituents gave satisfactory results (**5k-5m**, **Scheme 4.2**). In contrast, phenyl sulfinate salts with strong electron-withdrawing groups such as CF_3 and NO_2 led to a considerable decrease in yield, likely due to reduced nucleophilicity of the $PhSO_2^-$ anion (**5n** and **5o**, **Scheme 4.2**).[26] When methyl sodium sulfinate ($MeSO_2Na$) was used in place of aryl sulfinates, a noticeable decline in product yield was observed, which may be attributed to the absence of conjugation and reduced nucleophilicity of the sulfonyl sulfur (**5p**, **Scheme 4.2**).[27] Next, we examined hydrazines bearing halide substituents, which also resulted in decreased yields (**5q** and **5r**, **Scheme 4.2**). Interestingly, reaction gave corresponding product in 69% isolated yield when tosyl hydrazine was employed instead of phenyl hydrazine in the reaction (**5s**, **Scheme 4.2**).

4.2.3: Plausible mechanism

A proposed reaction mechanism for the regioselective synthesis of compound (**5a**) is depicted in **Scheme 4.3**. Initially, KI reacts with ACN and undergoes anodic oxidation to generate the iodinium species $[(CH_3CN)_2I^+]$.[28] This electrophilic iodinium species subsequently reacts with the *in situ* generated hydrazone **(4a)**, which is formed from the condensation of (**1a**) and (**2a**). Further, the abstraction of a proton by the acetate ion facilitates the formation of the indole

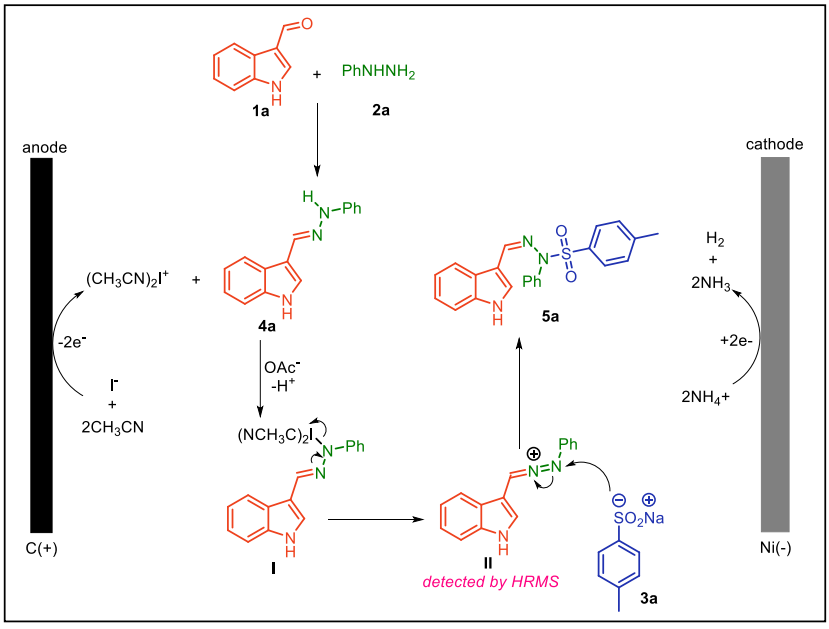

Scheme 4.3: Plausible mechanism

hydrazone iodinium intermediate (**I**), which undergoes a rearrangement to form intermediate (**II**) (confirmed using HRMS data). Thereafter, nucleophilic attack by the sulfinate anion on intermediate (**II**) leads to the formation of the final product (**5a**). The use of NH_4OAc in excess is crucial, as it serves not only as a proton abstractor but also undergoes reduction at the cathode during the electrochemical process.[28]

4.2.4: Control experiments

Further, to get more insight into the proposed reaction pathway, a series of control experiments were performed. First, the reaction was conducted in the presence of radical scavengers such as 2,2,6,6-tetramethylpiperidin-1-yl)oxidanyl (TEMPO) (4 equiv.) and butylated hydroxytoluene (BHT) (4 equiv.), the formation of product **5a** was still observed in good yield under these conditions, thereby ruling out a radical pathway and suggesting that no sulfinate radical intermediate is involved as reported previously by various groups.[25,29]

4.2.5: Cyclic voltammetry experiment

Next, cyclic voltammetry studies were carried out to get more insight about the proposed electrochemical reaction mechanism. In this context, hydrazone (**4a**) exhibited two distinct oxidation potentials at 0.43 V and 1.78 V (**Figure 4.2**). Separately, KI in acetonitrile showed oxidation waves at 1.00 V and 1.50 V. Interestingly, upon addition of KI to the reaction mixture, the first oxidation potential of hydrazone shifted to a more positive value (0.53 V), indicating the formation of the indole hydrazone iodinium intermediate (I).[28]

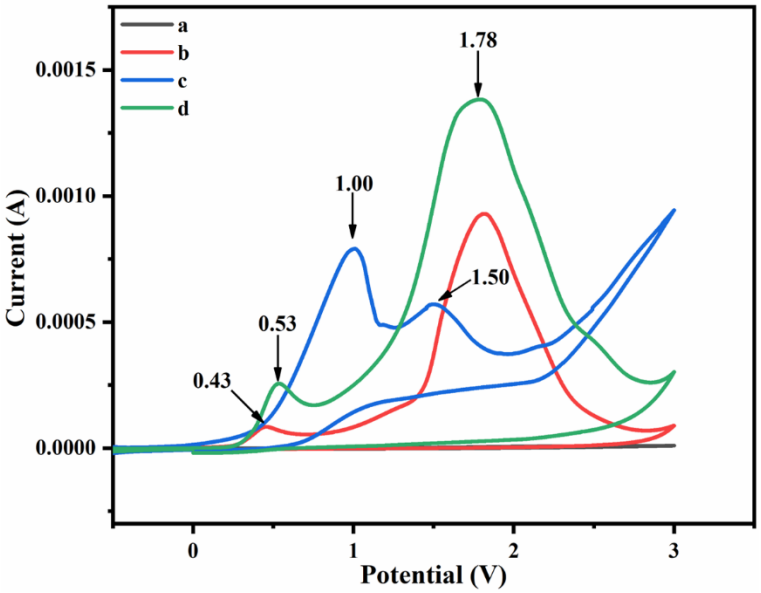

Figure 4.2: Cyclic voltammograms (IUPAC convention) recorded in 0.1 M $^{n}Bu_4NPF_6$/ACN at room temperature using a Pt working electrode, Pt wire counter electrode, and Ag/AgCl reference electrode. Scan rate: 0.05 V/s; initial potential: 0 V; scan direction: 0 → +3 V (oxidative). (a) ACN, (b) **4a** (0.001 M), (c) KI (0.024 M), (d) KI (0.024 M) and **4a** (0.001 M).

4.2.6: Antibacterial susceptibility analysis of the synthesized derivatives (*Done by our collaborator Dr. Kuljit Singh, CSIR-IIIM, Jammu*)

Primarily, the whole-cell screening of the (**5a-5s**) synthesized derivatives was conducted at a single concentration of 50 µM against representative Gram-positive and Gram-negative pathogens. This led to the identification of four potent hits, **5d, 5e, 5l,** and **5q**, that exhibited a growth inhibition of >85% against the *Staphylococcus aureus* pathogen. On the other hand, the synthesized derivatives showed a moderate inhibitory effect against Gram-negative pathogens. This experimental finding highlights the selective antibacterial potential of the identified

Table 4.2: Percentage viability of *S. aureus, K. pneumoniae, A. baumannii,* and *E. coli* pathogens in the presence of synthesized derivatives tested at 50 µg/mL. The results are expressed as mean ± standard deviation of three independent experiments.

Code	*S. aureus*	*K. pneumonia*	*A. baumannii*	*E. coli*
5d	**0.24 ± 0.12**	84.17 ± 2.31	80.52 ± 1.68	78.59 ± 1.77
5e	**10.26 ± 0.87**	94.93 ± 2.03	>100	82.79 ± 2.85
5l	**0.24 ± 0.11**	>100	>100	81.78 ± 2.59
5q	**1.73 ± 0.13**	73.27 ± 1.46	85.54 ± 2.24	98.15 ± 1.25

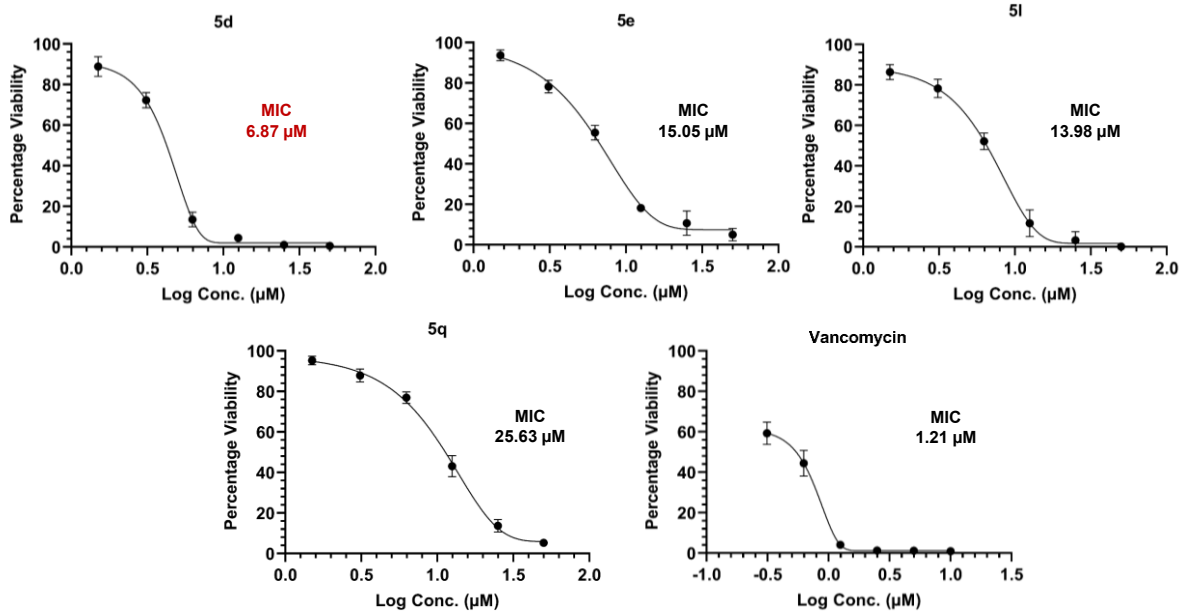

Figure 4.3: Dose-dependent curves of the four shortlisted hits against the *S. aureus* pathogen. Vancomycin was used as a standard drug control in the experiment. All the results are presented as the means ± standard deviations of three independent experiments.

molecules toward the Gram-positive pathogen *S. aureus*. The average percentage viability of the pathogens in the presence of the tested compounds is summarized in **Table 4.2**. Next, Minimum inhibitory concentration (MIC) of shortlisted hits was determined against *S. aureus* by broth micro-dilution assay to further assess their antibacterial potency. The active hits were tested at varied concentrations with vancomycin used as a positive control in the experimentation. The compounds **5d, 5e, 5l,** and **5q** exhibited effective antimicrobial activity against *S. aureus*. Among all the tested derivatives, the compound **5d** emerged as the most potent hit with an MIC value of 6.87 µM. The other three active hits (**5e, 5l,** and **5q**) displayed MIC values in the range of 10 to 26 µM. The dose-response curves of the four shortlisted hits and the standard drug (vancomycin) are represented in **Figure 4.3**.

4.2.7: Scanning electron microscopy (SEM) analysis

The SEM technique can be used to visualize the ultrastructural changes in the bacterial cell after treatment with biocidal molecules. Thus, in the present study, we have treated *S. aureus* cells with 1X and 2X MIC concentrations of the potent hit (**5d**) to investigate any structural

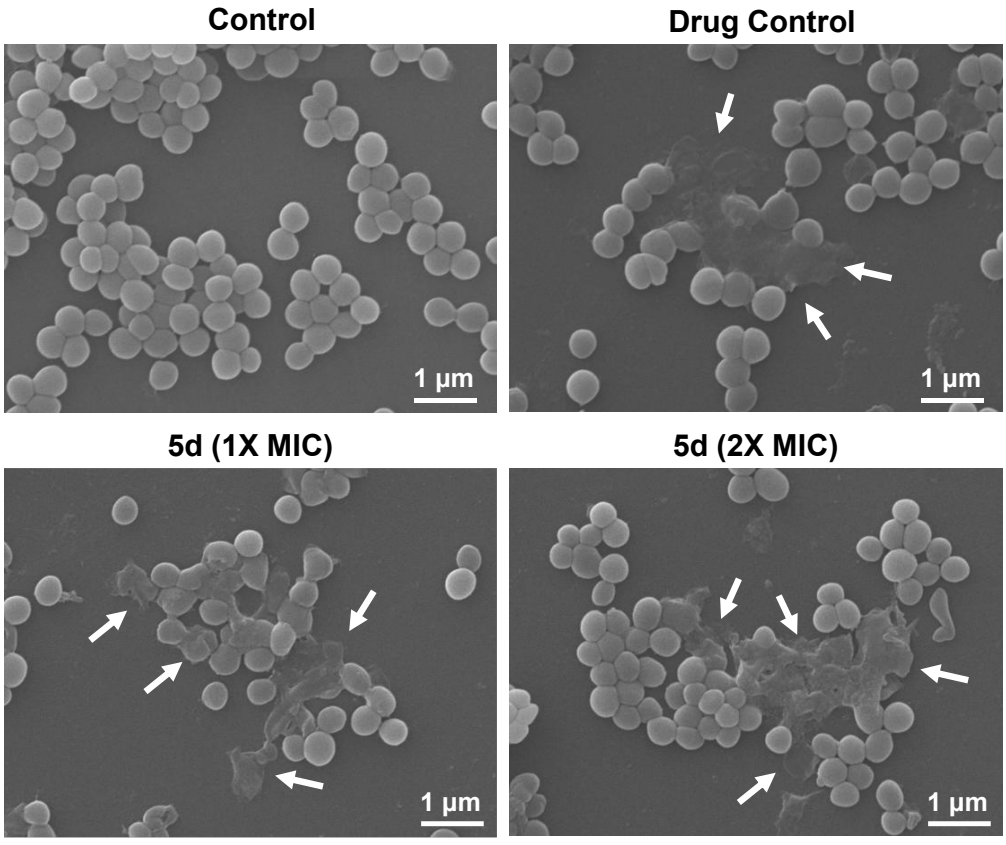

Figure 4.4: Scanning electron microscopy (SEM) analysis of *S. aureus* cells. Untreated control and drug control (vancomycin) at 1X MIC concentration. *S. aureus* pathogen exposed to potent hit (**5d**) at 1X and 2X MIC concentrations, respectively. White arrows in the figure depict the damage to the bacterial pathogen after treatment. (Scale bar = 1 µm).

irregularities and morphological alterations in the bacterial pathogen (**Figure 4.4**). SEM analysis revealed that untreated cells had smooth surfaces with round shapes and cells treated with drug control at 1X MIC concentration showed considerable damage. Upon treatment, with the potent hit (**5d**) at 1X and 2X MIC concentrations, substantial morphological changes, including surface depression, wrinkled and irregular appearance, are visible, leading to bacterial cell death**.**

4.3: Experimental Section

4.3.1: General information

All chemicals and solvents were obtained from commercial vendors and used without any further purification. All the glass and plasticware utilized in experimentation were sourced from Borosil Scientific (India) and Tarsons (India). Electrochemical reactions were carried out using an OWON (P4305) instrument in an undivided electrochemical cell equipped with a magnetic stirrer. Reaction progress was monitored by thin-layer chromatography (TLC), using silica gel-coated glass plates. Column chromatography was performed using silica gel (60-120 mesh) as the stationary phase, with a solvent system of diethyl ether and hexane serving as the mobile phase. ^{1}H and ^{13}C NMR spectra of the synthesized compounds were recorded on a Bruker spectrometer operating at 700/500/400 MHz and 176/126/101 MHz respectively. Tetramethylsilane (TMS) was used as an internal reference in $CDCl_3$. Chemical shifts (δ) are given in parts per million (ppm), and coupling constants (*J*) are reported in hertz (Hz). Residual solvent signals were used for calibration: $CDCl_3$ at 7.26 ppm (^{1}H) and 77.16 ppm (^{13}C). The NMR data were annotated using the following abbreviations: s (singlet), brs (broad singlet), d (doublet), t (triplet), q (quartet), dd (doublet of doublet), and m (multiplet). High-resolution mass spectrometry (HRMS) was performed on a Water QTOF (XEVO G2 XS) mass spectrometer using electrospray ionization in positive mode (ESI^{+}). Reaction conversions were quantified using high-performance liquid chromatography (HPLC) with 1,3-benzodioxole as an internal standard. The HPLC system consisted of a Shimadzu LC-20AD pump, a CTO-10AS column oven, and a photodiode array (PDA) detector. Cyclic voltammetry was conducted using a DY2300 potentiostat to study the redox behaviour relevant to the electrochemical process. Essential reagents like standard antibiotics and resazurin dye were received from Hi-Media (India). The bacterial strains, *Staphylococcus aureus* (ATCC 29213), *Klebsiella pneumoniae* (ATCC 15380), *Acinetobacter baumannii* (ATCC 19606), and *Escherichia coli* (ATCC 25922) were procured from the institutional microbial repository. For culturing bacterial strains, Luria Bertani (LB) broth and LB agar were procured from Hi-Media (India). Bacterial stocks were preserved in cryovials at -80 °C in 30% glycerol to maintain

viability. Fluorescence readings were taken using a Tecan Infinite M200-pro multimode plate reader. Centrifuge (Thermo Fisher- 5830R) and shaker incubator (REMI CIS-24-Plus) were utilized during the experimental procedure. All the biological assays were performed in a biosafety cabinet (ESCO AC2-4S1). The SEM study involved the utilization of GelBond film obtained from Lonza (Rockland, USA).

4.3.2: General procedure for the synthesis of compounds (5a-5s)

A mixture of indole-3-carboxaldehyde (100 mg, 0.68 mmol, 1.0 equiv.), phenylhydrazine (81 µL, 0.82 mmol, 1.0 equiv.), and sodium *p*-toluenesulfinate (245 mg, 1.37 mmol, 2.0 equiv.) was dissolved in 10 mL of ACN in a reaction vial. Thereafter, NH_4OAc (265 mg, 3.4 mmol, 5.0 equiv.) and KI (57 mg, 0.34 mmol, 0.5 equiv.) added to the reaction mixture. Electrolysis was then carried out by applying a constant current of 5 mA using a carbon anode and a nickel cathode, with the reaction mixture maintained at 40 °C in an oil bath. The mixture was stirred under these conditions for 12 hours. Upon consumption of starting materials, as confirmed by TLC, the electric current was turned off, and the solvent was removed under reduced pressure using a rotary evaporator. The resulting crude product was purified by column chromatography to afford the desired compounds.

4.3.3: General procedure for synthesis of starting materials (1 and 3)

4.3.3a: Procedure for synthesis of 1*H*-indole-3-carbaldehydes (1)[30]

In an oven-dried round-bottom flask equipped with a magnetic stir bar, dimethylformamide (DMF) and phosphorus oxychloride ($POCl_3$) are mixed in a 5:1 molar ratio by slowly adding $POCl_3$ (0.6 mL, 8.3 mmol, 1.5 equiv.) to DMF (1.6 mL, 21.2 mmol, 5 equiv.) under continuous stirring. The flask is kept in an ice bath throughout the addition while maintaining a low temperature. After 30 minutes, indole (500 mg, 4.2 mmol, 1 equiv.) is added to the cooled reaction mixture, and the solution is stirred for an additional hour to allow the reaction to proceed. Upon completion, the reaction is quenched by the slow addition of ice-cold water, followed by the dropwise addition of an aqueous sodium hydroxide solution (11 equiv.). This neutralization results in the formation of yellow precipitates. The solid product (**1**) is collected by filtration and thoroughly washed with cold water to remove any remaining impurities.

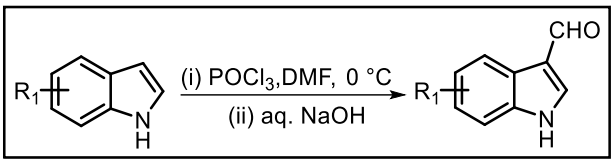

Scheme 4.4: General synthetic route for indole aldehydes

4.3.3b: Procedure for synthesis of sodium sulfinates (3)[7c]

Sodium sulfinates (**3a**, **3m**, **3p** and **3q**) were prepared by heating a mixture of sodium sulfite (600 mg, 4.8 mmol, 1.8 equiv.) and sodium carbonate (420 mg, 5 mmol, 2 equiv.) in 5 mL of water at 75 ◦C. After 15 minutes of stirring, sulfonyl chloride (484 mg, 2.5 mmol, 1 equiv.) was added slowly to the reaction mixture over a period of approximately 30 minutes. The reaction was then allowed to proceed for 3-4 hours. Upon cooling the mixture to room temperature, white precipitates began to form. The crude white solid was collected by filtration and used without further purification.

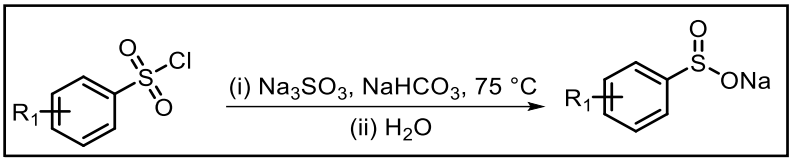

Scheme 4.5: General synthetic route for sodium sulfinates

4.3.4: Method for crystallization

Crystallization of compound **(5s)** was achieved using the vapor diffusion method. A solution of the compound (10 mg in 1 mL of dichloromethane) was placed in a small inner glass vial. This vial was then placed inside a larger, tightly sealed container holding 4 mL of hexane. As the hexane vapor slowly diffused into the DCM solution, the solvent environment gradually changed, promoting the slow formation of single crystals over time.[31]

4.3.5: Antibacterial susceptibility test (single point assay)

The antibacterial susceptibility of synthesized compounds was determined against Gram-positive (*S. aureus*) and Gram-negative (*K. pneumoniae*, *A. baumannii*, and *E. coli*) pathogens at a consistent test concentration of 50 µM. Briefly, the parent stocks of 20 mM concentration of the compounds were prepared by dissolving them in DMSO. The logarithmic phase of overnight-grown culture in LB medium was adjusted to 0.5 McFarland and then diluted 1:100 to obtain a final cell density of $1x10^6$ CFU/mL.[32,33] Subsequently, 100 µL of this freshly prepared bacterial suspension was dispensed into a 96-well flat-bottom plate containing 50 µM of synthesized compounds in triplicate and kept for incubation at 37 ºC for 24 hrs. After incubation, 10 µL of freshly prepared resazurin dye (0.04% dissolved in 1X PBS) was added to the culture plate, followed by another hour of incubation at 37 ºC. Finally, the Tecan Infinite M200-pro multimode reader was utilized to measure the fluorescence intensity with excitation and emission wavelengths set at 530 nm and 600 nm, respectively, to calculate the cell viability. The percentage viability of bacterial pathogens was calculated for each compound, and results

are represented as mean ± standard deviation of three independent measurements performed in triplicate.

4.3.6: Minimum inhibitory concentration (MIC)

The minimal inhibitory concentration (MIC), defined as the lowest compound concentration with no visible bacterial growth, was determined for the identified hits using a broth microdilution assay in accordance with the guidelines of the Clinical and Laboratory Standards Institute (CLSI).[34,35] Briefly, the compounds were serially diluted at a gradient concentration ranging from 50 µM to 1.56 µM in 96-well flat-bottom plates. Then, 100 µL of bacterial suspension with a cell density of $1x10^6$ CFU/mL was added to each well. Following incubation for 24 hrs, resazurin dye was added, and fluorescence was measured using a plate reader (as described above). Finally, the Gompertz equation was used to determine the MIC, and the data were plotted using GraphPad Prism 9 (Version 9.3.1). The experiment for MIC determination was performed in biological triplicate.

4.3.7: Scanning electron microscopy analysis

Scanning electron microscopy (SEM) was performed as reported previously.[33,36] Bacterial cultures of *S. aureus* in the exponential phase were treated with 1X and 2X MIC of potent hit (**5d**) and incubated at 37 °C for 4 hours. Following incubation, bacterial cultures were centrifuged at 5000 rpm for 5 minutes, and the pellet was washed thrice with 1X PBS. After this, the pellet was placed onto SEM sheets and left to air dry. Furthermore, the slides were fixed with 4% paraformaldehyde and 2.5% glutaraldehyde and air-dried overnight. After fixation, the slides were immersed in a graded ethanol series (30%, 50%, 70%, 90%, and 100%). The dried samples were coated with colloidal gold using a sputter coater, and morphological changes were examined under a JEOL JSM 6010 PLUS-LA (Akishima, Tokyo, Japan) scanning electron microscope.

4.3.8: Characterization of compounds

(*Z*)-*N*'-((1*H*-indol-3-yl)methylene)-4-methyl-*N*-phenylbenzenesulfonohydrazide (5a). off-white solid, ^{1}H NMR (400 MHz, $CDCl_3$): δ 9.26 (brs, 1H), 8.09 (s, 1H), 7.86 (d, J = 8.4 Hz, 2H), 7.71 (s, 1H), 7.50 (d, J = 8.4 Hz, 1H), 7.32 (s, 1H), 7.30 (s, 1H), 7.25 (s, 1H), 7.23 (s, 1H), 7.21 (s, 1H), 7.19 (s, 1H), 7.12 (t, J = 7.6 Hz, 1H), 6.96 (d, J = 7.6 Hz, 1H), 6.91 (d, J = 7.6 Hz, 2H), 2.45 (s, 3H) ppm. ^{13}C NMR (101 MHz, $CDCl_3$): δ 144.2, 142.7, 138.8, 136.4, 136.0, 129.6, 129.3, 128.8, 128.4, 124.6, 123.3, 122.1, 121.5, 119.7, 113.9, 112.5, 21.7 ppm. HRMS (ESI-TOF) m/z: $[M + H]^+$ calcd for $C_{22}H_{20}N_3O_2S$, 390.1276; found, 390.1263.

(*Z*)-*N*'-((5-methoxy-1*H*-indol-3-yl)methylene)-4-methyl-*N*-phenylbenzenesulfonohydrazide (5b). white solid, ^{1}H NMR (500 MHz, $CDCl_3$): δ 9.02 (brs,

1H), 8.02 (s, 1H), 7.83 (d, J = 8.5 Hz, 2H), 7.60 (d, J = 2.5 Hz, 1H), 7.33 (d, J = 9.0 Hz, 1H), 7.29-7.26 (m, 2H), 7.21-7.18 (m, 2H), 6.92-6.85 (m, 4H), 6.52 (d, J = 2.0 Hz, 1H), 3.63 (s, 3H), 2.42 (s, 3H) ppm. ^{13}C NMR (126 MHz, $CDCl_3$): δ 155.4, 144.2, 142.8, 139.1, 136.4, 129.5, 129.4, 129.0, 128.6, 125.2, 122.1, 113.9, 113.8, 113.3, 101.0, 100.1, 55.8, 21.7 ppm. HRMS (ESI-TOF) m/z: $[M + H]^+$ calcd for $C_{23}H_{22}N_3O_3S$, 420.1381; found, 420.1372.

(*Z*)-4-methyl-*N*'-((2-methyl-1*H*-indol-3-yl)methylene)-*N*-phenylbenzenesulfonohydrazide (5c). white solid, ^{1}H NMR (500 MHz, $CDCl_3$): δ 8.70 (brs, 1H), 7.90 (s, 1H), 7.79-7.76 (m, 2H), 7.33 (d, J = 8.0 Hz, 1H), 7.26 (s, 1H), 7.24 (s, 1H), 7.20 (t, J = 8.0 Hz, 2H), 7.15-7.12 (m, 1H), 6.99-6.98 (m, 2H), 6.93-6.90 (m, 3H), 2.41 (s, 3H), 2.32 (s, 3H) ppm. ^{13}C NMR (126 MHz, $CDCl_3$): δ 144.0, 142.6, 139.7, 138.5, 137.1, 135.8, 129.5, 129.3, 128.8, 126.4, 122.5, 122.2, 121.1, 118.9, 114.0, 111.2, 97.8, 21.7, 13.2 ppm. HRMS (ESI-TOF) m/z: $[M + H]^+$ calcd for $C_{23}H_{22}N_3O_2S$, 404.1432; found, 404.1422.

(*Z*)-*N*'-((5-bromo-1*H*-indol-3-yl)methylene)-4-methyl-*N*-phenylbenzenesulfonohydrazide (5d). off-white solid, ^{1}H NMR (500 MHz, $CDCl_3$): δ 9.43 (brs, 1H), 7.98 (s, 1H), 7.88 (d, J = 8.5 Hz, 2H), 7.62 (d, J = 3.0 Hz, 1H), 7.37 (d, J = 8.5 Hz, 2H), 7.30 (d, J = 3.0 Hz, 2H), 7.26-7.23 (m, 3H), 6.97 (t, J = 7.5 Hz, 1H), 6.89 (d, J = 8.0 Hz, 2H), 2.51 (s, 3H) ppm. ^{13}C NMR (126 MHz, $CDCl_3$): δ 144.6, 142.5, 138.3, 135.8, 134.7, 129.7, 129.4, 129.3, 129.1, 126.4, 126.3, 122.4, 121.9, 114.8, 114.0, 99.4, 21.8 ppm. HRMS (ESI-TOF) m/z: $[M + H]^+$ calcd for $C_{22}H_{19}BrN_3O_2S$, 468.0381; found, 468.0374.

(*Z*)-*N*'-((4-bromo-1*H*-indol-3-yl)methylene)-4-methyl-*N*-phenylbenzenesulfonohydrazide (5e). off-white solid, ^{1}H NMR (500 MHz, $CDCl_3$): δ 9.62 (brs, 1H), 7.89 (d, J = 6.5 Hz, 2H), 7.80 (s, 1H), 7.36 (d, J = 2.5 Hz, 1H), 7.33 (dd, J = 7.5, 4.5 Hz, 3H), 7.20-7.15 (m, 3H), 6.96 (t, J = 8.5 Hz, 1H), 6.89 (t, J = 7.5 Hz, 1H), 6.82 (d, J = 8.0 Hz, 2H), 2.45 (s, 3H) ppm. ^{13}C NMR (126 MHz, $CDCl_3$): δ 144.4, 142.6, 138.4, 137.1, 135.8, 129.5, 129.4, 129.3, 129.0, 125.3, 125.1, 124.2, 122.2, 114.1, 113.2, 111.7, 99.0, 21.8 ppm. HRMS (ESI-TOF) m/z: $[M + H]^+$ calcd for $C_{22}H_{19}BrN_3O_2S$, 468.0381; found, 468.0377.

(*Z*)-*N*'-((5-chloro-1*H*-indol-3-yl)methylene)-4-methyl-*N*-phenylbenzenesulfonohydrazide (5f). off-white solid, ^{1}H NMR (500 MHz, $CDCl_3$): δ 9.14 (brs, 1H), 7.92 (s, 1H), 7.82 (d, J = 8.5 Hz, 2H), 7.66 (d, J = 3.0 Hz, 1H), 7.36-7.30 (m, 3H), 7.22-7.15 (m, 3H), 7.08 (d, J = 2.0 Hz, 1H), 6.93 (t, J = 7.5Hz, 1H), 6.86 (d, J = 8.0 Hz, 2H), 2.44 (s, 3H) ppm. ^{13}C NMR (126 MHz, $CDCl_3$): δ 144.5, 142.6, 138.2, 136.0, 134.3, 129.6, 129.5, 129.4, 129.0, 127.4, 125.8, 123.9, 122.4, 119.0, 114.0, 113.4, 21.8 ppm. HRMS (ESI-TOF) m/z: $[M + H]^+$ calcd for $C_{22}H_{19}ClN_3O_2S$, 424.0886; found, 424.0883.

(*Z*)-4-methyl-*N*'-((5-nitro-1*H*-indol-3-yl)methylene)-*N*-phenylbenzenesulfonohydrazide (5g). yellow solid, ^{1}H NMR (500 MHz, $CDCl_3$): δ 9.69 (brs, 1H), 8.07-8.04 (m, 2H), 7.91 (s, 1H), 7.84 (d, J = 8.0 Hz, 2H), 7.76 (d, J = 2.5 Hz, 1H), 7.47 (d, J = 9.0 Hz, 1H), 7.34 (d, J = 8.0 Hz, 2H), 7.21-7.18 (m, 2H), 6.97-6.92 (m, 1H), 6.83 (d, J = 7.5 Hz, 2H), 2.45 (s, 3H) ppm. ^{13}C NMR (126 MHz, $CDCl_3$): δ 138.9, 135.4, 131.4, 129.8, 129.5, 129.4, 129.1, 124.5, 122.8, 118.9, 116.5, 114.1, 112.6, 102.4, 21.8 ppm. HRMS (ESI-TOF) *m/z*: $[M + H]^+$ calcd for $C_{22}H_{19}N_4O_4S$, 435.1127; found, 435.1119.

(*Z*)-*N*'-((5-cyano-1*H*-indol-3-yl)methylene)-4-methyl-*N*-phenylbenzenesulfonohydrazide (5h). yellow solid, ^{1}H NMR (500 MHz, $CDCl_3$): δ 9.56 (brs, 1H), 7.87 (s, 1H), 7.82 (d, J = 8.0 Hz, 2H), 7.73 (s, 1H), 7.49-7.46 (m, 2H), 7.42 (d, J = 8.5 Hz, 1H), 7.34 (d, J = 8.0 Hz, 2H), 7.22-7.18 (m, 2H), 6.95 (t, J = 7.5 Hz, 1H), 6.83 (d, J = 8.0 Hz, 2H), 2.47 (s, 3H) ppm. ^{13}C NMR (126 MHz, $CDCl_3$): δ 144.9, 142.3, 137.4, 135.6, 130.5, 129.8, 129.5, 129.1, 126.3, 124.9, 122.8, 119.7, 114.0, 113.5, 105.0, 101.0, 21.8 ppm. HRMS (ESI-TOF) *m/z*: $[M + H]^+$ calcd for $C_{23}H_{19}N_4O_2S$, 415.1228; found, 415.1223.

(*E*)-*N*'-benzylidene-4-methyl-*N*-phenylbenzenesulfonohydrazide (5i). yellow viscous, ^{1}H NMR (500 MHz, $CDCl_3$): δ 7.50 (d, J = 2.0 Hz, 1H), 7.48 (t, J = 2.0 Hz, 1H), 7.24 (s, 1H), 7.20 (d, J = 2.0 Hz, 1H), 7.19 (d, J = 2.0 Hz, 1H), 7.15 (d, J = 1.0 Hz, 1H), 7.14 (d, J = 2.0 Hz, 1H), 7.00-6.99 (m, 1H), 6.97 (s, 1H), 6.93 (t, J = 7.5 Hz, 1H), 6.83 (s, 1H), 6.82 (s, 1H), 6.80 (s, 1H), 6.78 (s, 1H), 6.74 (q, J = 4.0 Hz, 4.5 Hz, 1H), 2.24 (s, 3H) ppm. ^{13}C NMR (126 MHz, $CDCl_3$): δ 145.4, 144.8, 135.9, 134.0, 132.8, 132.4, 129.3, 129.1, 129.0, 128.6, 128.5, 128.3, 128.0, 127.9, 127.7, 126.7, 123.8, 122.7, 120.7, 112.8, 70.3, 21.6 ppm. HRMS (ESI-TOF) *m/z*: $[M + Na]^+$ calcd for $C_{20}H_{18}N_2NaO_2S$, 373.0986; found, 373.0978.

(*E*)-*N*'-(4-hydroxybenzylidene)-4-methyl-*N*-phenylbenzenesulfonohydrazide (5j). yellow viscous, ^{1}H NMR (500 MHz, $CDCl_3$): δ 7.84 (s, 1H), 7.79 (d, J = 8.0 Hz, 2H), 7.33 (d, J = 7.5 Hz, 2H), 7.26 (s, 1H), 7.22-7.18 (m, 3H), 6.94-6.91 (m, 3H), 6.88 (d, J = 9.0 Hz, 2H), 2.46 (s, 3H) ppm. ^{13}C NMR (126 MHz, $CDCl_3$): δ 158.3, 144.5, 142.9, 142.5, 136.0, 131.7, 129.7, 129.4, 129.1, 122.4, 117.4, 117.0, 113.9, 21.8 ppm. HRMS (ESI-TOF) *m/z*: $[M + H]^+$ calcd for $C_{20}H_{19}N_2O_3S$, 367.1116; found, 367.1111.

(*Z*)-*N*'-((1*H*-indol-3-yl)methylene)-4-methoxy-*N*-phenylbenzenesulfonohydrazide (5k). white solid, ^{1}H NMR (500 MHz, $CDCl_3$): δ 9.22 (brs, 1H), 8.03 (s, 1H), 7.86 (d, J = 9.0 Hz, 2H), 7.66 (d, J = 3.0 Hz, 1H), 7.45 (d, J = 8.0 Hz, 1H), 7.22-7.16 (m, 4H), 7.08 (t, J = 8.0 Hz, 1H), 6.93 (d, J = 9.0 Hz, 2H), 6.90 (s, 1H), 6.87 (d, J = 7.5 Hz, 2H), 3.84 (s, 3H) ppm. ^{13}C NMR (126 MHz, $CDCl_3$): δ 163.6, 142.8, 139.1, 136.0, 131.0, 130.7, 129.3, 128.4, 124.6,

123.3, 122.1, 121.5, 119.7, 114.2, 113.8, 112.5, 100.3, 55.7 ppm. HRMS (ESI-TOF) *m/z*: [M + H]$^+$ calcd for $C_{22}H_{20}N_3O_3S$, 406.1225; found, 406.1219.

(*Z*)-*N*'-((1*H*-indol-3-yl)methylene)-4-chloro-*N*-phenylbenzenesulfonohydrazide (5l). off-white solid, ^{1}H NMR (500 MHz, $CDCl_3$): δ 9.15 (brs, 1H), 8.10 (s, 1H), 7.88 (d, J = 8.5 Hz, 2H), 7.70 (s, 1H), 7.49-7.45 (m, 3H), 7.27-7.20 (m, 3H), 7.17-7.10 (m, 2H), 6.94 (t, J = 7.5 Hz, 1H), 6.88 (d, J = 7.5 Hz, 2H) ppm. ^{13}C NMR (126 MHz, $CDCl_3$): δ 142.5, 140.0, 138.2, 138.0, 135.9, 130.2, 129.4, 129.2, 128.5, 124.5, 123.5, 122.4, 121.7, 119.6, 113.9, 112.6, 100.0 ppm. HRMS (ESI-TOF) *m/z*: [M + H]$^+$ calcd for $C_{21}H_{17}ClN_3O_2S$, 410.0730; found, 410.0720.

(*Z*)-4-chloro-*N*'-((5-methoxy-1*H*-indol-3-yl)methylene)-*N*-phenylbenzenesulfonohydrazide (5m). brown solid, ^{1}H NMR (500 MHz, $CDCl_3$): δ 8.98 (brs, 1H), 8.07 (s, 1H), 7.88 (d, J = 9.0 Hz, 2H), 7.64 (d, J = 2.5 Hz, 1H), 7.46 (d, J = 8.5 Hz, 2H), 7.35 (d, J = 8.5 Hz, 1H), 7.23-7.20 (m, 2H), 6.93 (t, J = 7.0 Hz, 1H), 6.88 (d, J = 7.5 Hz, 3H), 6.51 (s, 1H), 3.65 (s, 3H) ppm. ^{13}C NMR (126 MHz, $CDCl_3$): δ 155.5, 142.6, 140.0, 138.5, 138.0, 130.8, 130.4, 129.4, 129.2, 128.6, 125.1, 122.4, 114.0, 113.8, 113.3, 100.9, 99.8, 55.9 ppm. HRMS (ESI-TOF) *m/z*: [M + H]$^+$ calcd for $C_{22}H_{19}ClN_3O_3S$, 440.0835; found, 440.0826.

(*Z*)-*N*'-((1*H*-indol-3-yl)methylene)-*N*-phenyl-4-(trifluoromethyl)benzenesulfonohydrazide (5n). light brown solid, ^{1}H NMR (500 MHz, $CDCl_3$): δ 9.02 (s, 1H), 8.12 (s, 1H), 8.07 (d, J = 7.5 Hz, 2H), 7.75 (d, $^3J_{H\text{-}F}$ = 3.0 Hz, 2H), 7.73 (s, 1H), 7.49 (d, J = 8.0 Hz, 1H), 7.20 (t, J = 7.7 Hz, 3H), 7.15-7.12 (m, 2H), 6.94 (t, J = 7.5 Hz, 1H), 6.84 (d, J = 7.5 Hz, 2H) ppm. ^{13}C NMR (126 MHz, $CDCl_3$): δ 143.3, 142.4, 137.8, 135.9, 129.5, 129.4, 128.5, 126.0, 124.4, 123.7, 122.6, 121.9, 119.6, 113.9, 112.5, 100.0 ppm. HRMS (ESI-TOF) *m/z*: [M + H]$^+$ calcd for $C_{22}H_{17}F_3N_3O_2S$, 444.0993; found, 444.0972.

(*Z*)-*N*'-((1*H*-indol-3-yl)methylene)-4-nitro-*N*-phenylbenzenesulfonohydrazide (5o). yellow solid, ^{1}H NMR (500 MHz, $CDCl_3$): δ 8.93 (brs, 1H), 8.28 (d, J = 8.5 Hz, 2H), 8.18 (s, 1H), 8.10 (d, J = 9.0 Hz, 2H), 7.79 (d, J = 3.0 Hz, 1H), 7.51 (d, J = 8.5 Hz, 1H), 7.31-7.27 (m, 1H), 7.24-7.21 (m, 2H), 7.14-7.10 (m, 2H), 6.96 (t, J = 7.5 Hz, 1H), 6.90 (d, J = 7.5 Hz, 2H) ppm. ^{13}C NMR (126 MHz, $CDCl_3$): δ 150.4, 145.8, 142.2, 137.2, 135.9, 130.0, 129.5, 128.6, 124.2, 124.0, 123.8, 122.9, 122.1, 119.5, 114.0, 112.6, 100.1 ppm. HRMS (ESI-TOF) *m/z*: [M + H]$^+$ calcd for $C_{21}H_{17}N_4O_4S$, 421.0970; found, 421.0959 ppm.

(*Z*)-*N*'-((1*H*-indol-3-yl)methylene)-*N*-phenylmethanesulfonohydrazide (5p). white solid, ^{1}H NMR (500 MHz, $CDCl_3$): δ 9.10 (brs, 1H), 8.06 (s, 1H), 7.65 (d, J = 2.5 Hz, 1H), 7.42 (d, J = 8.0 Hz, 1H), 7.37 (d, J = 8.0 Hz, 1H), 7.26-7.22 (m, 3H), 7.15 (t, J = 8.0 Hz, 1H), 7.00 (d, J = 8.0 Hz, 2H), 6.93 (t, J = 7.5 Hz, 1H), 3.24 (s, 3H) ppm. ^{13}C NMR (126 MHz, $CDCl_3$): δ 142.7, 138.9, 136.1, 129.5, 128.4, 124.5, 123.6, 122.3, 121.8, 119.8, 113.8, 112.6, 98.9, 40.0

ppm. HRMS (ESI-TOF) *m/z*: $[M + H]^+$ calcd for $C_{16}H_{16}N_3O_2S$, 314.0963; found, 314.0959 ppm.

(*Z*)-*N*'-((1*H*-indol-3-yl)methylene)-*N*-(4-chlorophenyl)-4-methylbenzenesulfonohydrazide (5q). Brown solid, ^{1}H NMR (500 MHz, $CDCl_3$): δ 9.23 (brs, 1H), 7.99 (s, 1H), 7.91 (d, J = 8.5 Hz, 1H), 7.78 (d, J = 8.0 Hz, 2H), 7.65 (s, 1H), 7.43 (d, J = 8.0 Hz, 1H), 7.24 (s, 1H), 7.19 (t, J = 7.0 Hz, 2H), 7.12 (s, 1H), 7.10 (s, 1H), 7.07 (d, J = 7.5 Hz, 1H), 6.76 (d, J = 9.0 Hz, 2H), 2.39 (s, 3H) ppm. ^{13}C NMR (126 MHz, $CDCl_3$): δ 144.4, 141.4, 139.7, 136.1, 136.0, 130.1, 129.6, 129.3, 128.9, 128.6, 126.9, 124.5, 123.4, 121.6, 119.6, 115.0, 112.6, 100.0, 21.7 ppm. HRMS (ESI-TOF) *m/z*: $[M + H]^+$ calcd for $C_{22}H_{19}ClN_3O_2S$, 424.0886; found, 424.0860 ppm.

(*Z*)-*N*'-((1*H*-indol-3-yl)methylene)-*N*-(2-bromophenyl)-4-methylbenzenesulfonohydrazide (5r). Brown solid, ^{1}H NMR (500 MHz, $CDCl_3$): δ 9.02 (s, 1H), 8.51 (s, 1H), 7.83 (s, 1H), 7.82 (s, 1H), 7.80 (d, J = 2.0 Hz, 2H), 7.48 (d, J = 8.0 Hz, 1H), 7.33 (d, J = 1.5 Hz, 1H), 7.32-7.31 (m, 2H), 7.30 (s, 1H), 7.28 (s, 1H), 7.21 (s, 1H), 7.13 (t, J = 7.5 Hz, 1H), 6.78 (t, J = 7.5 Hz, 1H), 2.41 (s, 3H) ppm. ^{13}C NMR (126 MHz, $CDCl_3$): δ 144.3, 143.7, 141.3, 140.0, 139.2, 136.2, 132.4, 129.8, 129.6, 128.9, 128.6, 128.4, 126.5, 123.5, 122.5, 121.5, 120.6, 115.3, 112.3, 108.2, 100.4, 21.7 ppm. HRMS (ESI-TOF) *m/z*: $[M + H]^+$ calcd for $C_{22}H_{19}BrN_3O_2S$, 468.0381; found, 468.0367 ppm.

(*Z*)-*N*'-((1*H*-indol-3-yl)methylene)-4-methyl-*N*-tosylbenzenesulfonohydrazide (5s). Light yellow solid, ^{1}H NMR (700 MHz, $CDCl_3$): δ 9.06 (brs, 1H), 8.62 (s, 1H), 7.99 (d, J = 7.7 Hz, 1H), 7.62 (d, J = 8.4 Hz, 4H), 7.47 (d, J = 9.1 Hz, 2H), 7.32 (t, J = 7.0 Hz, 1H), 7.23 (t, J = 7.7 Hz, 1H), 7.13 (d, J = 8.4 Hz, 4H), 2.42 (s, 6H) ppm. ^{13}C NMR (176 MHz, $CDCl_3$): δ 168.9, 144.9, 137.0, 134.0, 133.7, 129.4, 129.1, 124.6, 124.3, 122.7, 122.4, 112.1, 21.8 ppm. HRMS (ESI-TOF) *m/z*: $[M + H]^+$ calcd for $C_{23}H_{22}N_3O_4S_2$, 468.1051; found, 468.1051 ppm.

4.4: Conclusion

In summary, we have developed a novel electrochemical methodology for the regioselective *N*-sulfonylation of *in-situ* generated indole-based hydrazones. The scope and robustness of this eco-friendly protocol were demonstrated through the successful transformation of a wide variety of aldehydes, hydrazines, and sodium sulfinates, yielding the corresponding *N*-sulfonylated products in good yields. To confirm the essential role of electrical input in this transformation, a series of control experiments were carried out. Furthermore, cyclic voltammetry analyses were conducted to gain mechanistic insights and support the proposed reaction pathway. Next, synthesized compounds were tested at 50 µM to evaluate their antibacterial activity. Four compounds- **5d**, **5e**, **5l**, and **5q** stood out by showing strong

inhibition (over 85%) against *S. aureus*, a common Gram-positive bacterium. However, they were only moderately effective against Gram-negative bacteria. Further testing confirmed that these hits, especially **5d** with an MIC of 6.87 µM, have promising and selective activity against *S. aureus*. These findings suggest that the identified compounds could serve as potential leads for developing targeted treatments against Gram-positive infections. Other advanced antimicrobial biological studies are in progress in our lab and will be reported in due course. This study not only underscores the utility of electrochemical synthesis in modern organic chemistry but also opens new avenues for the sustainable development of medicinally important sulfonamide derivatives as antibacterial compounds.

4.5: References

1. (a) Patel, D. K.; Chaudhary, K. N.; Joshi, C. K.; Chaudhary, H. R.; Panchal, N. S.; Patel, D. D.; Patel, D. M. Green Synthesis, Spectral Characterization, In Silico and In Vitro Antimicrobial Investigations, and ADMET Profiling of Functionalized Hydrazone Derivatives. Russ. *J. Org. Chem.* **2024**, *60*, S213–S222. (b) Claraz, A. Harnessing the Versatility of Hydrazones through Electrosynthetic Oxidative Transformations. *Beilstein J. Org. Chem.* **2024**, *20*, 1988–2004. (c) Ali, A.; Khalid, M.; Abid, S.; Iqbal, J.; Tahir, M. N.; Rauf Raza, A.; Zukerman-Schpector, J.; Paixão, M. W. Facile Synthesis, Crystal Growth, Characterization and Computational Study of New Pyridine-Based Halogenated Hydrazones: Unveiling the Stabilization Behavior in Terms of Noncovalent Interactions. *Appl. Organomet. Chem.* **2020**, *34*, e5399. (d) Shao, B.; Aprahamian, I. Hydrazones as New Molecular Tools. *Chem* **2020**, *6*, 2162–2173.
2. (a) Rollas, S.; Küçükgüzel, Ş. G. Biological Activities of Hydrazone Derivatives. *Molecules* **2007**, *12*, 1910–1939. (b) Rajput, J. D.; Bagul, S. D.; Bendre, R. S. Synthesis, Biological Activities and Molecular Docking Simulation of Hydrazone Scaffolds of Carvacrol, Thymol and Eugenol. *Res. Chem. Intermed.* **2017**, *43*, 6601–6616. (c) Khan, M.; Ahad, G.; Alam, A.; Ullah, S.; Khan, A.; Kanwal, U.; Salar, U.; Wadood, A.; Ajmal, A.; Khan, K. M.; Perveen, S.; Uddin, J.; Al-Harrasi, A. Synthesis of New Bis(dimethylamino)benzophenone Hydrazone for Diabetic Management: In Vitro and In Silico Approach. *Heliyon* **2024**, *10*, e23323. (d) Boudiba, S.; Tamfu, A. N.; Hanini, K.; Selatnia, I.; Boudiba, L.; Saouli, I.; Mosset, P.; Ceylan, O.; Egbe, D. A. M.; Sid, A.; Dinica, R. M. Synthesis of a New Diarylhydrazone Derivative and an Evaluation of Its *In Vitro* Biofilm Inhibition and Quorum Sensing Disruption Along with a Molecular Docking Study. *J. Chem. Res.* **2023**, *47*, 17475198231184603. (e) Han, M. İ.; İmamoğlu, N. Design, Synthesis, and Anticancer Evaluation of Novel Tetracaine

Hydrazide-Hydrazones. *ACS Omega* **2023**, *8*, 9198–9211. (f) Demir, Y.; Tokalı, F. S.; Kalay, E.; Türkeş, C.; Tokalı, P.; Aslan, O. N.; Şendil, K.; Beydemir, Ş. Synthesis and Characterization of Novel Acyl Hydrazones Derived from Vanillin as Potential Aldose Reductase Inhibitors. *Mol. Divers.* **2023**, *27*, 1713–1733.

3. (a) Verma, S.; Lal, S.; Narang, R.; Sudhakar, K. Quinoline Hydrazide/Hydrazone Derivatives: Recent Insights on Antibacterial Activity and Mechanism of Action. *ChemMedChem* **2023**, *18*, e202200571. (b) Sreenivasulu, R.; Sujitha, P.; Jadav, S. S.; Ahsan, M. J.; Kumar, C. G.; Raju, R. R. Synthesis, Antitumor Evaluation, and Molecular Docking Studies of Indole–Indazolyl Hydrazide–Hydrazone Derivatives. *Monatsh. Chem.* **2017**, *148*, 305–314. (c) Verma, G.; Marella, A.; Shaquiquzzaman, M.; Akhtar, M.; Ali, M. R.; Alam, M. M. A Review Exploring Biological Activities of Hydrazones. *J. Pharm. Bioallied Sci.* **2014**, *6*, 69–80. (d) Sondhi, S. M.; Dinodia, M.; Kumar, A. Synthesis, Anti-Inflammatory and Analgesic Activity Evaluation of Some Amidine and Hydrazone Derivatives. *Bioorg. Med. Chem.* **2006**, *14*, 4657–4663. (e) Keskin, S.; Doğan, Ş. D.; Gündüz, M. G.; Aleksic, I.; Vojnovic, S.; Lazic, J.; Nikodinovic-Runic, J. Indole-Based Hydrazone Derivatives: Synthesis, Cytotoxicity Assessment, and Molecular Modeling Studies. *J. Mol. Struct.* **2022**, *1270*, 133936. (f) Farooq, U.; Khan, F.; Mali, S. N.; Ghaffar, U.; Hussain, J.; Khan, A.; Chaudhari, S. Y.; Al-Shwaiman, H. A.; Elgorban, A. M.; Jawarkar, R. D.; Islam, W. U.; Al-Harrasi, A.; Shafiq, Z. *In Vitro* and *In Silico* Analysis of Synthesized *N*-Benzyl Indole-Derived Hydrazones as Potential Anti-Triple Negative Breast Cancer Agents. *RSC Adv.* **2025**, *15*, 13284–13299.
4. Wahbeh, J.; Milkowski, S. The Use of Hydrazones for Biomedical Applications. *SLAS Technol.* **2019**, *24*, 161–168.
5. (a) Xu, X.; Zhang, J.; Xia, H.; Wu, J. C(sp^2)–H Functionalization of Aldehyde-Derived Hydrazones via a Radical Process. *Org. Biomol. Chem.* **2018**, *16*, 1227–1241. (b) Zhang, X.; Sivaguru, P.; Pan, Y.; Wang, N.; Zhang, W.; Bi, X. The Carbene Chemistry of *N*-Sulfonyl Hydrazones: The Past, Present, and Future. *Chem. Rev.* **2025**, *125*, 1049–1190. (c) Xu, P.; Li, W.; Xie, J.; Zhu, C. Exploration of C–H Transformations of Aldehyde Hydrazones: Radical Strategies and Beyond. *Acc. Chem. Res.* **2018**, *51*, 484–495. (d) Prieto, A.; Bouyssi, D.; Monteiro, N. Radical-Mediated Formal C(sp^2)–H Functionalization of Aldehyde-Derived *N,N*-Dialkylhydrazones. *Eur. J. Org. Chem.* **2018**, *20*, 2378–2393.

6. (a) Jamshidi, M.; Amani, A.; Khazalpour, S.; Torabi, S.; Nematollahi, D. Progress and Perspectives of Electrochemical Insights for C–H and N–H Sulfonylation. *New J. Chem.* **2021**, *45*, 18246–18267. (b) Colomer, J. P.; Traverssi, M.; Oksdath-Mansilla, G. Oxidation of Organosulfur Compounds Promoted by Continuous-Flow Chemistry. *J. Flow Chem.* **2020**, *10*, 123–138.
7. (a) Manasa, K. L.; Pujitha, S.; Sethi, A.; Mohammed, A.; Alvala, M.; Angeli, A.; Supuran, C. T. Synthesis and Biological Evaluation of Imidazo[2,1-b]thiazole-Based Sulfonyl Piperazines as Novel Carbonic Anhydrase II Inhibitors. *Metabolites* **2020**, *10*, 136. (b) Yan, Q.; Cui, W.; Song, X.; Xu, G.; Jiang, M.; Sun, K.; Lv, J.; Yang, D. Sulfonylation of Aryl Halides by Visible Light/Copper Catalysis. *Org. Lett.* **2021**, *23*, 3663–3668. (c) Sarkar, B.; Ghosh, P.; Hajra, A. Electrochemical C–H Sulfonylation of Hydrazones. *Org. Lett.* **2023**, *25*, 3440–3444. (d) Yu, S.; Yu, J. T.; Pan, C. Synthesis of Functionalized Tetrahydropyridazines from Hydrazones. *Org. Biomol. Chem.* **2024**, *22*, 7753–7766.
8. (a) Yu, M.; Lin, S.; Zhang, S.; Lin, X.; Huang, X. Direct C–H Sulfonylation of Hydrazones Involving the Insertion of SO_2. *Org. Chem. Front.* **2024**, *11*, 4284–4289. (b) Sridhar, R.; Srinivas, B.; Kumar, V. P.; Narender, M.; Rao, K. R. β-Cyclodextrin-Catalyzed Monosulfonylation of Amines and Amino Acids in Water. *Adv. Synth. Catal.* **2007**, *349*, 1873–1876.
9. (a) Noda, S.; Tanimori, S. Organic Solvent-Free Synthesis of Sulfonyl Hydrazides in Water. *Tetrahedron Green Chem.* **2023**, *1*, 100001. (b) Huang, C.; Kang, C.; Liu, H. J.; Wang, C. L.; Tang, S.; Qin, Y. S.; Wei, Z.; Cai, H. *N*-Sulfonylation of Azoles with Sulfonyl Hydrazides Enabled by Electrocatalysis. *Green Chem.* **2024**, *26*, 8706–8710.
10. (a) Hu, D.; Shen, L.; Chaw, S. S. H.; Liang, K.; Xia, C. Visible Light-Induced Sulfonylation with Sulfinates as Closed-Shell Radical Acceptors. *Org. Chem. Front.* **2024**, *11*, 3497–3502. (b) Johnson, T. C.; Elbert, B. L.; Farley, A. J. M.; Gorman, T. W.; Genicot, C.; Lallemand, B.; Pasau, P.; Flasz, J.; Castro, J. L.; Maccoss, M.; Dixon, D. J.; Paton, R. S.; Schofield, C. J.; Smith, M. D.; Willis, M. C. Direct Sulfonylation of Anilines Mediated by Visible Light. *Chem. Sci.* **2018**, *9*, 629–633.
11. (a) Kupwade, R. V. A Concise Review on Synthesis of Sulfoxides and Sulfones with Special Reference to Oxidation of Sulfides. *J. Chem. Rev.* **2019**, *1*, 99–113. (b) Parumala, S. K. R.; Peddinti, R. K. Metal-Free Synthesis of Sulfonamides via Iodine-Catalyzed Oxidative Coupling of Sulfonyl Hydrazides and Amines. *Tetrahedron Lett.* **2016**, *57*, 1232–1235.

12. Bourbon, P.; Appert, E.; Martin-Mingot, A.; Michelet, B.; Thibaudeau, S. Complementary Site-Selective Sulfonylation of Aromatic Amines by Superacid Activation. *Org. Lett.* **2021**, *23*, 4115–4120.
13. Yu, H.; Zhang, Y. NH_4I-Catalyzed Synthesis of Sulfonamides from Arylsulfonylhydrazides and Amines. *Chin. J. Chem.* **2016**, *34*, 359–362.
14. Laudadio, G.; Barmpoutsis, E.; Schotten, C.; Struik, L.; Govaerts, S.; Browne, D. L.; Noël, T. Sulfonamide Synthesis through Electrochemical Oxidative Coupling of Amines and Thiols. *J. Am. Chem. Soc.* **2019**, *141*, 5664–5668.
15. Dong, D. Q.; Han, Q. Q.; Yang, S. H.; Song, J. C.; Li, N.; Wang, Z. L.; Xu, X. M. Recent Progress in Sulfonylation via Radical Reaction with Sodium Sulfinates, Sulfinic Acids, Sulfonyl Chlorides or Sulfonyl Hydrazides. *ChemistrySelect* **2020**, *5*, 13103–13134.
16. (a) Hou, Y.; Shen, Q.; Zhu, L.; Han, Y.; Zhao, Y.; Qin, M.; Gong, P. Palladium-Catalyzed Three-Component Tandem Reaction of Sulfonyl Hydrazones, Aryl Iodides and Allenes: Highly Stereoselective Synthesis of (Z)-α-Hydroxymethyl Allylic Sulfones. *RSC Adv.* **2017**, *7*, 50372–50377. (b) Yang, B.; Lian, C.; Yue, G.; Liu, D.; Wei, L.; Ding, Y.; Zheng, X.; Lu, K.; Qiu, D.; Zhao, X. Synthesis of *N*-Arylsulfonamides through a Pd-Catalyzed Reduction Coupling Reaction of Nitroarenes with Sodium Arylsulfinates. *Org. Biomol. Chem.* **2018**, *16*, 8150–8154. (c) Tang, X.; Huang, L.; Qi, C.; Wu, X.; Wu, W.; Jiang, H. Copper-Catalyzed Sulfonamides Formation from Sodium Sulfinates and Amines. *Chem. Commun.* **2013**, *49*, 6102–6104.
17. Qiu, G.; Zhou, K.; Wu, J. Recent Advances in the Sulfonylation of C–H Bonds with the Insertion of Sulfur Dioxide. *Chem. Commun.* **2018**, *54*, 12561–12569.
18. (a) Chen, Y.; Murray, P. R. D.; Davies, A. T.; Willis, M. C. Direct Copper-Catalyzed Three-Component Synthesis of Sulfonamides. *J. Am. Chem. Soc.* **2018**, *140*, 8781–8787. (b) Lin, Z.; Huang, L.; Yuan, G. Electrosynthesis of Sulfonamides from DMSO and Amines under Mild Conditions. *Chem. Commun.* **2021**, *57*, 3579–3582.
19. (a) Reddy, R. J.; Kumari, A. H. Synthesis and Applications of Sodium Sulfinates (RSO_2Na): A Powerful Building Block for the Synthesis of Organosulfur Compounds. *RSC Adv.* **2021**, *11*, 9130–9221. (b) Fu, L.; Bao, X.; Li, S.; Wang, L.; Liu, Z.; Chen, W.; Xia, Q.; Liang, G. Synthesis of Sulfonamides from Azoles and Sodium Sulfinates at Ambient Temperature. *Tetrahedron* **2017**, *73*, 2504–2511. (c) Smith, J. M.; Dixon, J. A.; Degruyter, J. N.; Baran, P. S. Alkyl Sulfinates: Radical Precursors Enabling Drug Discovery: Miniperspective. *J. Med. Chem.* **2019**, *62*, 2256–2264.

20. (a) Su, X.; Aprahamian, I. Hydrazone-Based Switches, Metallo-Assemblies and Sensors. *Chem. Soc. Rev.* **2014**, *43*, 1963–1981. (b) Li, Q.; Zhang, Y.; Lin, J.; Zou, Y.; Wang, P.; Qin, Z.; Wang, Y.; Li, Y.; Zhang, Y.; Gao, C.; Zang, Y.; Hu, W.; Dong, H. Dibenzothiophene Sulfone-Based Ambipolar-Transporting Blue-Emissive Organic Semiconductors Towards Simple-Structured Organic Light-Emitting Transistors. *Angew. Chem. Int. Ed.* **2023**, *62*, e202308146. (c) Eid, N.; Karamé, I.; Andrioletti, B. Straightforward and Sustainable Synthesis of Sulfonamides in Water under Mild Conditions. *Eur. J. Org. Chem.* **2018**, *2018*, 5016–5022. (d) Şenkardeş, S.; İhsan Han, M.; Gürboğa, M.; Özakpinar, Ö. B.; Küçükgüzel, G. Synthesis and Anticancer Activity of Novel Hydrazone Linkage-Based Aryl Sulfonate Derivatives as Apoptosis Inducers. *Med. Chem. Res.* **2022**, *31*, 368–379. (e) Patoghi, P.; Sadatnabi, A.; Nematollahi, D. A New Type of Convergent Paired Electrochemical Synthesis of Sulfonamides under Green and Catalyst-Free Conditions. *Sci. Rep.* **2023**, *13*, 17582. (f) Blum, S. P.; Karakaya, T.; Schollmeyer, D.; Klapars, A.; Waldvogel, S. R. Metal-Free Electrochemical Synthesis of Sulfonamides Directly from (Hetero)Arenes, SO_2, and Amines. *Angew. Chem. Int. Ed.* **2021**, *60*, 5056–5062. (g) Liu, W.; Chen, J.; Su, W. Construction of Biaryl Sulfonamides via Pd(II)-Catalyzed Cross-Coupling of C(sp^2)-H Bonds with Iodobenzenesulfonamides. *Pharmaceut. Fronts* **2024**, *6*, e355–e381.

21. Xu, J.; Shen, C.; Qin, X.; Wu, J.; Zhang, P.; Liu, X. Oxidative Sulfonylation of Hydrazones Enabled by Synergistic Copper/Silver Catalysis. *J. Org. Chem.* **2021**, *86*, 3706–3720.

22. Qiao, J.; Zheng, K.; Lin, Z.; Jin, H.; Yu, W.; Shen, C.; Jia, A.; Zhang, Q. Heterogeneous Chitosan@Copper Catalyzed Selective C(sp^3)–H Sulfonylation of Ketone Hydrazones with Sodium Sulfinates: Direct Access to β-Ketosulfones. *Catalysts* **2023**, *13*, 726.

23. (a) Cembellín, S.; Batanero, B. Organic Electrosynthesis towards Sustainability: Fundamentals and Greener Methodologies. *Chem. Rec.* **2021**, *21*, 1–20. (b) Budnikova, Y. H.; Dolengovski, E. L.; Tarasov, M. V.; Gryaznova, T. V. Electrochemistry in Organics: A Powerful Tool for "Green" Synthesis. *J. Solid State Electrochem.* **2024**, *28*, 659–676.

24. (a) Martins, G. M.; Shirinfar, B.; Hardwick, T.; Murtaza, A.; Ahmed, N. Organic Electrosynthesis: Electrochemical Alkyne Functionalization. *Catal. Sci. Technol.* **2019**, *9*, 5868–5881. (b) Sbei, N.; Hardwick, T.; Ahmed, N. Green Chemistry: Electrochemical Organic Transformations via Paired Electrolysis. *ACS Sustainable Chem. Eng.* **2021**, *9*, 6148–6169.

25. Yang, Q. L.; Lei, P. P.; Hao, E. J.; Zhang, B. N.; Zhou, H. H.; Li, W. W.; Guo, H. M. Oxidative C–H Sulfonylation of Hydrazones Enabled by Electrochemistry. *SynOpen* **2023**, *7*, 535–547.
26. (a) Li, Z.; Chen, Q.; Mayer, P.; Mayr, H. Nucleophilicity Parameters of Arylsulfonyl-Substituted Halomethyl Anions. *J. Org. Chem.* **2017**, *82*, 2011–2017. (b) Kice, J. L.; Leganlc, E. Relative Nucleophilicity of Common Nucleophiles toward Sulfonyl Sulfur. II. Comparison of the Relative Reactivity of Twenty Different Nucleophiles toward Sulfonyl Sulfur vs. Carbonyl Carbon. *J. Am. Chem. Soc.* **1973**, *95*, 3912–3917.
27. (a) Kaiser, D.; Klose, I.; Oost, R.; Neuhaus, J.; Maulide, N. Bond-Forming and-Breaking Reactions at Sulfur (IV): Sulfoxides, Sulfonium Salts, Sulfur Ylides, and Sulfinate Salts. *Chem. Rev.* **2019**, *119*, 8701–8780. (b) Riddell, A. B.; Smith, M. R. A.; Schwan, A. L. The Generation and Reactions of Sulfenate Anions. An Update. *J. Sulfur Chem.* **2022**, *43*, 540–592. (c) Reddy, M. B.; McGarrigle, E. M. Iodine-Mediated Photoinduced Tuneable Disulfonylation and Sulfinylsulfonylation of Alkynes with Sodium Arylsulfinates. *Chem. Commun.* **2023**, *59*, 7767–7770.
28. Tanbouza, N.; Petti, A.; Leech, M. C.; Caron, L.; Walsh, J. M.; Lam, K.; Ollevier, T. Electrosynthesis of Stabilized Diazo Compounds from Hydrazones. *Org. Lett.* **2022**, *24*, 4665–4669.
29. (a) Lam, L. Y.; Ma, C. Chan–Lam-Type C–S Coupling Reaction by Sodium Aryl Sulfinates and Organoboron Compounds. *Org. Lett.* **2021**, *23*, 6164–6168. (b) Luo, Y. C.; Pan, X. J.; Yuan, G. Q. An Efficient Electrochemical Synthesis of Vinyl Sulfones from Sodium Sulfinates and Olefins. *Tetrahedron* **2015**, *71*, 2119–2123. (c) Lan, X. W.; Wang, N. X.; Bai, C. B.; Zhang, W.; Xing, Y.; Wen, J. L.; Wang, Y. J.; Li, Y. H. Ligand-Mediated and Copper-Catalyzed C(sp^3)-H Bond Functionalization of Aryl Ketones with Sodium Sulfinates under Mild Conditions. *Sci. Rep.* **2015**, *5*, 18391.
30. James, P. N.; Snyder, H. R. Indole-3-Aldehyde: Indole-3-Carboxaldehyde. *Org. Synth.* **1959**, *39*, 30.
31. Spingler, B.; Schnidrig, S.; Todorova, T.; Wild, F. Some Thoughts about the Single Crystal Growth of Small Molecules. *CrystEngComm* **2012**, *14*, 751–757.
32. Aktekin, M. B.; Oksuz, Z.; Turkmenoglu, B.; Istifli, E. S.; Kuzucu, M.; Algul, O. Synthesis and Evaluation of Di-Heterocyclic Benzazole Compounds as Potential Antibacterial and Anti-Biofilm Agents against *Staphylococcus aureus*. *Chem. Biol. Drug Des.* **2024**, *104*, e14601.

33. Tabassum, A.; Kumari, D.; Bhore, H. B.; Palmo, T.; Venkatesan, I.; Samanta, J.; Katare, A. K.; Singh, K.; Bharitkar, Y. P. Synthesis of Novel Spiroisoxazolidino Hybrids of Alantolactone and Isoalantolactone via 1,3-Dipolar Nitrone Cycloaddition and Its Antimicrobial Evaluation. *Bioorg. Chem.* **2025**, *154*, 108087.
34. Humphries, R.; Bobenchik, A. M.; Hindler, J. A.; Schuetz, A. N. Overview of Changes to the Clinical and Laboratory Standards Institute Performance Standards for Antimicrobial Susceptibility Testing, M100. *J. Clin. Microbiol.* **2021**, *59*, e0021321.
35. Humphries, R. M.; Ambler, J.; Mitchell, S. L.; Castanheira, M.; Dingle, T.; Hindler, J. A.; Koeth, L.; Sei, K. CLSI Methods Development and Standardization Working Group Best Practices for Evaluation of Antimicrobial Susceptibility Tests. *J. Clin. Microbiol.* **2018**, *56*, 10–1128.
36. Rani, D.; Kumari, D.; Bhushan, A.; Jamwal, V.; Lone, B. A.; Lakhanpal, G.; Nargotra, A.; Singh, K.; Gupta, P. Design, Synthesis, and Biological Evaluation of Eugenol-Isoxazoline Hybrid Derivatives as Potential Anti-Leishmanial Agents. *J. Mol. Struct.* **2024**, *1308*, 138105.

Conclusion of the thesis

Sustainability in organic synthesis refers to the development of chemical methodlogies that are efficient, environmentally friendly, cost-effective, and make use of renewable resources to ensure long-term ecological balance. It is deeply rooted in the twelve principles of green chemistry, which guide the sustainable production of pharmaceuticals and their precursors. Traditionally, organic synthesis has relied on resource-demanding and often hazardous practices that prioritize high yields and product purity, which often overlooking environmental and societal considerations. One promising strategy to enhance sustainability in organic synthesis is through catalyst-driven transformations. In addition, green catalysis includes approaches such as biocatalysis, electrocatalysis, and photocatalysis, each offering unique merits and demerits. Integrating these catalytic disciplines into one-pot systems can enable bi- or multicatalytic cascade reactions, which significantly reduce toxic waste generation, minimize solvent use, simplify work-up procedures, and lower energy consumption. However, combining these catalytic methods presents challenges. For example, enzymes typically require mild reaction conditions, making their integration with other catalytic approaches complex. Nevertheless, by carefully optimizing reaction parameters, such integration can be successfully achieved through sequential or concurrent addition of reagents. This combined strategy holds great promise for sustainable synthesis of structurally diverse and complex molecules. The first chapter of this thesis highlights such integrative approaches, focusing on the use of hydrolase enzymes in combination with chemical catalysis, electrocatalysis, and photocatalysis. It also provides a concise literature review on electricity-driven organic reactions and their applications in the synthesis of bioactive molecules.

In **Chapter 2**, we report the development of a bifunctional nanobiohybrid catalyst composed of palladium nanoparticles and the α-amylase enzyme from *A. oryzae*. This metal–enzyme hybrid catalyst was successfully applied in the chemoenzymatic synthesis of functionalized biphenyls and bis(indolyl)methanes with moderate to good yields. The reactions involved Pd-catalyzed Suzuki–Miyaura couplings and α-amylase-mediated aza-Michael additions or electrophilic substitution reactions, respectively. Notably, the developed catalyst demonstrated excellent reusability, enhanced thermostability, and a prolonged shelf life, making it highly effective for chemoenzymatic transformations.

Chapter 3 describes the sustainable synthesis of chiral sulfur-based organofluorine compounds through an integrative approach combining electrosynthesis and biocatalysis. A variety of thiophenols and fluorine-containing α,β-unsaturated alkenes were employed to generate a diverse range of 2-fluoro-3-mercaptopropionic acids in good isolated yields. Mechanistic

insights were gained through cyclic voltammetry studies, control experiments, and molecular docking analyses, which revealed the formation of radical species during the electrochemical reaction and highlighted the crucial role of the lipase's active site in enabling enantioselective synthesis. Furthermore, the practical applicability of the developed protocol was demonstrated by conducting a gram-scale reaction and synthesizing a key intermediate of an MMP-3 inhibitor.

In **Chapter 4**, we present a metal-free electrochemical methodology for regioselective *N*-sulfonylation of in situ generated indole-based hydrazones. The versatility of this protocol was demonstrated using a range of indole aldehydes, sodium sulfinates, and phenylhydrazines to afford N-sulfonylated products in good yields. Mechanistic insights were obtained through cyclic voltammetry studies and control experiments. The synthesized compounds were evaluated for their antibacterial activity against both Gram-positive and Gram-negative pathogens. Notably, compound (**5d**) exhibited promising antibacterial potential against *S. aureus* with a MIC value of 6.87 μM. Furthermore, SEM analysis revealed that compound (**5d**) induces significant morphological alterations in bacterial cells, exerting its effects by causing substantial cellular damage.

Outlook

- We developed a nanobiohybrid catalyst to overcome the challenges typically encountered in performing one-pot chemoenzymatic reactions involving Pd-catalyzed Suzuki-Miyaura coupling and α-amylase-mediated aza-Michael addition or electrophilic substitution. However, this nanobiohybrid catalyst exhibited certain substrate scope limitations, preventing it from efficiently facilitating diverse one-pot reactions. These constraints could potentially be addressed by designing hybrid catalysts that incorporate multienzyme systems or metal alloys immobilized on heterogeneous supports, enabling the execution of diverse multicatalytic reactions in a one-pot manner.
- We have also developed an integrative protocol combining electricity and lipase-mediated hydrolysis for the synthesis of chiral sulfur-based organofluorine compounds. This represents a sustainable approach, although so far it has been applied only to a limited set of electron-deficient fluorine-containing α,β-unsaturated alkenes. The methodology holds potential for expansion to a broader range of Michael acceptor alkenes. Additionally, we demonstrated its utility by synthesizing a key intermediate of an MMP-3 inhibitor. This integrative green protocol could be further applied to the synthesis of other biologically relevant sulfur-containing organofluorine compounds. Although moderate

enantioselectivity was achieved in these transformations, further optimization or enzyme engineering could enhance its efficiency and enable its application at an industrial scale.

- In our study, we elucidated a metal-free, oxidant-free, and reductant-free electrochemical approach for the functionalization of *in-situ* generated hydrazones. This strategy enables the regioselective synthesis of clinically important sulfonamides. Future research could further explore the potential of electricity-driven processes to facilitate diverse organic transformations with high selectivity. Moreover, integrating this electrochemical methodology with other catalytic disciplines holds promise for the sustainable synthesis of novel and complex molecules.

APPENDIX

Representative ^{1}H and ^{13}C-NMR spectra of Compound (5a) of Chapter 2

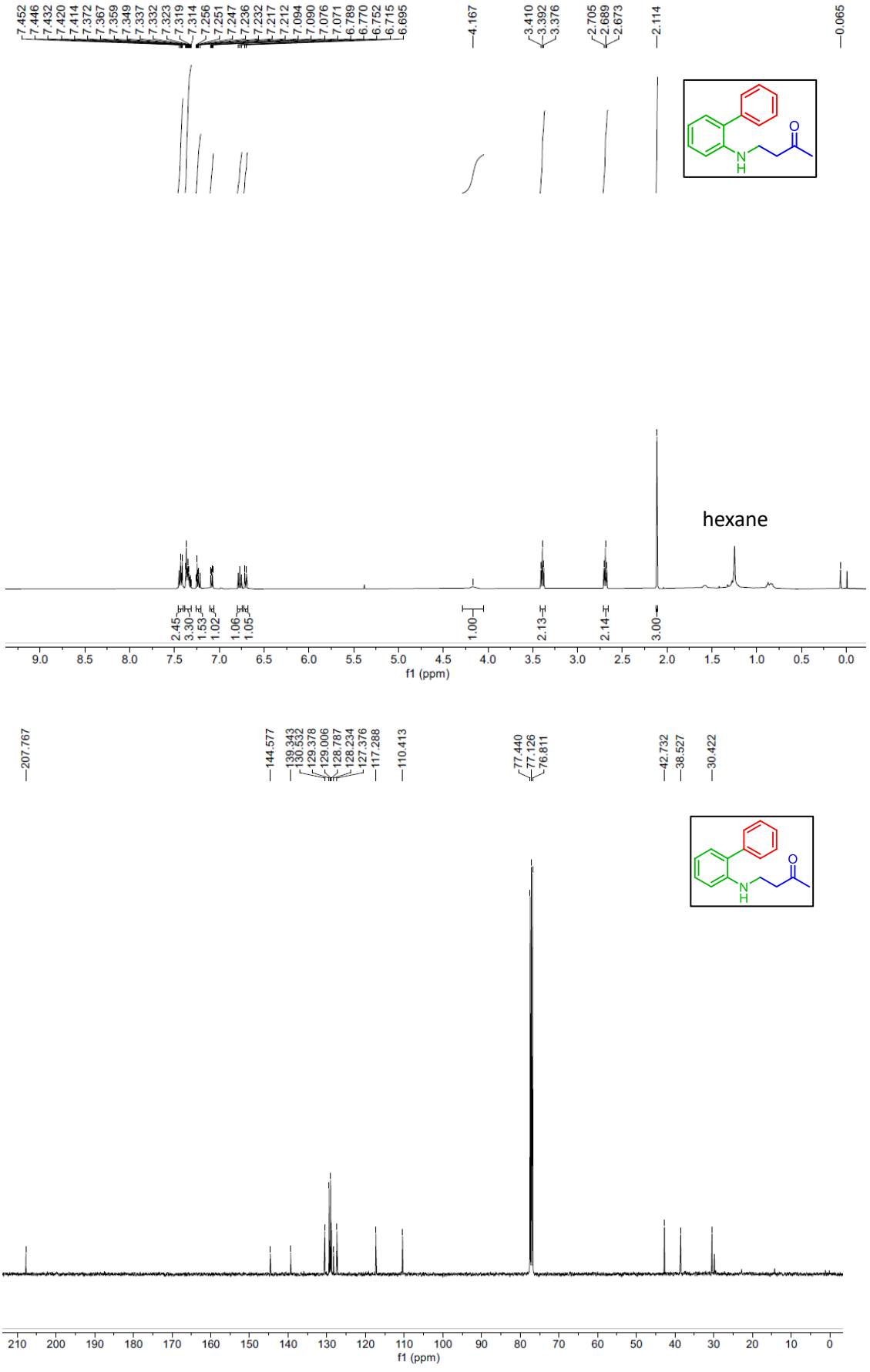

Representative ^{1}H and ^{13}C-NMR spectra of Compound (4a) of Chapter 3

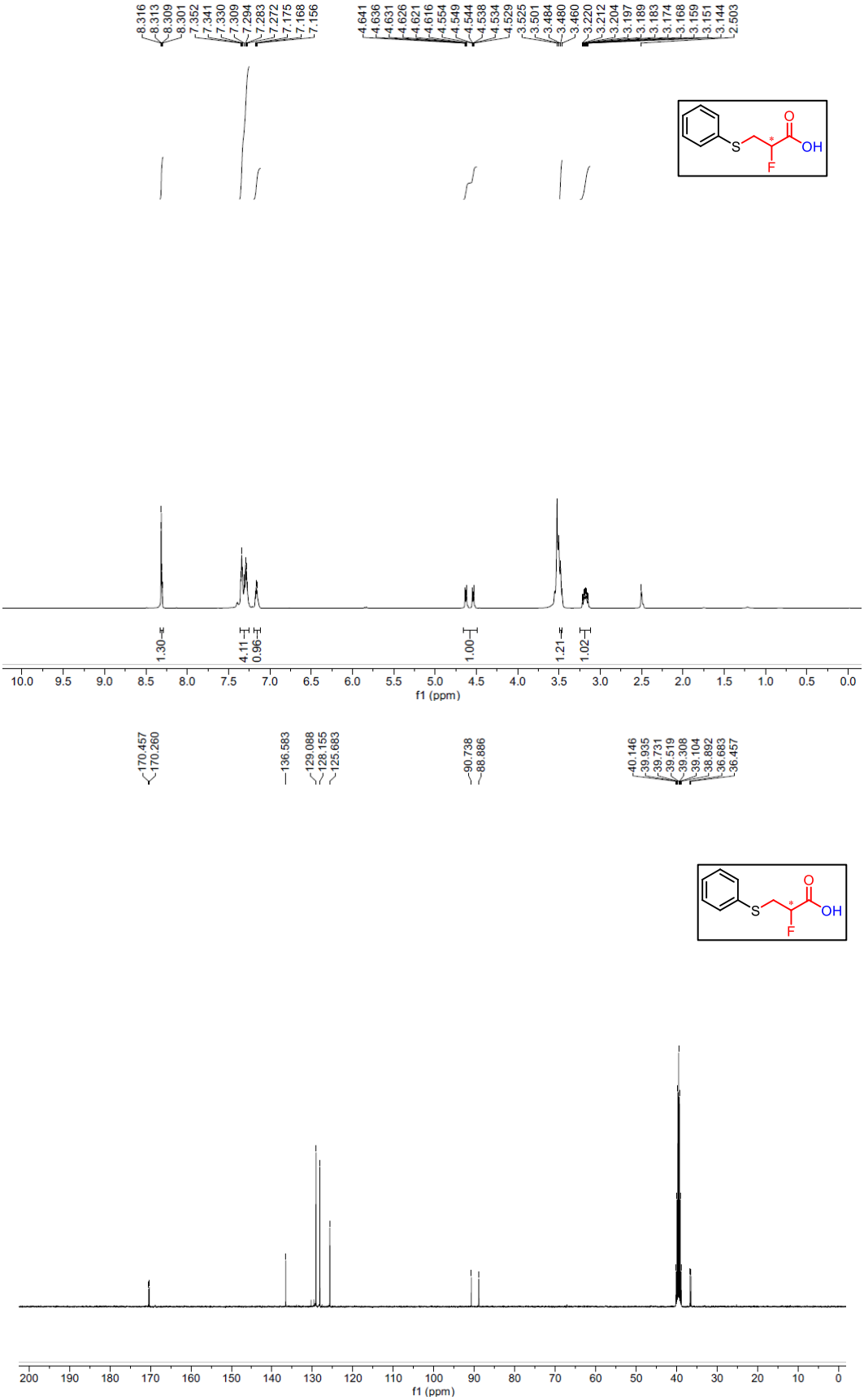

APPENDIX

Representative HPLC chromatograms of Racemic and Enantioselective Compound (4a) of Chapter 3

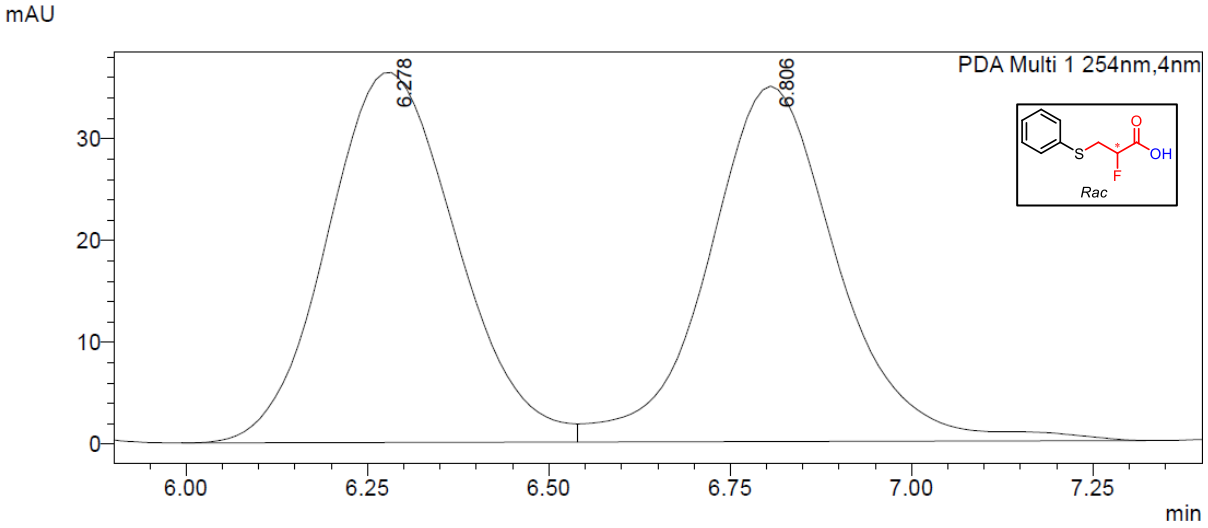

<Peak Table>

PM729 7 97 rac ref.lcd

PDA Ch1 254nm

Peak#	Ret. Time	Area	Height	Area%
1	6.278	451445	36360	50.901
2	6.806	435458	34926	49.099
Total		886903	71286	100.000

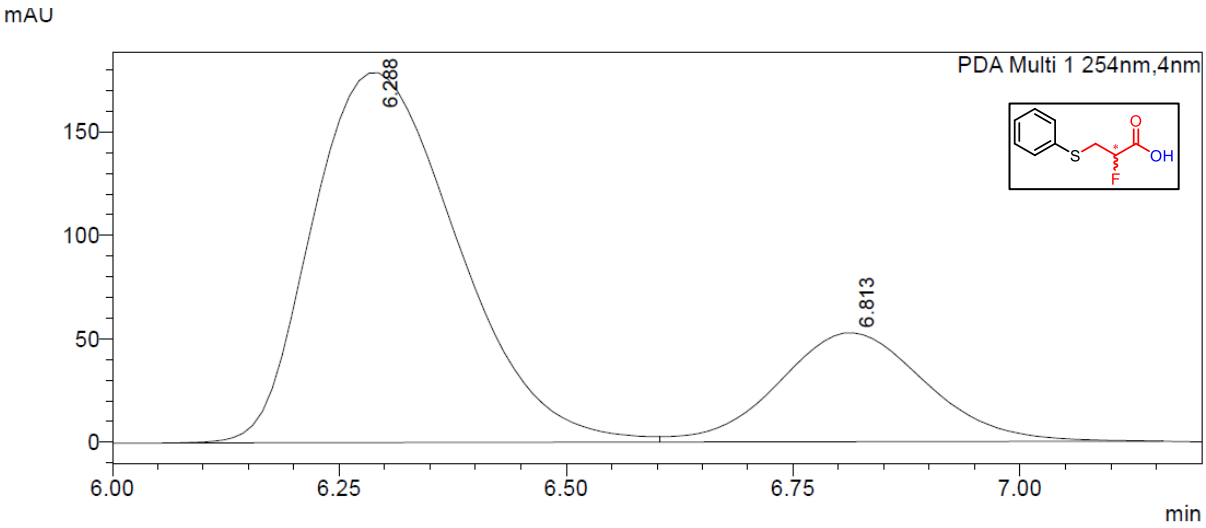

<Peak Table>

rep simple lip .lcd

PDA Ch1 254nm

Peak#	Ret. Time	Area	Height	Area%
1	6.288	1987545	178819	76.942
2	6.813	595624	52720	23.058
Total		2583169	231540	100.000

APPENDIX

Representative ^{1}H and ^{13}C-NMR spectra of Compound (5a) of Chapter 4

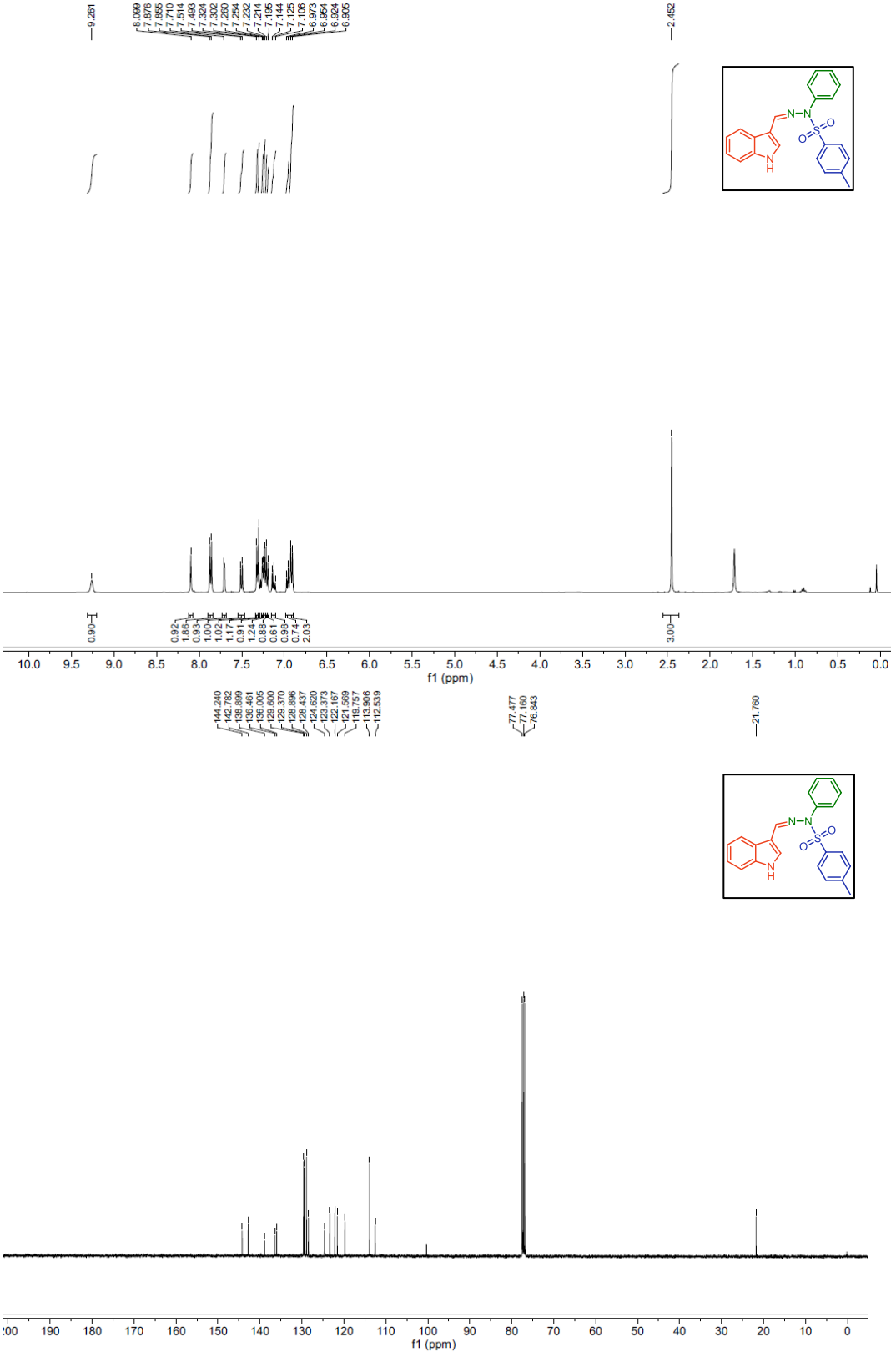

APPENDIX

Representative Crystallographic Data of Compound (5s) of Chapter 4

Identification code	Ex-PM908
Empirical formula	$C_{23}H_{21}N_3O_4S_2$
Formula weight	467.55
Temperature/K	293(2)
Crystal system	triclinic
Space group	P-1
a/Å	7.5075(5)
b/Å	10.2822(5)
c/Å	15.6878(9)
α/°	72.906(5)
β/°	88.731(5)
γ/°	80.529(5)
Volume/Å^3	1141.28(12)
Z	2
ρcalcg/cm3	1.361
μ/mm^{-1}	0.268
F(000)	488.0
Crystal size/mm^3	0.02 × 0.02 × 0.02
Radiation	Mo Kα (λ = 0.71073)
2Θ range for data collection/°	6.466 to 54.158
Index ranges	-9 ≤ h ≤ 9, -12 ≤ k ≤ 13, -19 ≤ l ≤ 18
Reflections collected	14961
Independent reflections	4595 [R_{int} = 0.1534, R_{sigma} = 0.1333]
Data/restraints/parameters	4595/0/291
Goodness-of-fit on F^2	0.957
Final R indexes [I>=2σ (I)]	R_1 = 0.0676, wR_2 = 0.1555
Final R indexes [all data]	R_1 = 0.1364, wR_2 = 0.1952
Largest diff. peak/hole / e Å^{-3}	0.22/-0.39

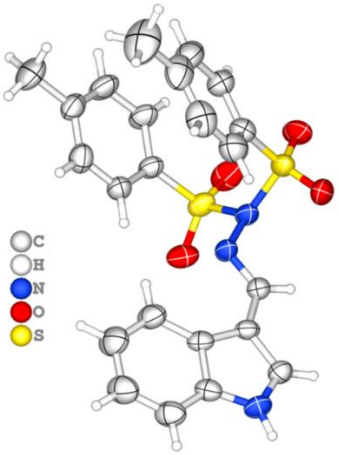

Figure (i): X-ray crystal structure of **5s** (CCDC 2471164)

LIST OF PUBLICATIONS

Thesis Publications

- **Kaur, P.**; Tyagi, V. Recent advances in iron-catalyzed chemical and enzymatic carbene-transfer reactions. *Adv. Synth. Catal.* **2021**, *363*, 877-905.

- **Kaur, P.**; Tyagi, V. Merging electrosynthesis and biocatalysis to access sulfur-based chiral α-fluorinated carboxylic acids. *J. Org. Chem.* **2025**, *90*, 5378-5392.

- **Kaur, P.**; Tyagi, V. Design and preparation of a bifunctional nanobiohybrid catalyst by combining palladium and α-amylase enzyme: application in one-pot chemoenzymatic catalysis. *ChemNanoMat* **2024**, *10,* e202300441.

Other Publications

- Soam, P.; Singh, K.; **Kaur, P**.; Tyagi, V. Synthesis of unsymmetrical urea derivatives via domino ring-opening/Pd-catalyzed decarboxylative cross-coupling reaction of isatin-3-oxime and isocyanide. *Tetrahedron* **2025**, *185*, 134809.

- Kamboj, P.; Bhardwaj, M.; **Kaur, P.**; Bajaj, P.; Tyagi, V. Chemoenzymatic synthesis of *N*-phenyl glycine derivatives via integration of Au/TiO_2 and enzyme as catalysts in water. *Biocatal. Biotransform.* **2024**, *43*, 158-165.

Manuscript under review/preparation

- **Kaur, P.**; Kumar, A.; Palmo, T.; Singh, K.; Tyagi, V. Electrochemical *N*-sulfonylation of *in-situ* generated indole-based hydrazones and antimicrobial evaluation. *Org. Biomol. Chem.* **2025** (major revision).

- **Kaur, P.**; Tyagi, V. Toward Sustainable Catalysis: Integrating Hydrolase Biocatalysis with Electro-, Photo-, and Chemical Catalysis. **2025**, *manuscript under preparation.*